Integrative ArcGIS Mapping Study of Direct Hydrocarbon Indicators within the Shelburne Subbasin of the Scotian Slope, Nova Scotia

by

Yaisa Dipna Owino

A Thesis Submitted to Saint Mary's University, Halifax, Nova Scotia in Partial Fulfilment of the Requirements for the Degree of Master of Science in Applied Science

April 23, 2023, Halifax, Nova Scotia

Approved: Dr. Todd Ventura
Supervisor

Approved: Dr. Danika Van Proosdij
Supervisory Committee

Approved: Dr. Adam MacDonald
Supervisory Committee

Approved: Randolph Corney
Supervisory Committee

Approved: Dr. Andrew MacRae
Supervisory Committee

Date: April 23, 2023

Integrative ArcGIS Mapping Study of Direct Hydrocarbon Indicators within the Shelburne Subbasin of the Scotian Slope, Nova Scotia

By Yaisa D. Owino

Abstract: Seepage data can provide evidence for hydrocarbon migration from underlying mature source rocks. In this study, ArcGIS coupled with seismic analysis of the Shelburne 3D seismic survey is used to better constrain the prospectivity of petroleum systems underlying the Scotian Slope. In this study, the seismic attributes root mean square amplitude (RMS) and coherence were used to identify near-surface expressions of hydrocarbon migration from the Shelburne 3D seismic volume. The RMS amplitude maps reveal amplitude anomalies including direct hydrocarbon indicators (DHIs) above salt features that are likely related to the presence of hydrocarbon-bearing sediments. Coherence maps were used to highlight seafloor and subsurface discontinuities such as paleo-pockmarks and polygonal faults, which are subsurface fluid escape mechanisms. The DHIs are commonly associated with these fluid escape structures. The presence of these two features suggest hydrocarbons are migrating from deeper within the Shelburne Subbasin implying the presence of an active petroleum system within the deeper Scotian Slope.

April 23, 2023.

Acknowledgements

I would like to acknowledge my thesis supervisor, Dr. Todd Ventura, for his consistent support before and throughout the pandemic to accomplish this thesis. I am truly grateful for his persistence and guidance. Great thanks to Adam MacDonald and Natasha Morrison of Nova Scotia Department of Energy and Mines without whom I would have probably suffered an existential crisis while learning to work on Petrel without prior geophysical skills, and who also gave counsel and support throughout the process. Many thanks to Randolph Corney and Dr. Andrew MacRae for always giving a listening ear and help with troubleshooting GIS problems, and for always asking great questions that develop understanding.

I wish to thank and acknowledge the financial and resource support from the following organizations: Mitacs (Scholarship), Faculty of Graduate Studies and Research at Saint Mary's University, Nova Scotia Department of Energy and Mines (Petrel and 3D seismic data access), Offshore Energy Research Association, Genome Atlantic and Genome Canada (GAPP grant).

Lastly, I would extend my sincere thanks to my family, my friends, and my fellow graduate students in the geology department. I really could not have done it without such a great network of support.

Table of Contents

List of Figures

List of Appendices

List of Abbreviations

APT – Applied Petroleum Technologies

ASCII – American Standard Code for Information Interchange

AUV – Autonomous Underwater Vehicle

Bbbls – Billion Barrels

BMP – Bitmap Image

CAD – Computer Aided Design

CD – Commercial Discovery

CMP – Common Mid-point

CNSOPB – Canada Nova Scotia Offshore Petroleum Board

CRS – Common Risk Segment

CT – Complex Trace

DEM – Digital Elevation Model

DHI – Direct Hydrocarbon Indicator

DMC – Data Management Centre

ESRI – Environmental Systems Research Institute

FGDBR – File Geodatabase Raster

GDE – Gross Depositional Environment

GIS – Geographic Information System

JPEG – Joint Photographic Experts Group

MTD – Mass Transport Deposit

MBSF – Meters Below Sea Floor

NSDEM – Nova Scotia Department of Energy and Mines

NRCAN – Natural Resources Canada

OERA – Offshore Energy Research Association (formerly OETR)

OETR – Offshore Energy Technical Research

PFA – Play Fairway Analysis

RMS – Root Mean Square

SD – Significant Discovery

SDR – Seaward-Dipping Reflectors

Tcf – Trillion cubic feet

TIFF – Tag Image File Format

Chapter 1 : Background and Introduction

1.1 Hydrocarbon Exploration History of Offshore Nova Scotia

Offshore development of natural gas from Nova Scotia and crude oil from Newfoundland and Labrador has been an important contribution to Canada's petroleum industry (Murillo, 2011). In Nova Scotia, offshore exploration began in 1959 (CNSOPB, 2018) and has mostly focused on shallow-water (<200 m) areas of the Scotian Shelf (Enachescu and Hogg, 2005; Murillo, 2011). Since 1967, two hundred and ten wells have been drilled, with 124 being exploratory, 29 delineation, and 57 development wells (Smith et al., 2014; CNSOPB, 2018; OERA, 2019). To date, 23 significant and eight commercial hydrocarbon discoveries have been made (CNSOPB, 2000; Smith et al., 2014). Total 2D and 3D seismic data acquired from 1960 to 2018 is 401,651.2 km and 48,376.9 km^2, respectively (CNSOPB, 2018).

Nova Scotia's exploration history is described in four distinct cycles of activity (CNSOPB, 2018). The first cycle (1960-1978) confirmed the existence of a thick Tertiary-Mesozoic stratigraphic succession in the Sable Delta with gas and oil shows in the Sable Island C-67 well (CNSOPB, 2018). Three significant discoveries were made in 1969 (Onondaga E-84), 1971 (Sable 1H-58), and 1972 (Primrose A-41) (CNSOPB, 2018). More significant gas discoveries were made in 1974 and the Sable Subbasin was considered the most prolific depocenter in the Scotian Margin at that time (CNSOPB, 2018).

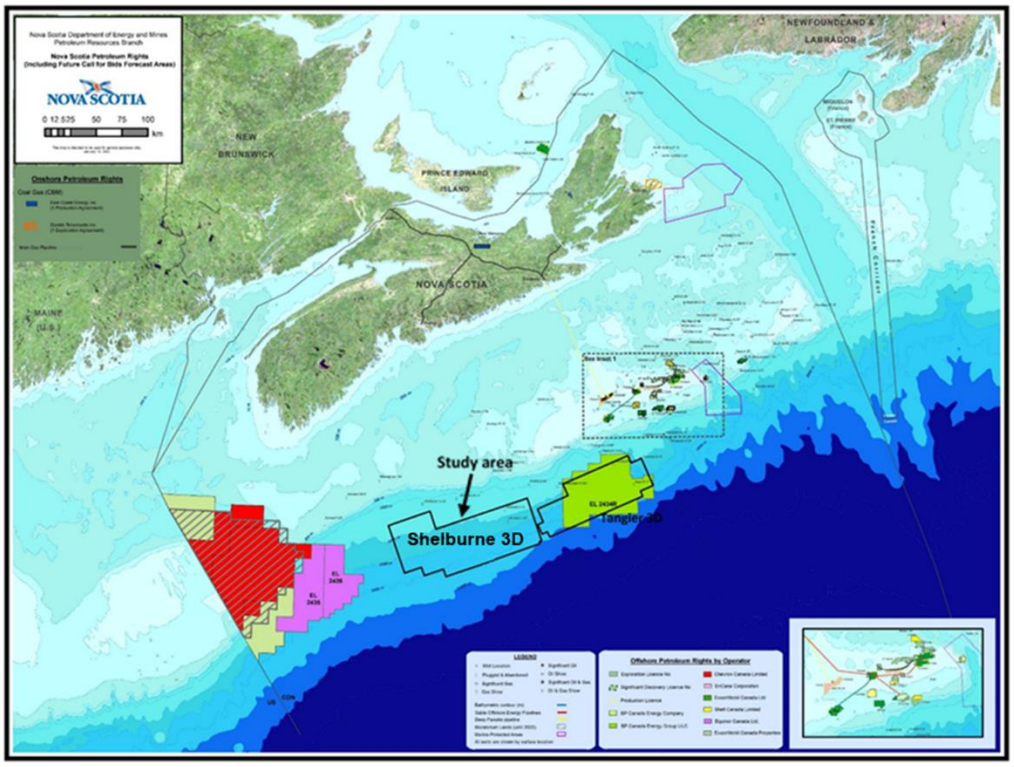

Figure 1.1. Offshore investments of Nova Scotia in the last decade total 1.28 billion. The Shelburne 3D seismic survey is the study area in this thesis. (*Adapted from NSDEM and CNSOPB web archive).*

The second exploration cycle (1979-1988) was sparked by a major gas discovery at Venture in 1979. The discovery was in very shallow waters east of Sable Island. More gas discoveries were made in this cycle and a few oil and gas shows were observed (see: CNSOPB, 2018). The cycle ended due to the fall of oil and gas prices.

In the third exploration cycle (1990-2005), drilling campaigns were undertaken in both the shallow Scotian Shelf and deepwater Scotian Slope with the development of several significant oil and gas discoveries (CNSOPB, 2018). The Cohasset-Panuke Project was considered as Canada's first offshore oil project, and it operated from 1992-1999. The project had a total of 14 production wells with 10 at Cohasset and four at Panuke. The oil field was a series of stacked reservoir sandstones in the Upper Missisauga Formation for the Panuke field, stacked reservoir sandstones within the lower Logan Canyon, Naskapi and Upper Missisauga formations for the Cohasset oil field

(CNSOPB, 2018). Decommissioning and abandonment were completed in 2006 for the Cohasset-Panuke Project. The fourth exploration cycle (2006-present) has had companies obtain exploration licences in the Scotian Slope deepwater portion. Shell (2013) and BP (2014) completed 3D Wide Azimuth seismic programs in the deepwater portion (CNSOPB, 2018).

The Sable Offshore Exploration Project (SOEP; Figure 1.2) was Canada's first offshore natural gas project and included the Venture, Thebaud, South Venture, North Triumph, and Alma gas fields (Kidston et al., 2002; Smith et al., 2014;). Production in the SOEP began in December 1999 and was shut down in December 2018. The project produced 60 billion cubic metres (2.1 tcf) of natural gas from the five gas fields (CNSOPB *web*). The *Deep Panuke* project, also in relatively shallow water (<250 m), sourced gas from the Abenaki Formation carbonate reservoir (Kidston et al., 2002; Enachescu and Hogg, 2005; Murillo, 2011). This carbonate reef play proved elusive over a 30-year period of well testing and hypothesis until it was confirmed (Eliuk, 1978; Harland et al., 2002; Enachescu and Hogg, 2005). Use of intensive 3D seismic data, seismic amplitude mapping, and reservoir-fluid recognition studies greatly helped in the confirmation of this play (Eliuk, 1978; Harland et al., 2002; Enachescu and Hogg, 2005). Production began in August 2013 for the Deep Panuke project and shut down in 2018.

Efforts to find new plays in the offshore of Nova Scotia is ongoing as the region is thought to host significant, underexplored resource potential estimated at 120 tcf of unrisked gas and eight Bbbls of oil in place (Kidston et al., 2002; Mukhopadhyay et al., 2003; Kidston et al., 2007; OETR, 2011). Utilization of multidisciplinary techniques

alongside conventional methods ought to reduce the exploration risks in the deepwater portion of the basin.

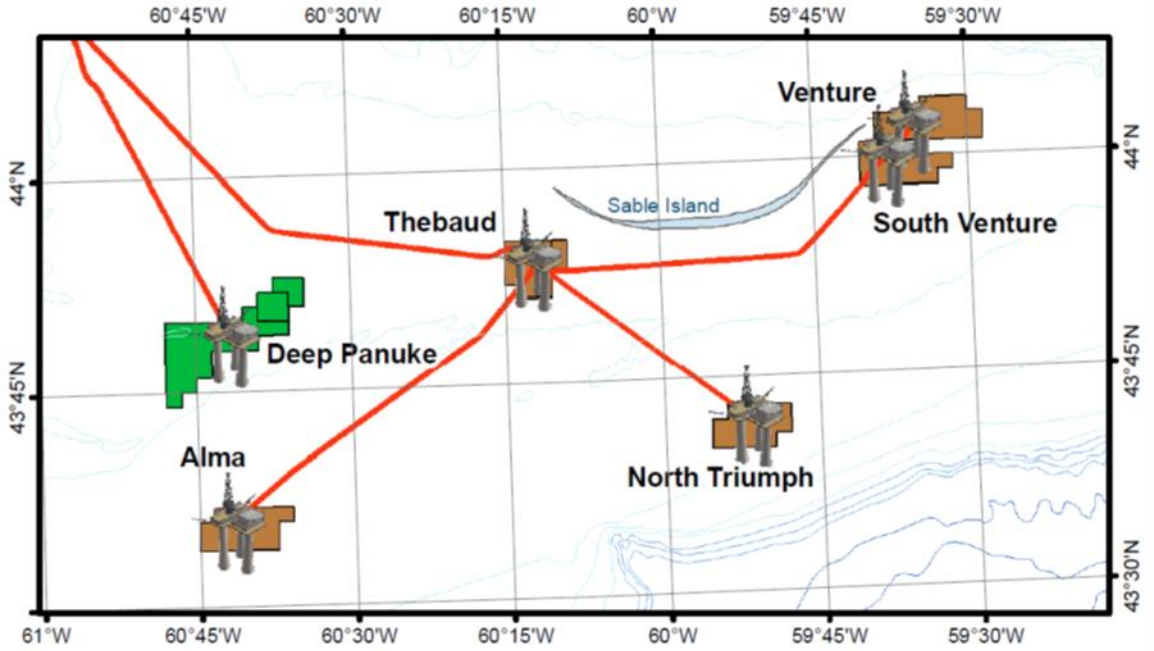

Figure 1.2. Sable area platforms showing the five gas fields of the SOEP and the Deep Panuke Platform. Image from CNSOPB web.

The Nova Scotia Department of Energy and Mines (NSDEM, currently Nova Scotia Department of Natural Resources and Renewables, NSDNRR) in collaboration with the Offshore Energy Research Association (OERA, formerly OETR), funded the Play Fairway Analysis (PFA) that re-evaluated the hydrocarbon potential in the basin (OETR, 2011). The program, launched in 2009, was a multidisciplinary research effort for a better geologic understanding of the basin's petroleum system and involved academic as well as industrial research teams (OETR, 2011). With newly acquired seismic grids and recent exploration well information becoming available and public, an effort to de-risk and better understand the hydrocarbon potential of the basin continues.

This thesis study proposes to identify surface and near-surface expressions of migrating hydrocarbons (seepage) in the Shelburne 3D seismic survey (Figure 1.1 –

Study area, Figure 2.2) using geophysical methods. Evidence of hydrocarbon migration implies the presence of source rock(s) and probable hydrocarbon charge of a prospect. Such evidence can contribute to de-risking efforts and may also be useful in comparing, ground truthing, and/or correlating different data types used in hydrocarbon exploration.

1.2 Thesis Question and Objectives

Geologic data of the Scotian Basin predicts the presence of a working petroleum system (OETR, 2011). Presence of hydrocarbon slicks in the basin may imply the presence of hydrocarbon seeps that leak hydrocarbons to the ocean water column (Mukhopadhyay et al., 2003). Hydrocarbon seeps are an indicator of possible prospectivity in frontier basins and surface core sampling of surficial sediment with geochemical analysis is a relatively inexpensive method to identify hydrocarbon occurrences in a play fairway prospect (Laubmeyer, 1933; Mukhopadhyay et al., 2003; Abrams and Dahdah, 2011).

In a multidisciplinary effort to find seeps in the Scotian Basin, this thesis seeks to answer two fundamental questions:

1. Does the deepwater portion of Scotian Basin show evidence for surface and near-surface expressions of subsurface hydrocarbon leakage?
2. Can surficial sediment analyses near potential seep locations help to increase understanding of the exploration risk and similarly help to validate seep presence in the Scotian Basin play fairway?

This study aims to utilize geophysical methods in conjunction with ArcGIS using the Shelburne 3D area to identify and map features that may represent evidence of subsurface hydrocarbon leakage and migration in the Shelburne Subbasin. This is done by:

1. Identifying seismic anomalies indicative of surface and near-surface expressions of hydrocarbon seepage and storage.

2. Integrating this geophysical data with prior geochemical surveys in areas where the high-resolution seismic data indicates a presence of hydrocarbon seepage and/or surface faulting that could serve as a migration pathway.

3. Checking for correlations between anomalies and surficial sediment hydrocarbon analyses to better identify potential migration pathways to the ocean floor.

In integrating the disparate datasets, an ArcGIS platform (ArcMap 10:3 and ArcGIS Pro 3) is used to display and visualize PFA 2011 data, seismic data, and geochemistry data in plan-view. Schlumberger's Petrel is used for interpretation of 3D seismic data.

Chapter 2 : Geological Setting and Prospectivity Potential of the Scotian Basin

2.1 Geological Setting of the Scotian Basin

Regionally, the Scotian Basin is a large sedimentary passive margin composed of a series of geologically distinct subbasins covering an approximate area of 300,000 km^2 (Jansa and Wade, 1975; OETR, 2011). The basin extends from Georges Bank to the Grand Banks, and from the near shoreline of Nova Scotia into deepwater (Jansa and Wade, 1975; MacLean and Wade, 1990; Hogg et al., 2001; Cullen et al., 2008; OETR, 2011).

Synrift redbeds, restricted marine dolomites and halite of the Eurydice, Iroquois and Argo formations (Hogg et al., 2001) characterized deposition in Middle to Late Triassic and Early Jurassic. Basin development in Middle-Late Jurassic to Tertiary was associated with accumulations of carbonate and clastic sequences ranging up to 10 – 12 km in depth (Jansa and Wade, 1975; MacLean and Wade, 1990; Enachescu and Hogg, 2005; Cullen et al., 2008; Mosher, 2008). Significant fluvio-deltaic and shelf sandstones (Hogg et al., 2001; Enachescu and Hogg, 2005) marked basin subsidence and fill in Middle Jurassic to the end of the Cretaceous.

Extensive basin-scale structural deformation was experienced from the halokinetic movement of Late Triassic-Early Jurassic Argo Formation halite coupled with high sediment input in the Jurassic and Early Cretaceous. This deformation produced complex salt tectonic features such as salt welds and pillows, extensional diapirs and canopies, swells, walls, ridges, and domes (Hogg et al., 2001; Adam and Krezsek, 2012; Deptuck and Kendell 2017, 2020). A salt province emerged, which strongly controls accommodation space in the basin and creates complex sediment

pathways with potential to host several distinct petroleum systems and with considerable variation in play-types (Hogg et al., 2001; Adam and Krezsek, 2012; Kendell, 2012; Deptuck et al., 2015; Deptuck and Kendell 2017, 2020).

2.2 Geological Setting of the Study Area

This study's research area is primarily focused on the Banquereau Formation (Figure 2.1, 2.3) in the Shelburne Subbasin (Figure 2.2). The Shelburne Subbasin is a subdivision of the southwestern part of the Scotian Basin and is one of several Mesozoic–Cenozoic sediment depocenters that interconnect to make-up the offshore passive-margin of Nova Scotia (Wade and MacLean, 1990; Cummings and Arnott, 2005; Albertz et al., 2010; OERA, 2019). The subbasin covers an approximate area of 100,000 km^2. It accumulated up to 14 km of clastic and carbonate sediment mostly deposited in the Jurassic through Cenozoic (Wade and MacLean, 1990a, b; OERA, 2019). Exploration in the slope area of the Shelburne Subbasin has been very limited with three older wells (Shelburne G-29, Albatross B-13, and Torbrook C-15), and two very recent wells (Cheshire L-97 and Monterey Jack E-43) (Figure 2.3, 2.4) on the slope in the Shelburne Subbasin (Shell, 2017, 2018). Well data tested favorable-looking hydrocarbon traps without new discoveries being realised. The area is also thought to host deepwater clastic reservoirs and source rocks, but whose identification and seismic interpretation is greatly affected by salt tectonics and a complex sediment system of alternating carbonates and clastics.

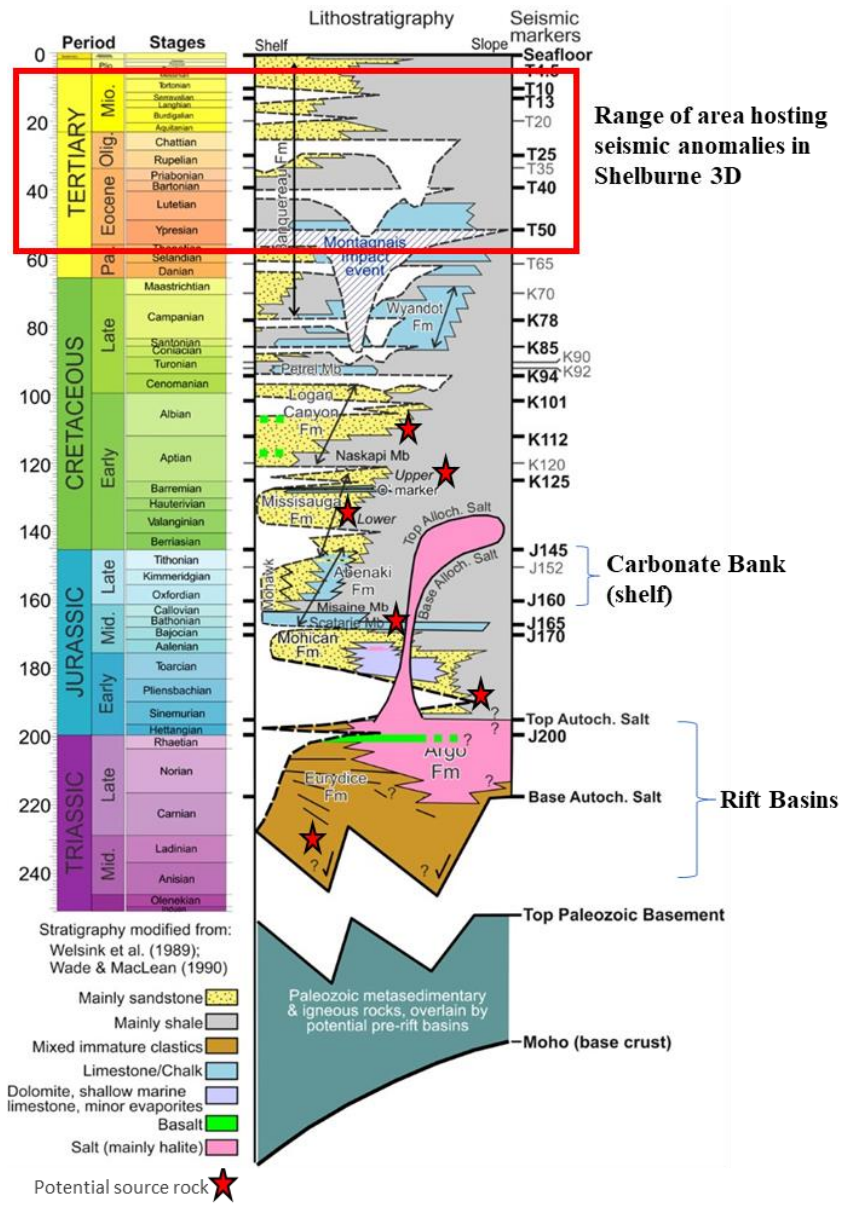

Figure 2.1. Basic litho-chronostratigraphic chart for the Scotian Basin. (Adapted and modified from Weston et al, 2012, Deptuck, and Kendell, 2020). The 3D data focused on the area in the red rectangle, hosted in the Banquereau Formation in the Shelburne subbasin (see also Figure 2.3.)

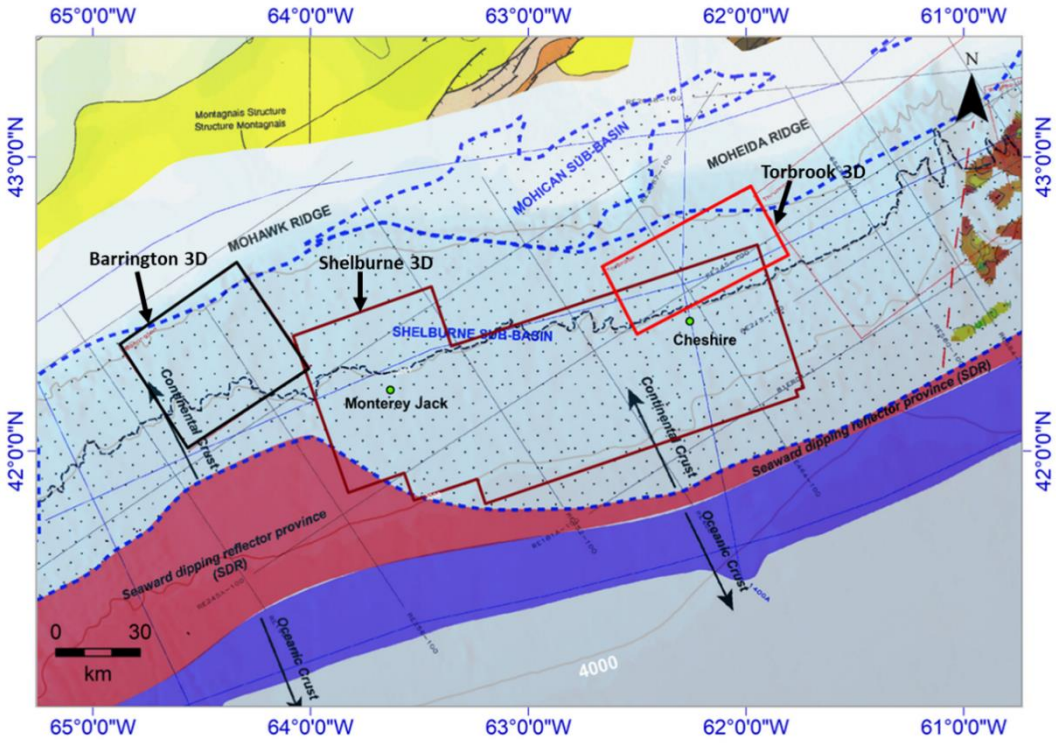

Figure 2.2. Shelburne 3D is located in the Shelburne subbasin's hyperextended domain (Deptuck and Kendell, 2020) just north of the seaward dipping reflector boundary (OETRA, 2011). Adapted and modified from OETRA (2011).

The Shelburne Subbasin is a subdivision of the southwestern part of the Scotian Basin and is one of several Mesozoic–Cenozoic sediment depocenters that interconnect to make-up the offshore passive-margin of Nova Scotia (Wade and MacLean, 1990; Cummings and Arnott, 2005; Albertz et al., 2010; OERA, 2019 earliest basin infilling formation occurred began during with Triassic-earliest Jurassic rifting and the deposition of consisted of red continental clastic and evaporitic sediments (Eurydice and Argo Formations). The basin transitioned to a passive margin within the Early Jurassic. By the Middle Jurassic, the basin was a succession of alluvial plains as well as, deltaic and carbonate environments. Deltaic progradation and shelf clastic deposits dominated the Early Cretaceous after the Avalon uplift in the north and New England hot spot uplift in the south (OERA, 2015). Transgressive shale, sporadic influxes of deltaic sands,

limestone, and chalk sequences dominated the Late Cretaceous-Early Tertiary sedimentation. During the Early Eocene transition, the Montagnais bolide destabilized the southern part of the margin causing mass transport of sediment down the slope (Wade and MacLean, 1990; Albertz et al., 2010; Deptuck and Campbell, 2012).

The late Cretaceous to early Quaternary aged Banquereau Formation is characterised by a stacked series of prograding sequences that downlap unconformably onto the chalk dominated Wyandot Formation (McIver, 1972). The lithology of this interval is mud dominated and generally coarsens upward with few intervals of silt and argillaceous sandstone (Figure 2.1). In general, the lower interval of the Banquereau Formation on the shelf is comprised of basinward–building, prograding deltaic clinoforms that consist of sandstone deposited in the topsets of clinoforms, and with mudstone fore-and -bottom sets (Fensome et al., 2008). Campbell et al. (2015) describe mudstone-dominated stratigraphic units of the Banquereau Formation on the slope and note an interval with sediment drift development, mass transport deposits, and channels near the modern seafloor surface (Figure 2.3) where the study area for this thesis is focused.

The Shelburne 3D seismic volume (Figure 2.2), located in the salt basin, was acquired on stretched continental crust of the Scotian passive margin. It is located SW of the main shelf break (a rimmed carbonate platform) that appears to have remained in approximately the same location since the Jurassic (OERA, 2019). It is bounded to the SW by a major NW-SE transverse fault separating the salt basin from the volcanic province, the latter characterized by seaward dipping reflectors (SDRs) (Figure 2.2., Deptuck and Kendell, 2020). This major fault affecting the continental crust may have acted as a transform fault during the first breakup event (OERA, 2019). In the Jurassic

and Cretaceous, a large drainage system from the northeastern flank of the Appalachian Orogeny extending from Massachusetts to New Brunswick fed clastic sediments to the subbasin at its southwestern end (Zhang et al., 2014; Chavez et al., 2018). In the northernmost part of the subbasin, wells record a probable secondary clastic source from the Meguma terrain (Zhang et al., 2014; Chavez et al., 2018; OERA, 2019). These secondary sources are inferred to be small, short rivers with sufficient relief to supply a significant quantity of lithic clasts. They are interpreted as being coastal rivers in an arid climate and likely to be flood dominated (Nagle et al., 2019; OERA, 2019).

In the seaward region of Shelburne 3D, the top autochthonous salt is dominated by a polygonal network of subcircular to elongated minibasins haloed by salt stems formed during syndepositional down-building process (i.e., the top of the salt diapir remains at the surface all the time) in the Jurassic and Cretaceous (Deptuck and Kendell, 2020). Salt bodies form isolated salt walls and stocks in the west, and salt tongues and amalgamated salt stock canopies in the east (Deptuck and Kendell, 2020). Salt overhangs are most prevalent in the eastern part of the block, and diapirs are bulbous or mushroom shaped with minor salt overhangs. The crests of most of the salt bodies range from 2800 to 3600 m below sea level with overburden varying between more than 2 km to less than 300 m (Figure 2.4A). Salt bodies in the distal parts of Shelburne are covered with the least amount of sediment, and the shallow buried diapirs are in areas of focused erosion or recent expulsion (Deptuck and Kendell, 2020).

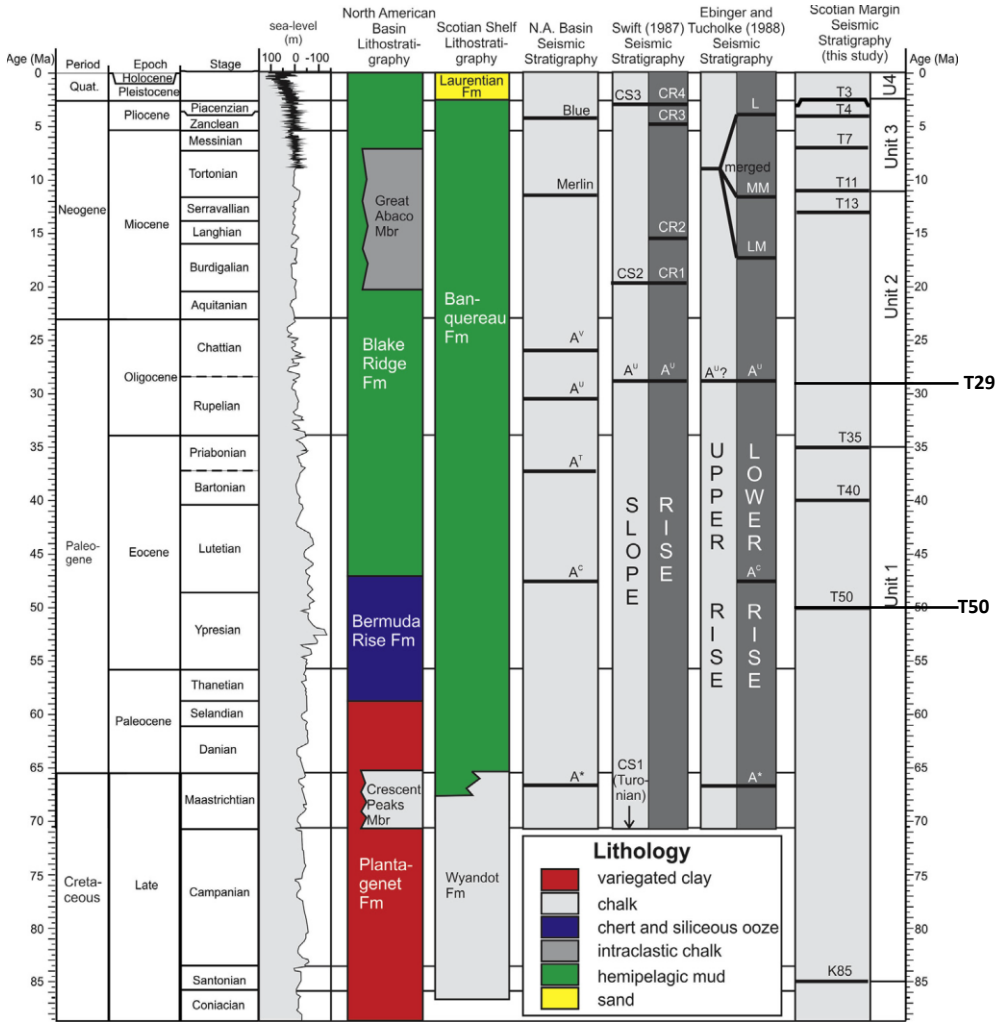

Figure 2.3. Stratigraphic framework for the Upper Cretaceous-Cenozoic of the southwestern Scotian Slope from Campbell et al. (2015). This study focused mainly on Units 2 and 3 (units as described in Campbell et al., 2015) above the T29 marker horizon to approximately the T4 marker and in the Banquereau Formation. The Banquereau Fm is considered to be one of the main vertical seals for hydrocarbon reservoirs (Mukhopadhyay et al., 2003). Unit 3 is described as an interval with sediment drift development, mass transport deposits, and channels. Unit 2 is described as an interval that is often eroded (especially between T11-T13) and with local sediment drift development observed until the T35 marker horizon. The horizon used to create the RMS amplitude map (see Chapter 3) is approximately between the T4 and T7 marker horizon.

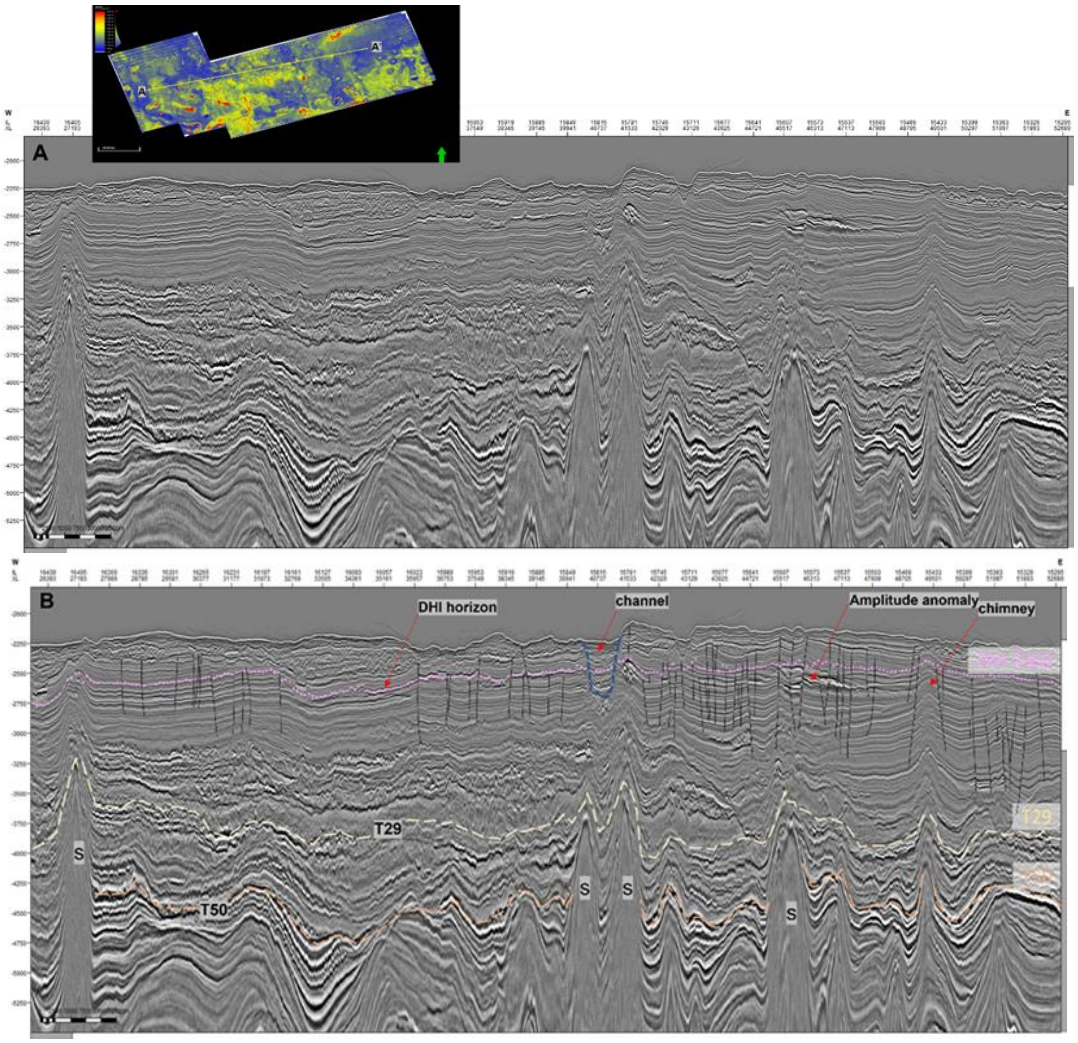

Figure 2.4. Regional strike line through the Shelburne 3D study area A) not annotated and B) annotated. The dotted pink line is the picked DHI horizon used to create an RMS amplitude map, which is described in detail in Chapter 3. S indicates salt structures.

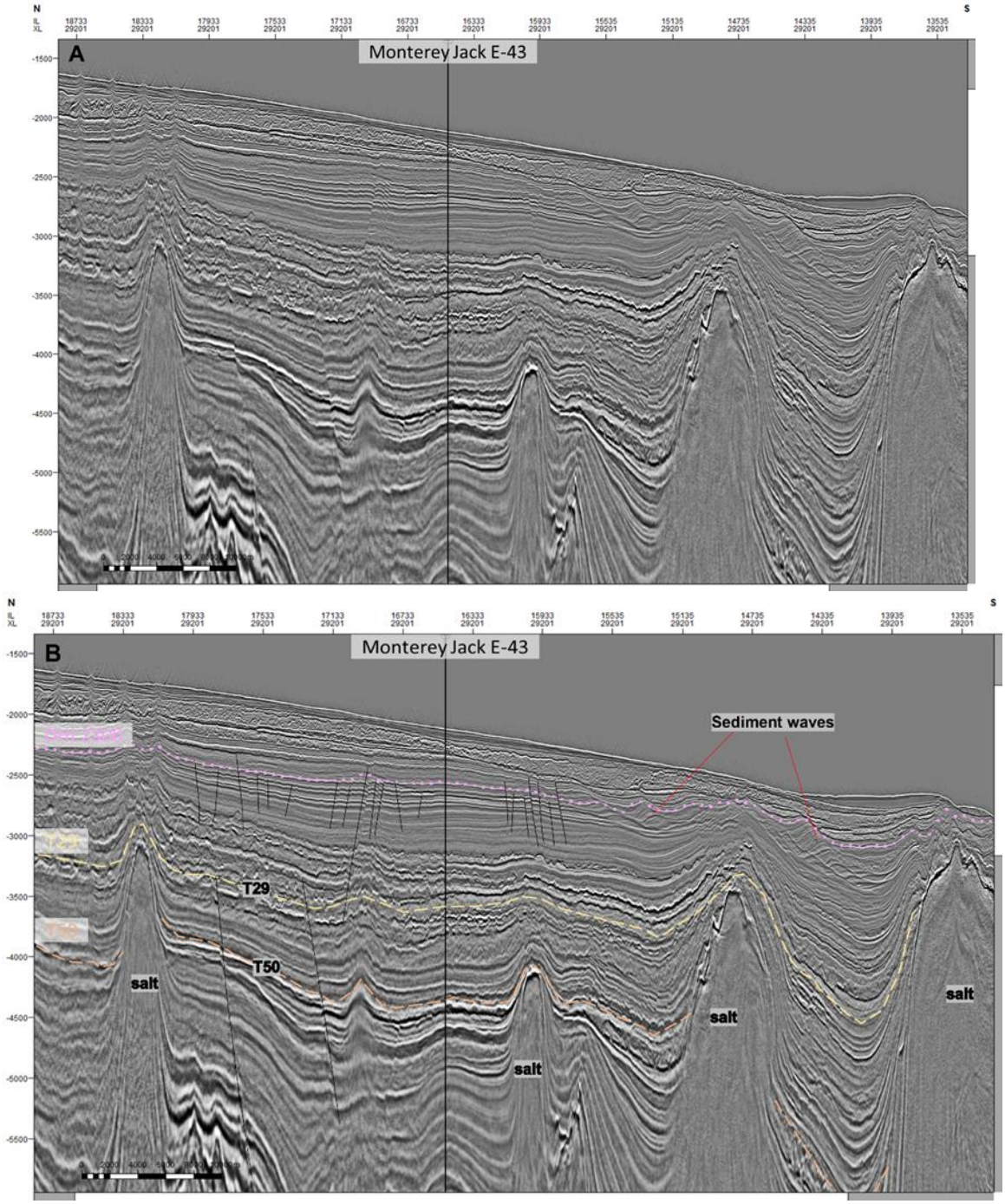

Figure 2.5. Dip-oriented seismic profile through the Monterey Jack exploration well in the western side of the Shelburne 3D study area (see Figure 2.2). A) not annotated, B) annotated.

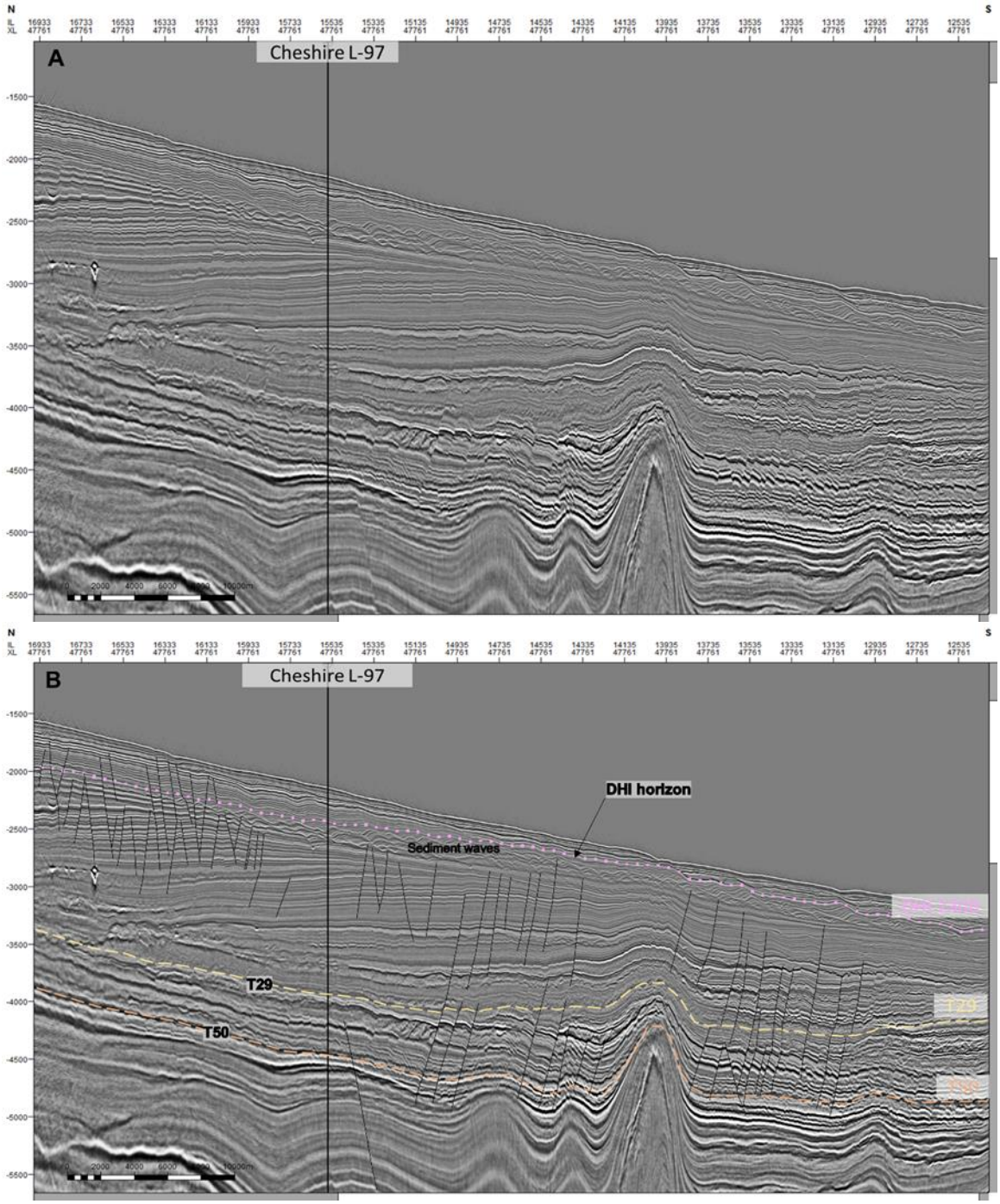

Figure 2.6. Dip-oriented seismic profile through the Cheshire L-97 exploration well in the eastern part of the study area (see Figure 2.2).

2.3 Source Rock, Reservoir, and Seal Potential in the Scotian Basin

Source rocks are organic-rich sediments that either have the potential to form or have already generated hydrocarbons when buried deeply within a sedimentary basin (Tissot and Welte, 1984; Magoon and Dow, 1994; Kennicutt, 2017). Source rocks are typically composed of sediments deposited in anoxic or suboxic conditions. However, if sedimentation rates are sufficiently high, oxic conditions can also lead to preservation of organic matter (Tissot and Welte, 1984).

In offshore Nova Scotia, most of the proven source rocks (Late Triassic to recent) derive from terrestrial organic matter deposited in a partially anoxic marine or deltaic environment and are gas- and condensate-prone due to high clastic dilution (Mukhopadhyay, 1990; Mukhopadhyay and Wade, 1990; Mukhopadhyay, 1993; Mukhopadhay et al., 1995; Mukhopadhyay et al., 2003). In some cases, source rocks are derived from partially oxidized marine organic matter (Mukhopadhay et al., 1995). The youngest hypothesised mature source rock interval in the Scotian Basin is in Upper Jurassic strata, centered on the Tithonian. In the deepwater portion of the basin, this source rock remains unconfirmed (OETR, 2011). Evidence exists for a regional Lower Jurassic and a Middle to Late Triassic source rock, which also remain unconfirmed (OETR, 2011).

The NSDNRR has publicly provided a 3D petroleum system model of the Scotian Basin identifying potential for a current, oil-generating, Lower Jurassic source rock in the Southwest part of the margin (OETR, 2011). The generation potential of the same source rock in the eastern part of the margin is thought to be over mature in the present day and already went through hydrocarbon generation earlier (OETR, 2011). In the Sable Subbasin, the basin model predicts an Upper Jurassic Tithonian sequence source rock that

is presently in the gas window. As the basin shallows at the margins, this source rock is predicted to be in the oil window implying an under-explored play with potential for an oil rim around the Sable delta and Huron subbasin (OETR, 2011).

The major offshore source rock systems proposed and identified are of deltaic and restricted marine facies (OETR, 2011). The Deep Panuke shallow water gas discovery is hosted in a Jurassic Abenaki carbonate reef play. It has been the only discovery in this play type in the western Atlantic margin (Enachescu and Hogg, 2005). In the deepwater, potential Cretaceous and Tertiary turbidite reservoirs are in areas extensively disturbed by salt tectonics with numerous structural and stratigraphic traps that are the main targets for exploration (Kidston et al., 2002; Enachescu and Hogg, 2005). Another play follows the listric fault trend in the Sable Basin targeting Late Jurassic –Early Cretaceous deltaic sandstones (Enachescu and Hogg, 2005). Aside from Deep Panuke there have not been any recent (over the last 20 years) commercial discoveries in offshore Nova Scotia either on the shelf or slope.

Regarding reservoirs and seals, earlier significant discoveries within the Scotian Shelf mostly lie within the Cretaceous (Missisauga and Logan Canyon formations) and Late Jurassic (Mic Mac Formation) sandstone reservoirs (Mukhopadhyay et al., 2003). EnCana Corporation's discovery of gas and condensate in reservoirs of the Late Jurassic Abenaki Formation led to further interest in exploration of the carbonate bank play in the basin (Mukhopadhyay et al., 2003). The main vertical seal for major hydrocarbon reservoirs of offshore Nova Scotia is shales of the Late Jurassic (Mic Mac), Middle Cretaceous (Naskapi Member, Logan Canyon Formation) and Early Tertiary (Banquereau Formation) (Mukhopadhyay et al., 2003).

After the PFA program completed, further analyses of the basin through basin modelling and new interpretation of 3D seismic data (see OERA, 2019) led to affirmations of some of the hypotheses in the PFA. The more recent review has also resulted in some clarifications as well as additional new leads. The PFA (2011) appears to be regionally accurate and predictive for reservoir distribution in the Shelburne Subbasin. The two most recent wildcat exploration wells (Cheshire L-97 and Monterey Jack E-93), however did not encounter any of the targeted reservoirs or an Upper Jurassic source rock as explained in the PFA (2011). Nonetheless, the predicted petroleum potential remains unchanged except for the lack of a Tithonian source rock (OETR, 2011; OERA, 2019).

The post-mortem report (OERA, 2019) advises the re-evaluation of new plays based on new data: a Tertiary play not previously evaluated ought to be explored, and there is potential for a Lower Cretaceous clastic turbidite play. The report (OERA, 2019) also discusses potential reservoirs with hydrocarbon accumulations hosted in the more proximal parts of the Lower-Middle Jurassic carbonate ramp play (OERA, 2019). A possibility for hydrocarbon charge of Lower Cretaceous turbidites south of the Cheshire well is suggested (OERA, 2019).

2.4 Basin Exploration and Seepage

There is a vast accumulation of geologic and geophysical legacy data for the offshore Nova Scotia from decades of exploratory efforts and research in the region (e.g., Jansa and Wade, 1975; Swift 1987; Jansa et al., 1989; Wade and MacLean, 1990; MacLean and Wade, 1993; Louden, 2002; Cummings, 2004; Piper et al., 2004; Cummings and Arnott, 2005; Enachescu and Hogg, 2005; Kidston et al., 2005; EnCana, 2006; Wierzbicki et al., 2006; Withjack and Schlische, 2006; Kidston et al., 2007; Eliuk,

2008; Natural Resources Canada, 2009; Piper et al., 2010; Gould et al., 2010; OETR, 2011). A visual display of selected datasets can illuminate the dynamic nature of the subsurface geology in the slope of the Scotian Basin and help to identify hydrocarbon indicators present in the region as well as features influencing their manifestation on the seafloor.

When a source rock generates hydrocarbons in an active petroleum system, the expelled hydrocarbons migrate and potentially accumulate within a trap (Magoon and Dow, 1994). For a hydrocarbon reservoir to form, the preservation of hydrocarbons within a trap must be greater than its leakage. For the hydrocarbons to remain entrapped, a seal is needed. A seal does not however prevent flow, as all rock types possess intrinsic permeability to a certain extent; therefore, it defines low permeability of a rock to an extent of halting or retarding the flow of petroleum toward the basin surface (Cartwright et al., 2007). Hydrocarbons migrate through sealing sequences on modest geological scales (Macgregor, 1996) through faults, fractures, and capillary pore systems (Losh et al., 1999; Gartrell et al., 2002; Nord-gard Bolas and Hermanrud, 2003; Boles et al., 2004); seepage is the most obvious indicator of leakage (Cartwright et al., 2007).

Most oil and gas accumulations leak hydrocarbons. When and if this leakage migrates to the ocean water column, it is commonly identified as a cold seep (Judd and Hovland, 2007; Hovland, 2012). Depending on the regional and local geologic conditions, migrating oil and gas can move both vertically and laterally in the subsurface (Macgregor, 1993; Reilly et al., 1996; Thrasher et al., 1996; Bolchert et al., 2000; Gay et al., 2007; Hou et al., 2008; Ding et al., 2010, Johansen et al., 2020). This makes the relationship between subsurface and surface hydrocarbons complex. Oil and gas from

mature source rock or a subsurface reservoir can leak to the near surface in detectable concentrations and their concentration and composition vary due to geological and biological processes (Abrams, 2005; Abrams and Dahdah, 2011; Abrams, 2020). Leythaeuser et al. (1982, 2000) describe how gases of thermal origin in near surface sediments are likely to generate at greater depths and migrate to the surface.

It is possible to detect and map near surface expressions of hydrocarbon seepage and microseepage by various direct and indirect methods (e.g., see Mukhopadhyay et al., 2003) including geochemical, geophysical, and non-geophysical methods. Surface geochemistry, or the detection of chemically identifiable seeps, has been a well-used evaluation tool in the petroleum industry (Laubmeyer, 1933; Link, 1952; Brooks and Carey, 1986; Huang et al., 2009; Abrams and Dahdah, 2011; Abrams, 2020). DHIs are a seismic anomalous feature that result from large volumes of migrating gas (Phipps and Carson, 1982) and present in various ways in seismic traces (Carlson et al., 1985; Abrams, 1992; Heggland, 1998; Whelan et al., 2005; Rollet et al., 2006; Dembicki and Samuel, 2007; Løseth et al., 2009; Gay et al., 2011). When seepage data is integrated with conventional exploration data, it can be effective in de-risking a prospect.

To study the hydrocarbon survival after charge and leakage from reservoirs, evidence of seepage and presence of faults and breach of vertical and lateral seals for target reservoirs are necessary components (Mukhopadhyay et al., 2003). Surficial sediments acquired via piston coring from near and on seeps are great for direct analysis of hydrocarbon seepage (Kennicutt, 2017) and especially in predicting hydrocarbon type and properties (Hood et al., 2002; Kennicutt, 2017). The presence of gaseous hydrocarbons in near-surface sediment is of interest due to the mobility of gases. It can

signal the presence of deeper and more extensive hydrocarbon accumulations (Kvenvolden et al, 1981). The 3D seismic interpretation is also useful in identifying and predicting hydrocarbon migration pathways through the analysis of a diverse set of seismically resolvable geological features that appear to breach sealing sequences, allowing for vertical or subvertical fluid flow and cross stratal migration across seals (Cartwright et al. 2007). Seismic data provides an avenue for the visualisation of near-surface expressions of hydrocarbon migration, and integration on a GIS platform makes it possible to display disparate data types as plan-views.

The deepwater portion of the Scotian Basin is considered a frontier basin in terms of exploration and play fairway analysis. To de-risk exploration, the legacy exploration data from the shelf and any new datasets obtained in the slope region can be useful in delineating the hydrocarbon potential of this region. As the 2011 PFA infers the presence of a mature source rock in the study area, this study seeks to find evidence of hydrocarbon leakage in the near-surface and surface sediment that can further be useful in the exploration of this frontier basin by implying the possibility of charge from a deeper trap. To achieve this, seismic and geological data is analysed and used to identify and map seepage features in the Shelburne 3D volume that is located on the Scotian Slope offshore Nova Scotia.

Chapter 3 : Methods

3.1 Piston Coring and Sediment Sampling in the Scotian Basin

To obtain evidence of direct hydrocarbon seepage in the deep portion of the Scotian Basin, surficial sediments were acquired by piston and gravity coring surveys (Campbell and MacDonald, 2016; Campbell, 2019; Campbell and Normandeau, 2019). The geochemical data collected from these surveys were used for this study (Fowler and Webb, 2015, 2017, 2019). Piston and gravity coring expeditions were undertaken in 2015, 2016, and 2018 (Campbell and MacDonald, 2016; Campbell, 2019; Campbell and Normandeau, 2019) to search for evidence of a working petroleum system in the deepwater Scotian Slope (note: a 2017 Sydney Basin expedition is not a focus of this study, but the core locations were mapped on the ArcMap geodatabase, see below). Core locations (Figure 3.1) within the Shelburne data block were selected based on targets initially identified through analysis of slicks data from satellite imaging and 2D and 3D seismic data provided by NSDEM.

For this study, the results of the geochemical analyses were compiled and mapped in plan-view. The locations of the cores in the study area were organized by their acquisition year, and the summary hydrocarbon signatures for the core samples. In Chapter 4, the results from this endeavor are further integrated with geophysical data to check for correlations between geochemical signatures of hydrocarbon seepage and any geologic subsurface structures that would facilitate its migration.

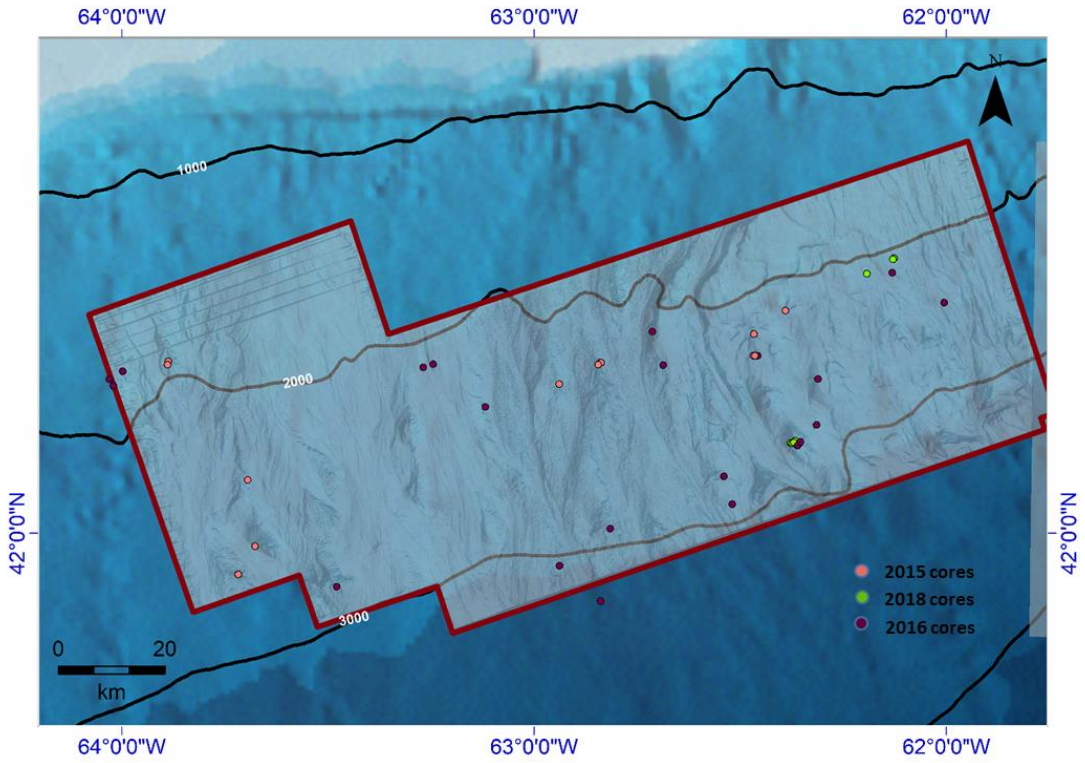

Figure 3.1. Piston and gravity cores retrieved in the study area during coring surveys displayed on a high-resolution sea floor bathymetric map of the Shelburne 3D study area (red polygon).

3.2 GIS Methodology

A geographic information system (GIS) is a spatial system that creates, manages, analyzes, and maps various types of data by incorporating geographical features with tabular data (Environmental Systems Research Institute (ESRI) online, Burrough, 1986). In this study, ArcMap v10:3 and later ArcGIS pro were used to visualize and display integrated datasets of information on exploration efforts in the deep-sea region of the Scotian Basin (OETR 2011, OERA 2019) into a geodatabase as plan-view maps.

This ArcGIS project organises the different datasets into four main parent layers: Seep Mapping Surveys, Basin Geology, Basin Exploration and Prospectivity, and Geography (Figure 3.2).

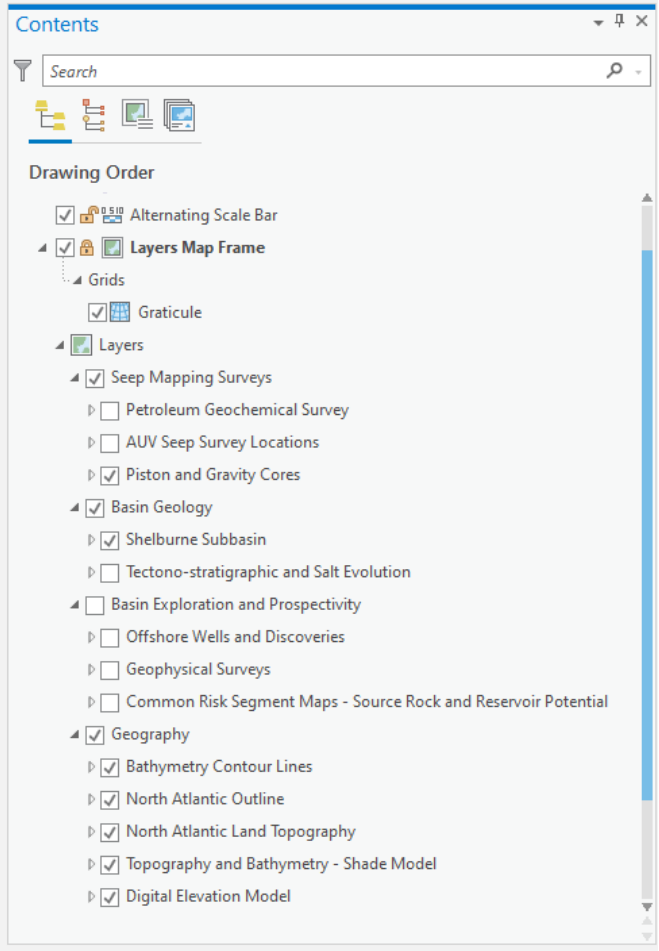

Figure 3.2. Table of contents (TOC) as seen in ArcGIS Pro for the ArcGIS database created in this study.

3.2.1 Geography Layer

This layer provides base-level geographic maps of the North Atlantic. These feature classes include a North Atlantic Land Topography map, a North Atlantic Outline, a digital elevation model (DEM), and hill shade relief map of the North Atlantic (Geological Survey of Canada, 1991; Keppie, 2000; Shaw et al., 2004; OETR, 2011). The source for these layers is found in the basemap geodatabase (basemap. gdb) on ArcCatalog.

The topographic map of the North Atlantic (Figure 3.3A) was imported to the project as a 2D raster (FGDBR format). To better visualize the topographic elevation in

the North Atlantic, a DEM (Figure 3.3B) and a hill shade model of the region were added (Figure 3.3C). As the focus study area was the slope region, 1000 m step isobaths were added to indicate bathymetry (Figure 3.4)

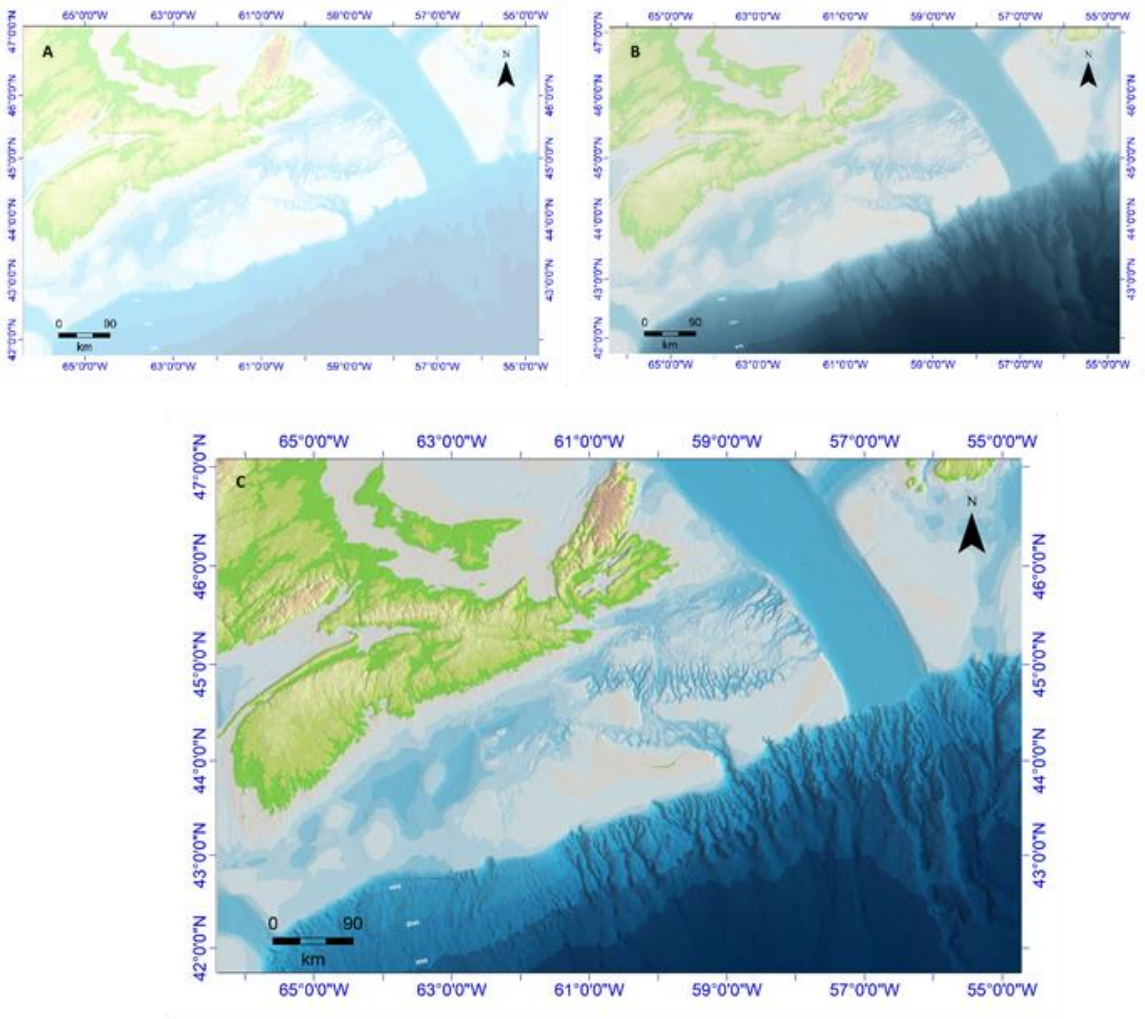

Figure 3.3. A) topographic map of North Atlantic focused on Nova Scotia, B) with a DEM applied, and C) Hill shade model also applied.

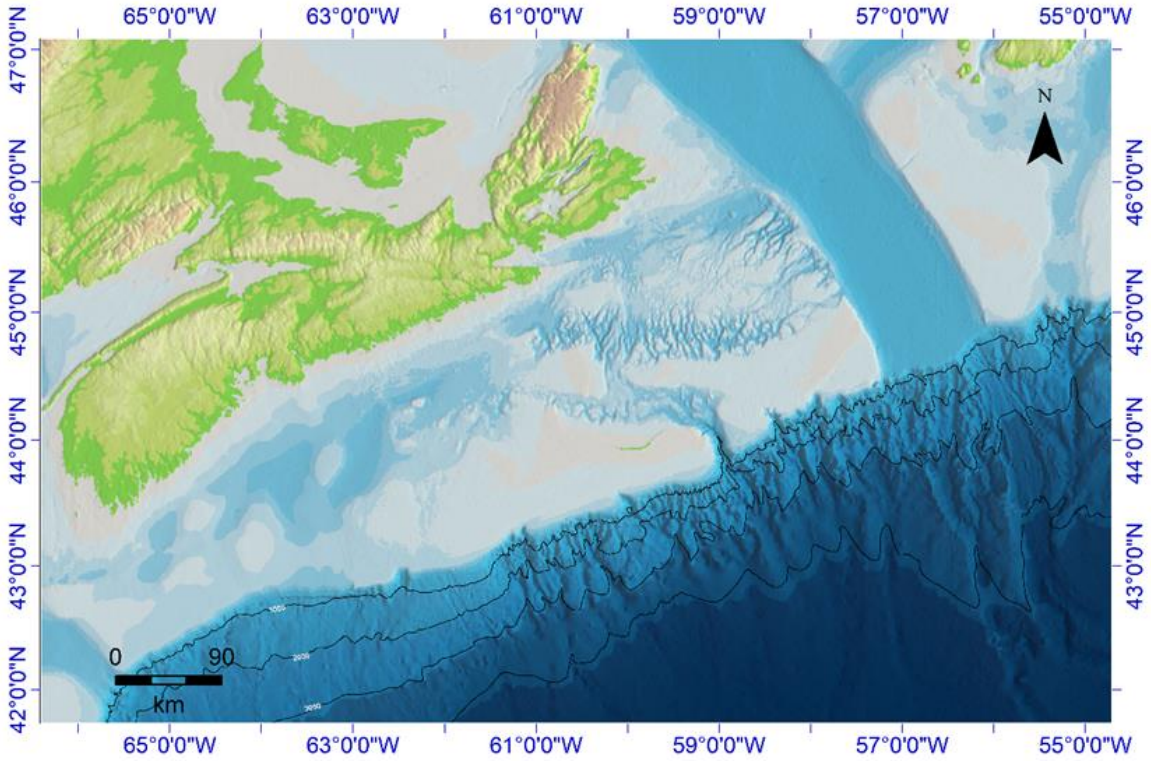

Figure 3.4. Offshore Nova Scotia with bathymetric contour lines along the slope. In ArcGIS, the user can control the contour line spacing and visualization.

3.2.2 Basin Geology Layer

The basin geology layer is organised in two major sections: I) the Shelburne 3D seismic survey, which has sub-layers including the study area boundary, a high-resolution sea floor bathymetry map of the study area, seismic RMS amplitude, and coherence surface maps of the study area; and II) the tectonostratigraphic and salt evolution layer, which is further discussed below.

3.2.2.1 Tectonostratigraphic Evolution Layer

Tectonostratigraphy, a stratigraphic technique developed by Berthelsen (1978), differentiates packages of deformed sediment and rock based on their deformation histories (Lee, 2018). The sediment packages are reconstructed in sequential order of

formation to show stratigraphic evolution in time and space. These sequences are significant in understanding the distribution of resources in a studied terrain (Lee, 2018).

In the Scotian Margin PFA, the prospective sedimentary section of the basin is sub-divided into four stratigraphic mega-sequences: Triassic to Callovian, Oxfordian to Tithonian, Berriasian to Aptian, and Albian to Cenomanian (CNSOPB, 2000; Keppie, 2000; Kidston et al., 2007; Piper et al., 2010; OETR, 2011). The architectural aspects of these sequences were designed along seismic cross-sections at a regional scale and based on 20 key wells (Jansa and Wade, 1975; Swift 1987; Jansa et al., 1989; Wade and MacLean, 1990; MacLean and Wade, 1993; Kidston et al., 2002; Louden, 2002; Wierzbicki et al., 2002; Cummings, 2004; Piper et al., 2004; Cummings and Arnott, 2005; Kidston et al., 2005; Enachescu and Hogg, 2005; EnCana, 2006; Withjack and Schlische, 2006; Kidston et al., 2007; Eliuk, 2008; Natural Resources Canada, 2009; Gould et al., 2010; Piper et al., 2010; OETR, 2011).

The sub-layers display both digitized (heads-up method) and geotiff images of salt canopies and diapirs, isopach maps, and structural depth maps of the Scotian Basin all obtained from the PFA 2011 analysis project (Eliuk, 1978; Jansa et al., 1989; Wade and MacLean, 1990b; Maclean, 1991; Keen, 2000; Kidston et al., 2005; Thomas, 2005; Ings and Shimeld, 2006; OETR, 2011). Seismic marker horizons and biostratigraphy were used in the PFA to date the geologic formations through the basin architecture and to update the stratigraphic chart of the Scotian Basin (Jansa et al., 1989; Welsink, 1989; GSC, 1991; MacLean, 1991; Shaw et al., 2004; Gemmer et al., 2005; Thomas, 2005; Vendeville, 2005; Ings and Shimeld, 2006; Ings et al., 2009; Weston et al., 2012).

3.2.2.1.1 Salt Canopies and Diapirs Sub-Layer

The slope domain of the Scotian Margin is subdivided into various structural sub-provinces (Shimeld, 2004; Albertz et al., 2010). In this section, we focus on the canopy and diapir provinces of the slope. The canopy province is characterized by autochthonous and allocthonous salt bodies and large canopy structures (Deptuck et al; 2009, 2010a, b; Deptuck and Kendell, 2020). To show the spatial extent and distribution of salt bodies in the slope at different stratigraphic sequences for the region, salt canopies and diapirs of the Argo Formation were manually digitized (heads-up digitizing) from georeferenced isopach maps for tectonostratigraphic evolution and petroleum systems (Chapter 6 of OETRA, 2011).

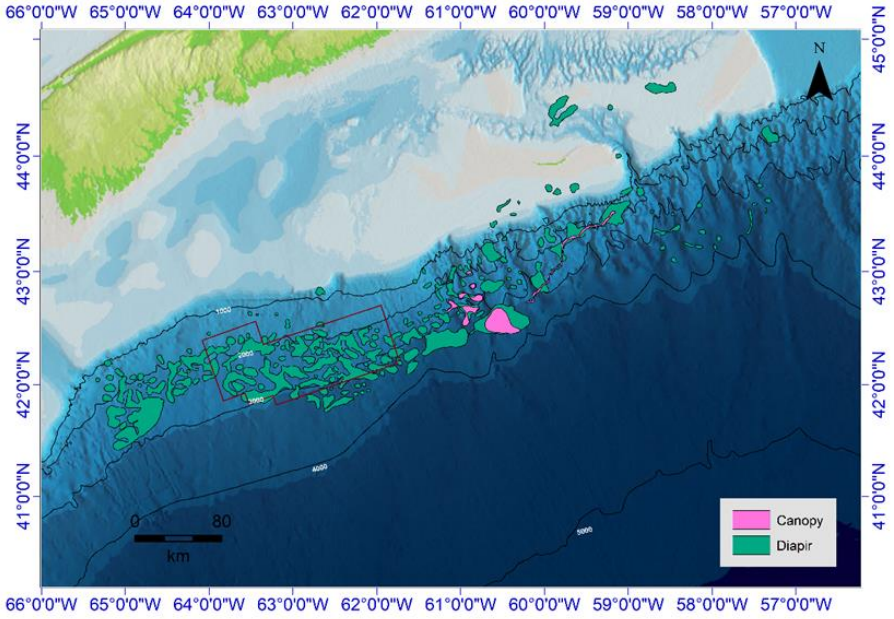

Figure 3.5. Salt canopies and diapirs at the J150 – K137 (Tithonian-Berriasian) interval, which encompasses a transgressive phase at the base of Tithonian aged shales and a major regressive Berriasian sands sequence associated with the Avalon uplift (OETR, 2011). Sediment thickness in this interval varies around the slope and deep offshore area of the basin. The variations are attributed to ponded basins found between salt diapirs (OETR, 2011).

3.2.2.1.2 Isopach and Depth Structure Maps sub-layers

An isopach map portrays the variation in stratigraphic thickness between an upper and lower horizon (Hintze, 1971). A depth structure map is a depth-converted, seismic-derived map that displays the geometry of a subsurface structure. The isopach and depth structural maps in this geodatabase were imported as georeferenced raster images (e.g., Figure 3.6). This dataset had a locked system and the projection (Universal Transverse Mercator –Zone 20; Datum – NAD27) would plot incorrectly on conversion. With the projection still being Mercator, it was left as transverse instead of Mercator ISP, which is the projection used in the data frame of the project. The plotting matched the dataframe for all the imported images.

Metadata of all downloaded and georeferenced images can be found in the item description for the maps in ArcMap.

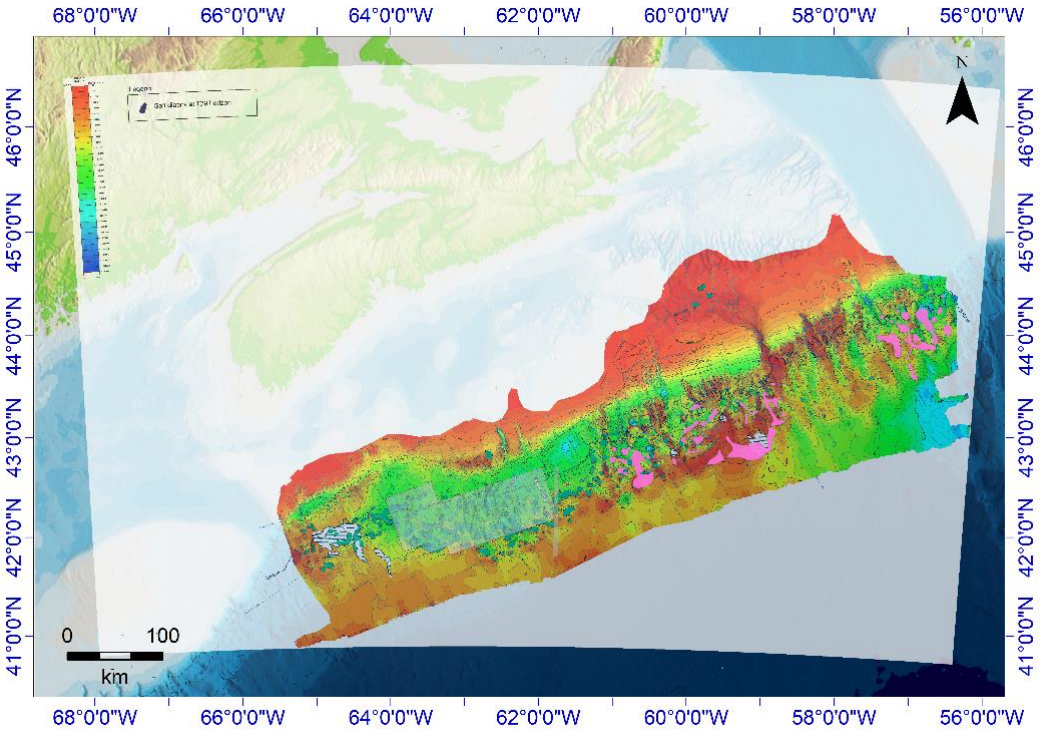

Figure 3.6. The T29 (Mid Oligocene to Pliocene) Seabed Isopach unit GeoTiff image overlaying topographic map. The legend describes increasing thickness with blue zones being thickest (~3000 m) and orange zones ranging between 0-600 m. In the study area the average

3.2.2.2 Shelburne 3D Seismic Survey Layer

Shell Canada Limited acquired a 3D seismic survey of this block named Shelburne 3D (RPS, 2013; Brown, 2018; OERA, 2019; Deptuck and Kendell, 2020). The seismic data was made available by NSDEM, and it was interpreted for this study using Schlumberger's Petrel software platform. After the interpretation, three attribute surface maps were extracted and imported to ArcMap: a high-resolution seafloor bathymetry map (Figure 3.7), an RMS amplitude map (Figure 3.8), and coherence surface maps at different depths (see Appendix III). A georeferenced polygon shape file delineating the boundary of the survey (Figure 3.7) was also imported to ArcMap.

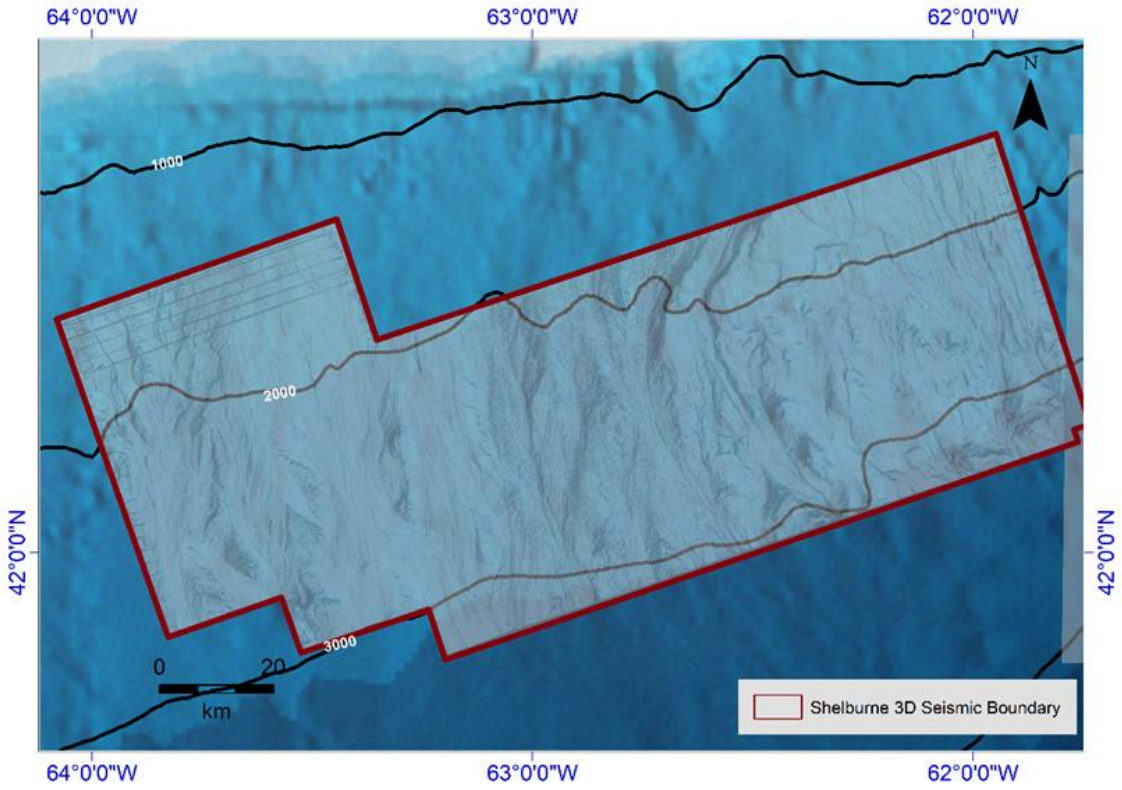

Figure 3.7. High-resolution bathymetric map of the Shelburne 3D survey.

The attribute maps were exported out of Petrel as Zmap plus Grid (zmap + Grid) files, which are a format readable by a GIS. The Zmap+ file type format stores gridded elevation data in a plain text line format for transport and storage.

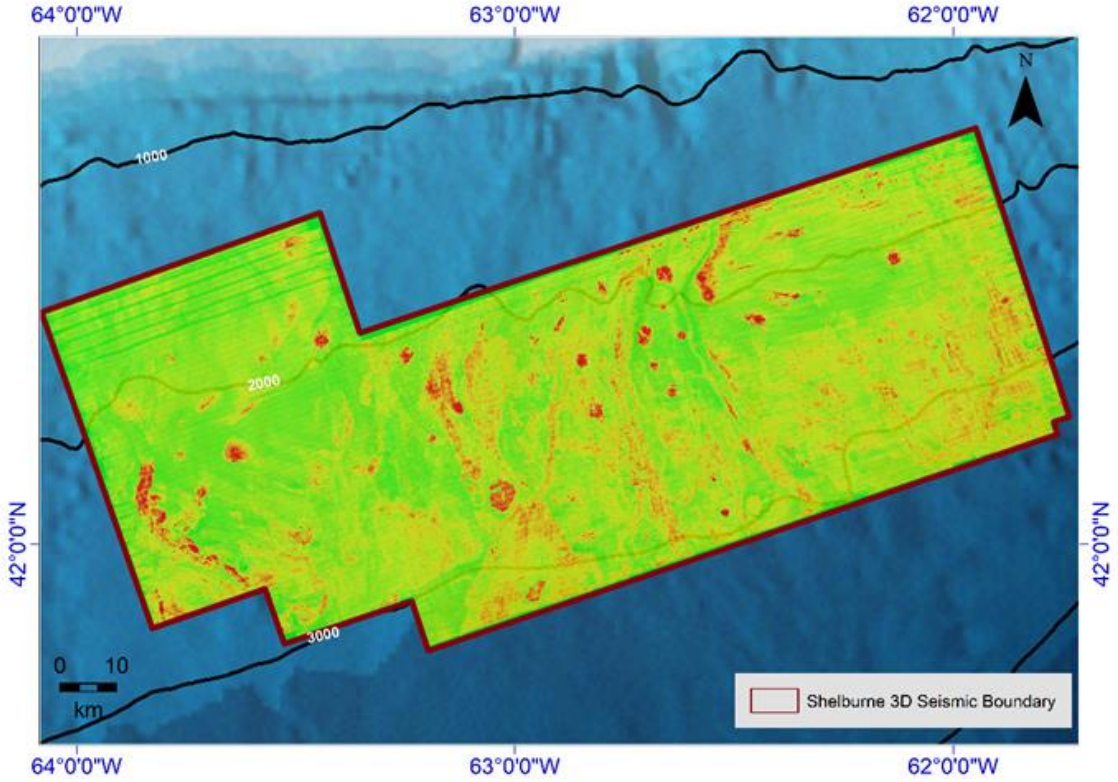

Figure 3.8. RMS amplitude map extracted from Shelburne 3D seismic volume, one of the attributes imported in from Petrel that highlights high amplitude anomalies on an interpreted horizon (Figure 3.17).

3.2.3 Seep Mapping Survey Layer

This layer displays recent exploration and de-risking data of the Nova Scotia offshore region including locations where piston and gravity core samples were collected in the slope region (Figure 3.9); results of geochemical analysis on the samples recognizing hydrocarbon presence (or absence); and the locations where the most recent AUV data has been collected by NSDEM and its collaborative partners.

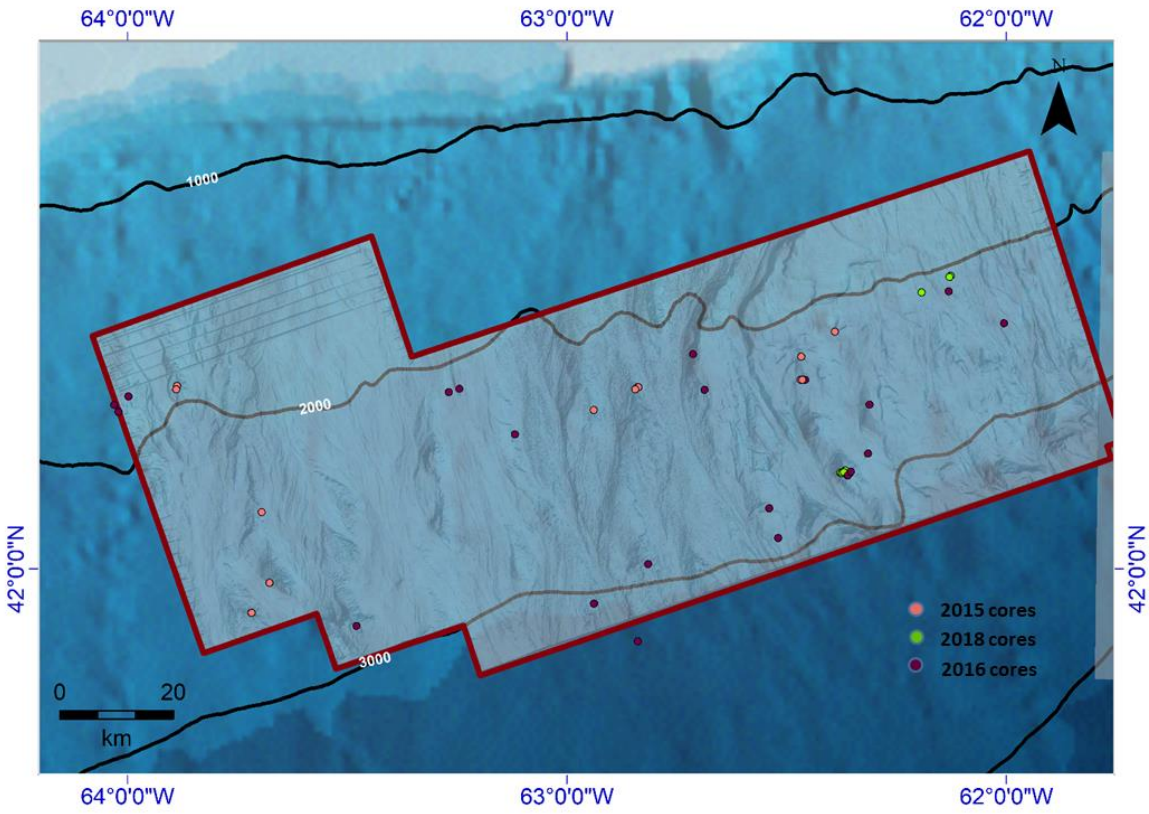

Figure 3.9. Piston and gravity core locations in the study area on a high-resolution, seafloor bathymetric surface.

Piston and gravity cores from the deepwater portion of the Scotian Basin were collected during 2015, 2016, 2017 and 2018 seep survey cruises aboard the CCGS Hudson (Campbell and MacDonald, 2016; Campbell, 2019; Campbell and Normandeau, 2019 respectively) and the RV Coriolis II (2017) (Fowler and Webb 2017, 2019). In the petroleum geochemical surveys layer, the samples with positive hydrocarbon signatures are displayed as shows. A 'show' represents any indications of subsurface petroleum fluid. Oil shows indicate signatures for light oil and condensates. Gas shows indicate signatures for gas of biogenic, thermogenic, or indeterminate origins. Sampled sites without geochemical signatures implying no hydrocarbon presence are displayed in the

hydrocarbon negative layer (geochemical data obtained from Fowler and Webb, 2015, 2017, 2019).

3.2.4 Basin Exploration and Prospectivity Layer

3.2.4.1 Offshore Wells and Discoveries Sub-Layer

To date, 210 offshore wells have been drilled in the Scotian Basin (CNSOPB, 2018). The Canada Nova Scotia Offshore Petroleum Board (CNSOPB) provides access to the directory of wells on its data management centre (DMC) website (see Appendix IV). The data was obtained in a tabular format was formatted in Microsoft Excel and imported into ArcCatalog once coordinate properties were defined. The data was then displayed in ArcMap. The associated data table can be viewed in the layer's attribute table. Well types were classified using symbology based on metadata in the attribute (Figure 3.10). Most of the wells are located around the Sable Basin, in the shelf portion of the basin. Most recently, two wells (Cheshire L-97 and Monterey Jack E-43) (Figure 2.5, 2.6) have been spudded in the deeper portion of the slope to test hydrocarbon prospects, but failed to find commercial quantities (Shell, 2017, 2018; OERA, 2019).

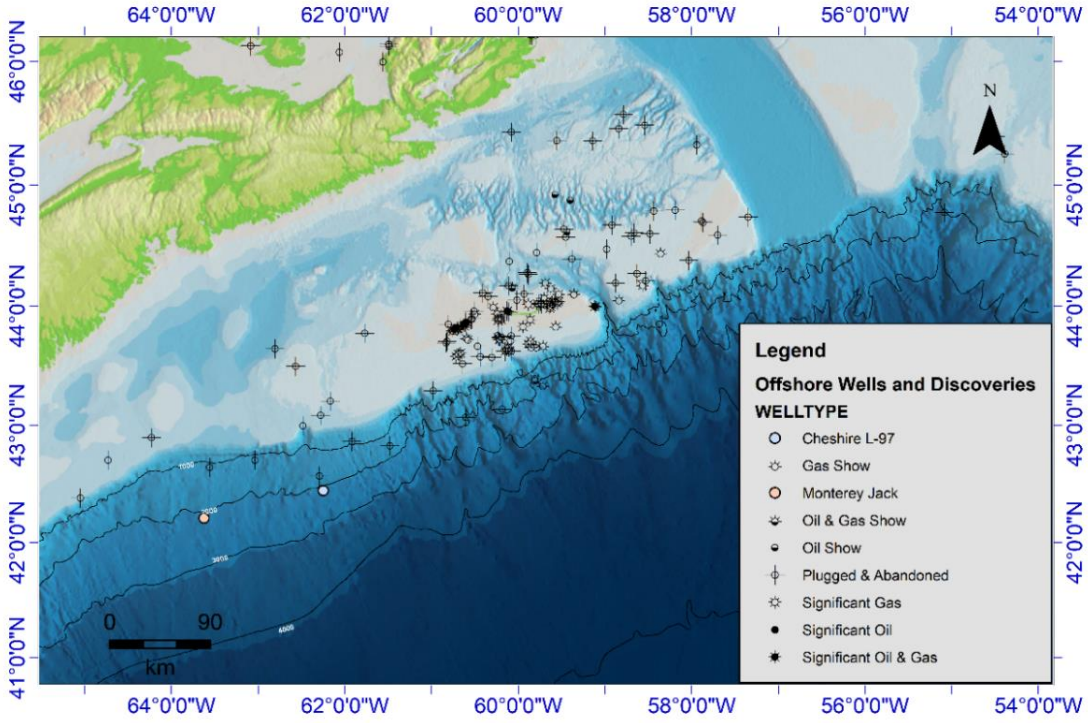

Figure 3.10. Wells in offshore Nova Scotia. Monterey Jack and Cheshire wells (indicated with a blue and pink circle, respectively) are among two of four most recent wells drilled in the deepwater portion of the basin.

3.2.4.2 Common Risk Segment (CRS) Maps of the Scotian Basin Sub-Layer

A common risk segment (CRS) map is an objective map-based understanding of the distribution of petroleum in a basin that easily highlights sweet spots and critical risk zones where focus can be applied for further data collection and analysis (OETR, 2011; Bump et al., 2021).

In the PFA of the Scotian Basin, CRS maps were generated based on risk determination in reservoir and seal, source rock presence, and petroleum evaluation along the Scotian Margin (see Chapter 8.2 of the Play Fairway Analysis, 2011). These CRS maps were imported as Microstation V8 design files (.dgn) from the PFA atlas. In this dataset obtained from the Nova Scotian fairway analysis atlas, the model contained different features used in the construction of the CRS maps including point, polygons, polyline and multipatch features. As is conventional for composite CRS maps, this study

adheres to the three-color scheme of red (high risk), yellow (moderate risk), and green (low risk) for visualization in ArcMap (e.g., Figure 3.11).

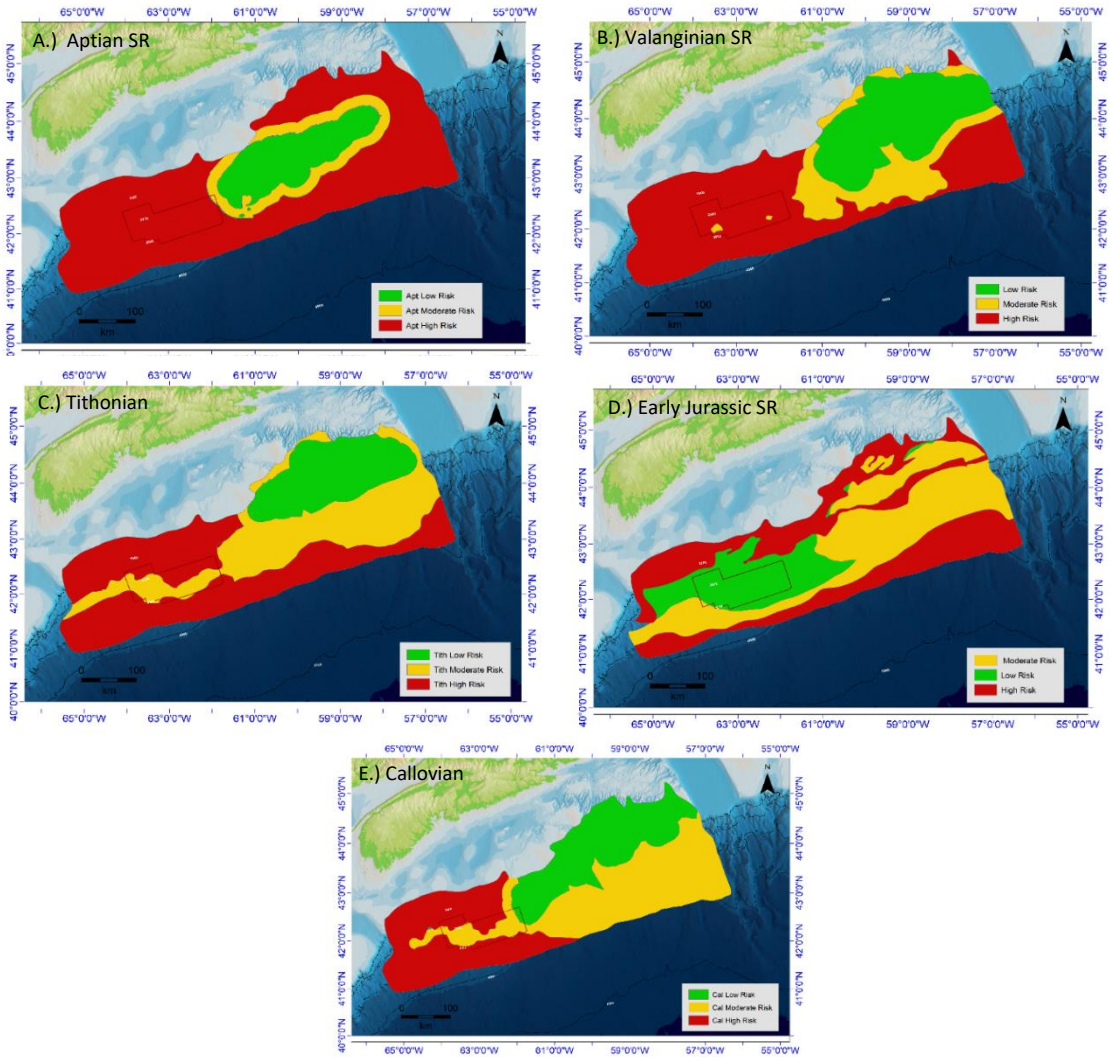

Figure 3.11. CRS maps at different stratigraphic sequences. The source rock (SR) CRS maps are a composite of presence, maturity, and migration. In-depth information can be found in Chapter 8 of PFA 2011. Five potential source rocks were identified from geochemical analyses and petroleum system modeling. The study area appears to have a low risk for hosting an Early Jurassic source rock (D). This source rock is yet to be found or confirmed.

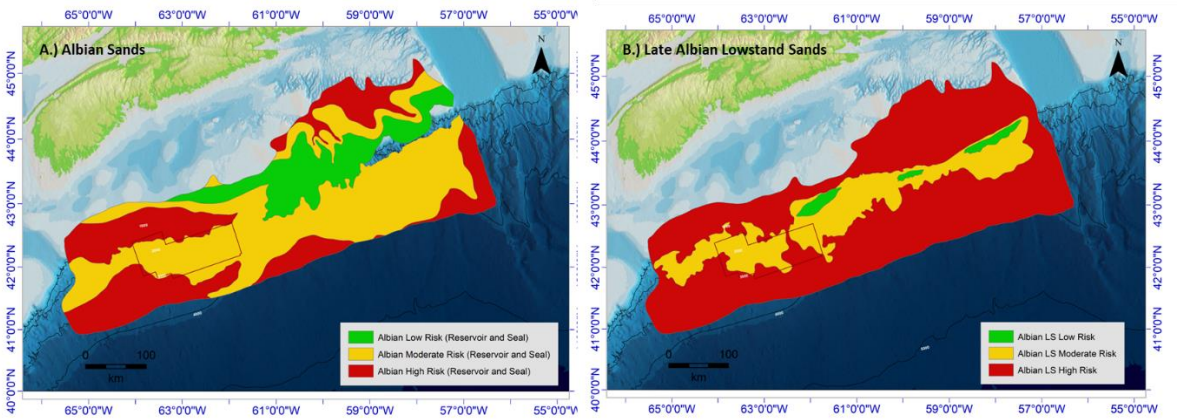

Figure 3.12. Reservoir and seal composite maps for Albian sands and Albian lowstand sands. The study area is predicted to have a moderate risk in hosting Albian sands with effective reservoirs and seal potential based on PFA 2011 evaluation.

The reservoir and seal maps (e.g., Figure 3.12) are a composite of three different maps: *i*) a reservoir presence map controlled by well data, seismic data, and gross depositional environment (GDE) maps, *ii*) a reservoir effectiveness map controlled by well data and porosity prediction, and *iii*) a seal presence and effectiveness map controlled by well data and GDE maps. More maps predicting potential plays are found in the CRS maps layer and details on parameters can be found in Chapter 8 of the PFA 2011 (OETR, 2011).

To extract what was useful for this study, a source rock and reservoir geodatabase was created in ArcCatalog. From this file geodatabase, the georeferenced DGN files were imported as a feature class and the appropriate elements for thematic precision (play elements chance of success/critical risks) were digitized and the projection was converted to match that of the data frame. The digitized polygons are saved as new feature layers in the Common Risk Segment Maps layer.

3.3 Seismic Methodology

Seismic attributes are mostly used in seismic exploration and reservoir studies to image subsurface geologic structures (Pramanik et al., 2002; Pramanik et al., 2003).

Attributes work well for extracting subtle and easy to overlook features on high quality seismic data (Marfut and Alves, 2015). Seismic attribute analysis uses procedures to extract corresponding subsurface geologic information from seismic sections (McQuillin, 1984; Avseth, 2005; Alistair, 2011). The attributes are quantities of geometric, kinematic, dynamic, or statistical features from the seismic data (Taner et al., 1995; Liner, 2004; Chopra and Marfut, 2005a, b; Oyeyemi et al., 2015). Two seismic attributes, RMS amplitude and coherence (or variance), were applied to the Shelburne 3D seismic data volume in this study to identify and map near-surface expressions associated with hydrocarbon migration in the deepwater region of the Scotian Slope.

3.3.1 Study Area (Shelburne 3D)

The Shelburne 3D seismic volume (CNSOPB program number NS24-S6-3E) was acquired by Shell in 2013 (RPS, 2013; OERA, 2019). It is a large, wide azimuth survey that covers approximately 10,400 km^2 (is approximately 50 – 100 × 200 km) and covers the deep offshore domain of the Southwestern Scotian Margin in water depths ranging from 1435 to 3460 m (Figure 3.13). It spans the dip GXT 1400 and strike GXT 5300 reference 2D survey lines (OERA, 2019). The survey is mainly located above the Shelburne Subbasin, east of the Barrington 3D seismic survey and overlaps the Torbrook 3D seismic survey on the western side (Figure 3.13). Two wells have been drilled in this survey block: the Cheshire well, located on reference line 1400, and the Monterey Jack well, which is very close to reference line 5300 (OERA, 2019). The volume was already depth converted (by the operators) and this work assumes that the velocity model is correct.

In this study, the workflow guiding the interpretation of the seismic volume took three forms: (1) amplitude anomaly identification; (2) horizon picking and interpretation;

and (3) extraction of surface-based attributes and transfer to ArcMap. Horizons were mapped and gridded to produce continuous surfaces with a grid cell size of 25 m.

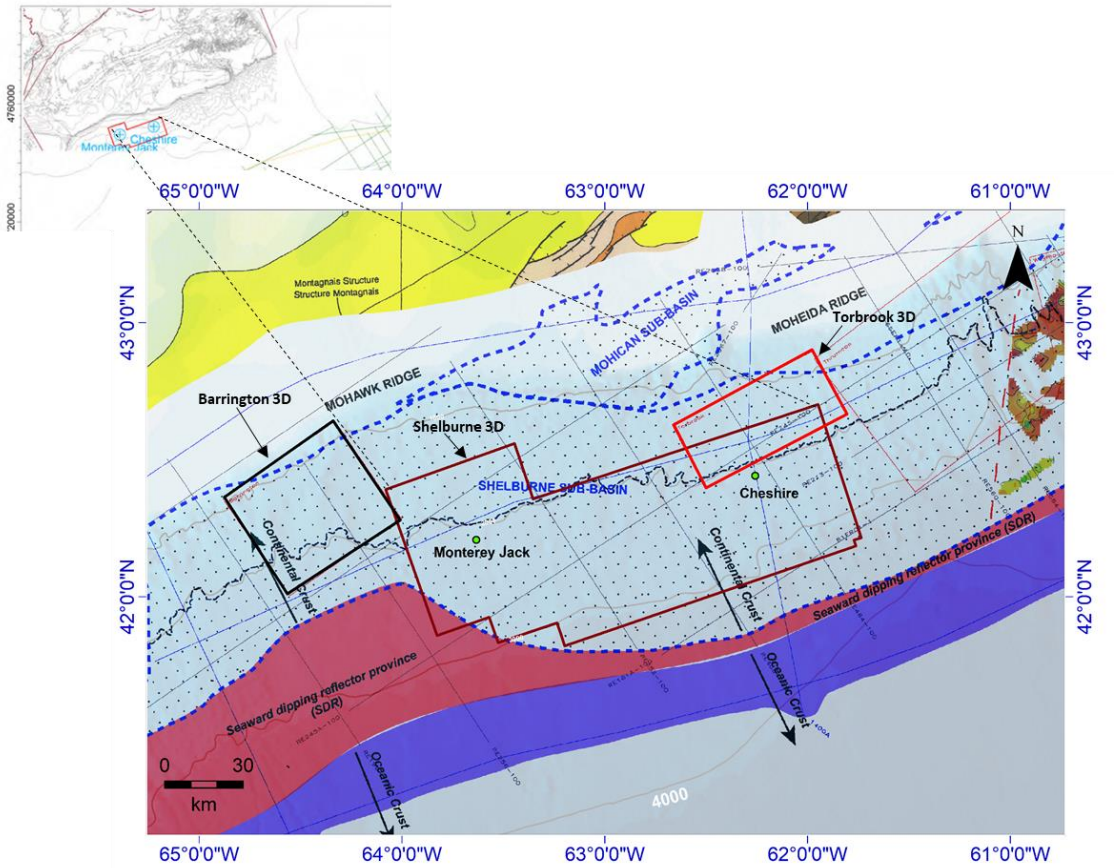

Figure 3.13. Shelburne 3D wide azimuth seismic volume boundary located east of Barrington 3D and overlapping Torbrook 3D survey. Adapted and modified from PFA (OETR, 2011).

3.3.2 Seismic Analytical Techniques

3.3.2.1 Amplitude Anomaly Identification

When seismic waves encounter an impedance contrast of rocks at interfaces in the subsurface, seismic reflection amplitudes are produced (Nanda, 2021). The inherent characteristics of rocks that determine their impedance include its matrix, density, and pore fluid, each of which influences elasticity and mainly, the compressibility of the rock layer (bulk modulus) (Nanda, 2021). Gas (or light oil) in porous sediment significantly lowers the bulk modulus and can create high amplitude seismic anomalies (Figure 3.14). This represents one type of a direct hydrocarbon indicator (DHI) (Roden et al., 2012; Nanda, 2021). Such DHIs were identified in the 3D vertical seismic cross sections of the study area (e.g., Figure 3.14). It is acknowledged that not all amplitude anomalies are DHIs and not all geologic settings equally exhibit DHIs.

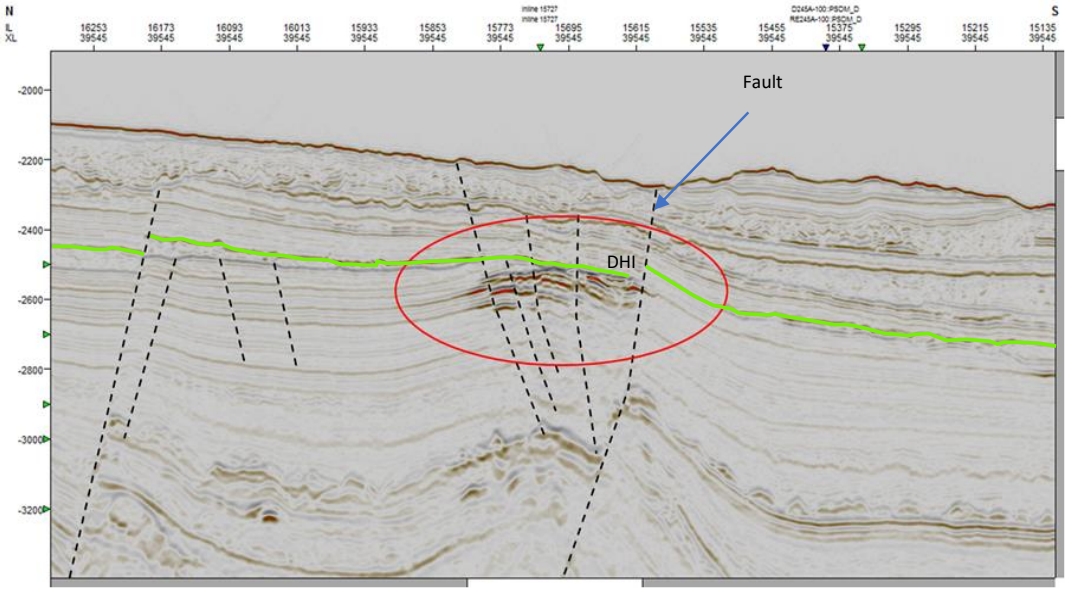

Figure 3.14. Seismic section with amplitude anomaly identified as a DHI circled in red. Faults are highlighted with a black dotted line, and the green line is the reference horizon used to create the RMS amplitude map discussed later.

In the analyzed 3D seismic volume of this study, an intensive survey of the 3D data block led to the discovery that DHIs appear to be largely confined to depths of 400

mbsf over regions of the slope with water depths ranging from 2300 to 3800 m (in observation and personal communications with Natasha Morrison at the NSDEM). The mapped DHI horizon (Figure 2.4, 3.14) was therefore not a known reference horizon, but was picked as one that topped most of the anticipated DHIs in the Shelburne 3D volume.

3.3.2.2 Horizon Window Picking

When a feature is interpreted on a seismic section by selecting and tracking a horizon or other events, it is known as a pick. Seismic horizon interpretation involves picking and tracking laterally consistent seismic reflectors with the aim of resolving basin structural patterns for the detection and delineation of extent of potential hydrocarbon accumulations.

In choosing a horizon to pick, a scan of the volume was done to identify amplitude anomalies (amplitude anomaly identification) and the depths at which they occurred. Once the depths of occurrence were known, an arbitrary continuous and strong reflection (no specific geologic tie) that captured the top of the anomalies and showed good lateral continuity was chosen for correlation as a horizon (e.g., Figure 2.4, 3.14). To pick this horizon, a new interpretation window was opened that displays the seismic trace to be interpreted. From the seismic interpretation window, the seeded 2D autotracking tool was used to manually digitize across the reflector of interest in the seismic trace. The horizon was correlated along a peak. Seeded 2D autotracking uses a single digitized point to track the horizon and continues until the tracked event no longer meets the defined tracking parameters due to a fault, amplitude decay, or polarity reversal. The procedure is repeated for the segment across a disturbance.

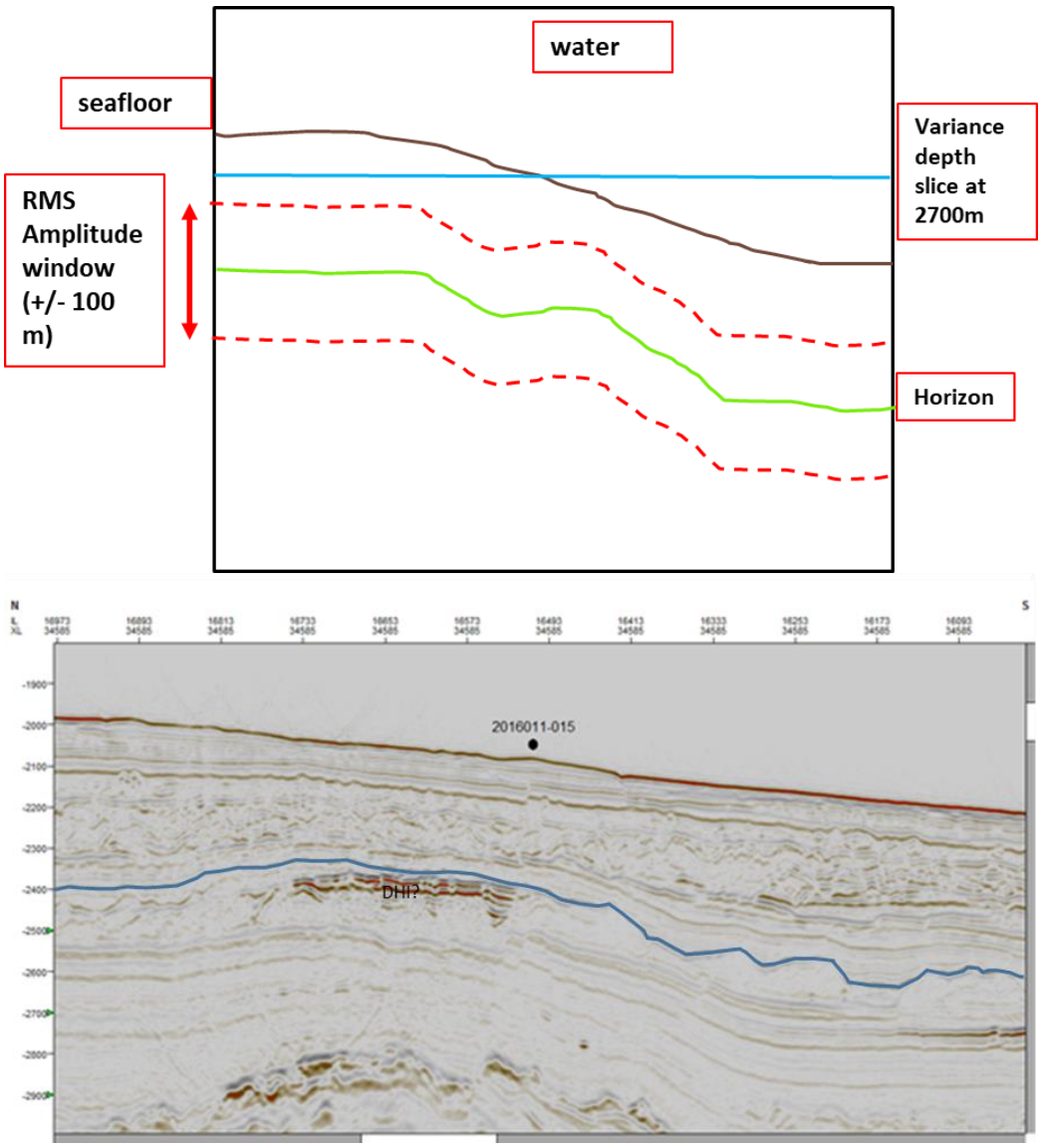

Figure 3.15. Cartoon of a seismic section illustrating the seismic methodology process where: i) a DHI horizon is picked that tops most of the DHIs in the Shelburne 3D survey and is used to create a surface (Figure 3.17) that is then used to extract an amplitude attribute map with a window of 100 m above and below the horizon (Figure 3.18); ii) Variance depth slices extracted from seismic volume at different depths.

Once the picking is complete across the volume, the interpreted horizon (Figures 2.4, 3.17) is displayed in the interpretation window (can be 2D or 3D) and obvious mis-ties can be noted and corrected. Once the horizon interpretation is complete, it is converted into a surface where various attributes can be generated and draped on the surface.

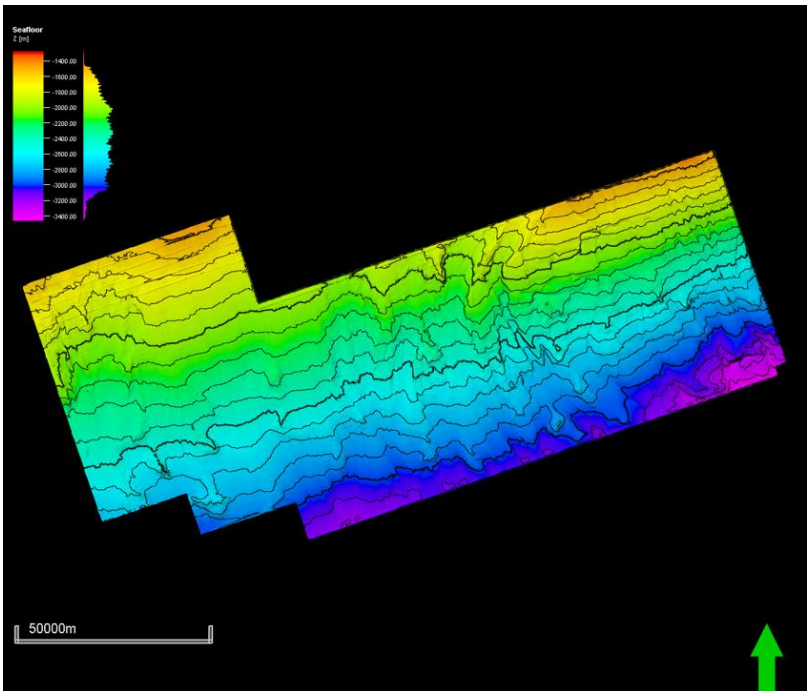

Figure 3.16. Structural map of the Shelburne 3D seafloor surface with 5× vertical exaggeration.

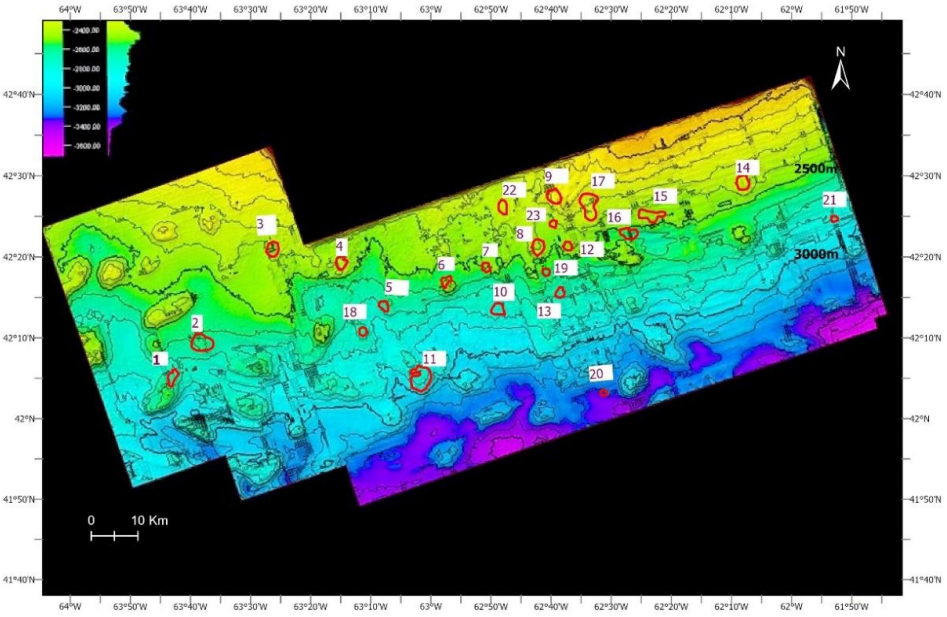

Figure 3.17. Structural map (V.E = 5× with 100 m step isobaths) of the picked reference horizon, which is approximately 300–400 mbsf and captured a strong reflector topping amplitude anomaly and whose shape varied across the study area and was used to create selected attributes. The positions of identified DHIs are circled and labeled with numbers.

3.3.2.3 Extraction of Surface Based Attributes

Seismic attributes are a quantitative measurement of a seismic characteristic performed through a suite of deterministic calculations on a computer (Chopra and Marfut, 2005b). A seismic amplitude is the maximum (positive or negative) amplitude value at each sample along a picked horizon. In many cases, an amplitude of reflection strongly correlates to porosity or saturation (oil/water or gas) of an underlying formation as these properties have a strong effect on both velocity and density.

As an intrinsic property of a seismic wave signal derived from seismic data, good seismic attributes represent key aspects of an underlying geology (Brown, 1996). Attributes are not independent of each other but are different ways of presenting and studying a limited amount of basic seismic information, which includes time, amplitude, frequency, and attenuation (Brown, 1996).

Seismic attributes are generally classified into either physical or geometric attributes. Physical attributes are defined as those directly related to wave propagation, lithology, and other parameters. Physical attributes can be further classified as pre-stack and post-stack attributes. Post-stack attributes are derived from stacked data and are a result of properties derived from the complex seismic trace signal (Taner et al., 1979). The complex trace is defined as presented in Equation (1):

$$CT(t) = T(t) + iH(t) \quad (1)$$

Where *CT(t)* is the complex trace, *T(t)* is the real seismic trace, *H(t)* is Hilbert's transform (imaginary trace) of *T(t)*. In a multi-dimensional space, the real trace is in vertical display with the imaginary trace perpendicular to it. The complex signal, therefore, is a vector with one axis pointing in the real direction and the other in the Hilbert transform direction. The complex trace makes it possible to define instantaneous amplitude

(envelope), phase, and frequency (Taner et al., 1979; Taner, 2001). The envelope (*E(t)*) is computed by taking the square root of the sum of the squares of the real and imaginary components as presented in equation (2).

$$E(t) = \sqrt{\{T^2(t) + H^2(t)\}} \quad (2)$$

where *E(t)* is the instantaneous amplitude (envelope), T(t) is the square of the real seismic trace, and $H^2(t)$ is the square of Hilbert's transform (imaginary trace) of T(t).

The phase (ϕ(t)) is computed by taking the double argument (ATAN2) inverse tangent of the imaginary and real components as presented in equation (3). The frequency is computed as the rate of change of the phase.

$$\emptyset(t) = tan^{-1}\left[\frac{H(t)}{T(t)}\right] \quad (3)$$

Where ϕ(t) is the phase, *H(t)* is Hilbert's transform, and *T(t)* is the real seismic trace.

The instantaneous envelope (reflection strength) is sensitive to changes in acoustic impedance and therefore to lithology, porosity, hydrocarbons, and thin-bed tuning. Instantaneous phase is useful in detecting unconformities, faults, and lateral changes in stratigraphy. Instantaneous frequency is useful in identifying abnormal attenuation and thin-bed tuning (Taner, 1979; Chopra and Marfut, 2005b, Koson et al., 2014).

Root Mean Square (RMS) Amplitude

The root mean square amplitude (Figure 3.18) was extracted from a horizon (Figure 3.17) interpreted from the seismic data. RMS amplitude provides a scaled estimate of a seismic trace envelope offering a smoother version of reflection strength (Koson et al., 2014). It is the square root of the arithmetic mean of the squares of the trace values in a

specified window (Koson et al., 2014; Nanda, 2016). Petrel uses an inbuilt formula as presented in Equation (4) to compute the RMS attribute:

$$X_{rms} = \sqrt{\frac{1}{N}\sum_{n-1}^{N} w_n x_n^2} \quad (4)$$

Where X_{rms}= root mean square amplitude, w_n = window values, N = number of samples in the window, x = trace value. In this study, the RMS amplitude map is extracted from an interpreted horizon (Figures 2.4, 3.17) created in the study area that is approximately 300–400 m below the seafloor and delineated the upper limit of shallow DHIs with water depths starting at 2300–3200 m across the study area.

Once the attribute was computed, it was processed to output a colour-coded amplitude map which was imported to ArcMap.

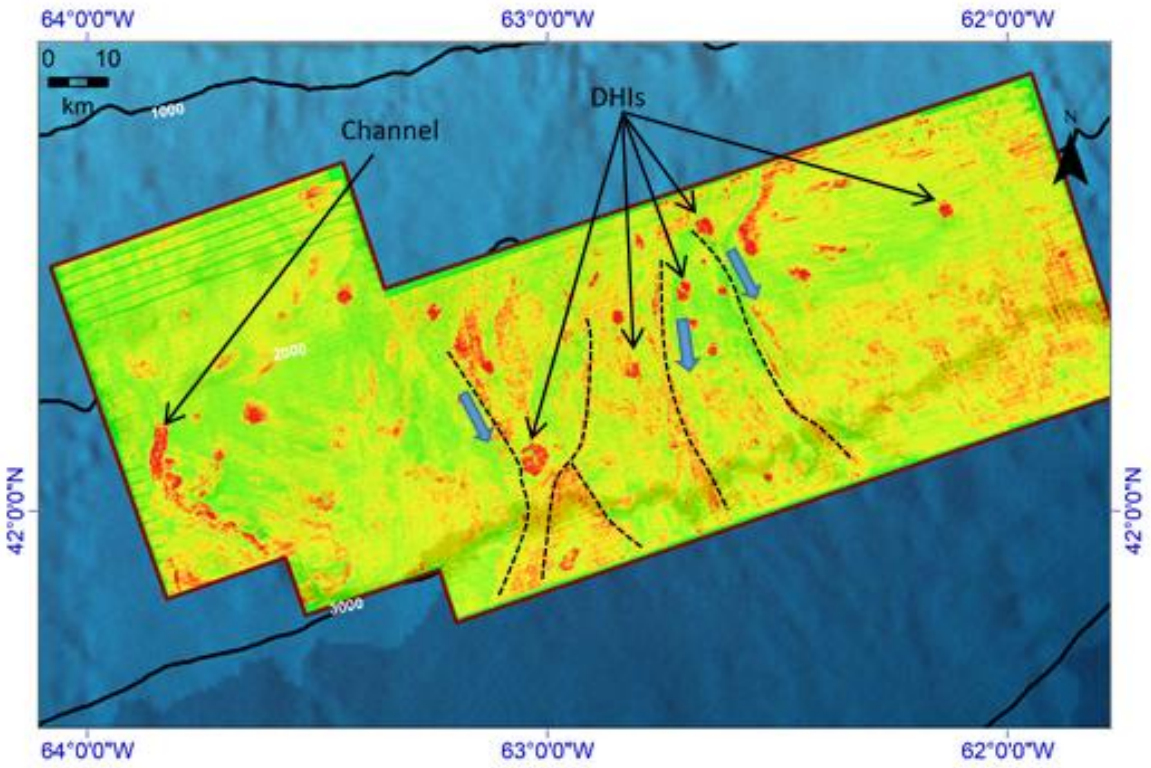

Figure 3.18. An RMS amplitude map with effects of down-slope gravity-flow-dominated processes indicated in dotted lines (generating mass transport deposits, canyons, and migrating submarine channels transporting sediment) further discussed in Chapter 4.

Variance (Coherence) Attribute

Variance is a coherence-based measure of how well a seismic trace fits an adjacent reference waveform trace (Chopra and Marfut, 2005b). In Petrel, the variance attribute applies an algorithm to compute the local variance of the seismic data from a user-defined surface. The variance attribute is implemented to identify structural discontinuities (Figure 3.19) e.g., faults, fluvial channels, chimneys, and fractured zones by emphasizing lateral changes of acoustic impedance by calculating trace-to-trace variability in a specified sample interval (Pigott et al., 2013; Koson et al., 2014). Geologically, highly coherent seismic waveforms indicate laterally continuous lithologies. Abrupt changes in waveform can indicate faults, fractures, and other discontinuities in the sediments.

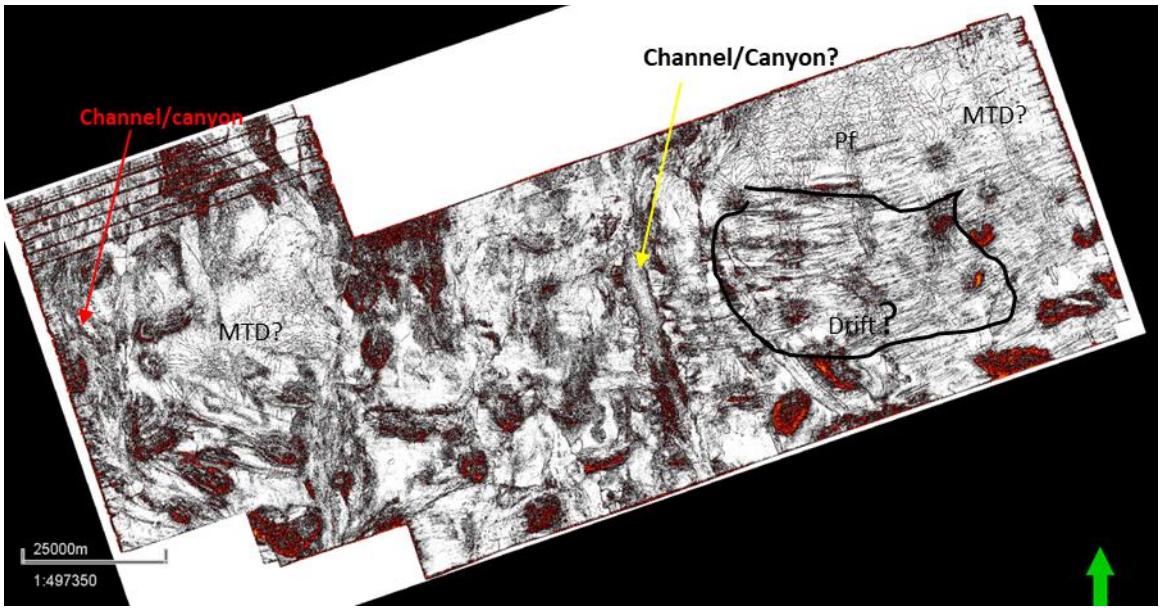

Figure 3.19. Dip-corrected (to seafloor) coherence attribute depth slice at 2700 m. MTD = Mass transport deposit; pf = polygonal faulting.

The coherence attribute depth slices were extracted from the 3D seismic volume. The depths chosen for the coherence maps include the seafloor surface, 2500 m, 2700 m, 3000 m and 3500 m from the Shelburne 3D seismic volume. These depths were selected because they captured above and below the horizon window used in creating the RMS amplitude map when identifying DHIs. The 3500 m slice was selected to extrapolate features that manifested below the described horizon, and the 2500 m slice was included to capture sea floor attributes. The attributes are imported to GIS in gray scale (see images in Chapter 4 and original Petrel images in Appendix III).

Chapter 4 : Integration and Results

In this study, the shallow level Shelburne 3D seismic data is interpreted to identify seepage events and their associated subsurface structural features in the Scotian Slope offshore Nova Scotia. Previously acquired geochemical data is then used to establish and/or further validate correlations with geophysical data within a GIS platform. Collectively, these separate platforms are applied as a means of visualizing the integrated datasets.

4.1 DHIs in Shelburne 3D

Various high amplitude anomalies were identified within an RMS amplitude map created from an interpreted horizon in the Shelburne 3D study area. Many of the anomalies were further interpreted as being DHIs (Figure 4.1A) based on their depth (~300–400 mbsf), indications of migratory pathways to the anomaly, and with guidance from a geophysicist familiar with the data. DHIs in Shelburne 3D were identified on seismic cross sections interpreted for the study area (Appendix II). For the integration component, the focus remained on DHIs with piston and gravity cores sampled previously collected on or near the anomaly.

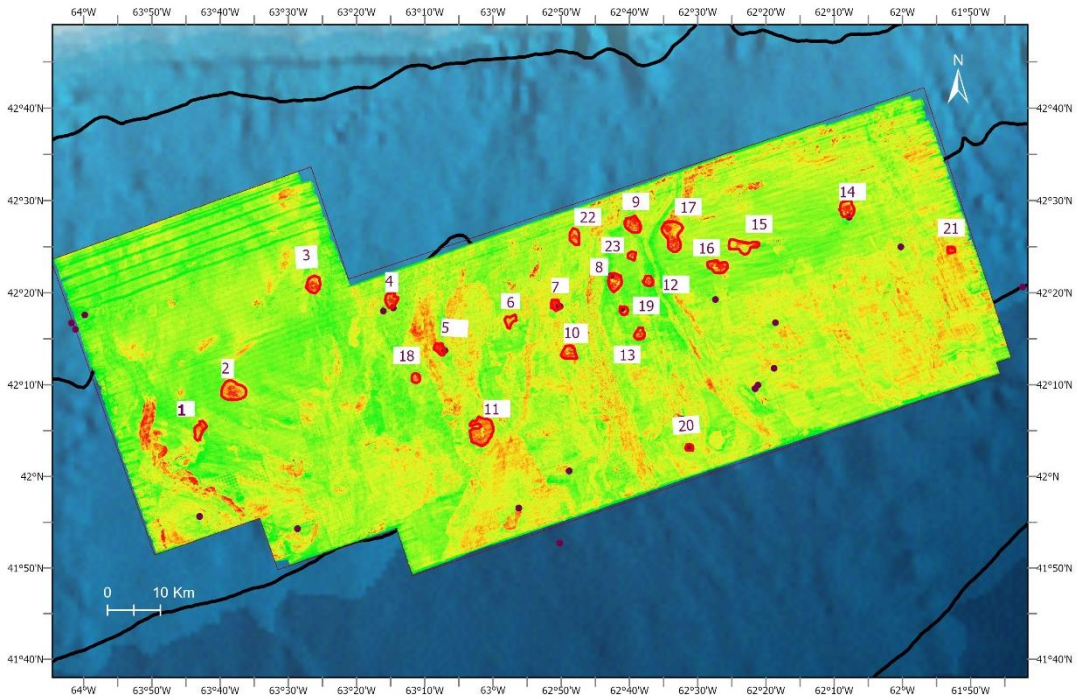

Figure 4.1A. RMS amplitude map of Shelburne 3D. Resolved DHIs are outlined with red polygons and numbered to enable their comparative description.

4.2 Surface and Near-Surface Expressions of Seepage Correlative with Surficial Sediment Geochemical Analysis in the Shelburne 3D Seismic Volume

In this study, an attempt was made to validate the presence of prospective petroleum seeps in the Scotian Basin based on identifying near-surface expressions of hydrocarbon migration from the subsurface. The piston and gravity coring program of the Scotian Slope from 2015, 2016 and 2018 survey expeditions (Campbell and MacDonald, 2016; Campbell, 2019; Campbell and Normandeau, 2019) targeted several of the DHIs found in the Shelburne data block. The recovered sediment cores were sub-sampled and geochemically analyzed for the presence of hydrocarbons. The detection of hydrocarbon provides evidence of cold seeps overlying the DHIs in the region (Fowler and Webb, 2015, 2017, 2019). Using the results from the samples in Shelburne 3D (Figure 4.1), we looked at the surface and near-surface seismic data in the sampled areas and checked for

correlations between the geochemical, seismic, and geologic features. Based on geological and basin modelling data (OETR, 2011; OERA, 2019), it is predicted that the subbasin has at least one working petroleum system. We therefore hoped to observe additional evidence for this based our survey of potential hydrocarbon migration in the seismic data.

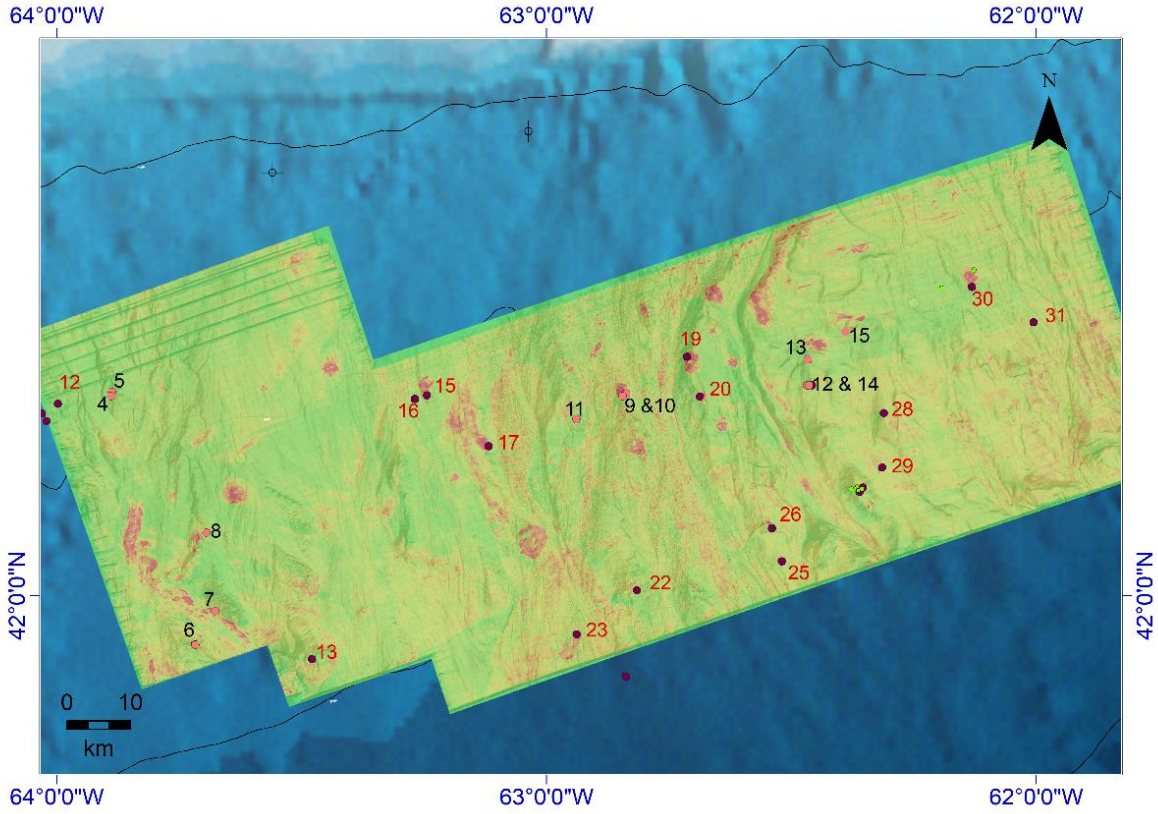

Figure 4.1B. Piston and gravity cores sampled in the Shelburne 3D displayed on an RMS amplitude surface interlayered with a high-resolution seafloor bathymetry map. Cores collected in 2015 are labeled black, 2016 samples in red and 2018 samples are green dots.

Seismic attributes in the Shelburne 3D data block indicate the presence of shallow-level, high amplitude anomalies (some of which are interpreted as DHIs), paleo-pockmarks, radial and polygonal faulting. These features can be indicators of a working petroleum system in differing capacities. Fluid based DHIs imply the presence of leaking hydrocarbons from a reservoir or source rock deeper in the subsurface. Pockmarks are

seabed depressions believed to be created by the release of over-pressured pore water and/or gas emission from the subsurface (Hovland et al., 2010; Cathles et al., 2010; Callow et al., 2021). Pockmarks are a visible example of seabed fluid expulsion features that can overlie deeper migration conduits such as faults (Harrington, 1985; Roberts et al., 1990; Judd and Hovland, 2007; Johansen et al., 2020). Fluid advective transport is driven by buoyant forces along the path of least resistance following the same pathway as the water (Abrams, 2020). Faults can act as both leaking and sealing features. If leaking, they are conduits for migration, and if sealing, they trap and seal hydrocarbons. The piston and gravity cores in Figure 4.1B will be discussed in the following section. Figure 4.1B gives a guide to the locations of the samples at a regional scale of the Shelburne 3D survey considering their proximity to high amplitude anomalies.

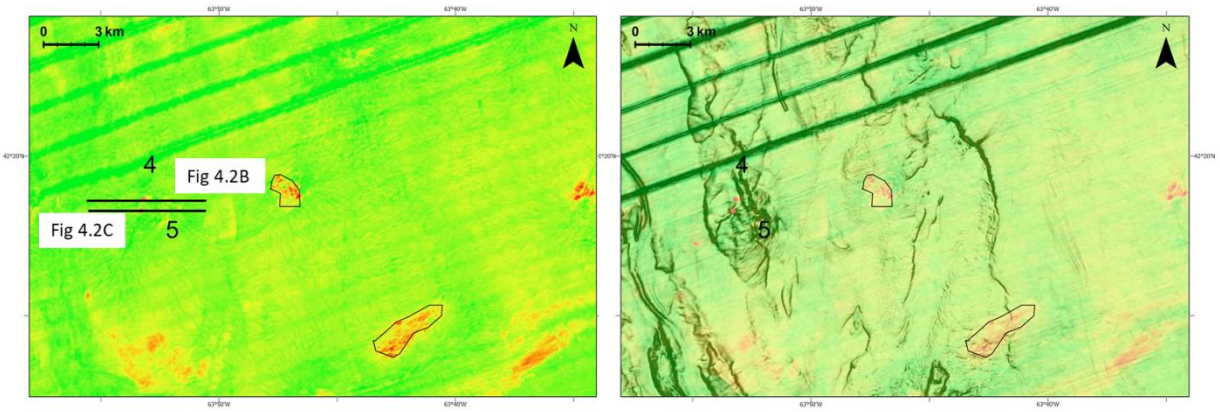

Figure 4.2A. Snapshot of Core 4 and 5 on RMS amplitude map (left) and the RMS amplitude overlain on a variance map of the seafloor surface (right) from the 2015 expedition. The black polygons indicate high amplitude anomalies not captured on the seismic sections for the two cores.

Cores 4 and 5 collected in 2015 are about 1 km from each other along the East Mohawk Canyon System (see: Chapter 5: T13 – Mid to Late Miocene Unconformity; Deptuck and Kendell, 2020). These cores targeted the surface sediments overlying the crest of a diapir (Figure 4.2B to 4.2C). The area around the diapir appears to be a highly faulted interval (HFI) with networks of diapir-related or polygonal faults (pf) (Figure 4.2E at 2500 and 2700 m). For this area, no DHIs were found on the seismic sections or the RMS amplitude maps; however, there are indications of low-amplitude zones (washouts possibly related to gas presence).

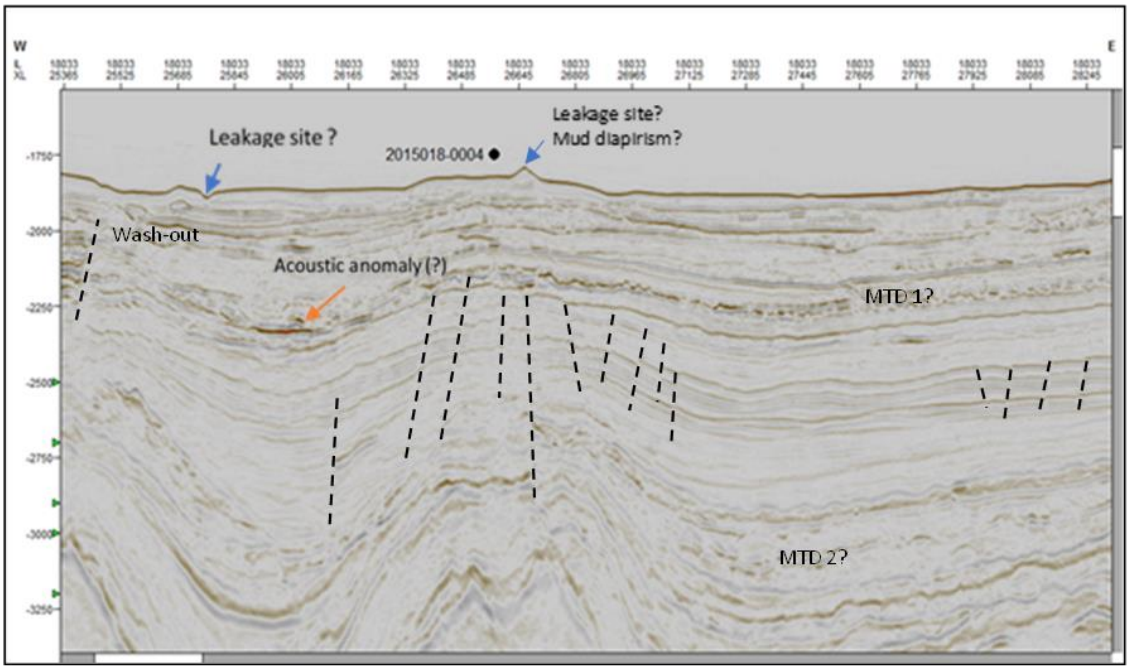

Figure 4.2B. Seismic cross-section showing seafloor relief (potentially related to active seepage), a diapir with a thick roof of sediment with an unconformity in the upper strata near surface (likely erosional and due to a mass transport deposit (MTD 1)). The sediment on the crest of the diapir has polygonal faults (pf) that are seen on the coherence attribute at 2500 m (Figure 4.2E). It is likely that the washout zone is gas rich sediment. Location of Core 4 from the 2015 expedition is indicated with a black diamond. No evidence of hydrocarbon seepage was obtained from the geochemical analyses performed on the related site's gravity core (Fowler and Webb, 2015). The acoustic anomaly noted here could be a tuning effect or a change in lithology on an erosive surface if not related to hydrocarbons.

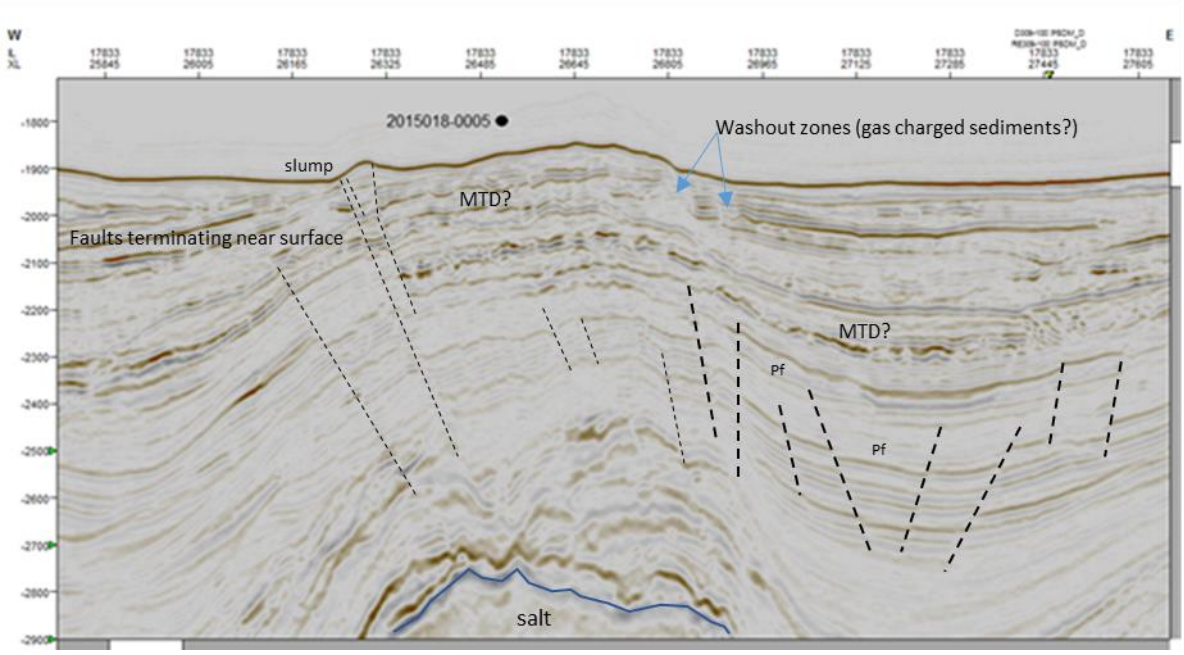

Figure 4.2C. Inline cross-section of the survey site where Core 5 was collected. Faults to surface emanate from a diapir-produced relief. The crest and flanks of the diapir appears to be thickly draped with unconformity-bounded sedimentary packages on either side of the salt. The overburden on the right side looks coherent and interrupted by faults between 2300–2700 m, while the left side is more chaotic. Evidence of gas washout zones are present above fault zones that flank the diapir. Geochemical analysis of this site also produced evidence of some gas seepage supporting the idea of gas presence in the sediment (Fowler and Webb, 2015).

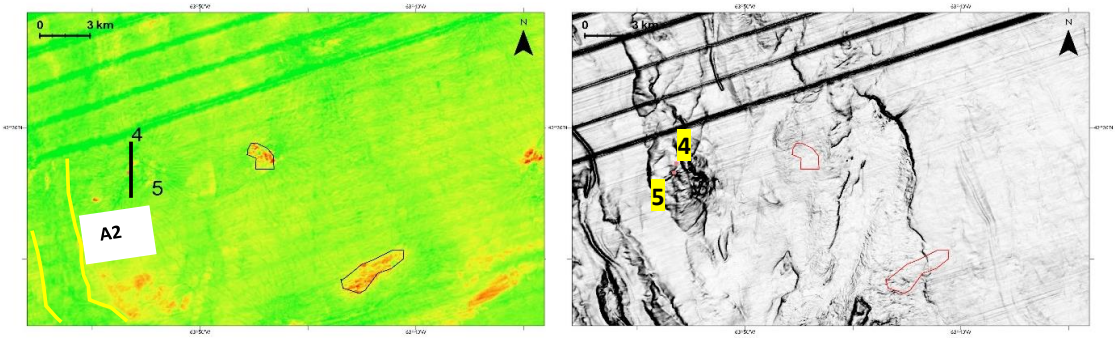

Figure 4.2D. Snapshot of Site 4 and 5 on RMS map (left) and the seafloor surface (right) in the same location. An inline cross section that cuts through locations for Core 4 and 5 is in Appendix II (A2).

The observed seafloor map captures morphological features (Figure 4.2D) also visible in the vertical seismic cross section (Figures 4.2B and C). Cores 4 and 5 were collected on the edge of a slump (Figure 4.2B, 4.2C, and 4.2D). A canyon or a paleochannel is also observed (Figure 4.2D yellow lines) potentially marking a sediment pathway down the slope of the margin. While there is no acoustic anomaly at Site 5

(Figure 4.2C), the vertical seismic sections show a protruding feature with faults approximately 100–300 m from the sampling point terminating near the ocean floor. The acoustic anomaly seen in the seismic cross section at Site 4 (Figure 4.2B) is likely a gas pocket or a change in sediment lithology change draped over an erosive surface.

Site 5 showed evidence of hydrocarbons. Sample headspace gas analyses recorded elevated concentrations of C_1-C_4 hydrocarbons. However, the relatively low concentration of ethane and propane compared to methane alongside isotopically depleted methane ($\delta^{13}C$ -84.6‰) indicates the site hosts mostly biogenic gas. No hydrocarbons were detected at Site 4 (Fowler and Webb, 2015).

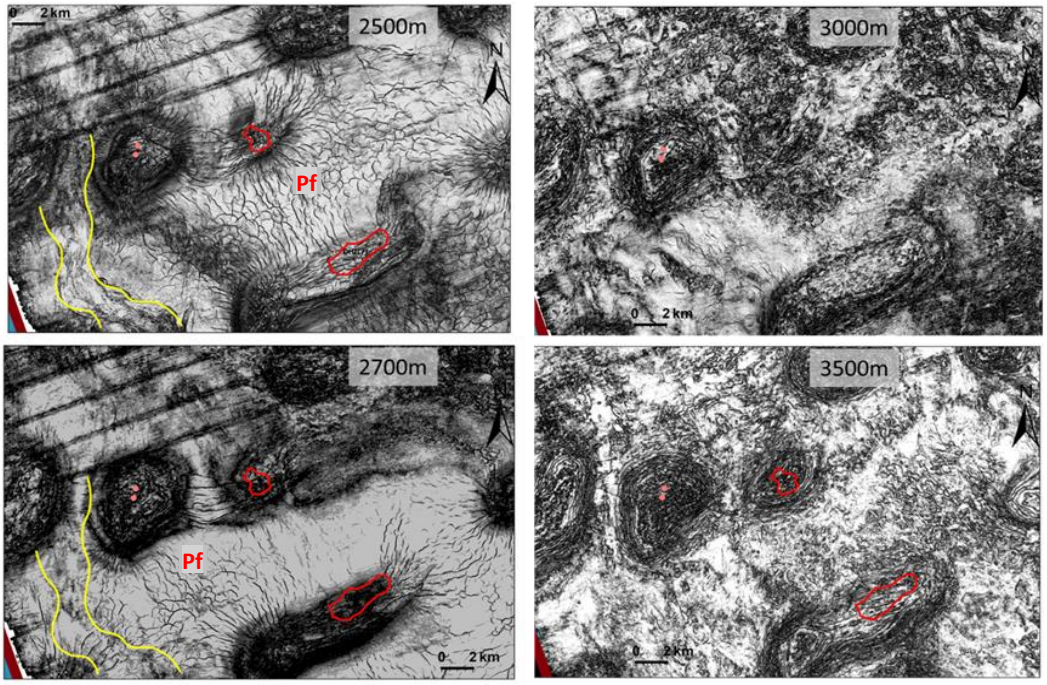

Figure 4.2E. Coherence attribute maps of different seismic depths for samples from Core 4 and 5. At 2500 m, the surface shows a high density of radial and interconnected polygonal faults (pf) that could act as conduits for migrating fluids. The samples are collected atop the crest of a thick-roofed diapir with faulting visible at a depth of 2500 m. By 3000 m and 3500 m salt diapirs are intersected below the overlying polygonal and radial fault structures.

The two sites show evidence for faults but there were no indications of hydrocarbon accumulation in the subsurface at this location when looking at the seismic section, although the nearby washout zones may imply gas charged sediment. If there is a source rock or reservoir in the subsurface in this location, the absence of a DHI in seismic data could imply a failure or absence of a seal.

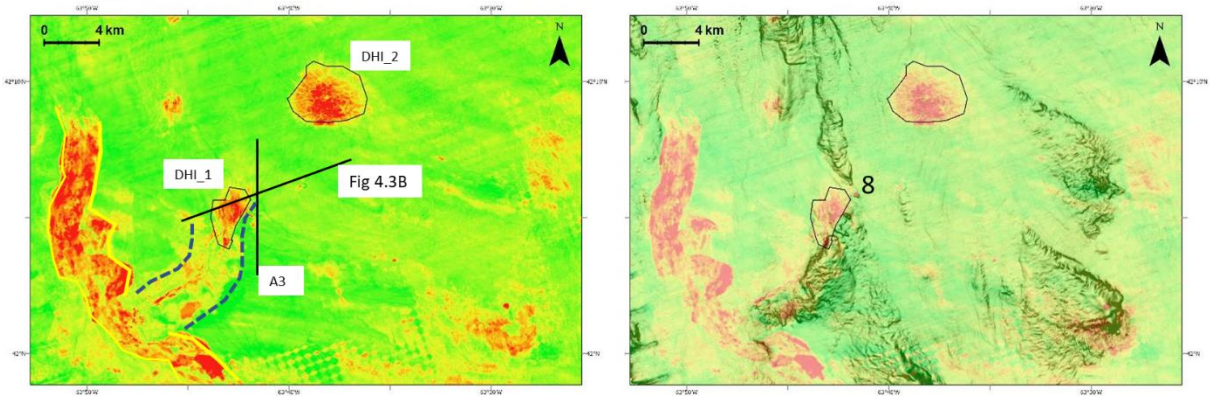

Figure 4.3A. An RMS amplitude snapshot of Core 8 (left) overlain on a variance snapshot of the seafloor surface (right).

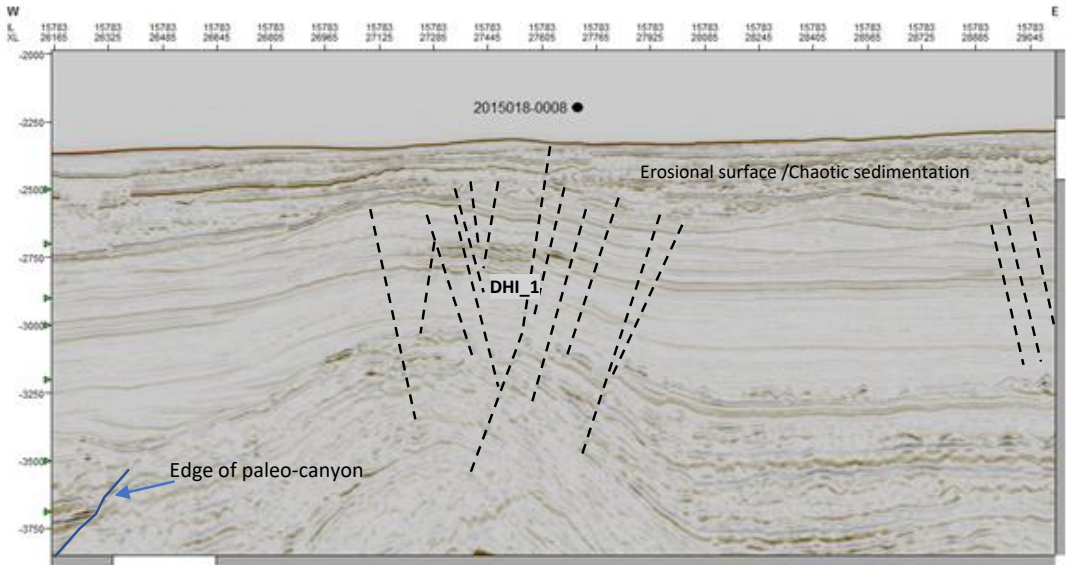

Figure 4.3B. An inline seismic cross-section of Core 8 showing the roof of a diapir with crestal faults reaching to Banquereau Formation mass transport deposits. Flanking the western edge of the diapir is a paleo-canyon. This site showed no geochemical evidence of hydrocarbon seepage (Fowler and Webb, 2015).

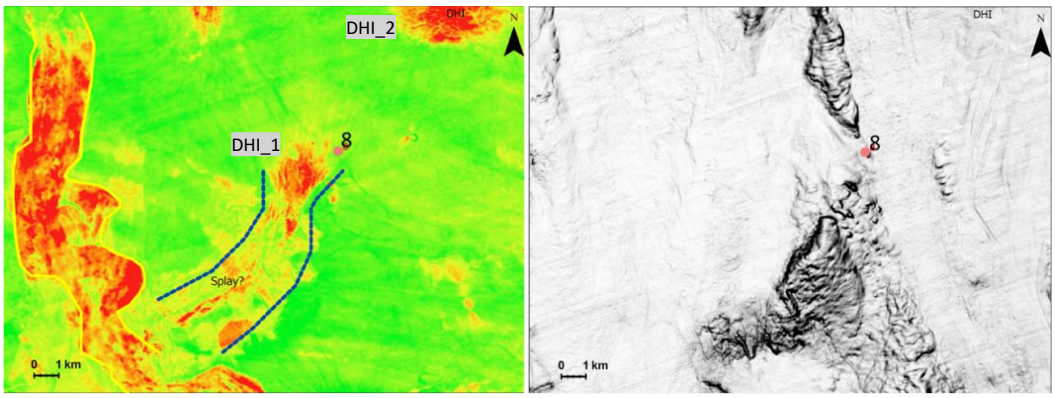

Figure 4.3C. An RMS amplitude attribute near Core 8 on the left, and the variance map of the seafloor surface at the same location on the right. The high amplitude anomaly may both be a DHI signature and a fine-tuning artefact from a canyon or channel system erosional surface and sediment transport system. The yellow-outlined amplitude anomaly shows the meandering geometry of a slope canyon system, the Mohawk East Canyon of Deptuck and Kendell (2020). The blue outlined area interpreted as a crevasse splay from breach of the levee system of the canyon.

Gas shows was not observed in Core 8. Like Site 4 and 5 is on a canyon/channel system pathway and at the site is likely to be a crevasse splay from a levee breach that is indicated by the geometry of the high amplitude zones to the southwest of the sampling site (Figure 4.3C). The vertical section shows no obvious acoustic anomaly, but a highly faulted interval is observed (Figure 4.3B). Even with a high density of faults (Figure 4.3D) as seen at 2700 m of the coherence attribute, DHI_2 (Figure 4.3A, 4.3C) north and east of Site 8 is likely too far away and on a different structure to have supplied hydrocarbons to Site 8.

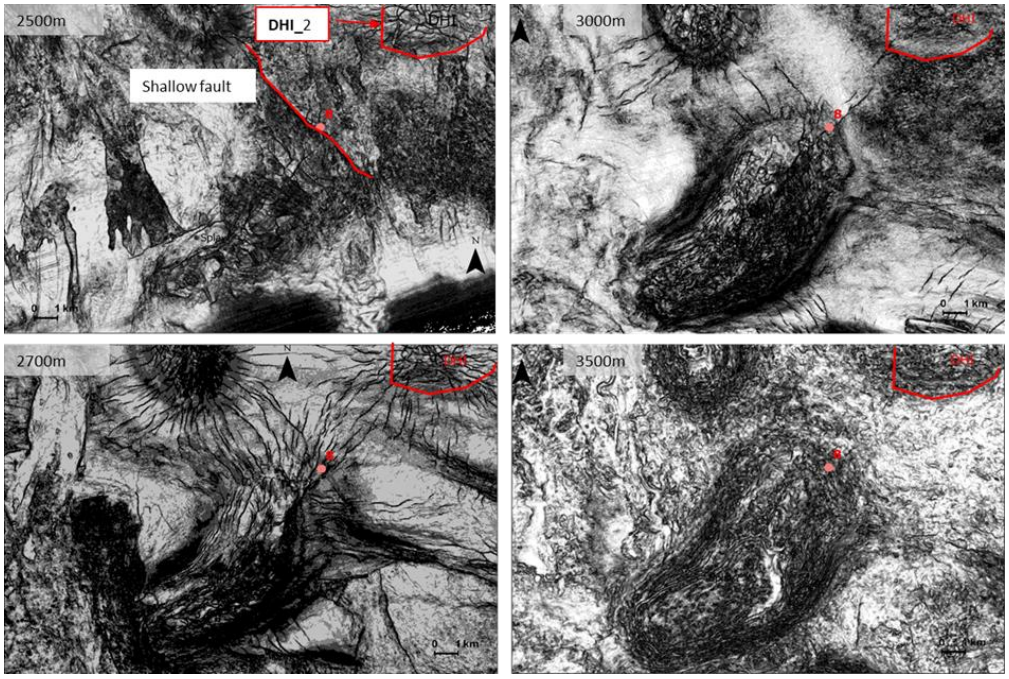

Figure 4.3D. Coherence attributes at different water depths for sample 2015 Core 8. A DHI is identified in the northeast of Site 8. Radial faulting is most visible at 2700 m and is likely caused by salt-induced shearing and associated fracturing. At 2500 m, the surface appears rough as inferred on the seismic cross section and a shallow fault is observed. Interconnected crestal faulting is seen at 2700 m and dissipates at 3000 m in the variance maps. The faulting occurs most prominently at 2400 to 3100 m on the vertical section (see A3 in Appendix II).

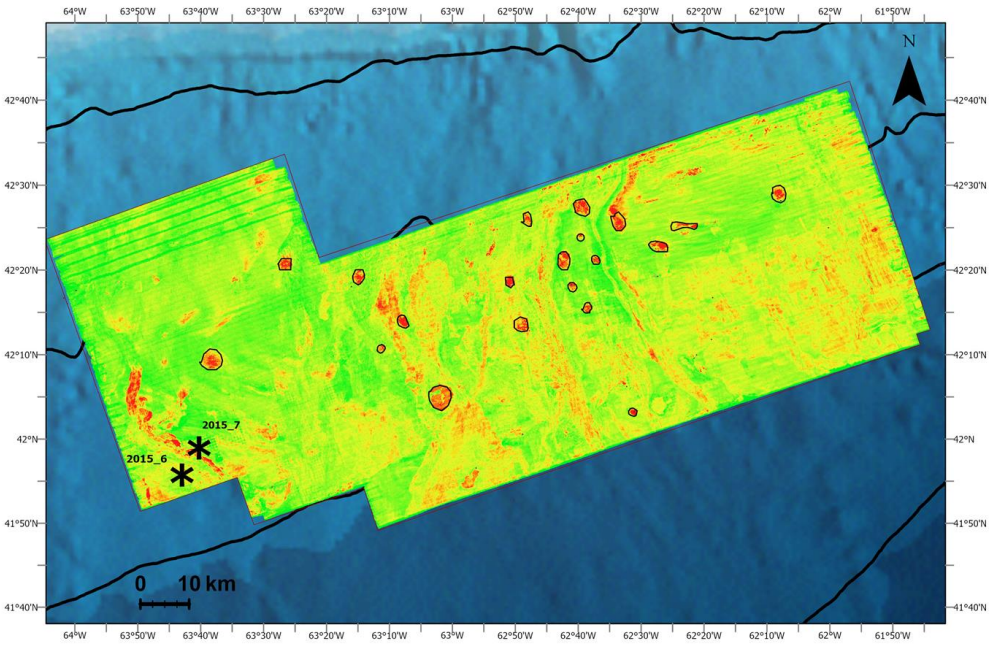

Figure 4.4A. The RMS attribute map showing the location for sample 2015 Site 6 and 7 marked by asterisks. The two sites are separated by a canyon channel transporting sediment down the slope.

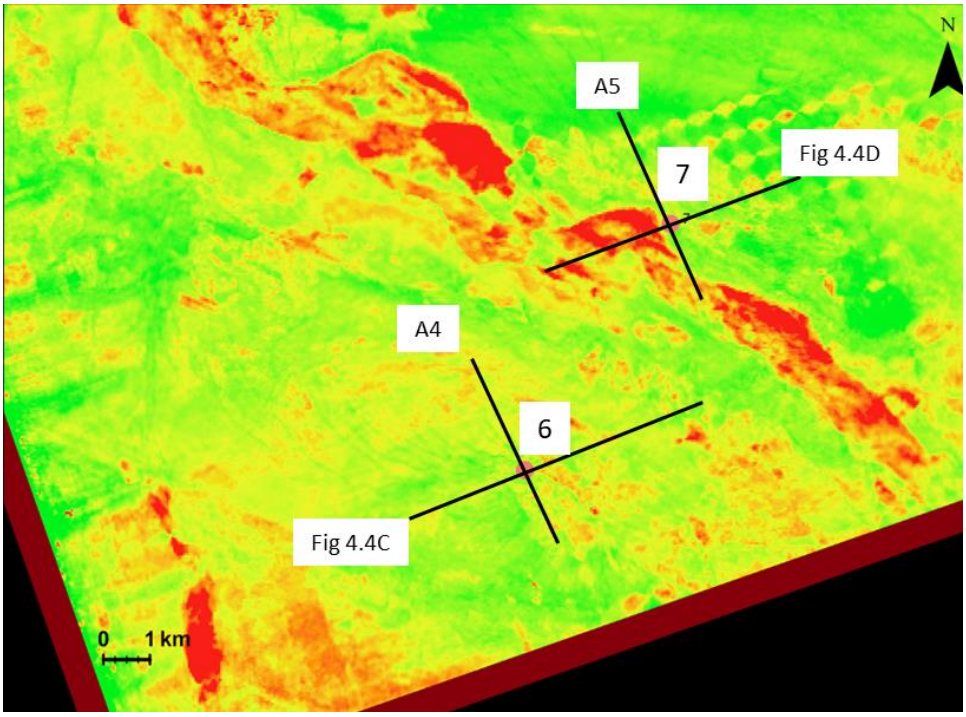

Figure 4.4B. A zoomed-in RMS amplitude attribute snapshot of sample 2015 Core 6 and 7. Core 7 is sampled on a channel/canyon system. Core 6 is likely sampled in a sediment flow path. Cross-sections A4 and A5 are in Appendix II.

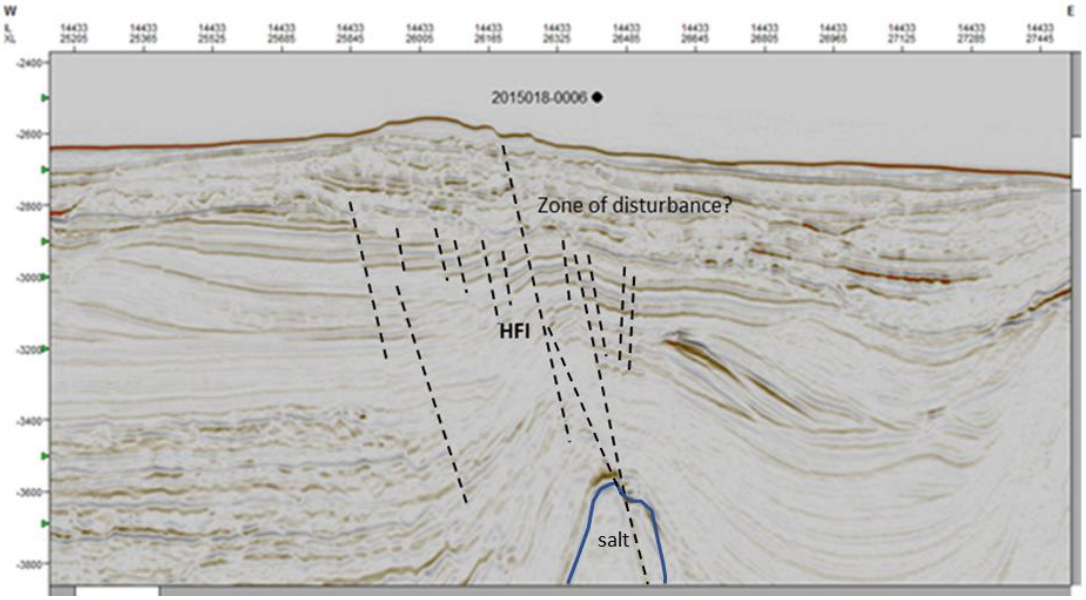

Figure 4.4C. Seismic inline cross-section for 2015-006 (of Site 6) that is located slightly askew of a paleo-canyon system. This was the only site where the core was collected in water depth greater than 2500 m during the 2015 expedition and showed evidence of hydrocarbon gas seepage in the geochemical analysis (Fowler and Webb, 2015).

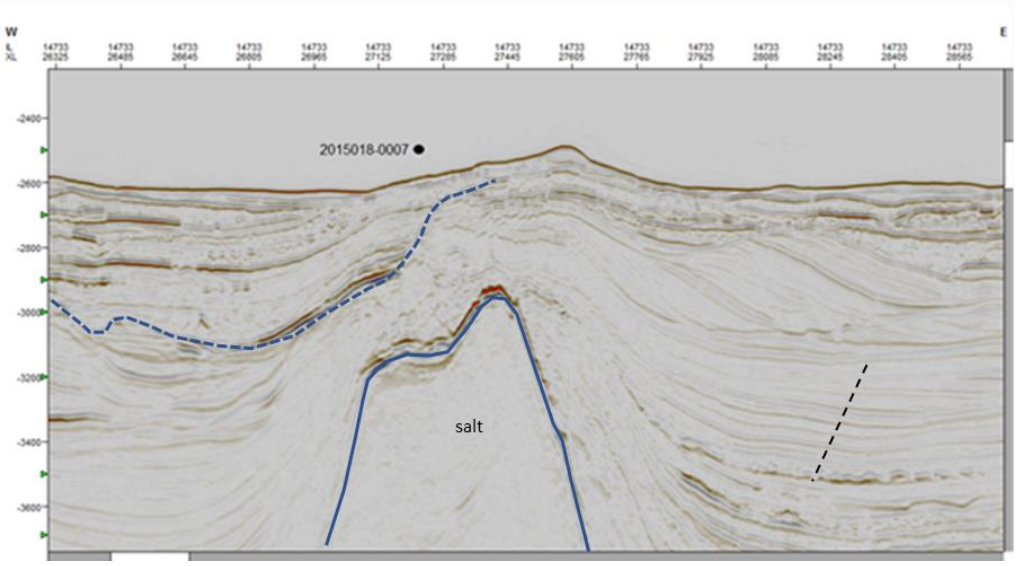

Figure 4.4D. Seismic inline cross-section for sample 2015 Core 7 sampled from a paleo-canyon system (note the variation in sediment deposition) whose sediment drapes the flanks of the salt crest. The blue dotted line delineates the canyon boundary.

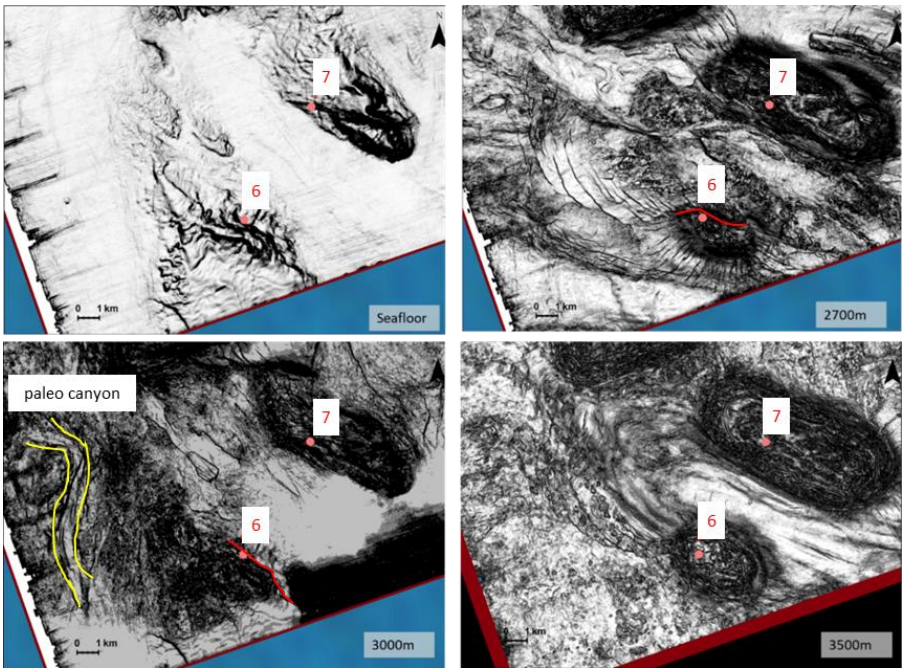

Figure 4.4E. Coherence attributes at different water depths for sample 2015 Core 6 and 7. The salt diapir in site 6 appears to cause salt-induced shearing and fracturing. The flanks and roof of the salt in Site 7 are onlapped by a mass transport complex as overburden. The yellow lines at 3000 m are interpreted as a paleo-canyon, and the red lines on core 6 at 2700 and 3000 m are plausibly the fault that reaches the surface from Figure 4.4C.

The vertical seismic cross section for Site 6 (Figure 4.4C) indicates a highly faulted interval at 2700 m to around 3200 m. In the variance maps, faulting is mostly

visible at 2700 m and is mostly radial. The areas of high relief at the seafloor variance map (Figure 4.4E) make it hard to distinguish between it being a fault or the erosional edge of a high relief area. However, from the vertical section, it could be that both are present. There are no apparent indicators for hydrocarbon migration in the seismic section. The high amplitude anomaly (Figure 4.4B) shows the downslope, meandering structure of the East Mohawk Canyon.

Site 6 had the highest reported concentrations of C_2–C_4 gases and show evidence for methane being a mixed of biogenic-thermogenic origin ($\delta^{13}C$ -60.8 to -68.6‰) (Fowler and Webb, 2015). Based on the biomarker distributions (see Fowler and Webb, 2015 for detailed explanations and parameters), it is inferred that the thermogenic hydrocarbons are in fact an artifact rather than being derived from deeper petroleum seepage.

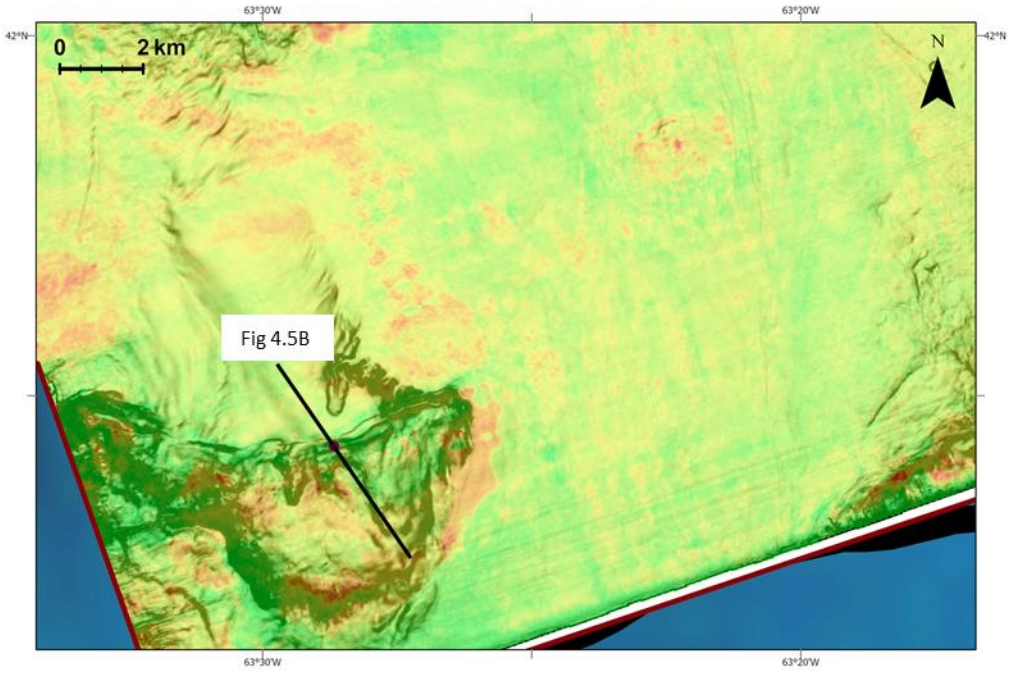

Figure 4.5A. An RMS amplitude snapshot overlain on a seafloor variance map showing the location for sample 2016 Core 13.

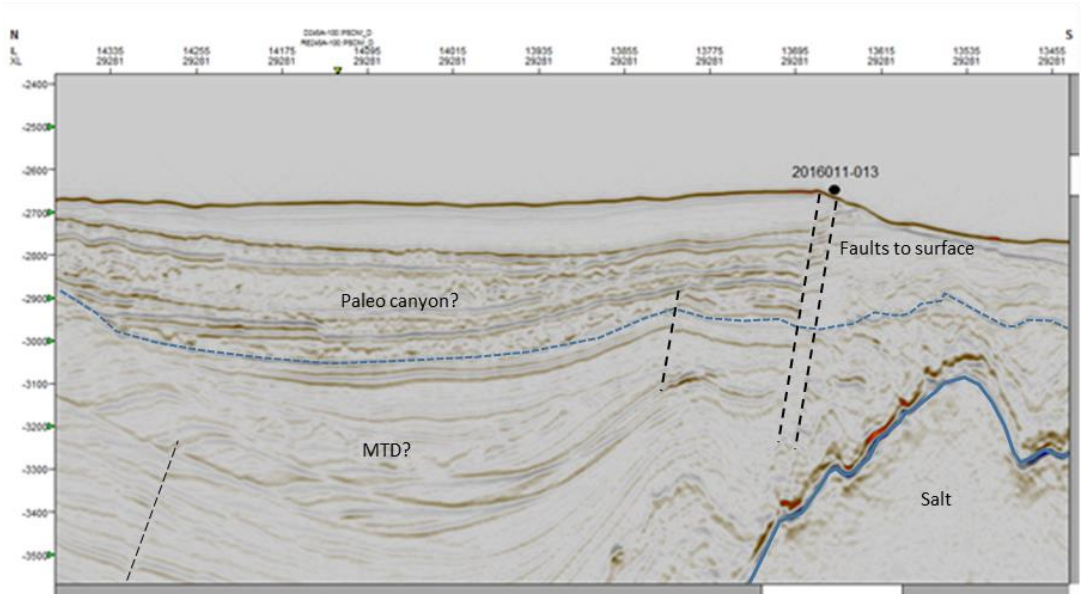

Figure 4.5B. Seismic crossline cross-section for Site 2016-013 that was close to Site 2015-006. The sample showed no geochemical evidence for hydrocarbon seepage (Fowler and Webb, 2017).

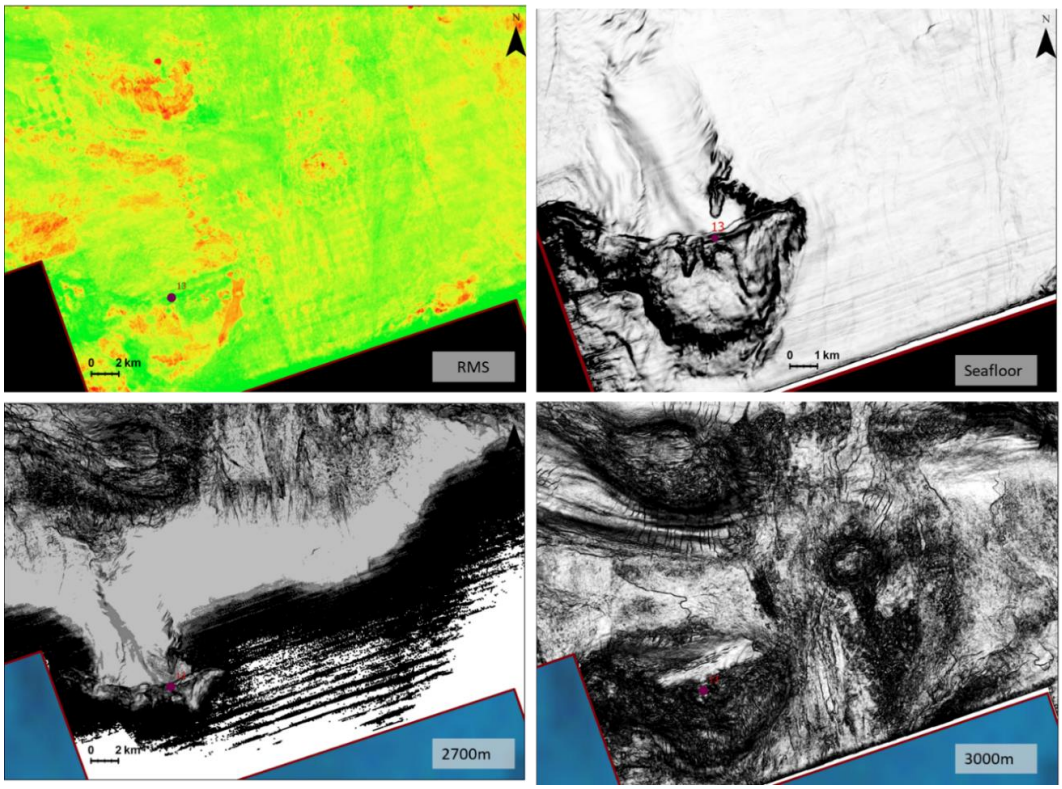

Figure 4.5C. Site 2016-013 area of down-slope gravity-flow-dominated processes (i.e., likely mass transport deposit (MTD) canyon and/or migrating submarine channels). On the variance seafloor map, Core 13 appears to be on top of headwall scarps from slumps generated by the relief from the uplifted diapir crest. Faults radiating from a salt body (salt halo) can be seen at 3000 m.

Core 13 was sampled in a region experiencing a considerably higher volume of downslope sediment transport and with tall salt stocks. There were no obvious indicators for hydrocarbon migration in the seismic section (Figure 4.5B) and available geochemical data did not indicate a presence of hydrocarbons. Paleo-pockmarks are observed deeper in the subsurface at 3500 m (Figure 4.5D). As the features are only observed at 3500 m, they are not active fluid escape features. Even so, there could still be fluid migration from the subsurface at this depth that may be transient or without pathways that lead to the surface.

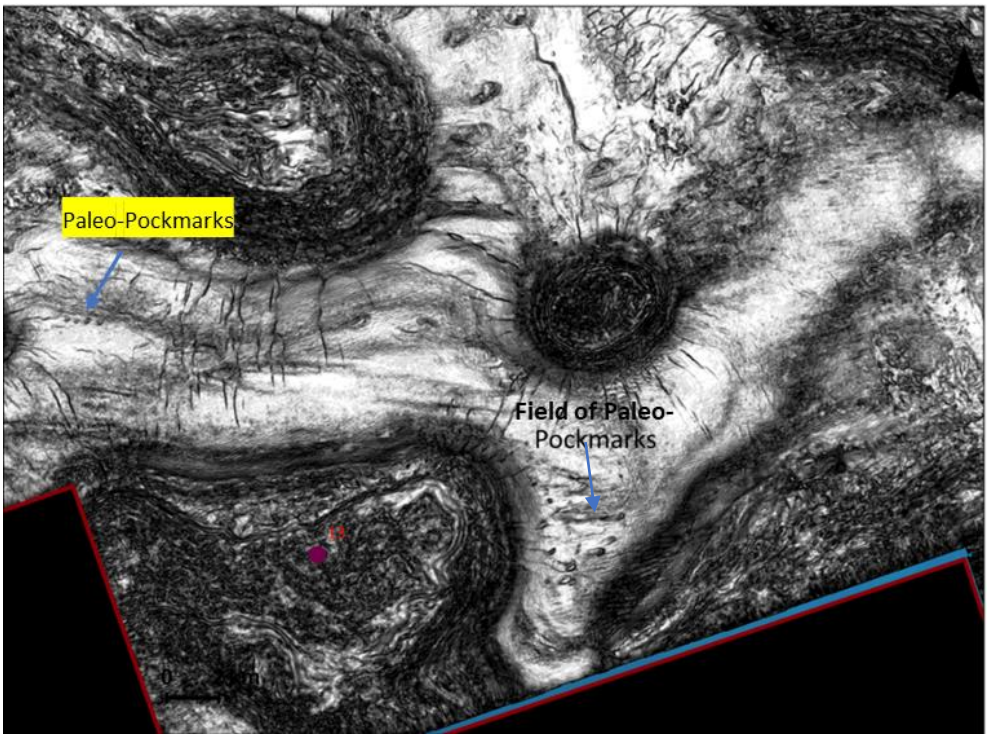

Figure 4.5D. Coherence attribute for sample 2016 Core 13 at 3500 m showing features interpreted as paleo-pockmarks (blue arrows). Four are seen on the upper right, and a field of paleo-pockmarks on the lower side. A seismic section that goes down to this depth would be useful in confirming if the features are indeed paleo-pockmarks.

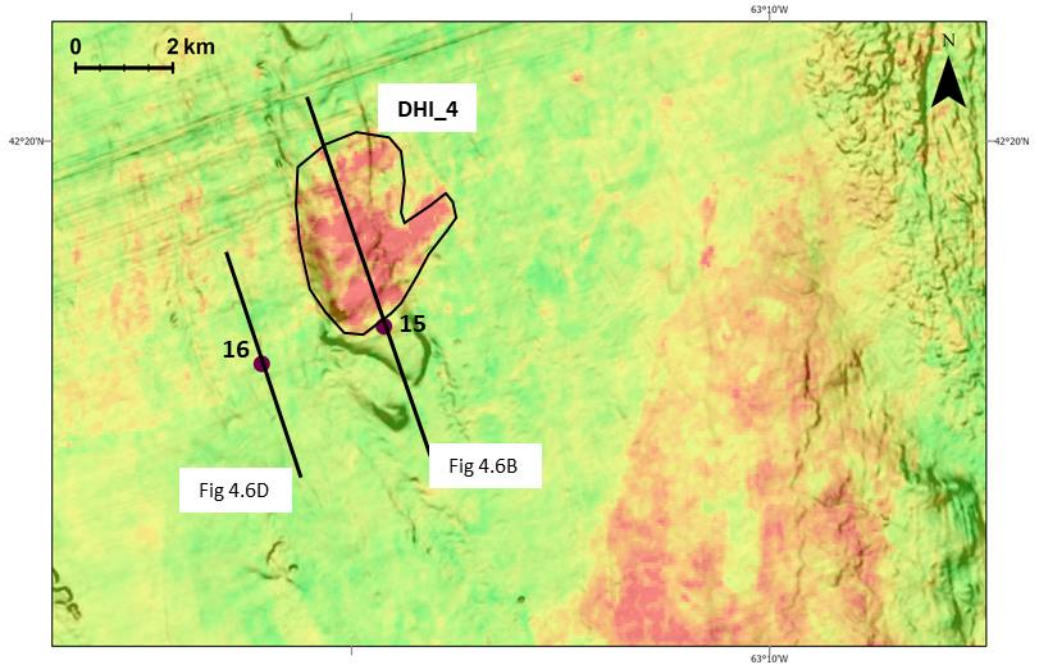

Figure 4.6A. An RMS amplitude snapshot overlain on a seafloor variance map showing location of samples 2016 Core 15 and 16.

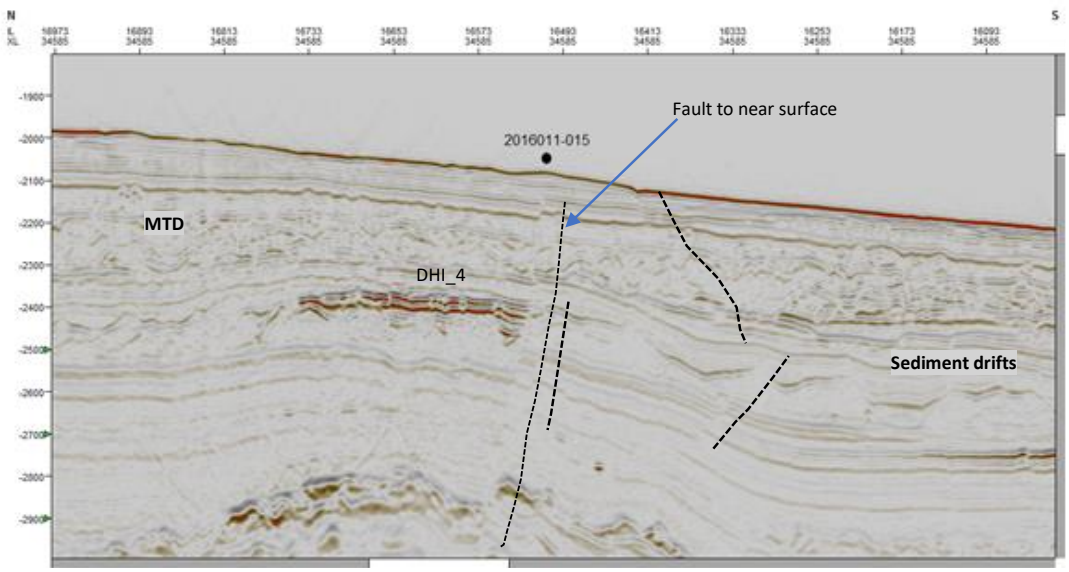

Figure 4.6B. Seismic crossline cross-section for sample 2016 Core 15. There are no records for geochemical analysis for this site. The DHI is approximately 400 m from the surface which could hinder migration of hydrocarbons and limit its migration potential to sediment type were it not for the presence of the fault which would be a possible conduit. Whether the fault is leaking or sealing remains indeterminate for this case. A positive geochemical indication for hydrocarbon would imply a leaking fault.

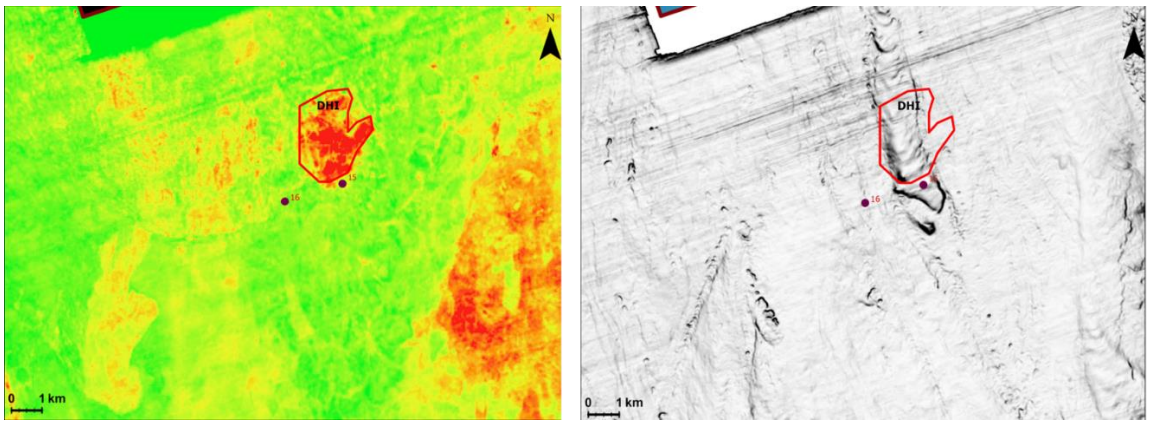

Figure 4.6C. An RMS snapshot (left) and seafloor surface coherence attribute (right) for Core 15 and 16. The red polygon is DHI_4.

Sample 2016 Core 15 targeted sediment on top of an acoustic anomaly and with a fault terminating near surface (Figure 4.6B). There is some indication for gravity related sediment flow through this zone between 2100 to 2300 m. On the seafloor surface (Figure 4.6C), no faults are visible.

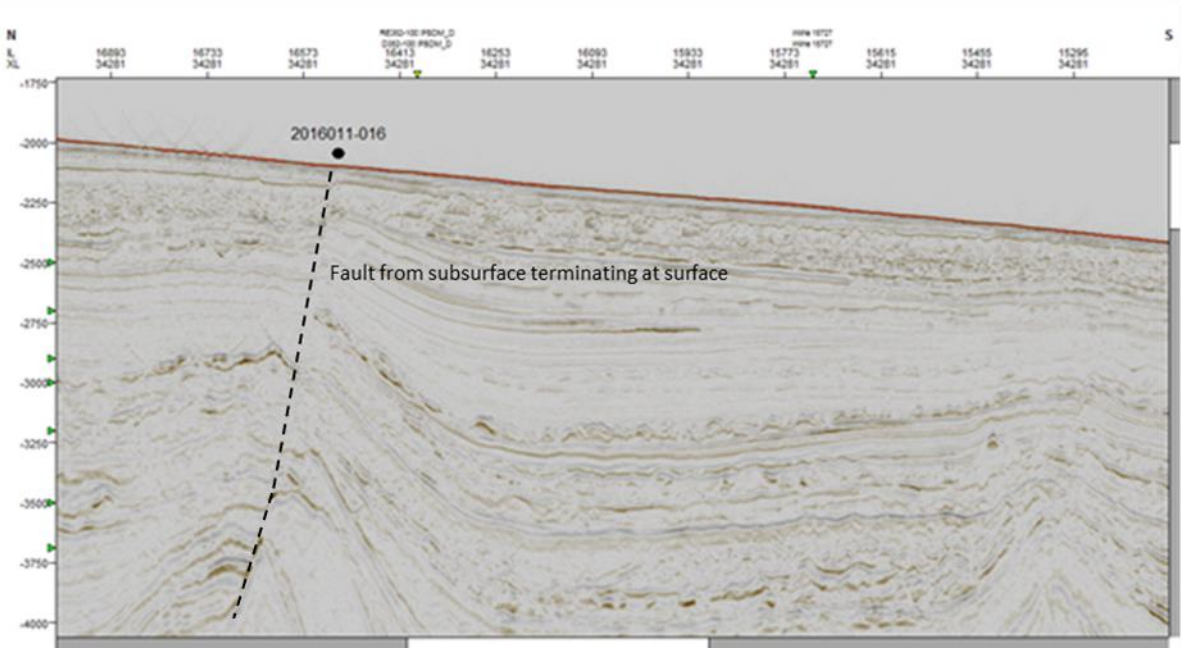

Figure 4.6D. Seismic crossline cross-section for 2016 Core 16. There is no record for a geochemical analysis of sediment from this site.

Core 16 is approximately 2 km away from Core 15 and further from the acoustic anomaly, but also on the crest of the same diapir structure as Core 15 (see Figure 4.6E).

The vertical seismic section (Figure 4.6D) shows a fault terminating at the surface, but no apparent indication of hydrocarbon migration is evident in the near surface units. There does not seem to be any geochemical records for both sites and only the core data was retrieved for this study. Core 2016_015 contained sandy beds with dewatering in some portions of the core. It was sampled at a water depth of 2050 m. Core 2016_016 included a sandy bed deposited between grey and red mud. It was sampled at a water depth of 2054 m (Fowler and Webb, 2017).

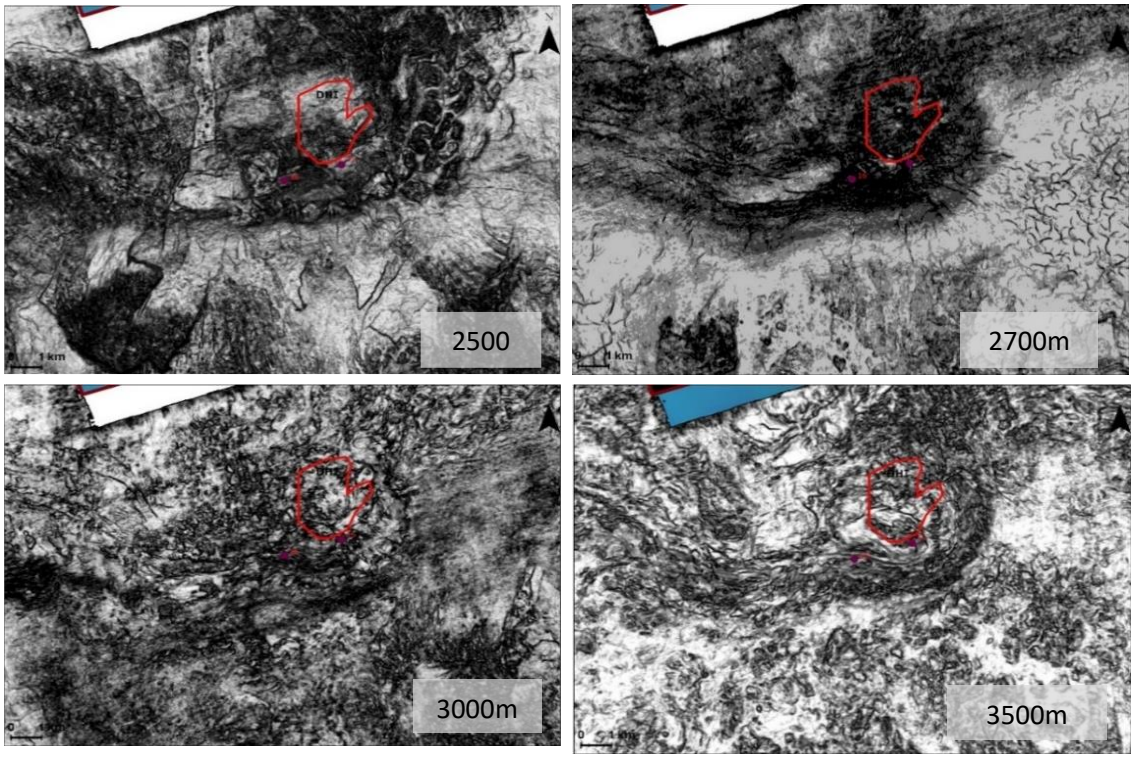

Figure 4.6E. Coherence attributes for Core 15 and 16 at different water depths. The DHI polygon is overlaid on the coherence maps at the different depths, but the DHI itself appears at approximately 2450 m water depth. No faulting is observed at deeper depths in this location.

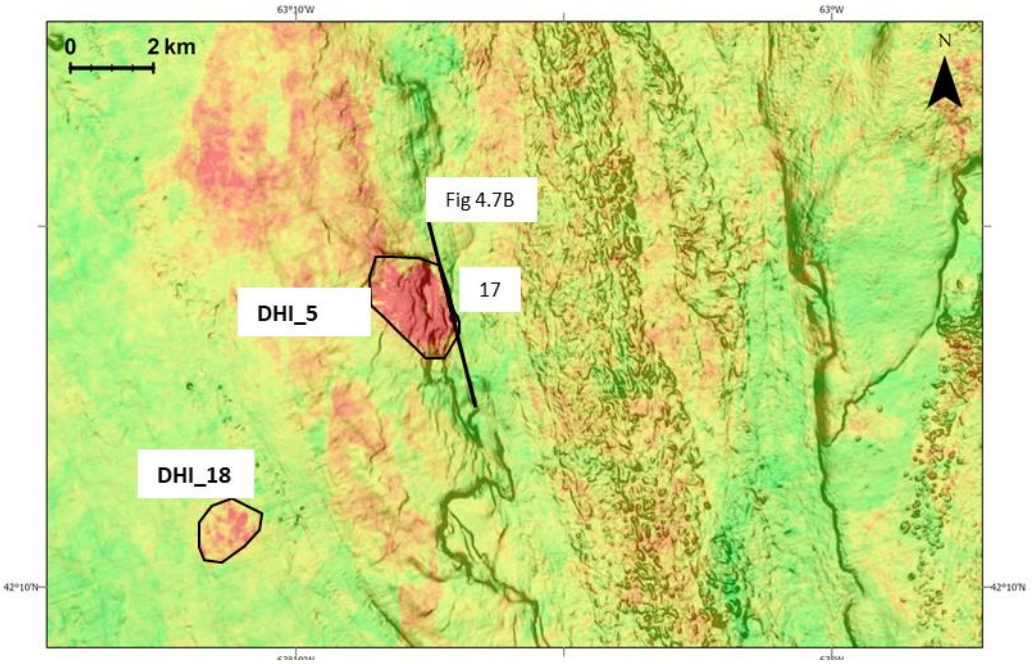

Figure 4.7A. An RMS amplitude snapshot overlain on a variance seafloor map showing the location for Core 2016-017.

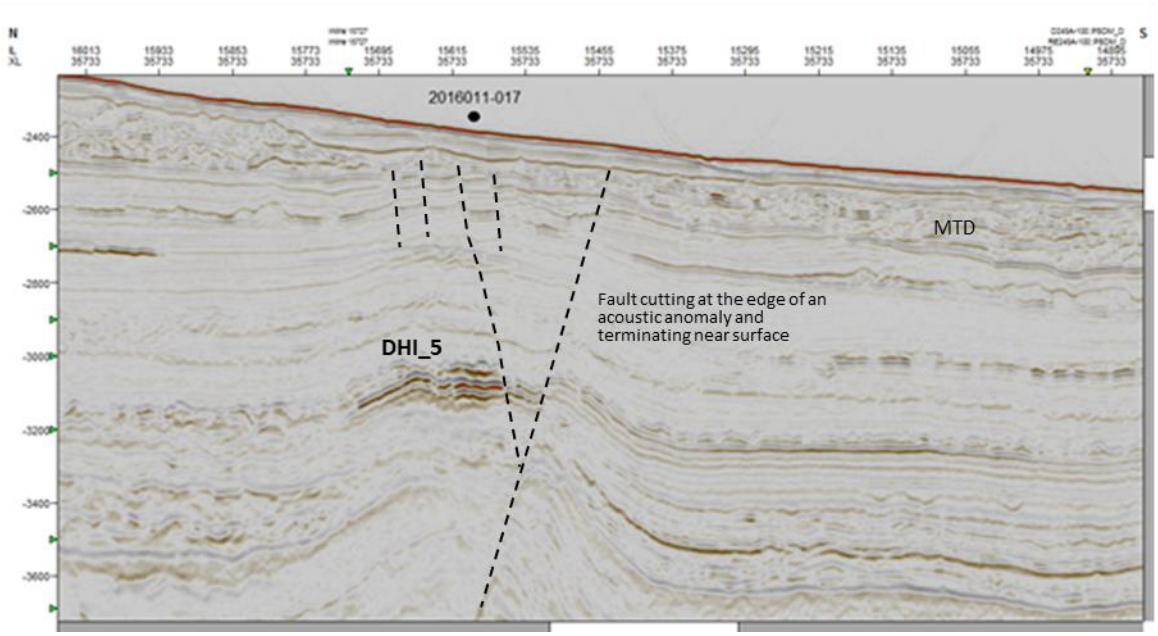

Figure 4.7B. Seismic crossline cross-section for Core 2016-017. The DHI sits in sediment draped over the crest of a diapir and is ~600 m below the seafloor. It is plausible that there is some fluid migration from the subsurface through the DHI and towards the seafloor.

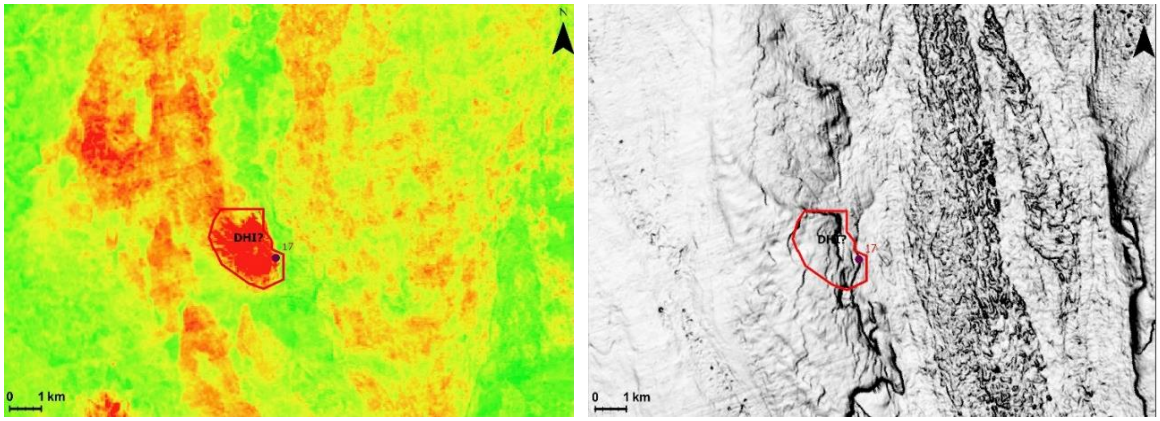

Figure 4.7C. An RMS amplitude map (left) indicating DHI_5 and Core 2016-17. The seafloor surface coherence attribute map (right) for the same site showing an area of high relief.

Core 17 at a water depth of 2315 m overlies high-amplitude reflections in sediments draped over the crest of a salt diapir, and seemingly truncated by one of the crestal faults. The reflections are interpreted as DHIs and occur approximately 600 mbsf (Figure 4.7B). The coherence seafloor surface map shows no sign of near-surface gas indications, only down-slope linear trends related to seafloor sedimentation or erosion (Figure 4.7A, C). The samples analyzed from Core 17 were without discernable geochemical evidence of hydrocarbons (Fowler and Webb, 2017).

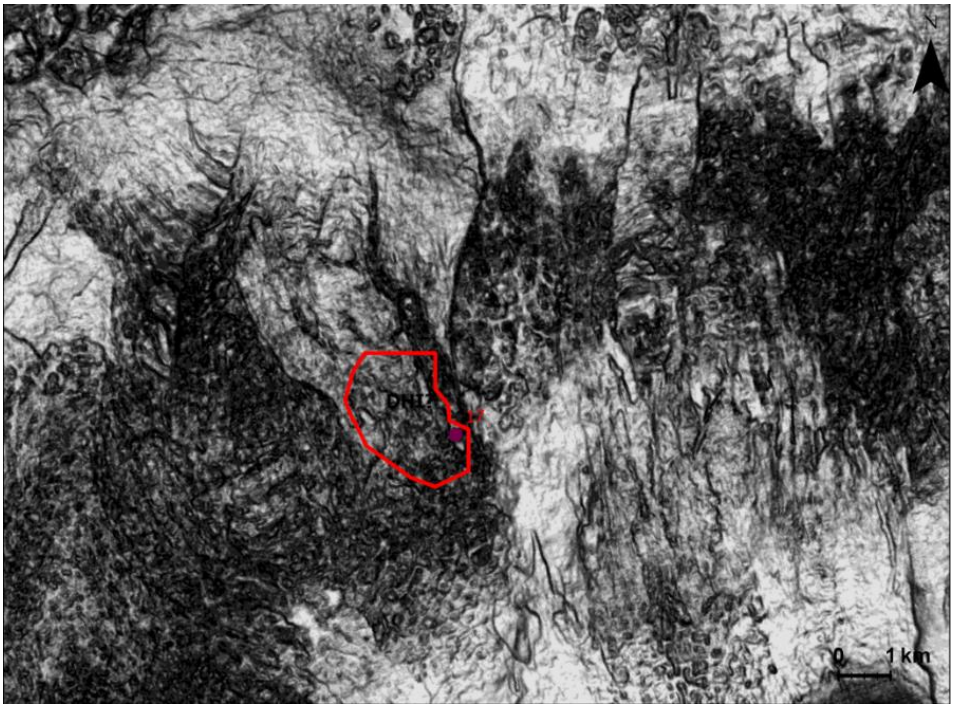

Figure 4.7D. Coherence attribute at 2500 m for Site 17 showing an incoherent and irregular geometry at this depth that is possibly related to MTD development. No seepage/leakage mechanisms are noted. Core 17 was collected on the edge of a paleo-scarp.

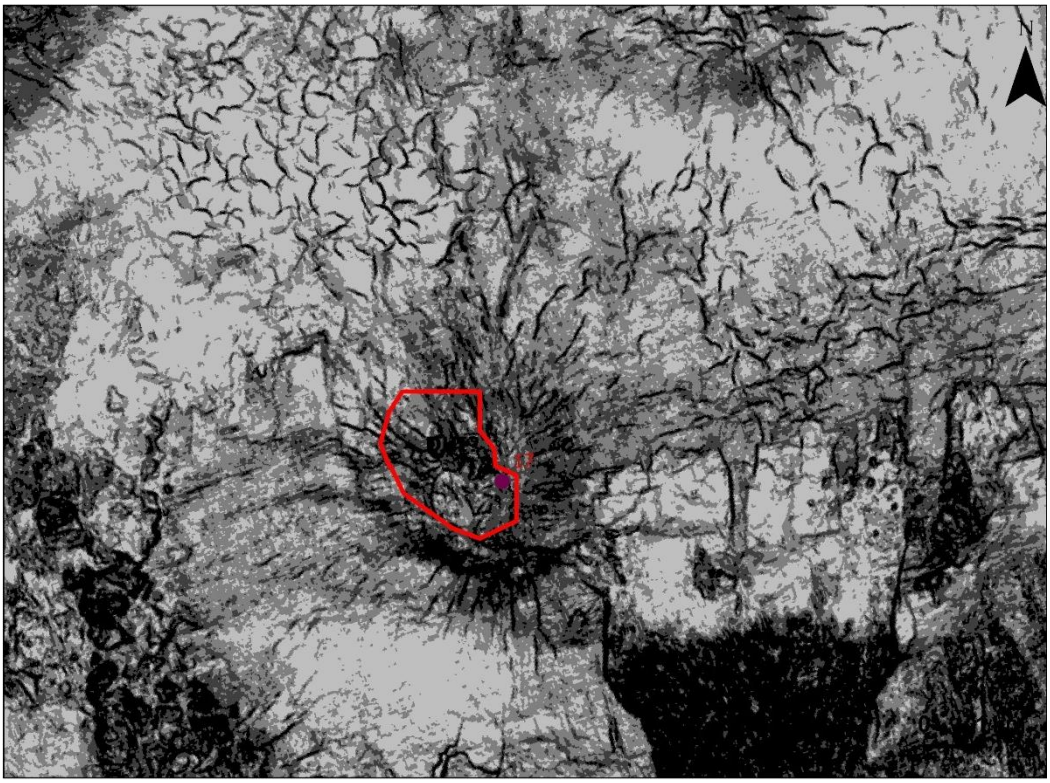

Figure 4.7E. Coherence attribute at 2700 m for Core 2016-017. Polygonal faulting and faults radiating from a salt body (salt halo) are observed. The faulting does not appear to propagate to surface but is localised at this depth.

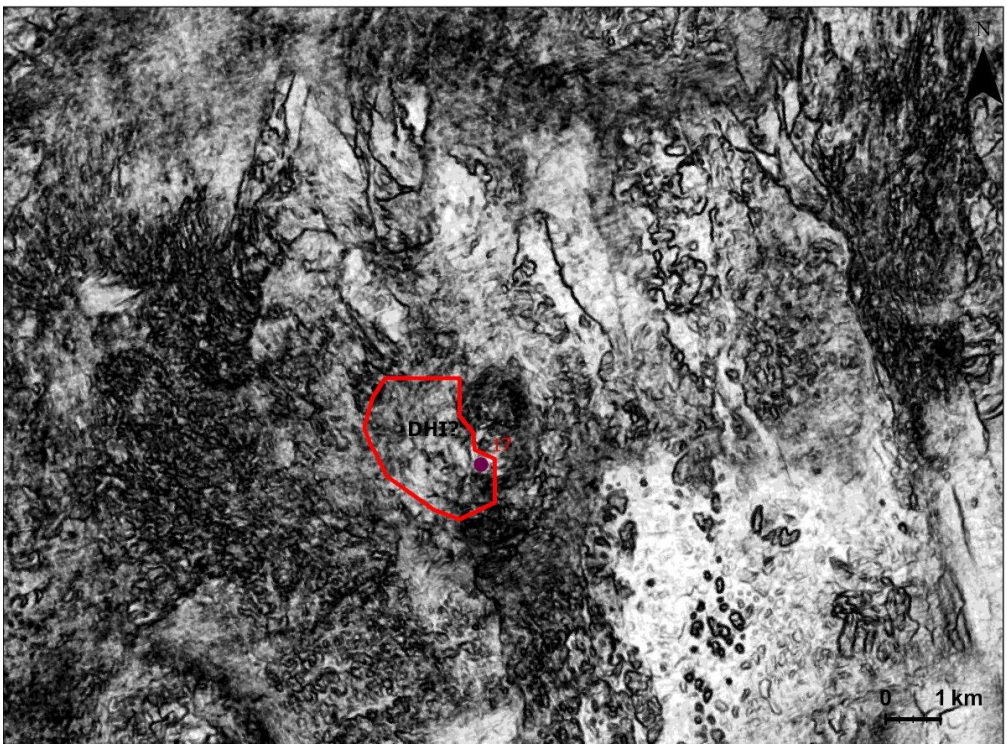

Figure 4.7F. Coherence attribute at 3000 m for sample 2016 Core 17. No seepage features are observed.

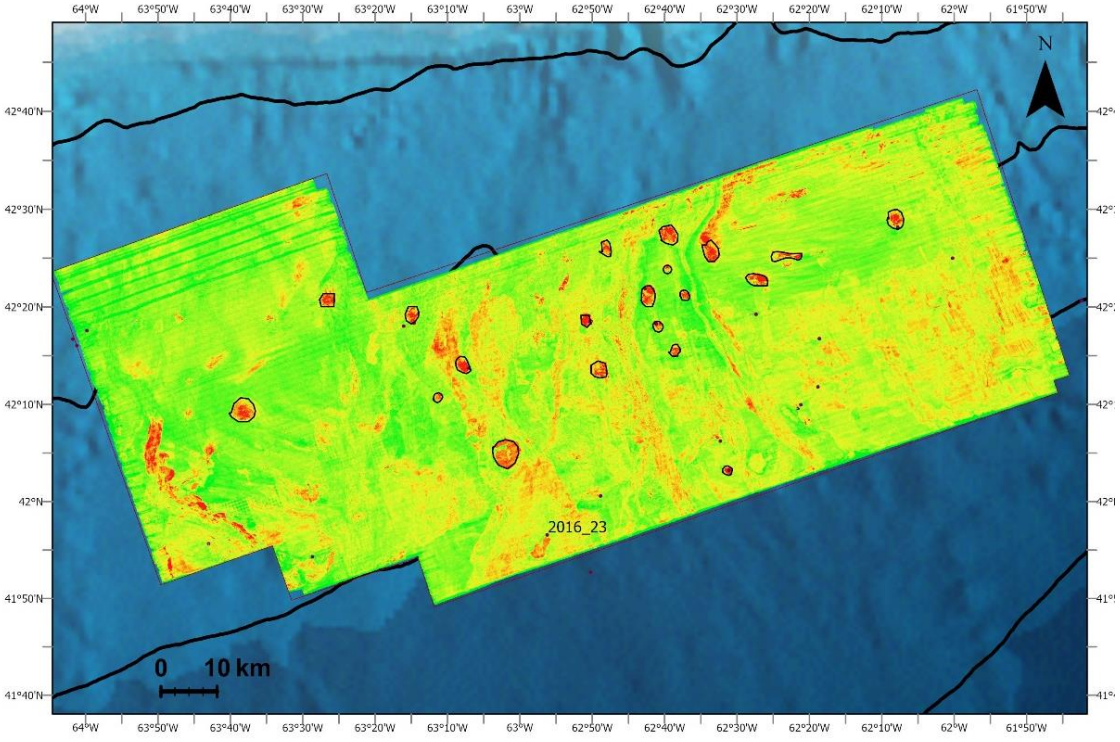

Figure 4.8A. The RMS amplitude map showing location of sample 2016 Core 23.

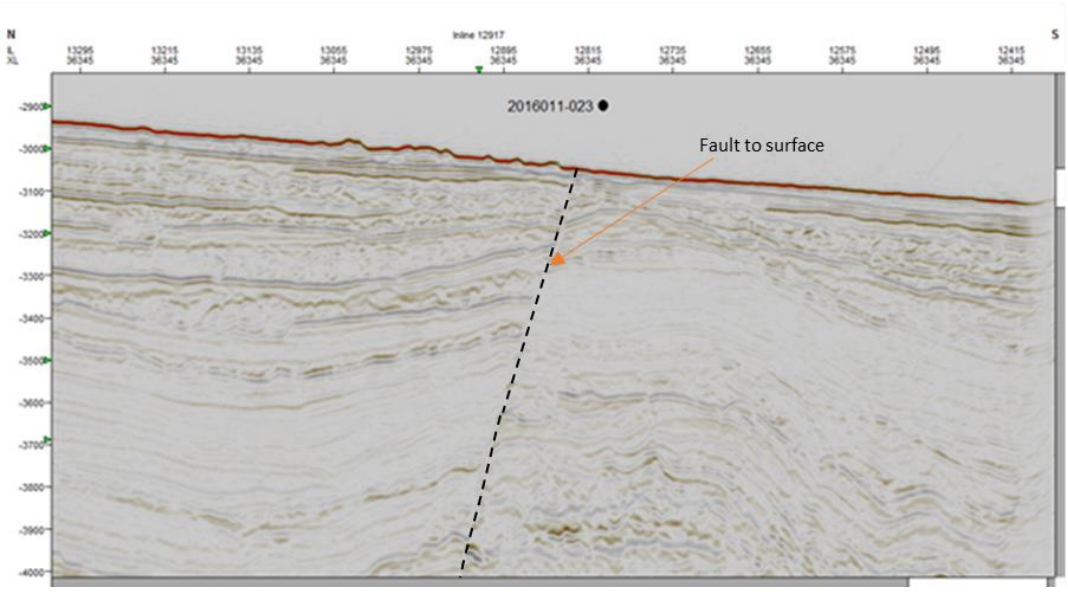

Figure 4.8B. Seismic crossline cross-section for sample 2016 Site 23. The seafloor surface shows rugosity in some sections likely to indicate erosional processes in a channel system. This seismic cross section may have just missed the high amplitude anomaly or is picking up the tuning effects from the erosive sediment at ~3000 m (and at 3100 m).

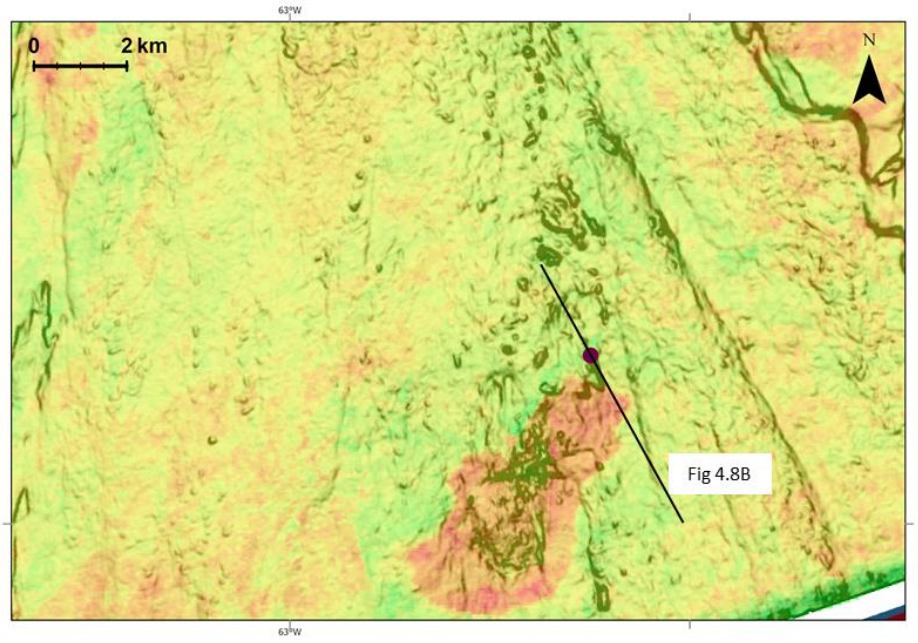

Figure 4.8C. An RMS amplitude snapshot of sample 2016 Core 23 overlaid on a variance seafloor map. The high amplitude anomaly is not picked up on the section. From Figure 4.8A, this area appears to be receiving sediment from channels that begun up-slope. The high amplitude anomaly is likely to be produced by sediment debris flow in an erosive environment.

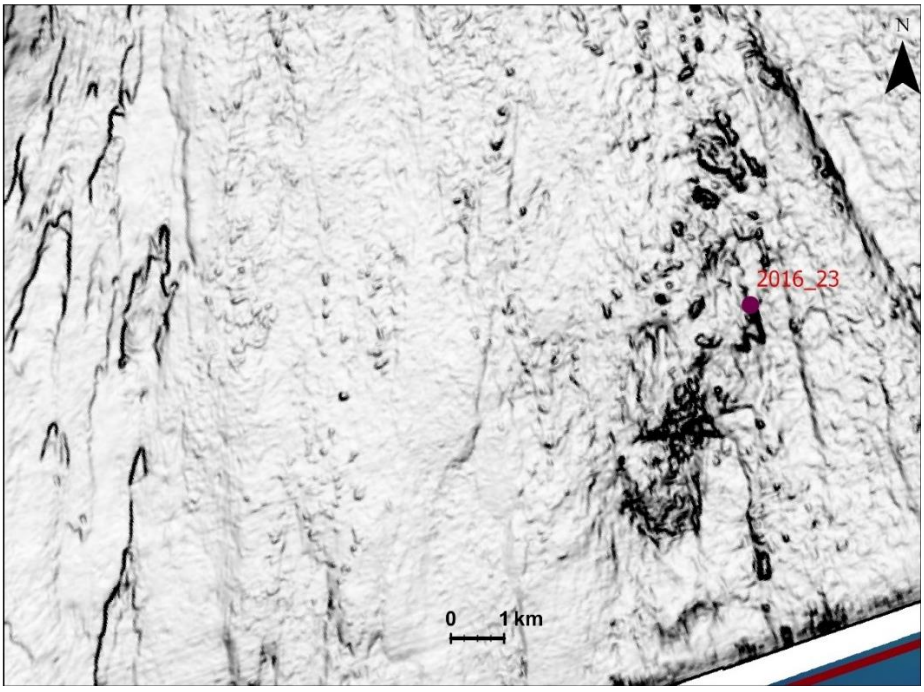

Figure 4.8D. Coherence attribute showing the seafloor surface at Core 23. The rugosity observed on the seismic cross section is also noted on this surface which appears rough and mottled.

Core 23 was located in a deeper portion of the slope (Figure 4.8A and 4.8E). The RMS amplitude map (Figure 4.8A and 4.8C) shows an area of high amplitude anomalies, likely produced by sediment debris flows on a channel pathway (see: Figure 3.18). The seismic section (Figure 4.8B) did not show indications of hydrocarbon migration. The piston core from this site had very low recovery and had no samples were analyzed (Fowler and Webb, 2017). Seismic crosslines to the left of the one interpreted on Figure 4.8 would clarify if the anomaly is a DHI or not.

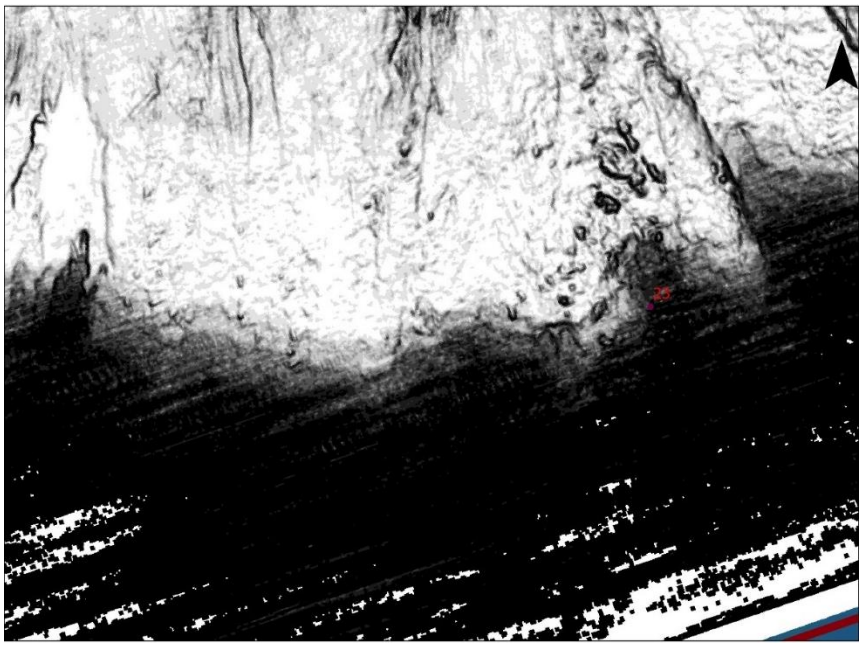

Figure 4.8E. Coherence attribute showing the Site 23 at 3000 m water depth. Rugosity is observed on surface at this depth. This coherence slice tapers off as this depth slice is not dip corrected.

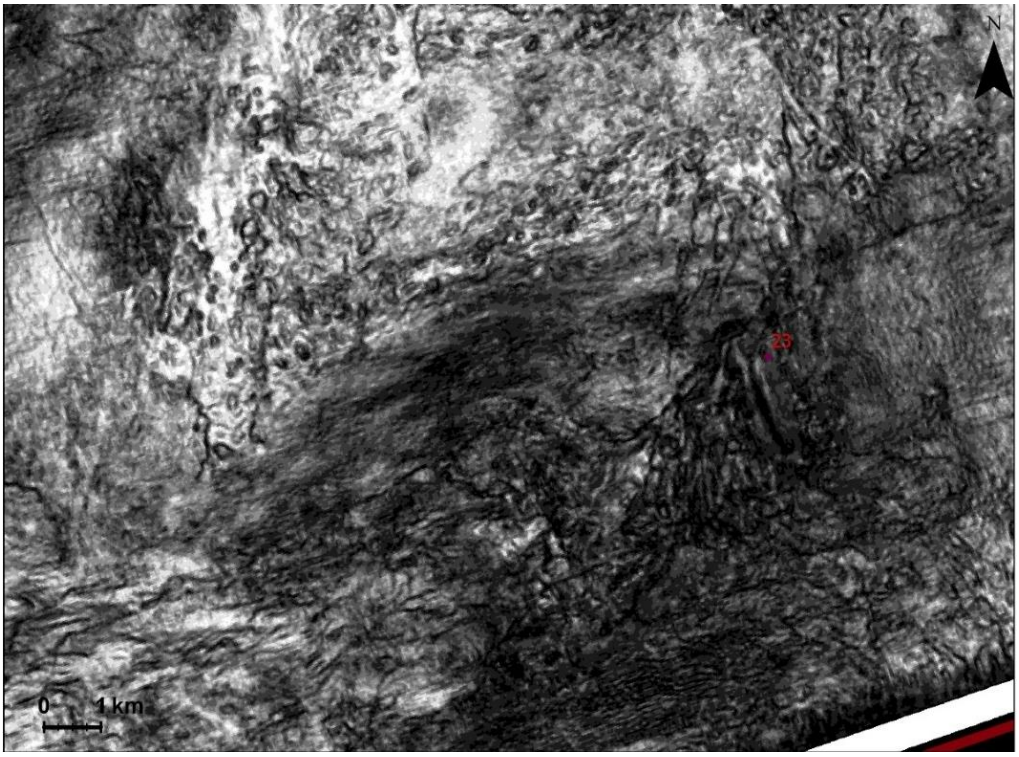

Figure 4.8F. Coherence attribute at 3500 m for Core 2016-23.

.

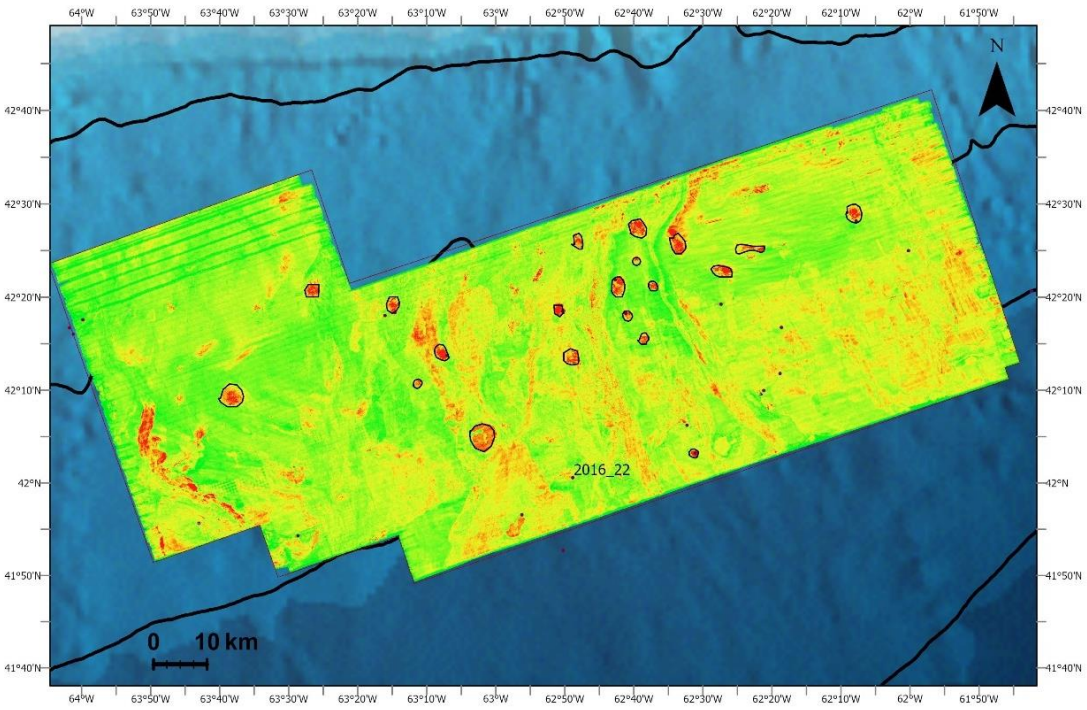

Figure 4.9A. The RMS amplitude map showing location of sample 2016 Site 22.

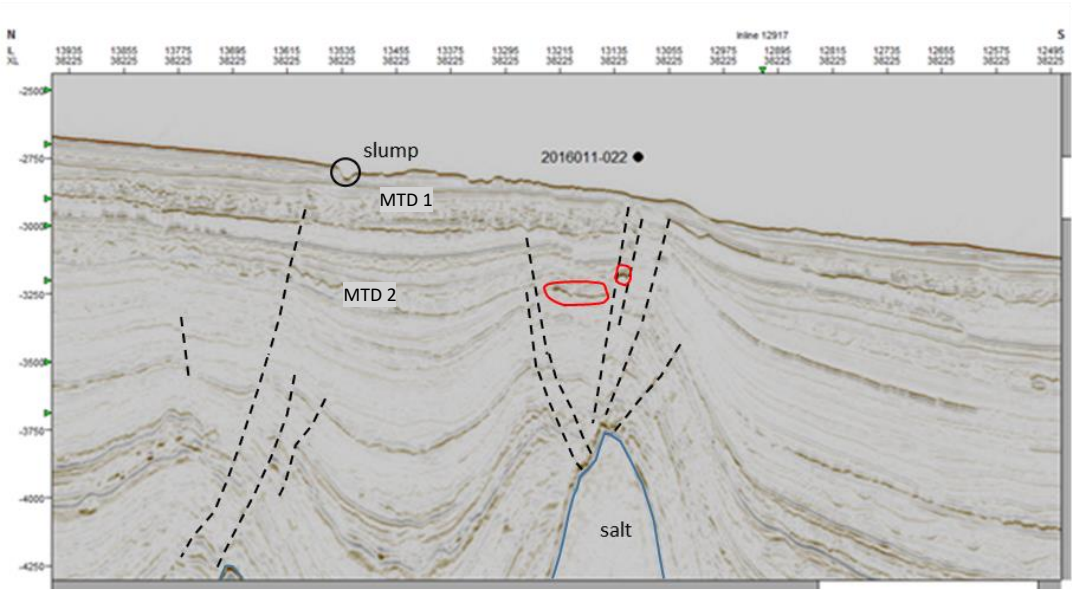

Figure 4.9B. Seismic crossline cross-section for sample 2016 Core 22 with fault-disrupted sedimentation and some rugosity on seafloor likely caused by modern erosional processes in a mass transport sediment system. The amplitude anomalies indicated by the red polygons could be picking up an erosive surface at that depth (~3200 m).

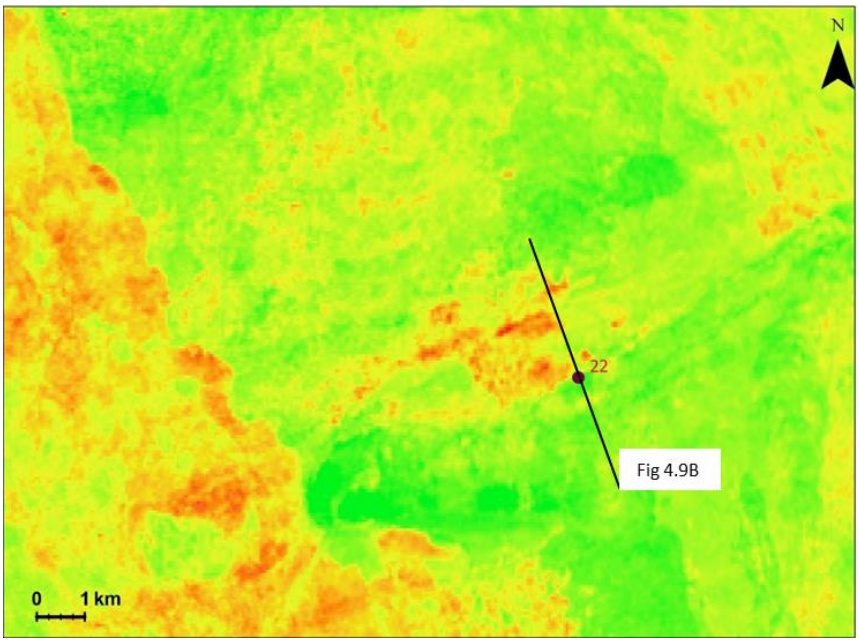

Figure 4.9C. An RMS amplitude map showing some high amplitudes most likely from sediment flow on erosional surfaces in a sloping area.

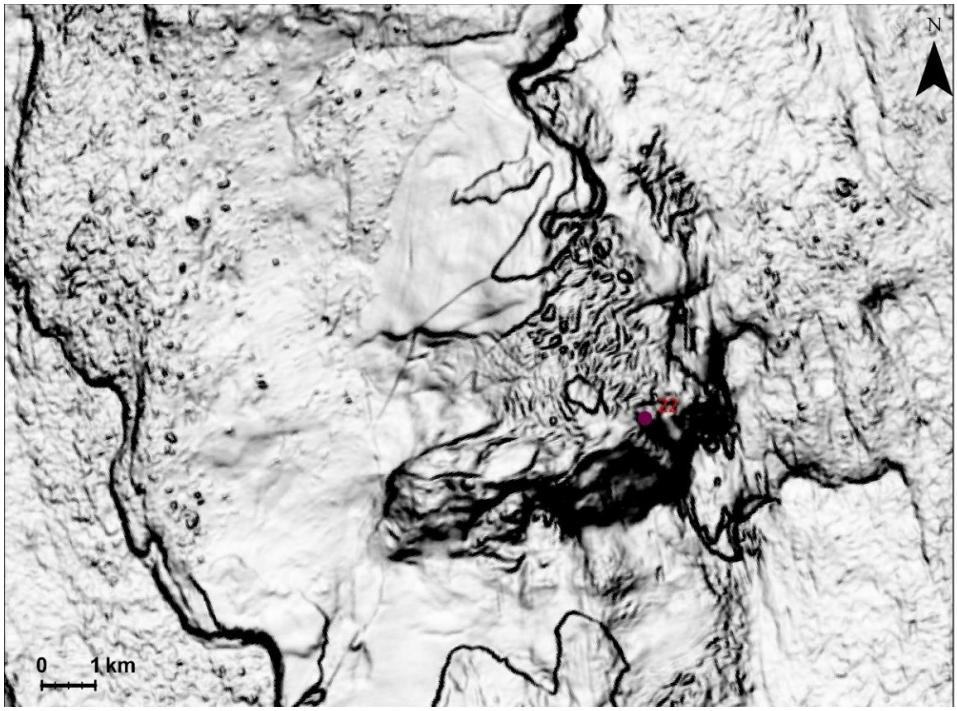

Figure 4.9D. Coherence attribute at site of Core 22 showing the seafloor surface. A high relief and pitted surface are observed for this location. The resolution is not high enough to determine the presence of leakage/escape features.

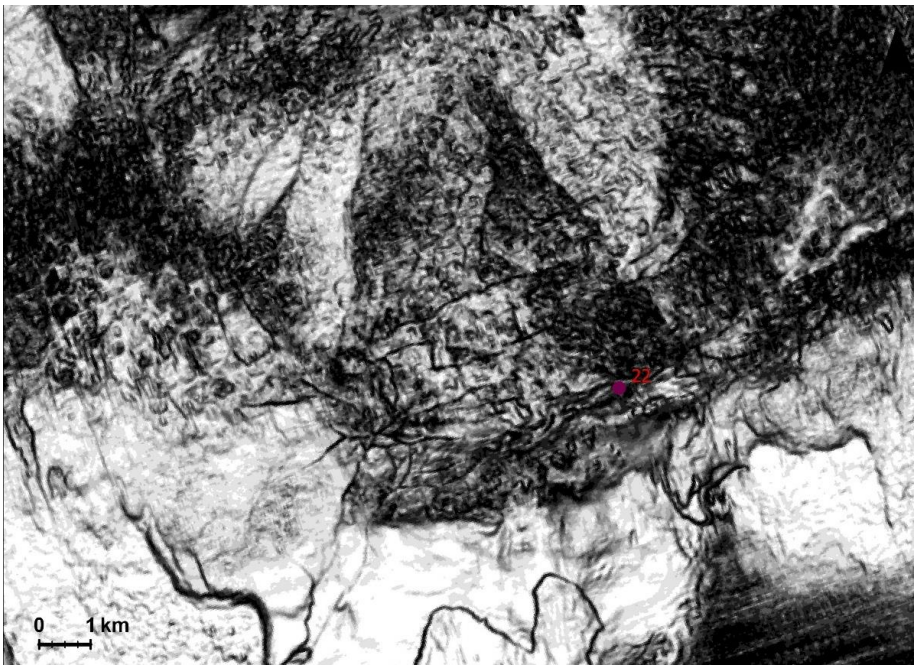

Figure 4.9E. Coherence attribute at 3000 m for Site 22.

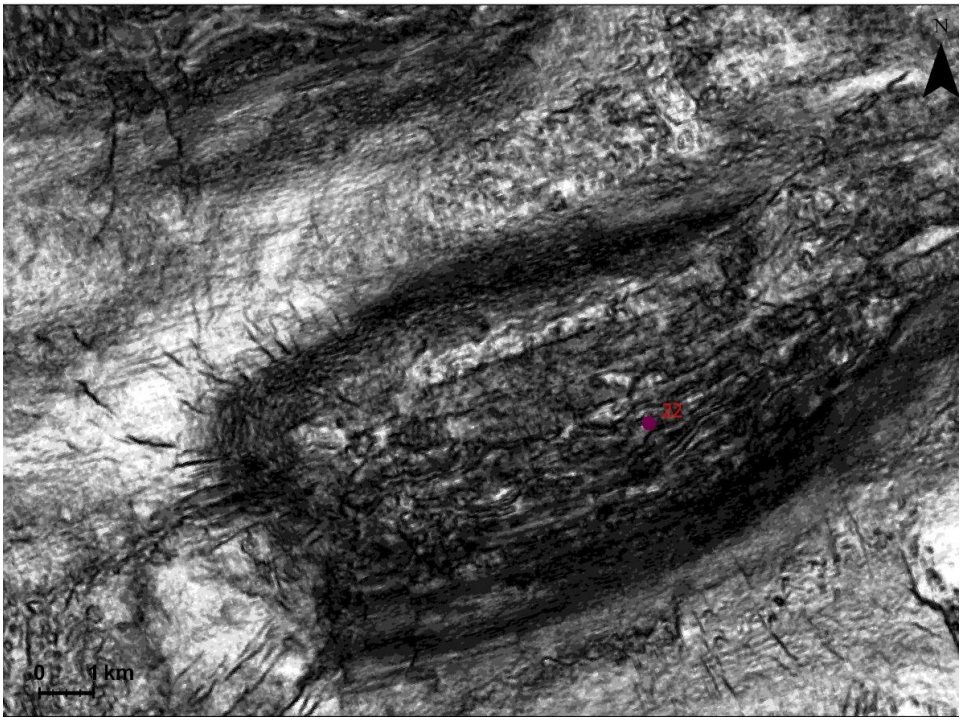

Figure 4.9F. Coherence attribute at 3500 m for Site 22. The ascending salt body is flanked by radiating faults and a series of WSW-ENE-oriented faults at the crest of the diapir structure.

Core 22 does not show indications of hydrocarbon migration in the seismic cross sections (Figure 4.9B) or in geochemical analyses of collected piston core sediments (Fowler and Webb, 2017). This site is in a zone of downslope sediment flow and like Site

23, abruptly deepens into even deeper water such that the seafloor is then at around 3000 m (Figure 4.9E and no surface at 2500 m and 2700 m). Additionally, the site had reported low total organic carbon content (0.2 mg) and did not produce signatures of thermogenic hydrocarbons (Fowler and Webb, 2017).

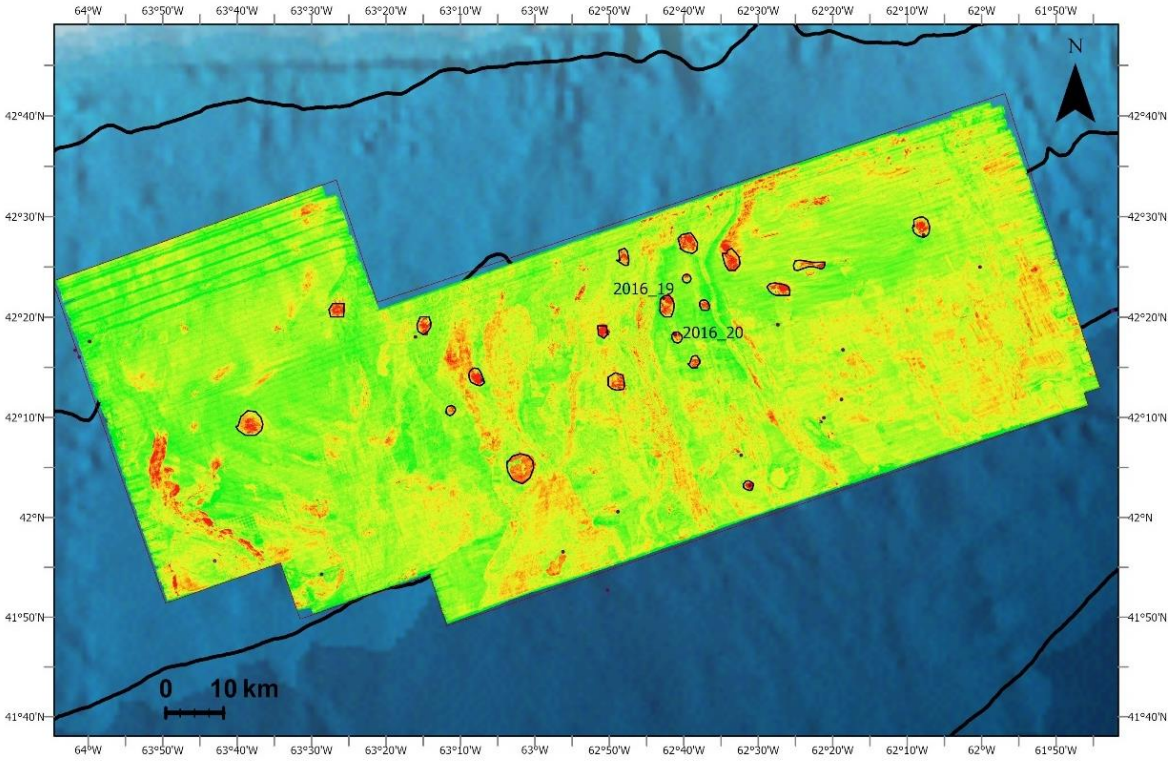

Figure 4.10A. The RMS amplitude map showing location of samples 2016 Site 19 and 20.

Sites 19 and 20 are located in between two channel/canyon systems that transport sediment down the slope (Figure 4.10A and 4.10C). The area is rich with a zone of anomalous, high-amplitude acoustic anomalies, some of which are interpreted as DHIs (Figure 4.10A those circled in black).

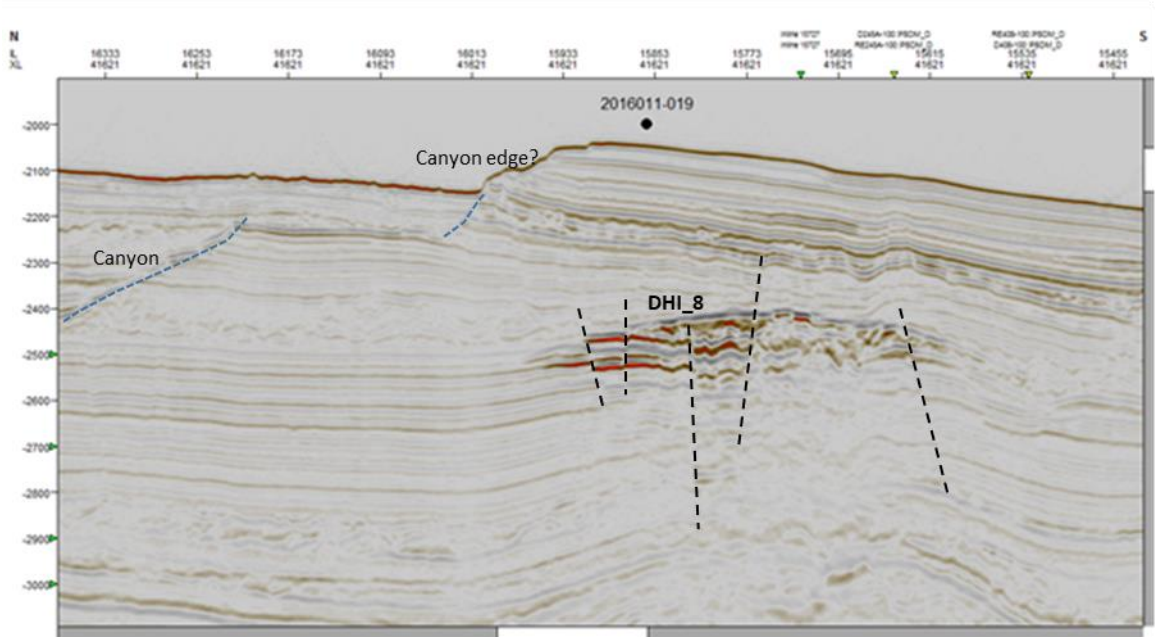

Figure 4.10B. Seismic crossline cross-section for Core 2016-19 collected near the edge of what appears to be a canyon system. The disruption of reflections near the crest of the DHI_8 likely indicates unresolved faulting and/or the effects of gas migration or other fluids within the sediments.

The seismic cross section for Core 19 (Figure 4.10B) indicates the presence of an anomaly interpreted as a DHI at 2400–2600 m. The piston core was collected next to a modern canyon system (Mohican Canyon). Core 19 was retrieved at a water depth of 2043 m, while the DHI is more than 300 m below the sampling point and without an obvious migratory pathway leading to the sampling point. However, the presence of seafloor pockmarks (Figure 4.10E) supports the likelihood of escaping gas from the underlying sediments. The core lithology included sand and mud (Fowler and Webb, 2017). Further scrutiny of this site is recommended to search for pockmarks on the surface.

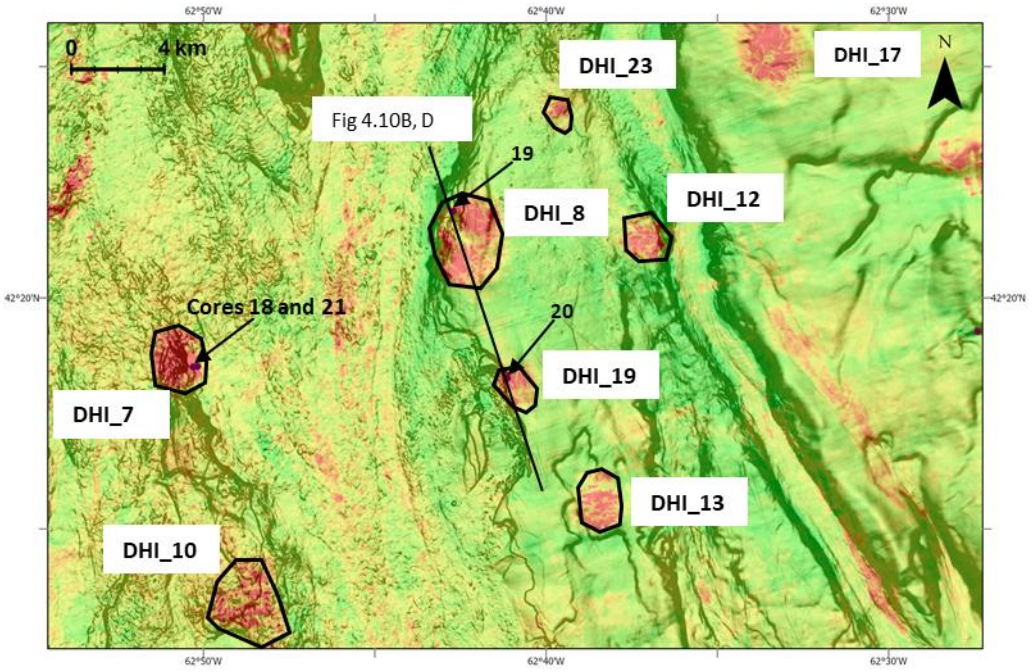

Figure 4.10C. An RMS amplitude snapshot map overlaid on variance seafloor map showing the locations for Cores 19 and 20 and highlighting an area rich with high amplitude anomalies interpreted here as DHIs.

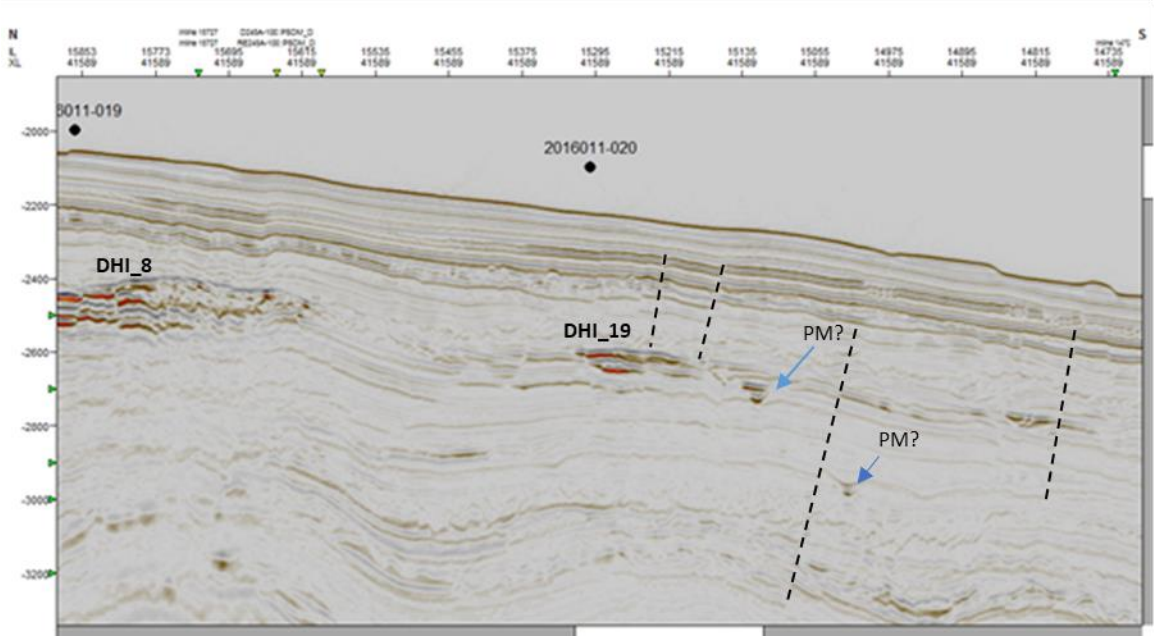

Figure 4.10D. Seismic crossline cross-section for Core 20 2016 Site 20, which is a continuation of the seismic line 4.10B.

Site 20 (Figure 4.10E) appears to have been sampled at what would be the edge of a canyon and down slope from Site 19. The piston core from Site 20 was retrieved at 2190 m and contained sediments composed of sand and mud. The acoustic anomaly was more than 200 m below the seafloor. No notable hydrocarbon signatures were observed (Fowler and Webb, 2017).

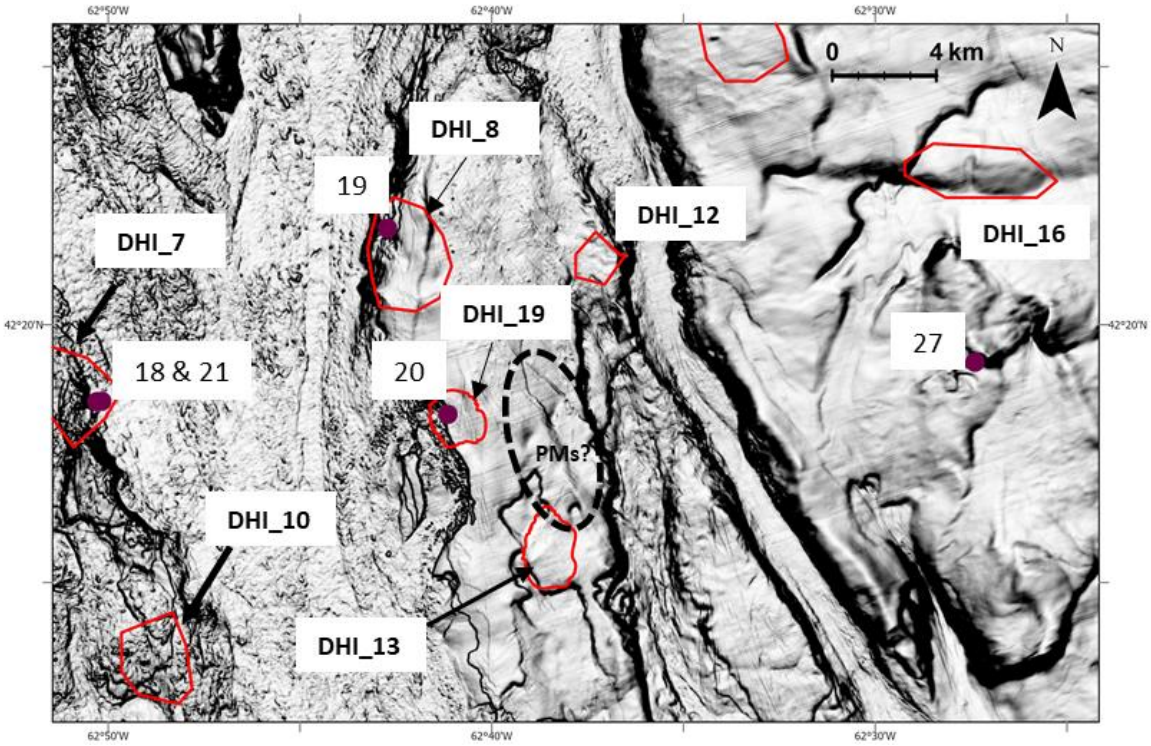

Figure 4.10E. Coherence attribute showing the seafloor surface at Cores 19 and 20 (Cores 18, 21, and 27 also seen here). Red polygons indicate DHI locations. The DHIs appear in between and besides the channels, in an area that likely received considerable sedimentation compared to adjacent canyon systems. The dotted ellipse could potentially be pockmarks (PM) manifesting on the seabed. The 'pockmarks' are also visible in deeper coherence slices.

Coherence attributes at 2500 m (Figure 4.10F) and 2700 m (Figure 4.10G) indicate a high-density network of polygonal and radial faults that interconnect the salt bodies in the area. The complex structures can act as conduits for migrating fluids. Features interpreted as paleo-pockmarks (and contour currents) are also observed at 2700

m below the seafloor (Figure 4.10G) indicating the presence of fluid escape features in this area.

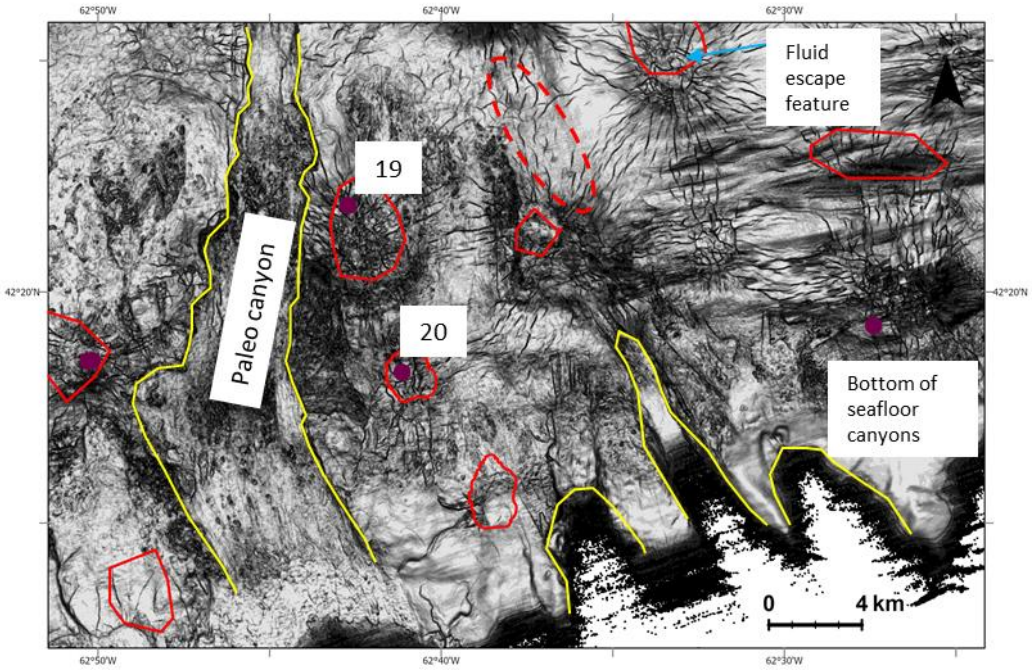

Figure 4.10F. Coherence attribute at 2500 m for Cores 2016-19 and -20. Sediment scouring can be observed on the eastern side of this profile as the wavy variations. The protrusions bounded in the dotted red line are interpreted to be paleo-pockmarks (close to DHI_12) and are better seen when further zoomed in (current scale 1:150000).

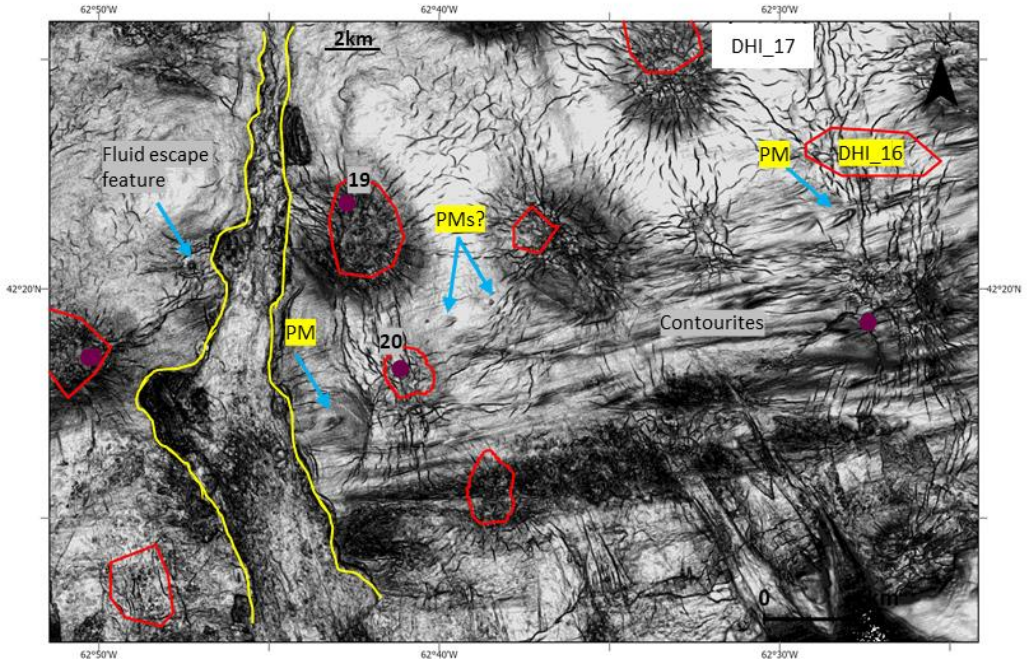

Figure 4.10G. Coherence attribute at 2700 m for Core 2016-19 and -20. PM indicates paleo-pockmarks.

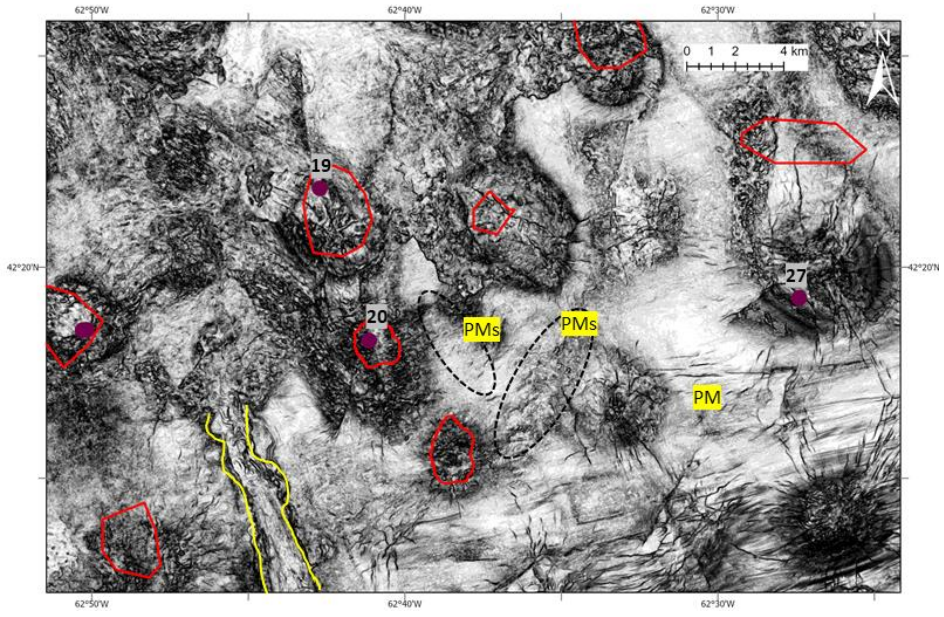

Figure 4.10H. Coherence attribute at 3000 m. Fluid escape features interpreted to be PMs are identified in dotted black ellipses.

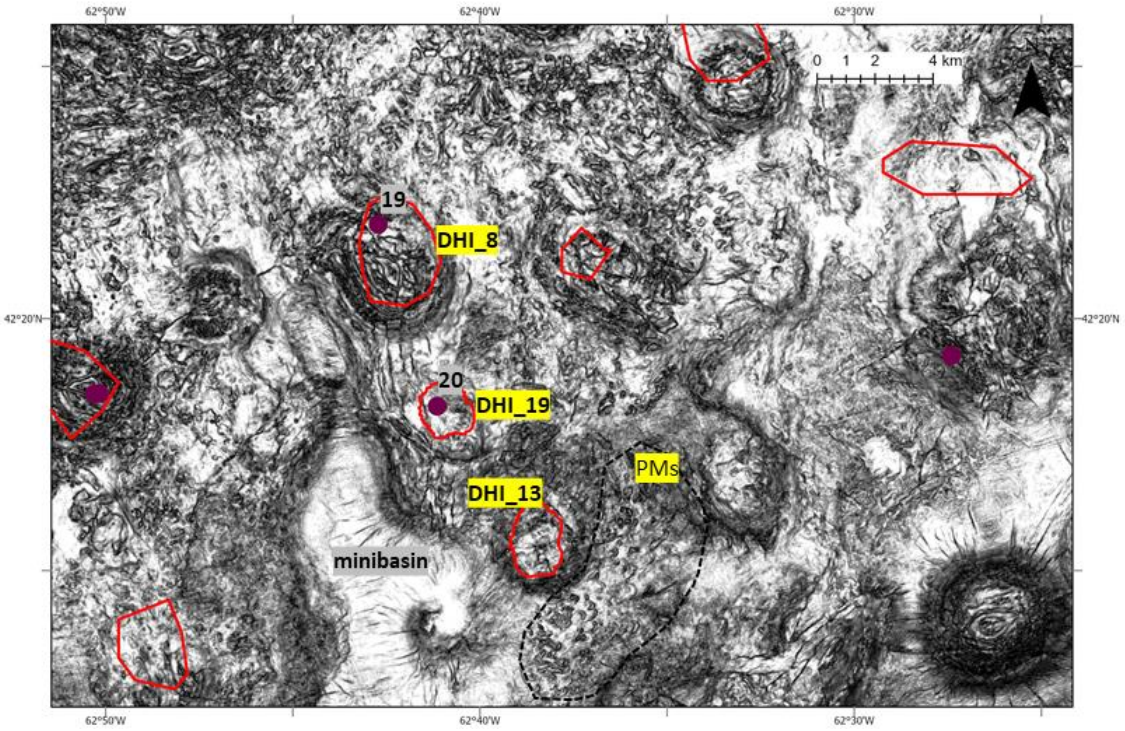

Figure 4.10I. Coherence attribute at 3500 m. Paleo-pockmarks are still visible at this depth and their area seems to expand deeper in the subsurface.

The coherence attribute maps from these two core sites (19 and 20) show paleo-channels (Figure 4.10E) and faulted zones in the shallow subsurface (Figure 4.10F and 4.10G). Based on the interpreted DHI and a network of faults, there would be expectation for Site 19 to show some geochemical indications for hydrocarbon seepage, but this was not so (Fowler and Webb, 2017). It is possible that the corer was too shallow to retrieve sediment with detectable hydrocarbons, or that it did not hit the target.

As pockmarks are an indicator of fluid escape from the subsurface, at this location high amplitude anomalies are interpreted as DHIs. With a network of faults, it is possible that it experiences periodic leaking from a source deeper in the subsurface.

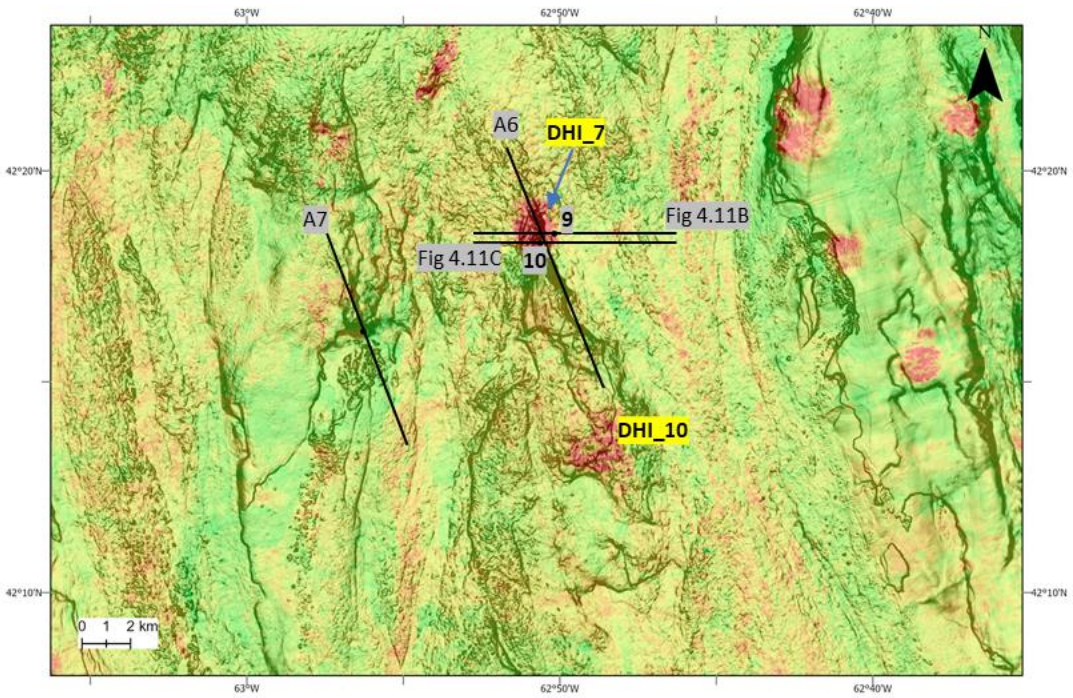

Figure 4.11A. The RMS amplitude map overlaid on a variance seafloor map and showing the location of Cores 9, 10 and 11 (seismic section in Appendix II -A7) from the 2015 expedition. Sites 9 and 10 appear to be on a sediment flow pathway.

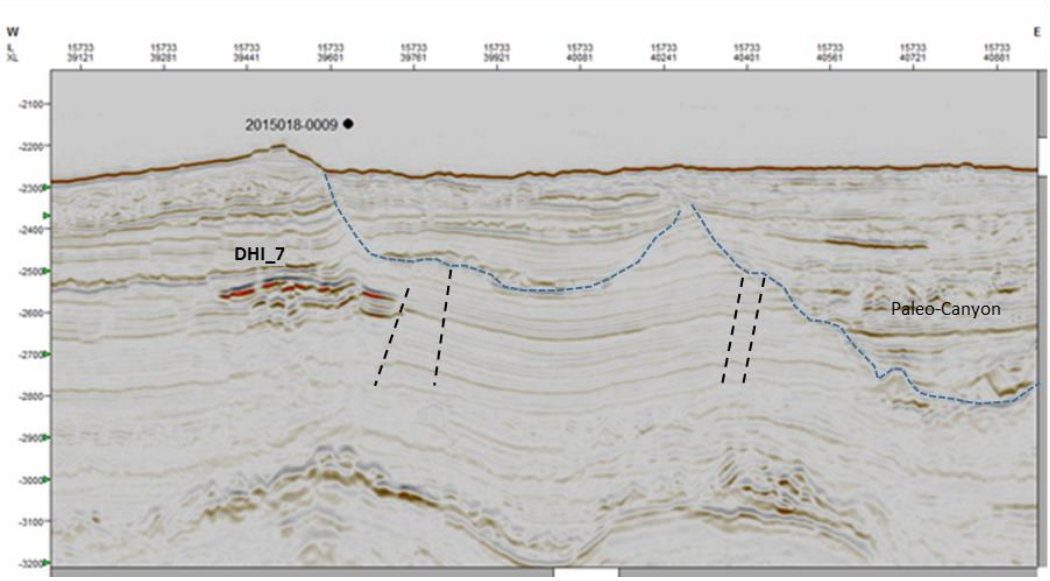

Figure 4.11B. Seismic in-line cross-section for Core 2015-009, which targeted sediment on top of a DHI. The blue dotted line delineates a paleo-canyon margin.

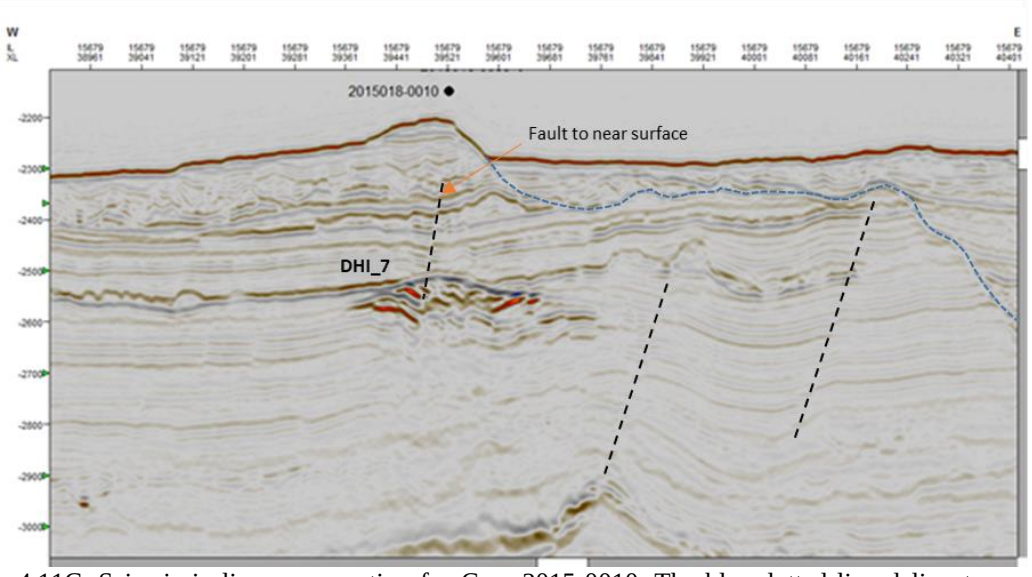

Figure 4.11C. Seismic in-line cross-section for Core 2015-0010. The blue dotted line delineates a paleo-canyon margin.

Site 9 (Figure 4.11B) and 10 (Figure 4.11C) show acoustic anomalies in the seismic sections that are interpreted as DHIs. The crossline (Appendix II-A6) indicates a fault that propagates to surface.

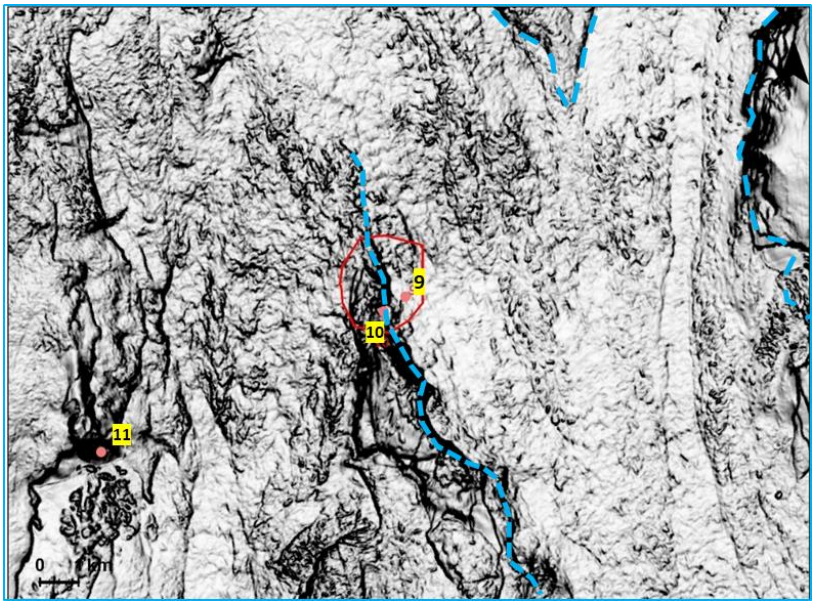

Figure 4.11D. Coherence attribute showing the seafloor surface at Cores 9 and 10 were collected at the margin of a canyon system. The blue dotted lines show the modern canyon relief.

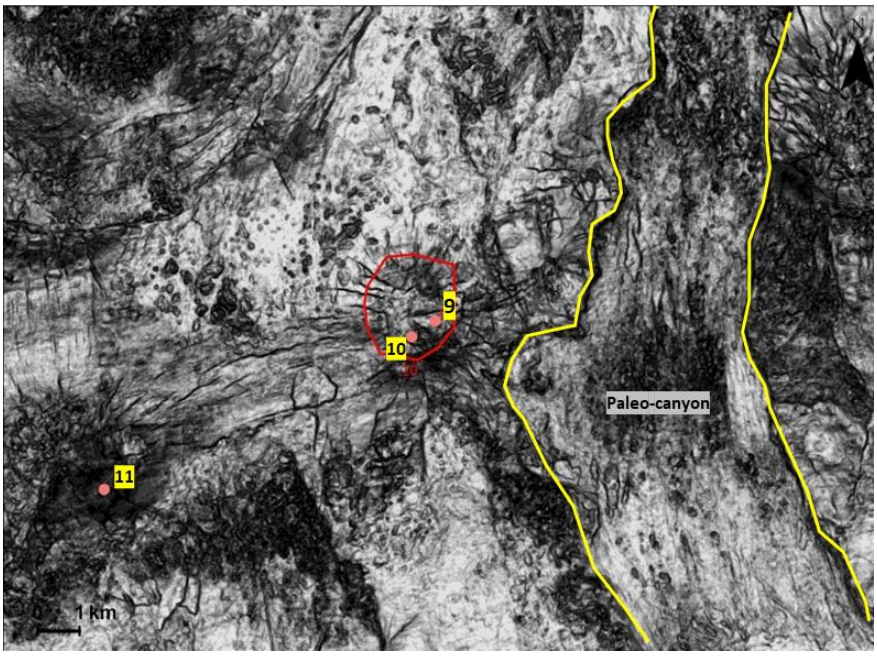

Figure 4.11E. Coherence attribute at 2500 m for sample 2015 Core 9 and 10. DHI_7 in the red polygon. Salt induced radial fracturing above the diapir crest is observable with faults linking the doming crests of diapir roofs.

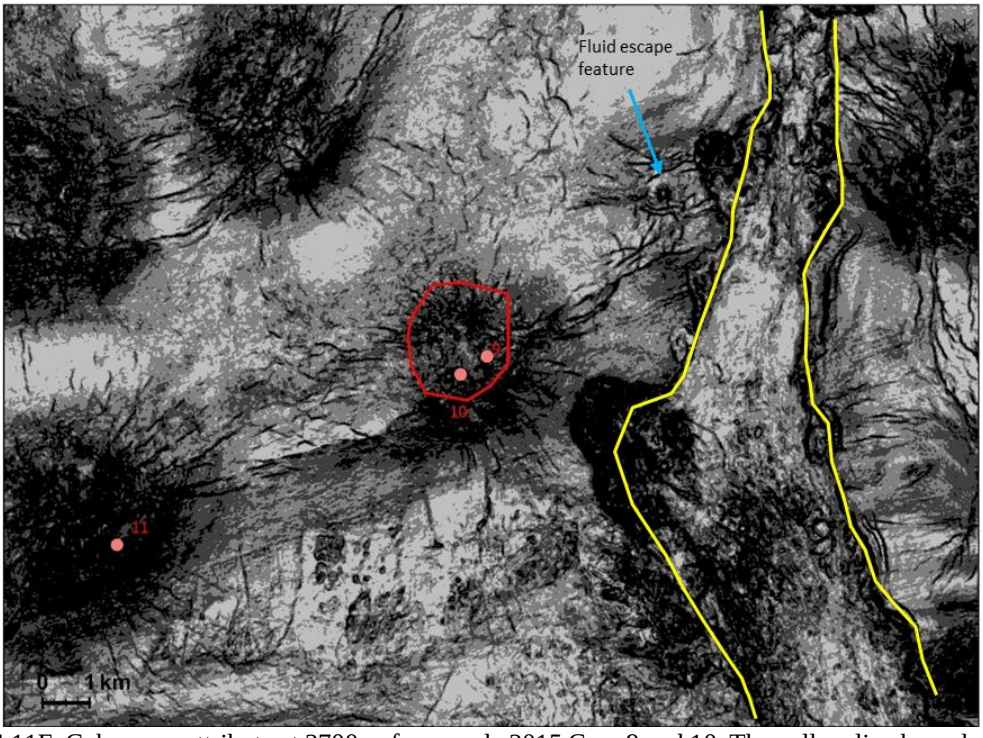

Figure 4.11F. Coherence attribute at 2700 m for sample 2015 Core 9 and 10. The yellow line bounds a paleo-canyon.

The sediment core samples were collected on an area with a high relief, likely the edge of a channel/canyon system as visible from the coherence attribute surface map

(Figure 4.11D). Underlying the surface geomorphology is a network of faults observed at 2500 m (Figure 4.11E) and 2700 m (Figure 4.11F). The piston core samples were collected right on top of an anomaly interpreted as DHI_7. The seismic sections did not indicate the presence of a highly faulted interval but there was a fault terminating near surface for Site 10 (Figure 4.11C; A6 in Appendix II). In geochemical analysis, Site 9 did provide evidence of a mixed biogenic-thermogenic methane with the thermogenic hydrocarbons likely derived from a petrogenic source (Fowler and Webb, 2015). Sediment coring at Site 10 did not produce geochemical evidence of gas seepage. It is plausible that the corer might have sampled sediment some distance away from the hosting sediment or did not penetrate deep enough into the subsurface to reach hydrocarbon bearing sediments.

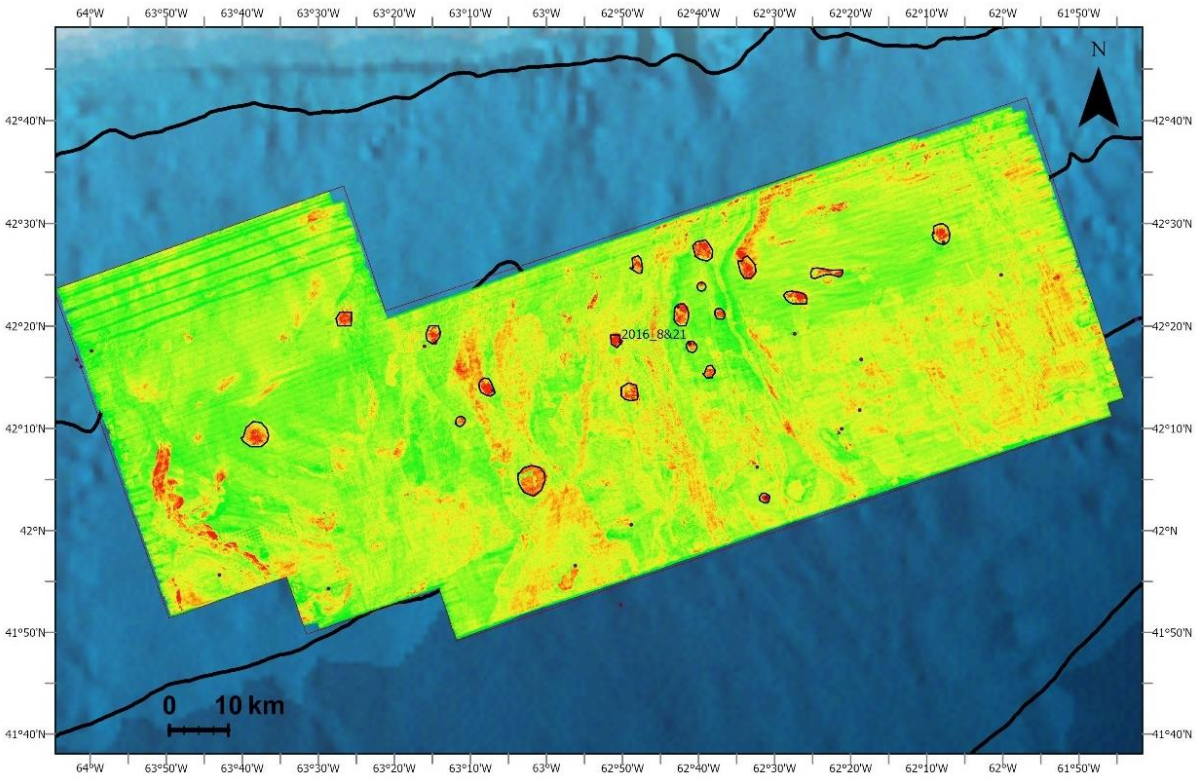

Figure 4.12A. The RMS amplitude showing the location for sample 2016 Site 18 and 21.

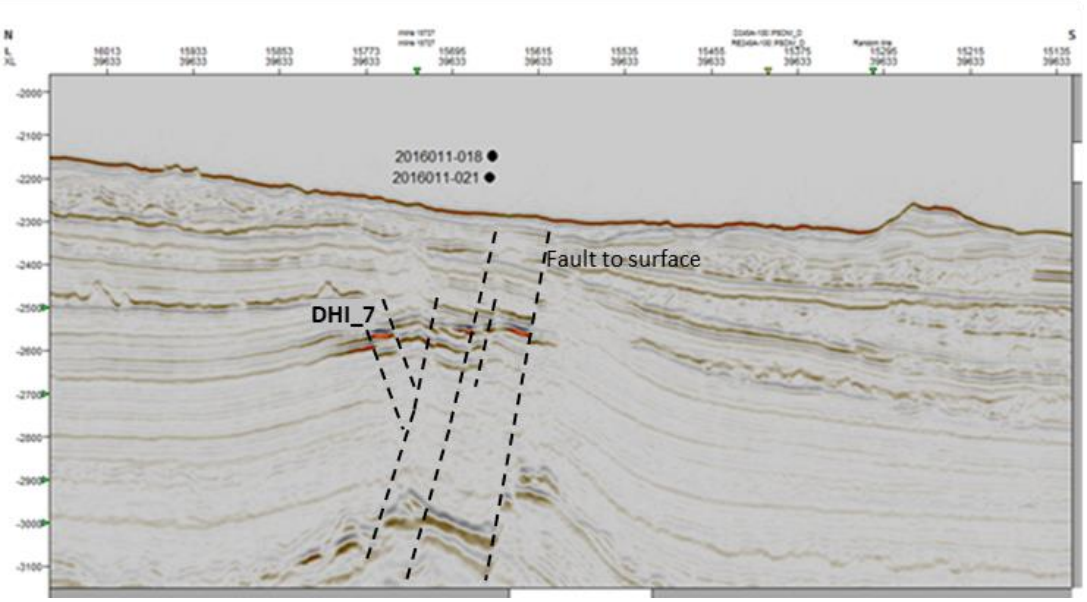

Figure 4.12B. Seismic crossline cross-section for Core 2016-018 and -021 targeting sediments overlying a DHI that is about 300 m from the seafloor surface.

Cores 2016-018 and -021 targeted the same feature as Core 2015-009 and -010. Because Site 009 had shown geochemical evidence of thermogenic hydrocarbons, the site was re-visited in the 2016 coring cruise. The vertical seismic cross-sections (Figure 4.12B) may indicate hydrocarbon migration with the presence of a high-amplitude anomaly that is interpreted as a DHI (i.e., DHI_7). The DHI at this location is intersected by a fault that terminates at the ocean seabed. In the geochemical analysis, Site 18 and 21 both showed evidence for gas seepage and cores had a strong sulfuric smell (Fowler and Webb, 2017). Sediment from Site 18 did not display contributions of petrogenic hydrocarbons and is likely biogenic gas. The headspace gas samples from the core taken at Site 21 produced a component of thermogenic gas. Like Site 9 from the 2015 coring program, Site 21 showed indications of having thermally mature hydrocarbons (Fowler and Webb, 2017). It is plausible hydrocarbons are migrating from a subsurface leaky reservoir that lacks continuous sealing capacity through the pathway to the surface.

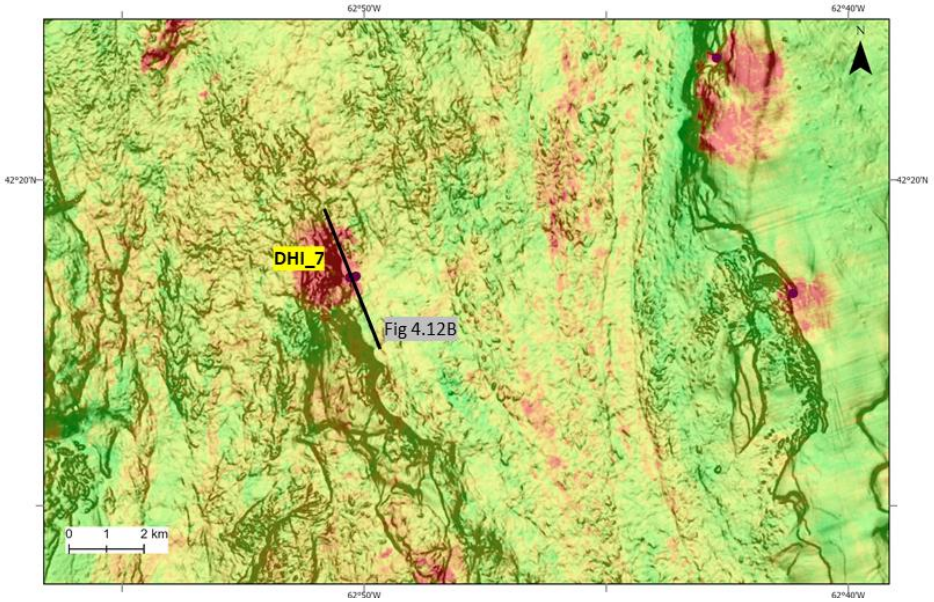

Figure 4.12C.The RMS amplitude snapshot at Core 2016_18 and _21 overlaid on a variance seafloor map.

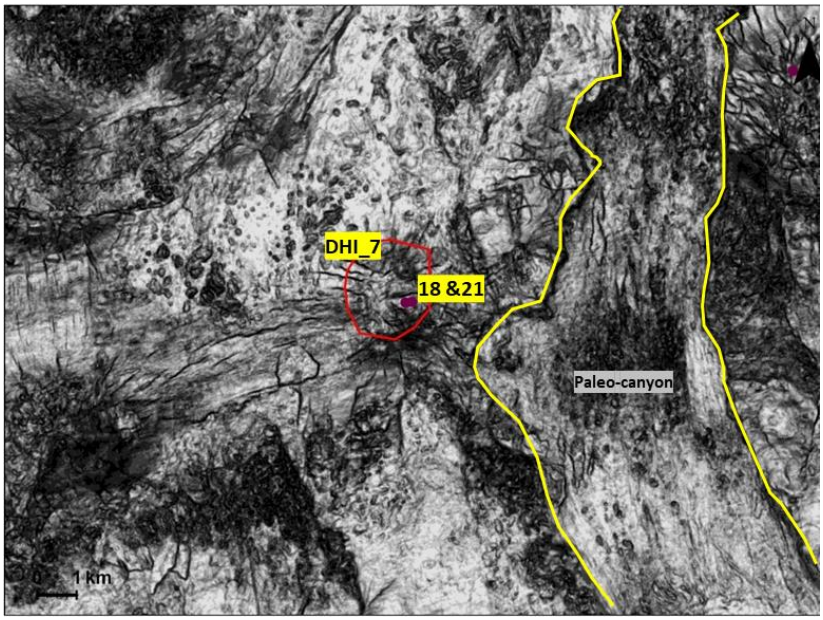

Figure 4.12D. Coherence attribute for cores 2016 Sites 18 and 21 at 2500 m, same as that of Core 2015-9 and -10.

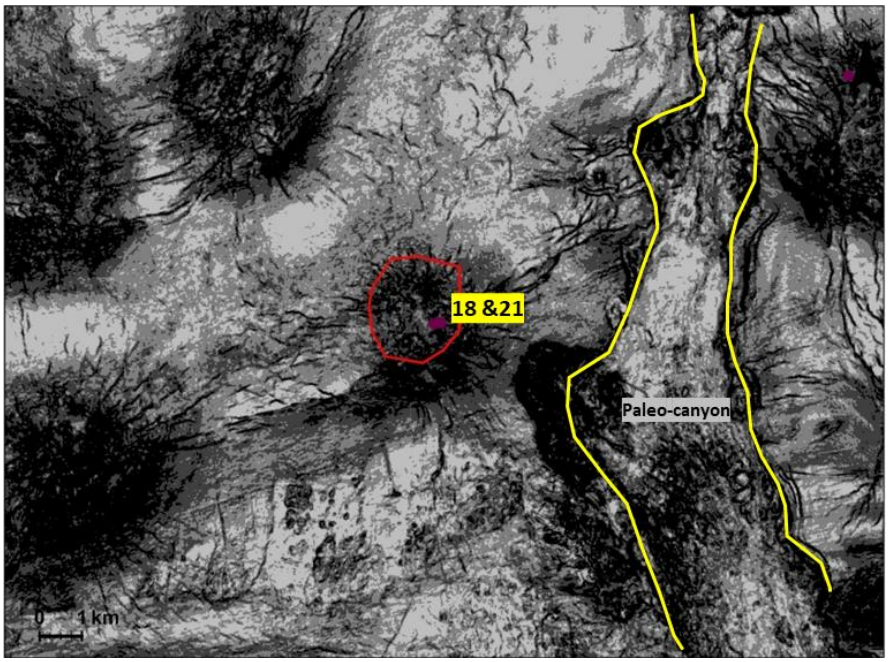

Figure 4.12E. Coherence attribute at 2700 m for Core 2016-18 and -21. It is hard to interpret what the mottled features on this depth slice are in both the 2015 and 2016 samples.

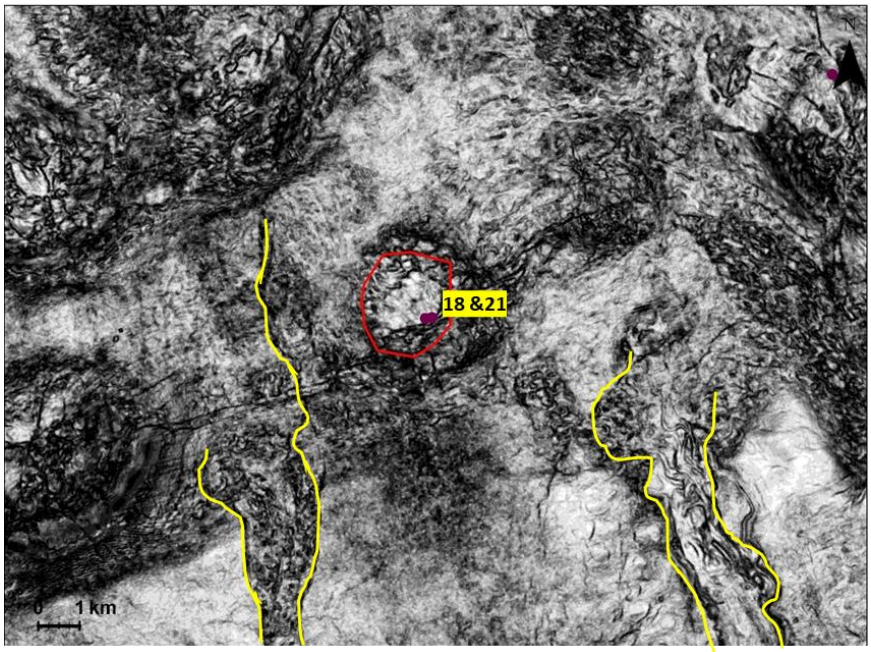

Figure 4.12F. Coherence attribute at 3000 m. Paleo-canyons bounded in yellow lines can be observed at this depth. The red polygon is DHI_7.

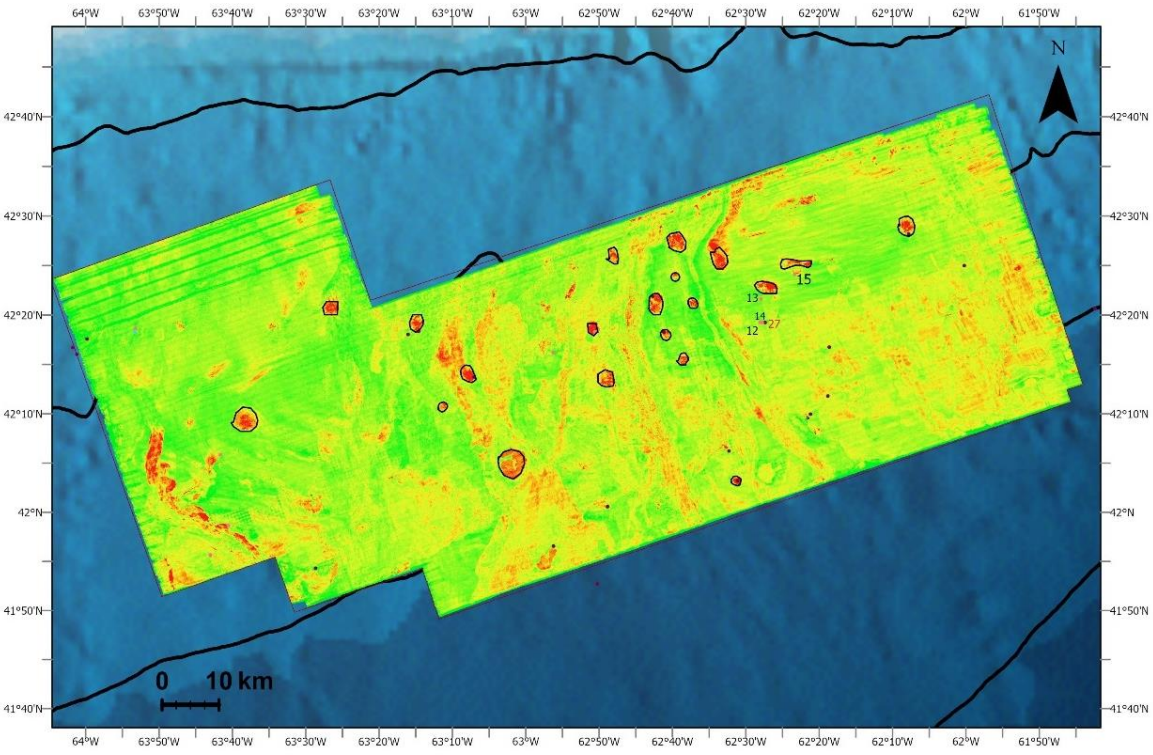

Figure 4.13A. The RMS amplitude map showing the location for samples 2015 Sites 12, 13, 14 and 15; and sample 2016 Site 27.

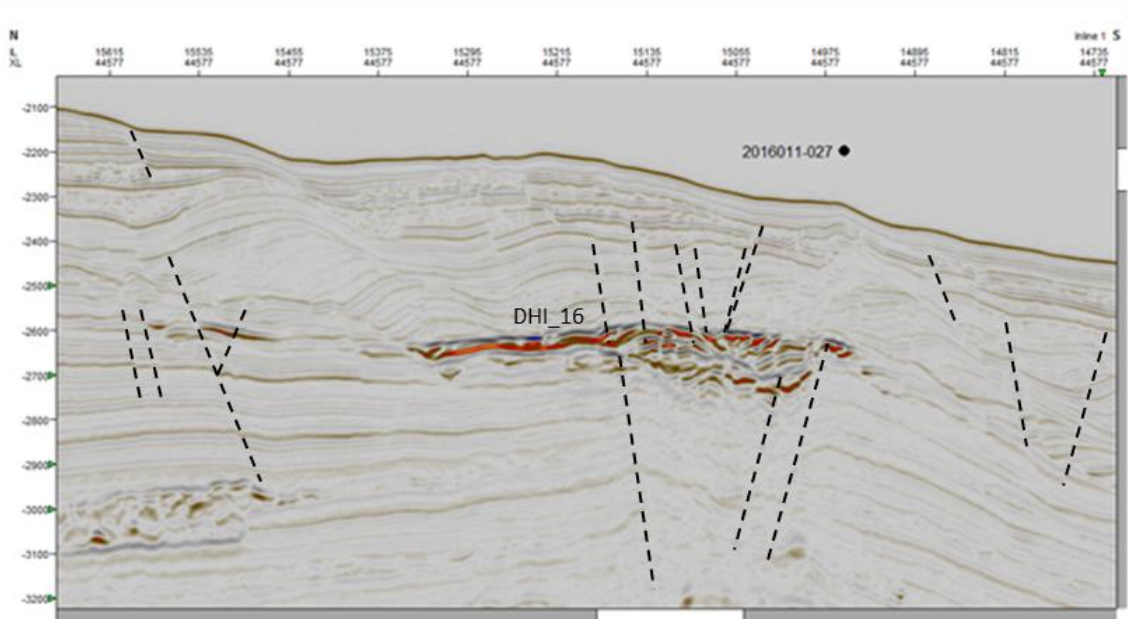

Figure 4.13B. Seismic crossline cross-section for sample 2016 Core 27, which did not show any notable hydrocarbon signatures in the geochemistry analysis and core.

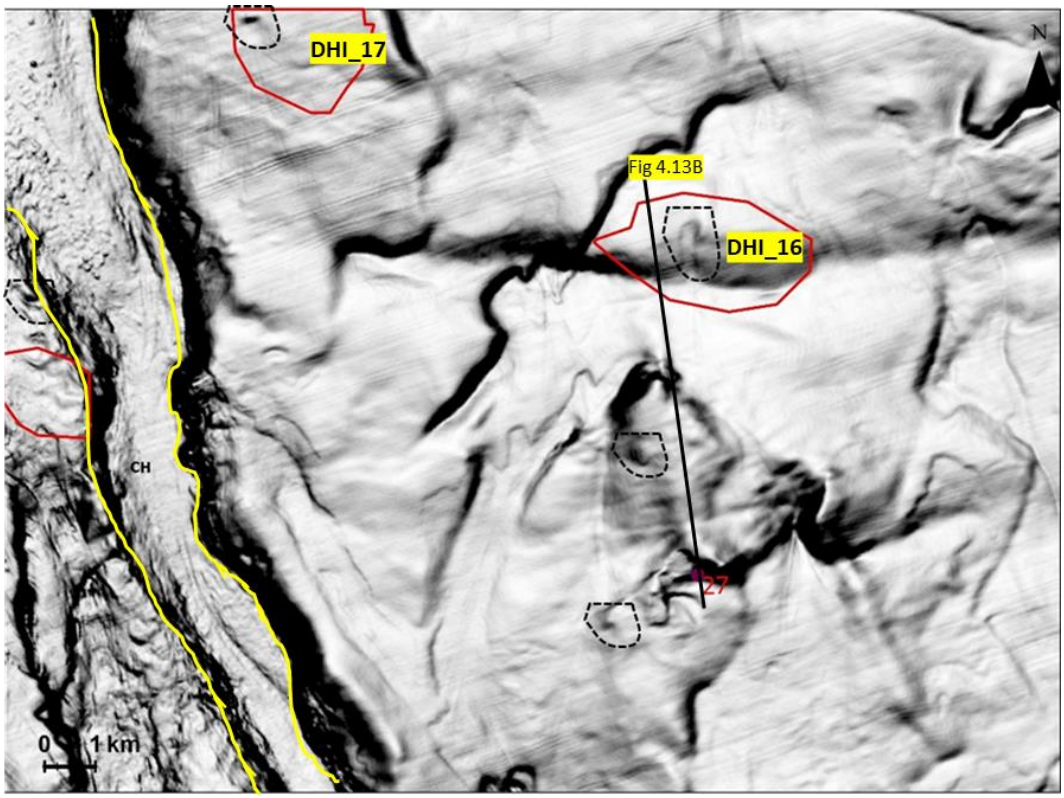

Figure 4.13C. Coherence attribute showing the seafloor surface at sample 2016 Core 27. CH indicates a channel/canyon system. The red polygons indicate locations of anomalies interpreted as DHIs. The dotted black polygons are hypothesised to be fluid escape features.

Core 2016_027 was collected in proximity of sites 12 and 14 from the 2015 cruise. In the seismic section (Figure 4.13B), the near surface sediment indicates presence of an acoustic anomaly, which is interpreted as a DHI in a highly faulted zone west of the Mohican Canyon channel system. It appears the core did not retrieve sediment with hydrocarbon signatures for this site (Fowler and Webb, 2017).

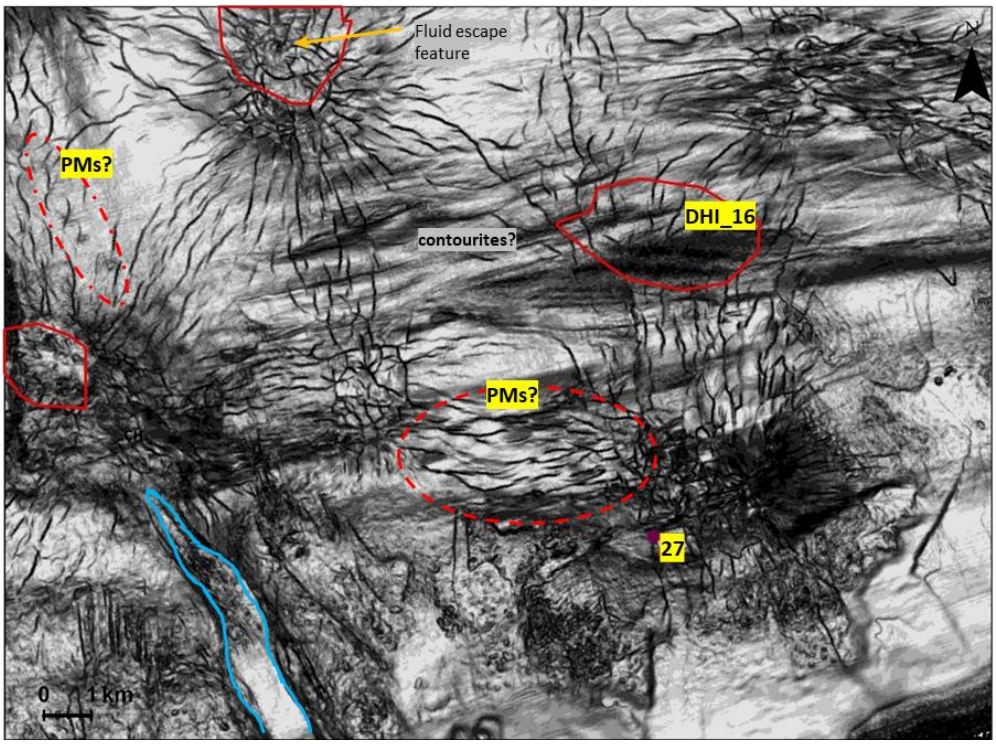

Figure 4.13D. Coherence attribute at 2500 m for Core 2016-027. The surface shows a network of crestal faults interconnecting the salt bodies. Sediment waves caused by contour currents are also observed. The blue lines indicate a canyon.

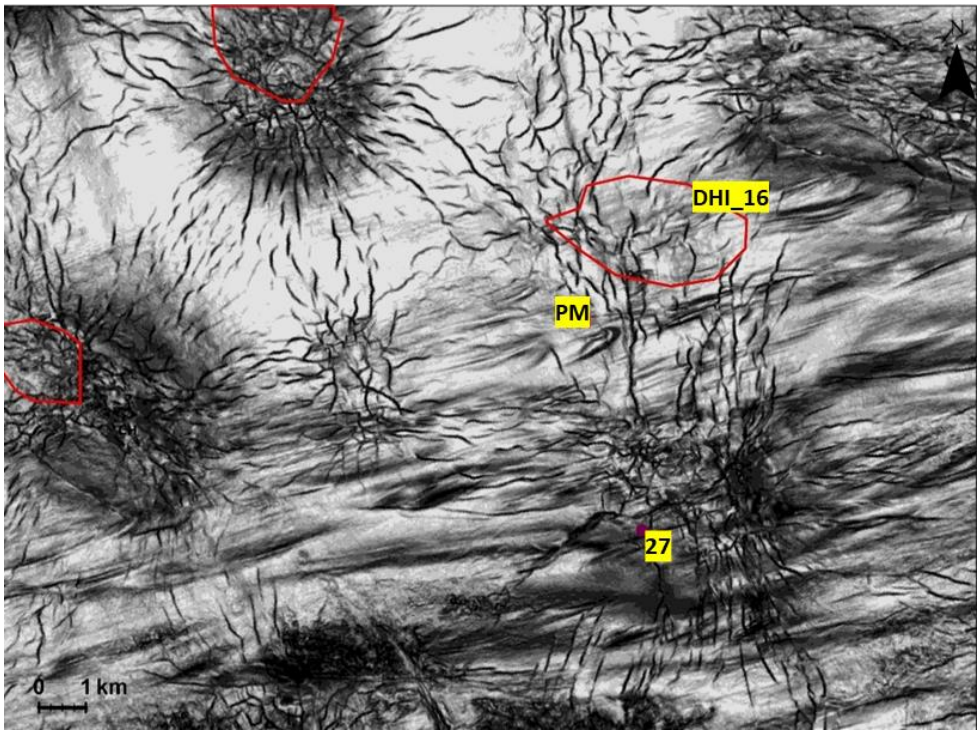

Figure 4.13E. Coherence attribute at 2700 m for Core 2016-27.

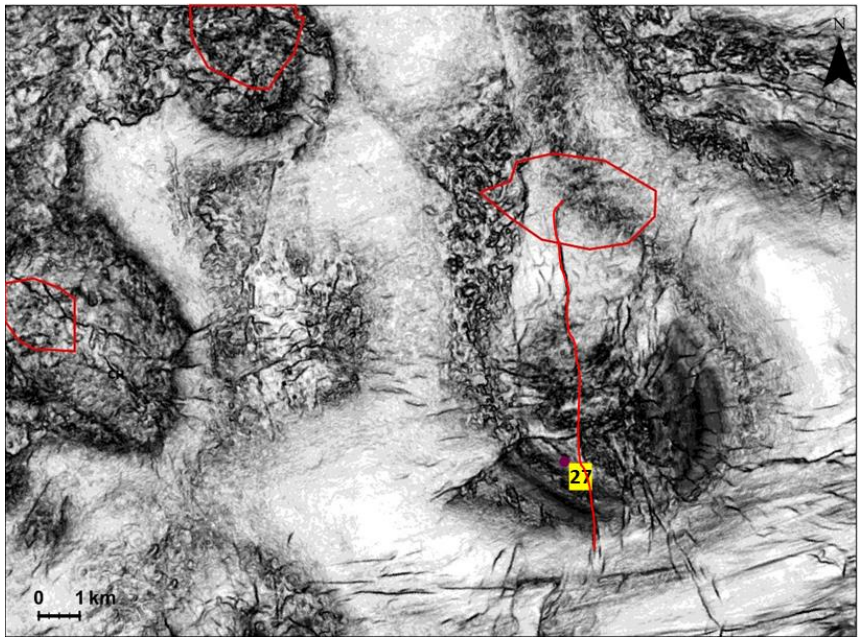

Figure 4.13F. Coherence attribute at 3000 m for Core 2016-27. The red vertical line is interpreted as the fault that originates from the subsurface and that terminates just below the surface on Figure 4.13G.

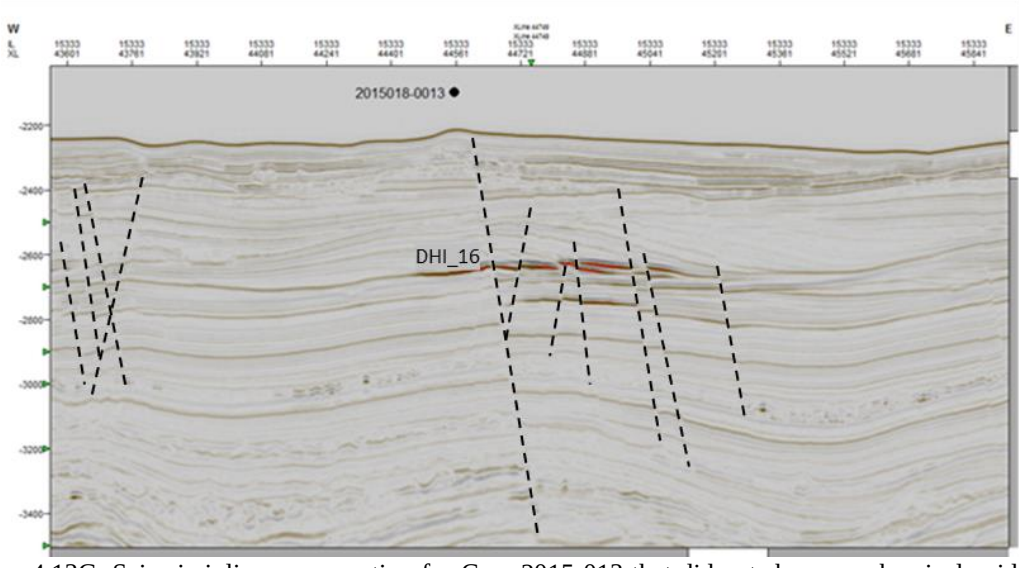

Figure 4.13G. Seismic inline cross-section for Core 2015-013 that did not show geochemical evidence for gas.

Site 2015-013 is located north of Sites 2015-012, -014, and 2016-027 (Figure 4.13A). The vertical seismic section (Figure 4.13G) indicates an acoustic anomaly in a highly faulted interval of relatively uniform stratigraphic sequence below the anomaly. Above is a canyon that onlaps the anomaly. A fault terminating at surface cuts through

the anomaly and a bump is observed on the seafloor that could potentially be a feature relating to fluid migration (see 4.14D and F) for fluids migrating through the fault. However, the geochemical data for this core sample did not show indications of hydrocarbon seepage. It is possible the corer did not sample deep enough or hit the seep. It is also likely that migration from the shallow accumulation, if present, is impeded.

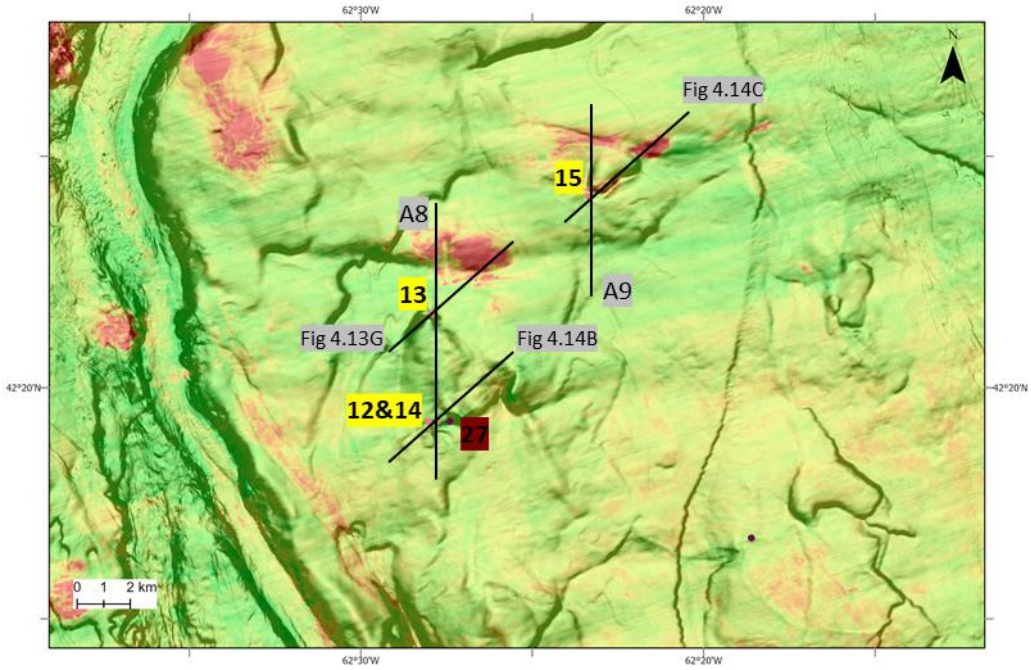

Figure 4.14A. An RMS amplitude map snapshot overlaid on variance seafloor map for Cores 2015-12, -13, -14, and -15.

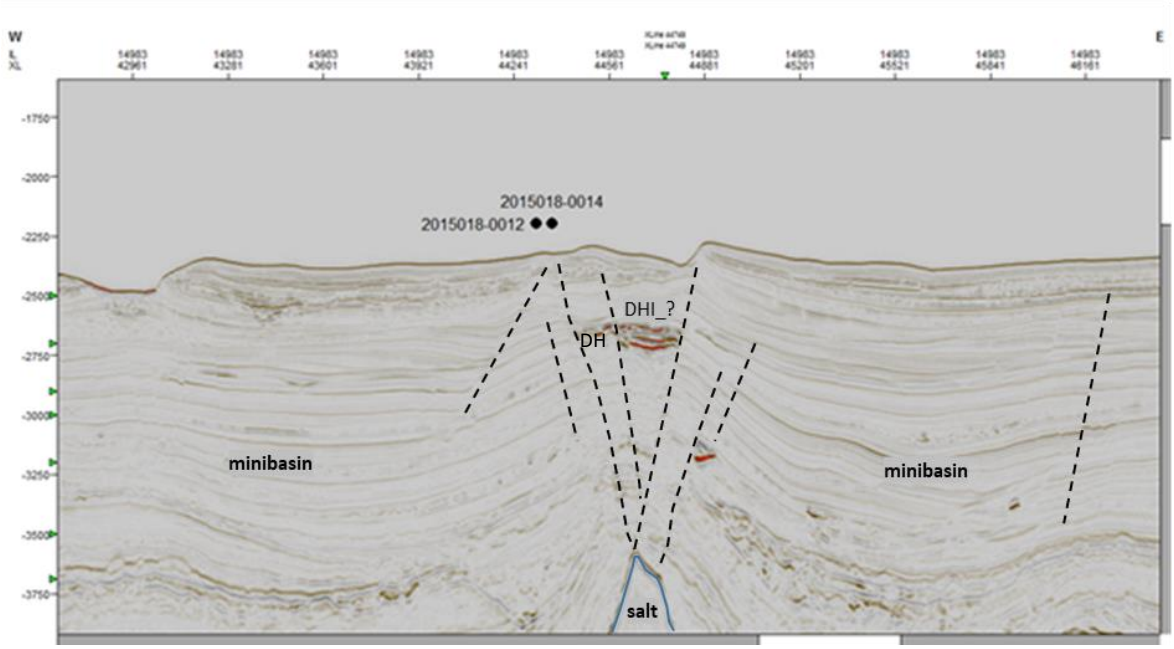

Figure 4.14B. Seismic inline cross-section. Cores 2015-012 and -014 did not show any geochemical evidence for gas seepage and appears to have sampled some distance away from the anomaly. While this DHI is not apparent on the RMS amplitude map, it is plausible that it is sourcing form DHI_16 (e.g., see A8 in Appendix II that cuts through Cores 13 and 14 with DHI_16 being observed in a highly faulted interval).

Cores 2015-012 and 14 show the presence of a DHI in the vertical seismic section (Figure 4.14B). The seafloor surface on the seismic section shows slump scarps (Figure 4.14D). The coherence attributes indicate salt-related faults reaching the surface, and a fault cutting through the salt that could be the cause of the slump to the east of the piston coring location. The geochemical data did not show indications of hydrocarbon seepage (Fowler and Webb, 2015), and it is plausible these samples were off target.

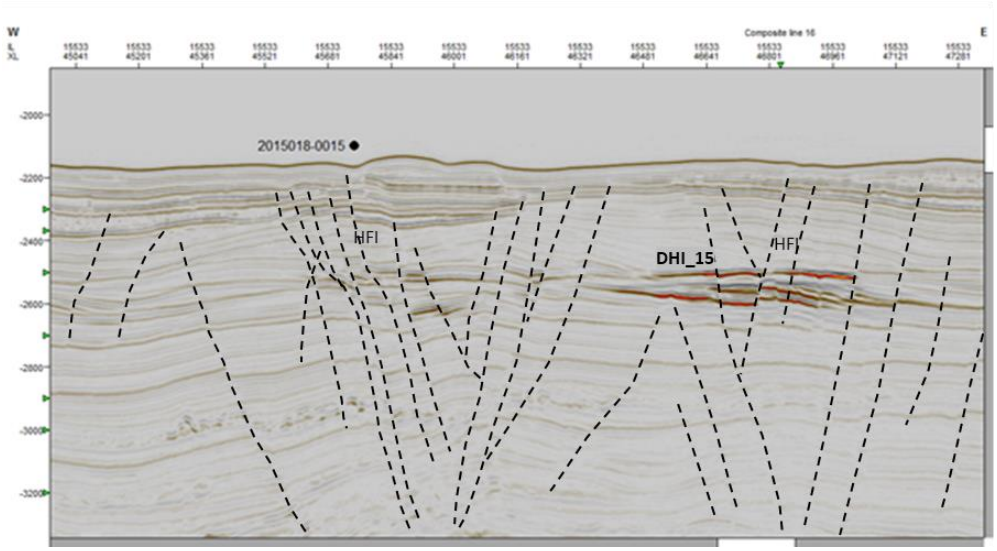

Figure 4.14C. Core 2015-0015 did not show geochemical evidence for gas. It was sampled in a zone with faults terminating at surface but away from DHI_15.

Site 2015-015 shows a highly faulted interval in the vertical seismic (Figure 4.14C; A9). In the coherence attributes, it becomes clear that this region has a system of interconnected salt-related anticlinal structures linked by a network of faults (e.g., Figure 4.14E). Geochemical analysis for this site did not show any indications of hydrocarbon seepage.

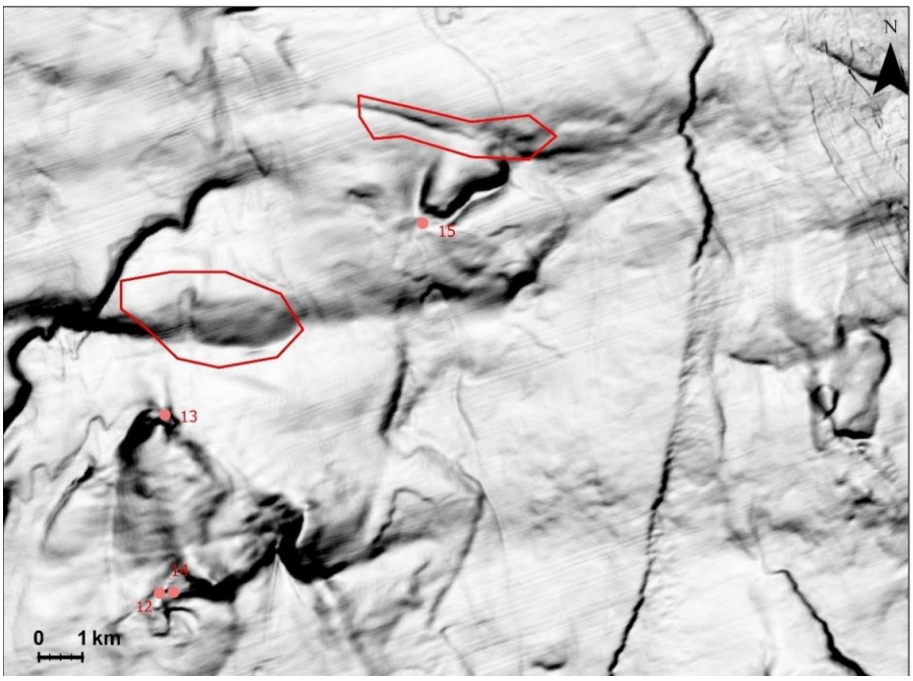

Figure 4.14D. Coherence attribute showing the seafloor surface for Cores 2015-12, -13, -14 and -15.

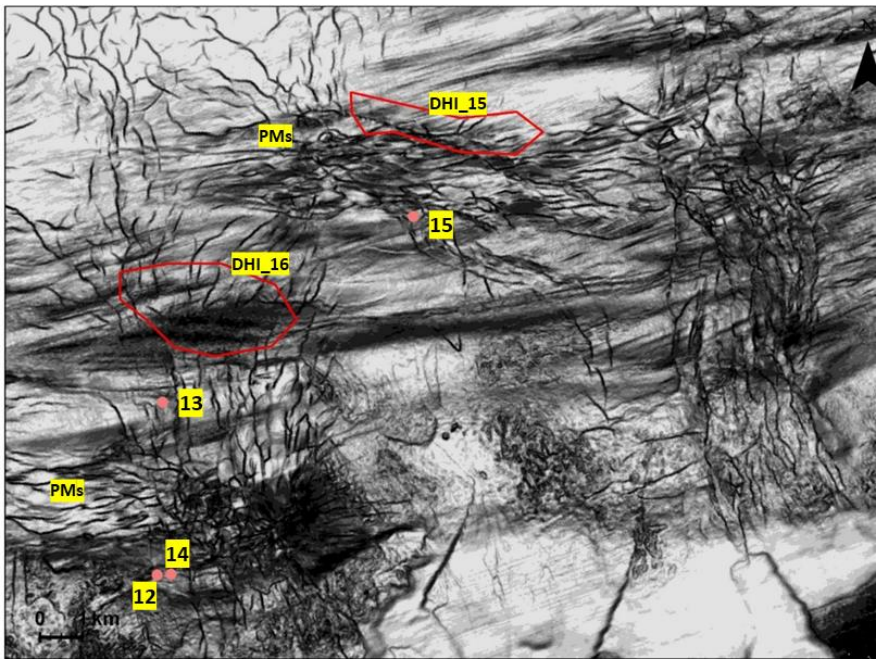

Figure 4.14E. Coherence attribute at 2500 m for cores 2015-12, -13, -14 and -15. Sediment waves are observed, and the salt-related anticlines are interconnected by a network of faults and salt-induced fractures.

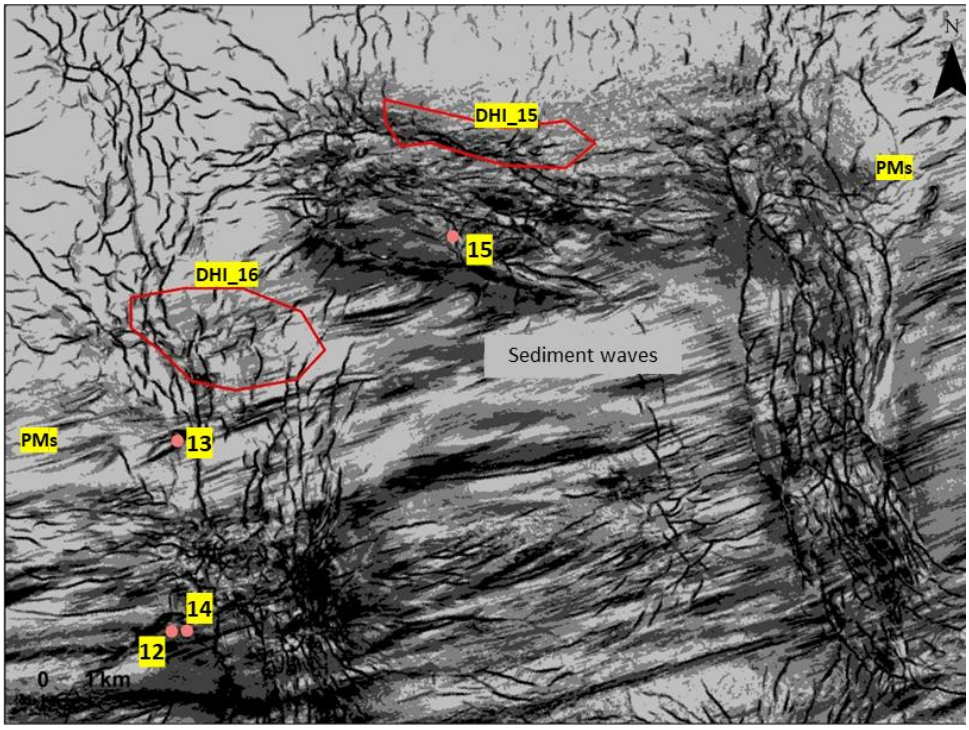

Figure 4.14F. Coherence attribute at 2700 m.

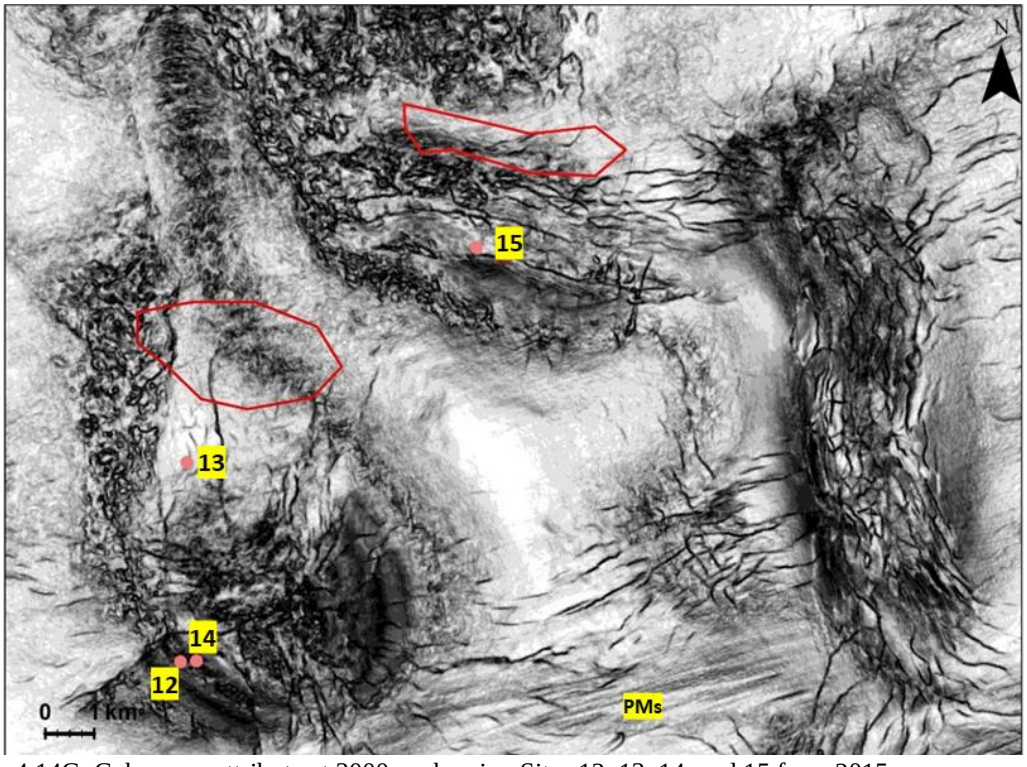

Figure 4.14G. Coherence attribute at 3000 m showing Sites 12, 13, 14, and 15 from 2015.

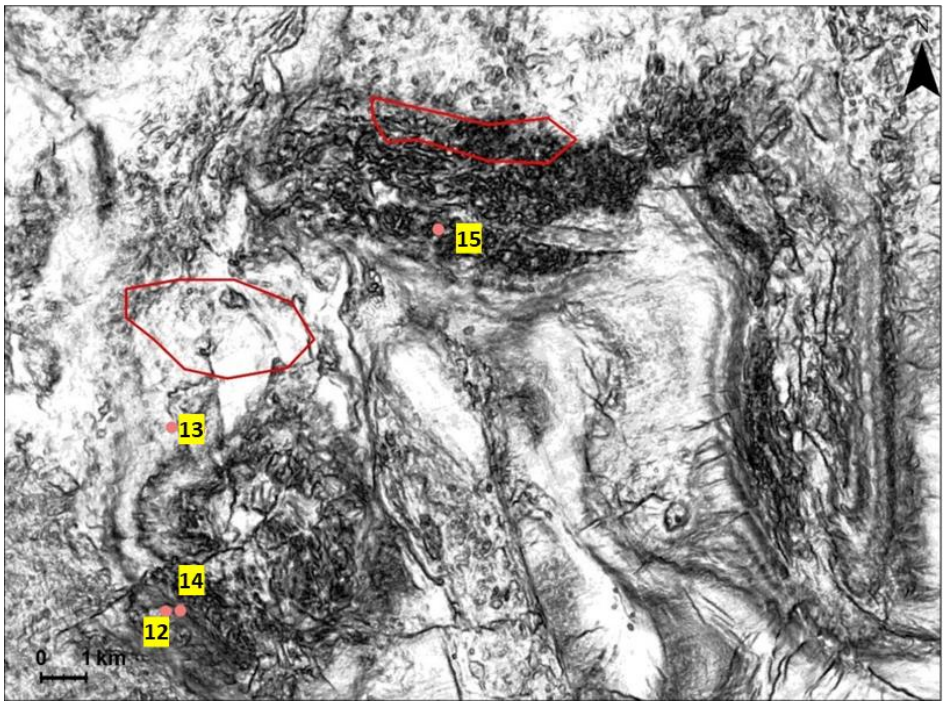

Figure 4.14H. Coherence attribute at 3500 m showing Sites 12, 13, 14, and 15 from 2015. No fluid escape features are observed at this depth.

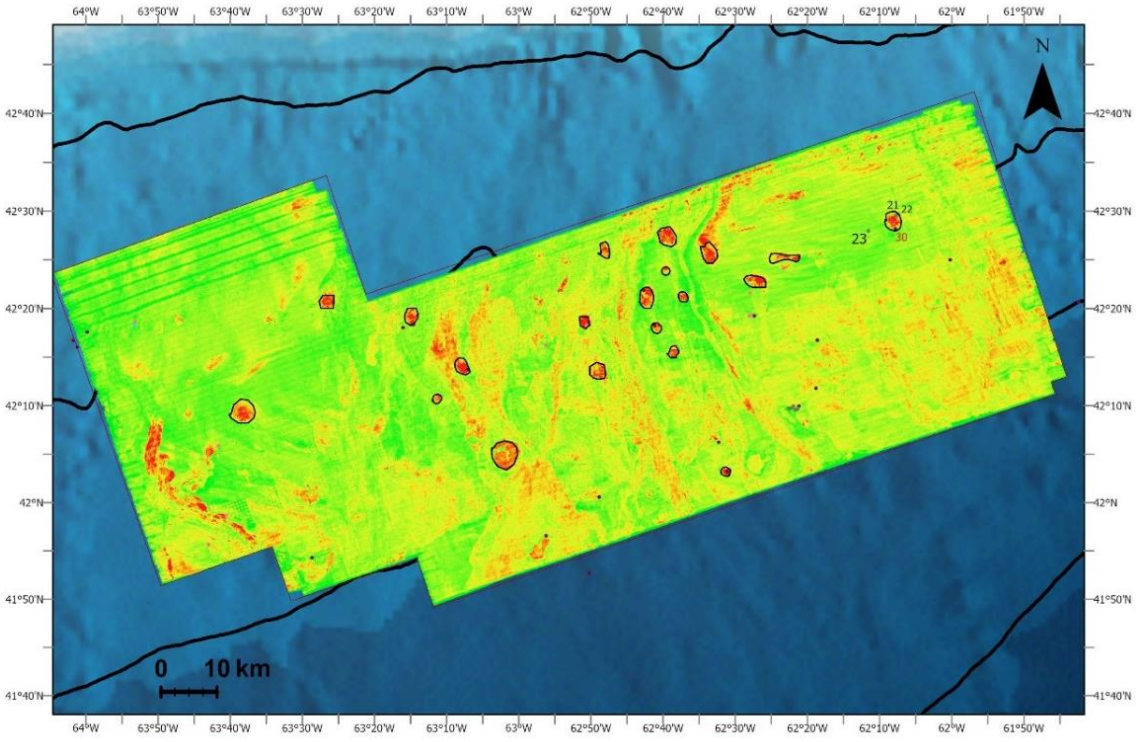

Figure 4.15A. The RMS amplitude map showing locations for sample 2016 Site 30 and 2018 Sites 21, 22, and 23. Samples targeted sediment atop an acoustic anomaly interpreted as a DHI.

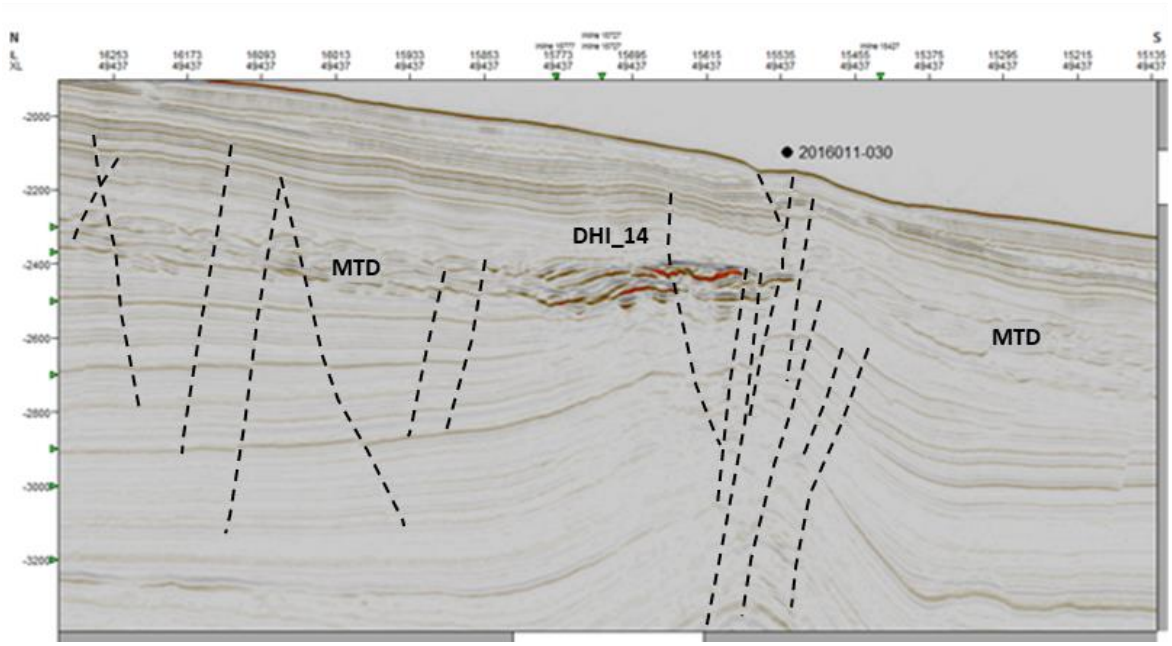

Figure 4.15B. The seismic crossline cross-section for sample 2016 Site 30 (retrieved at a water depth of 2106 m) shows a DHI about 400 m below the sea floor in this location. The sample did show large amounts of light hydrocarbons in the geochemical analysis but not of a thermogenic origin. The DHI is accumulated in a zone of chaotic/incoherent reflections (MTD) and could be hydrocarbons of biogenic origin.

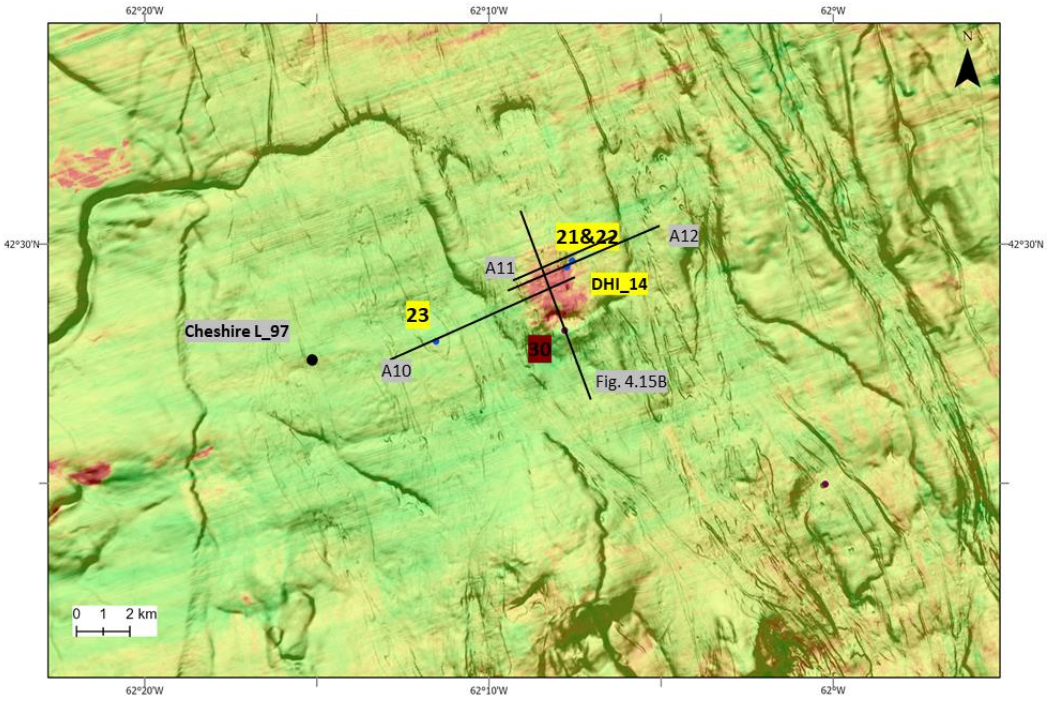

Figure 4.15C. The RMS amplitude map snapshot overlaid on variance seafloor map for Cores 2018-21, -22 and -23; and Core 2016-030. See Appendix II for A10, 11, 12.

Core 2016-030 is located above a DHI in the near surface sediment (Figure 4.15C). The vertical seismic section (Figure 4.15B) shows disturbance along the length of the salt-related anticline on whose crest the acoustic anomaly is hosted. In the coherence attributes, possible fluid escape features are observed west of this site in the form of rounded and crescent-shaped structures interpreted as paleo-pockmarks (Figure 4.16C). The geochemical analysis did indicate presence of hydrocarbon seepage for site 30, but not from a petrogenic source (Fowler and Webb, 2017).

Sites 2018-021 and -022 were located approximately 3 km north of Site 2016-030. The coherence attributes show the zone is highly faulted (Figure 4.16B; see seismic sections in A11, A12) and the RMS amplitude map indicates they were retrieved at the edge of a high amplitude anomaly interpreted as a DHI (Figure 4.15C). Geochemical analysis of 2018 Site 21 showed signatures of *n*-alkane biodegradation and shows the possibility of being in proximity to a hydrocarbon seep. However, the sediment analysis did not have supporting evidence for the presence of thermogenic gases; Site 22 did not have indications of being in proximity of a seep even though it was sampled only 100 m away from Site 21 (Fowler and Webb, 2019). Seismic sections (Appendix II A11, A12) indicate the possibility of a seep at this site.

Site 2018-023 located west of the Cheshire well was sampled closest to the field of pockmarks seen in the coherence attributes (Figure 4.16C). The seismic cross section (A10) indicates a highly faulted zone and pockmark like features at approximately 2650 m water depth. Geochemical analysis indicates modest TOC content (0.69%) but did not show evidence of petroleum seepage (Fowler and Webb, 2018). The core may have been off target.

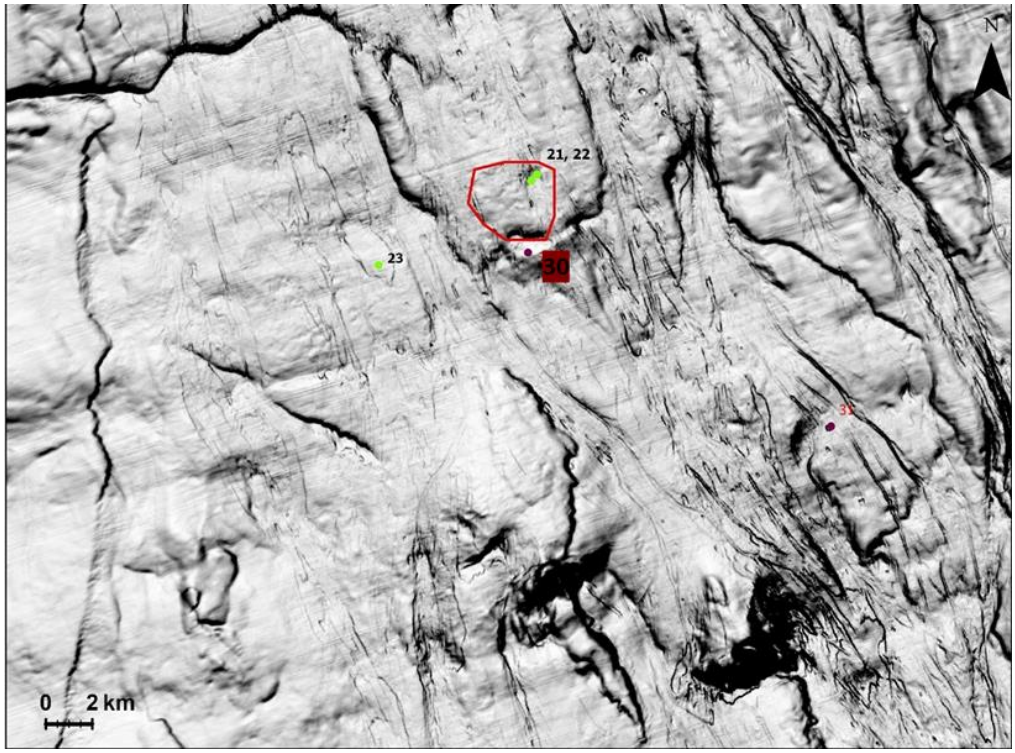

Figure 4.16A. Coherence attribute showing seafloor surface.

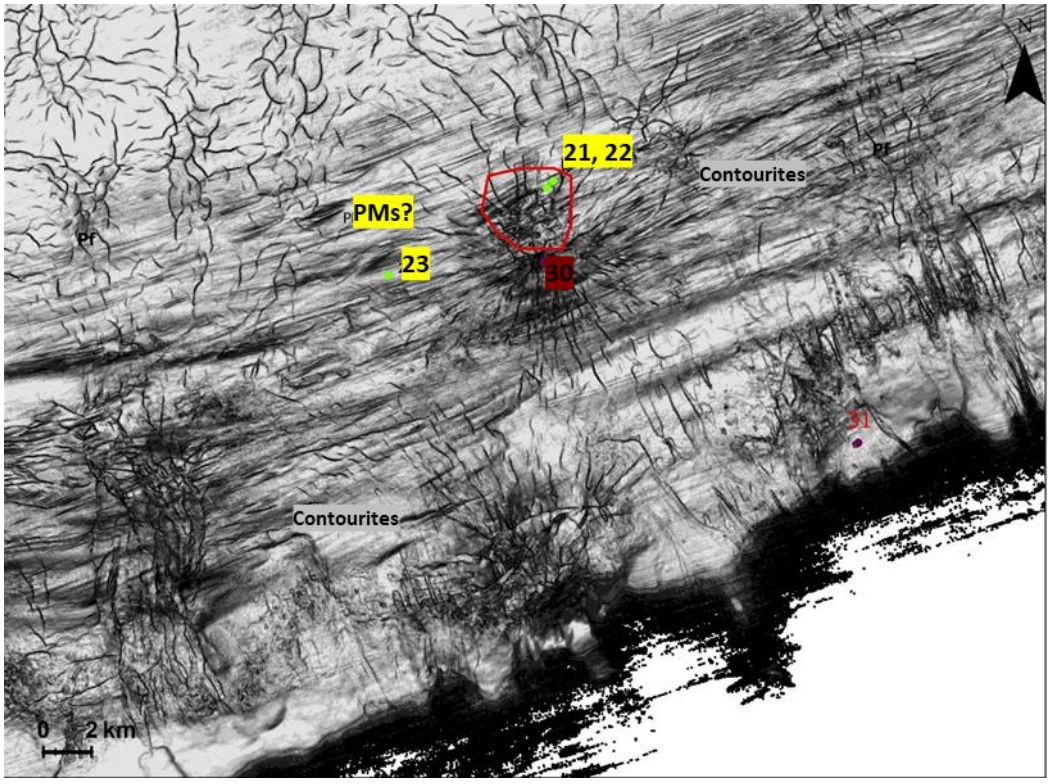

Figure 4.16B. Coherence attribute at 2500 m.

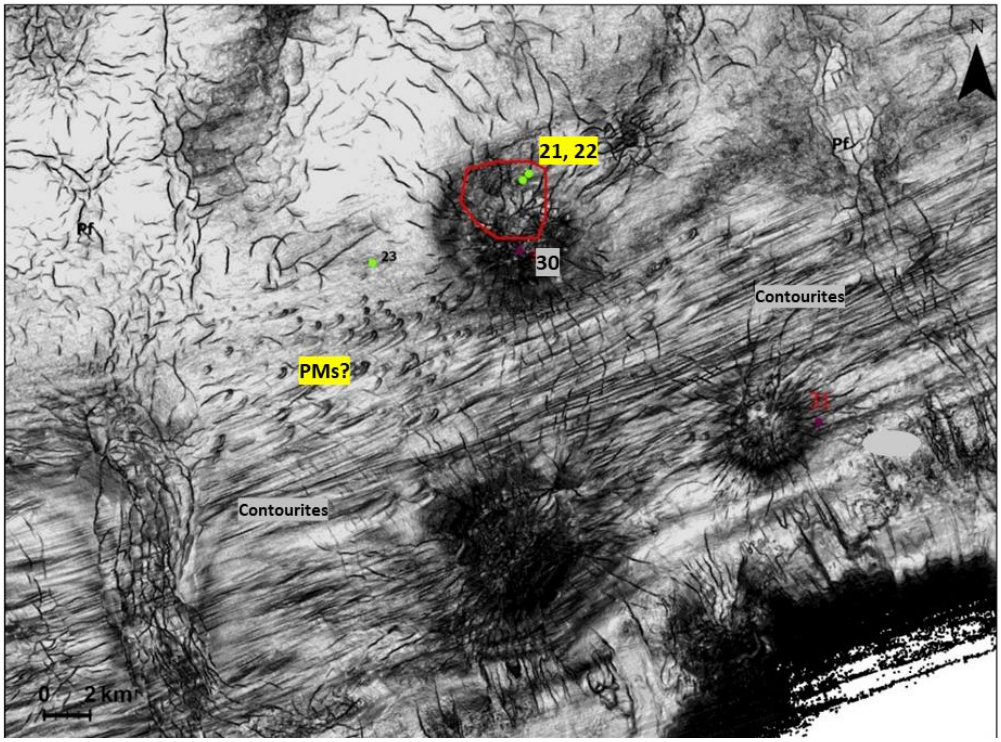

Figure 4.16C. Coherence attribute at 2700 m. Site 2018-23 is the closest location to a field of what looks like paleo-pockmarks whose shapes may have been modified due to slope-parallel contour currents. The features could also be contourite-related crescentic dunes.

The presence of DHIs within a polygonal faulted zone suggests the fault system is part of a shallow gas fluid migration system (Callow et al., 2021). Coupled with the presence of pockmarks, it is plausible that there is a seep near Site 2016-030 and 2018-023.

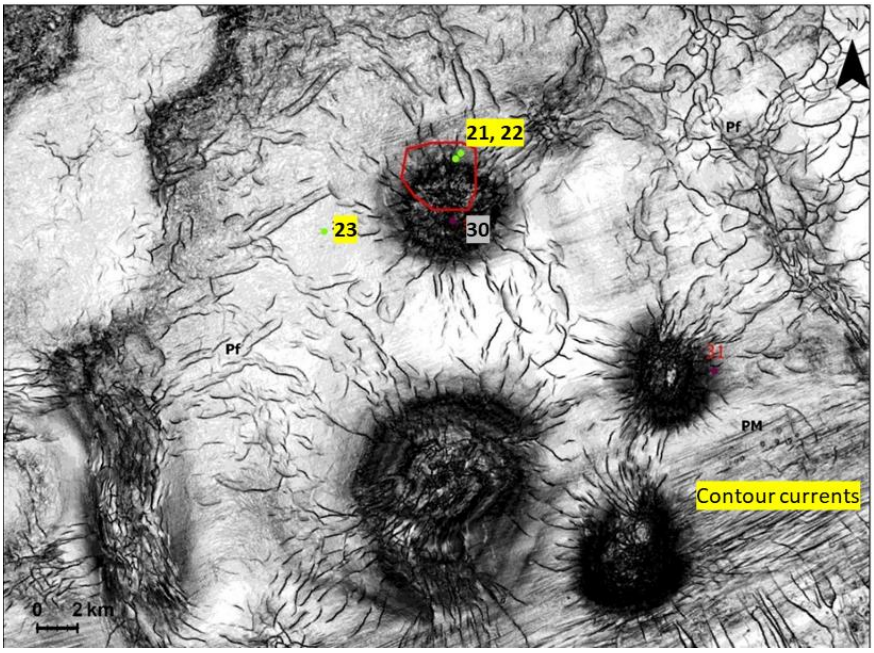

Figure 4.16D. Coherence attribute at 3000 m for cores 2018 Sites 21, 22, and 23.

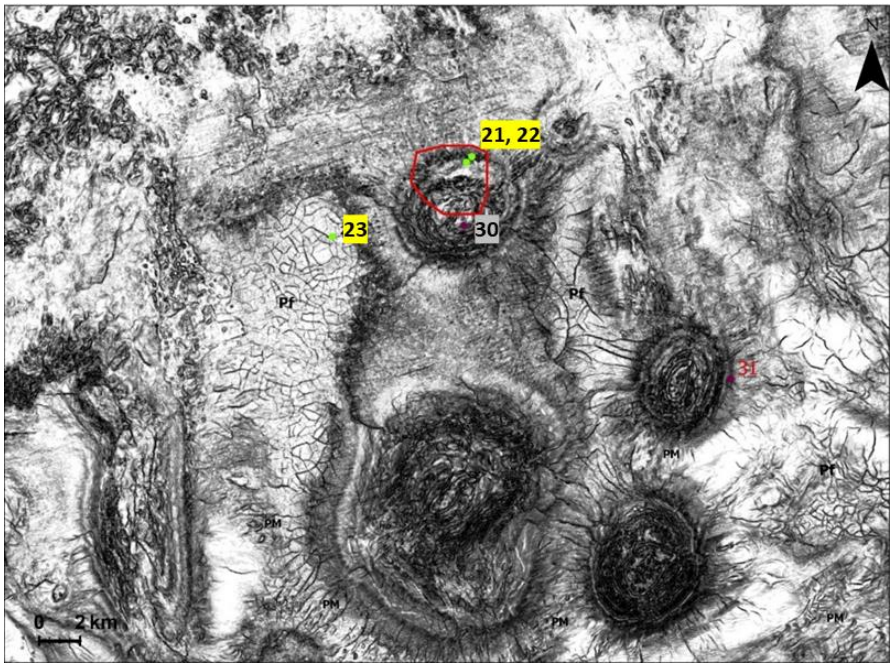

Figure 4.16E. Coherence attribute at 3500 m samples 2018 Sites 21, 22, and 23

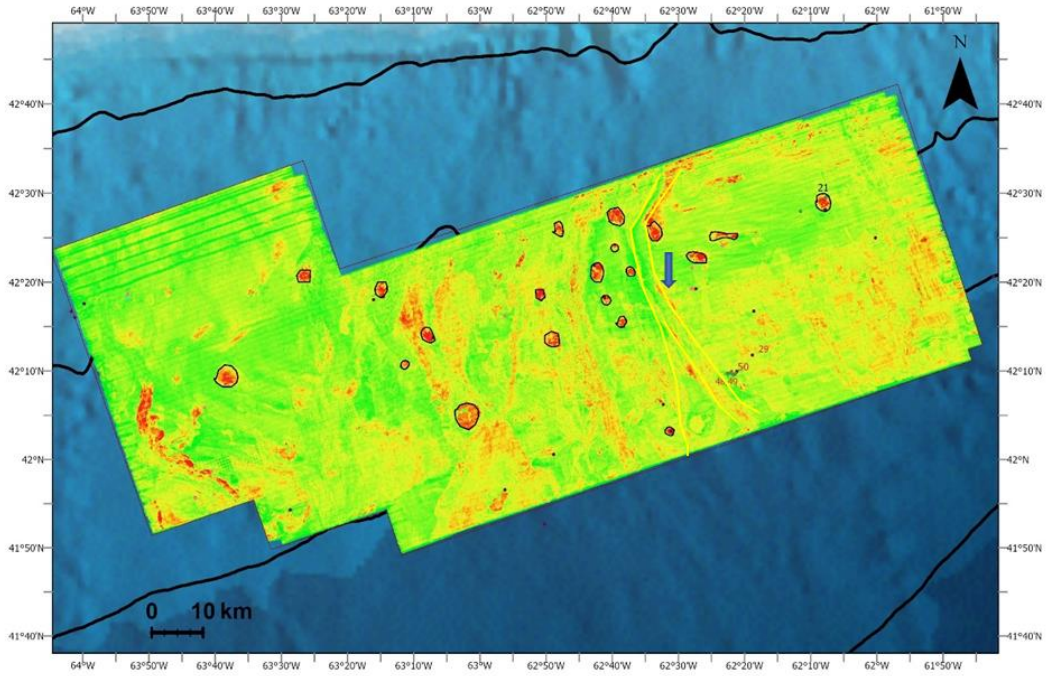

Figure 4.17A. The RMS amplitude map showing locations for sample 2016 Sites 48, 49, and 50. Yellow lines delineate a channel system.

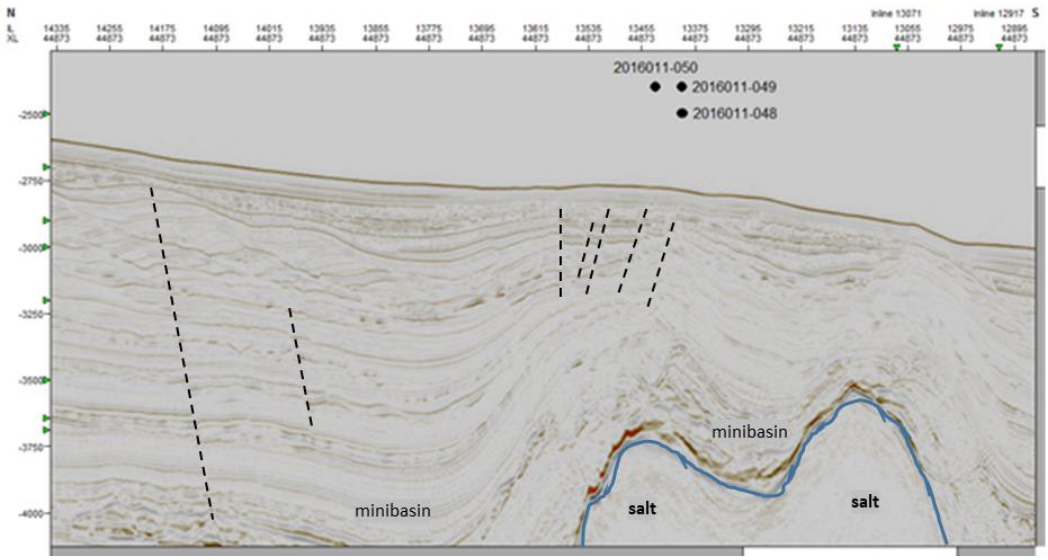

Figure 4.17B. Seismic crossline cross-section for samples 2016 Sites 48, 49, and 50.

Vertical seismic section for Sites 2016-049 and -048 do not indicate presence of high-amplitude anomalies in the near surface (Figure 4.17B). There could be gas from the

subsurface migrating into the sediment near surface and hence having gas charged sediment.

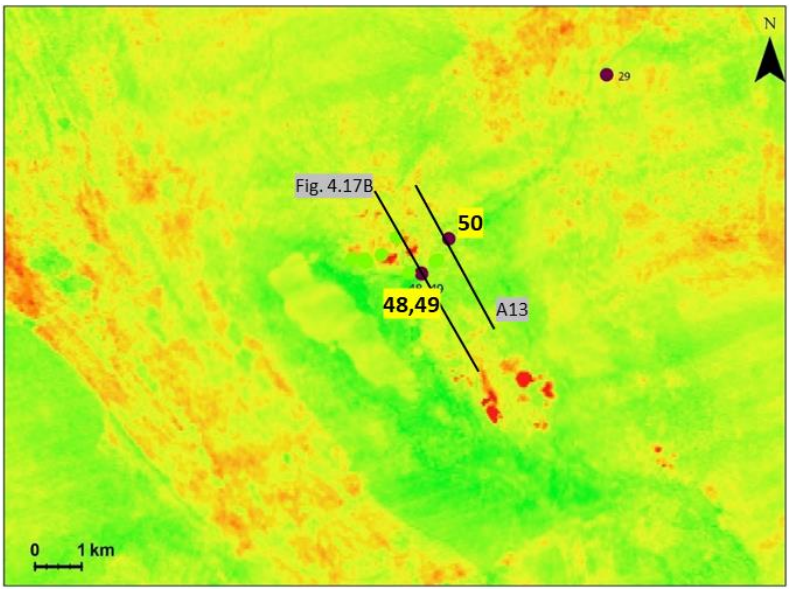

Figure 4.17C. An RMS amplitude snapshot of Sites 48, 49, and 50. The high amplitude anomalies are not visible on the seismic section and may have been tuning effects on erosive surface experiencing down-slope sediment transport (Figure 3.18, 4.7A). More seismic sections from this area are to be considered for interpretation.

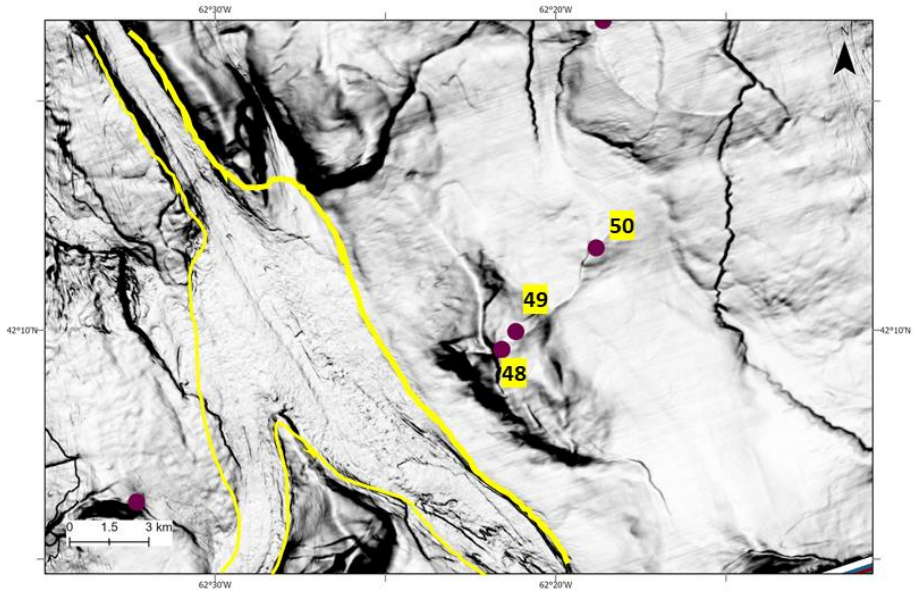

Figure 4.17D. Coherence attribute showing seafloor surface at Cores 48, 49, and 50 from 2016.

Sediment Cores 48 and 49 had a strong sulfur smell and were found to contain gas hydrates (Fowler and Webb, 2017). The gas from the two cores is of biogenic origin and

showed no evidence of a petrogenic source (Fowler and Webb, 2017). Site 50 was a slick sample retrieved during coring at Site 49 and showed geochemical characteristics of a weathered petroleum (Fowler and Webb, 2017) suggesting the presence of a seep near this site. Surface slicks are a helpful source of geochemical information in defining potential petroleum systems in deepwater settings (Dembicki, 2020). Slicks may result when seafloor sediments around a seep site become saturated with leaking oil (Dembicki, 2020). Slicks can also form from oil spills, pollution, or biological activity. In 2018, resampling was done near Sites 48 and 49, but there was no further evidence of a significant thermogenic component (Fowler and Webb, 2018). This raises a question: is the slick from episodic seepage and/or ephemeral seepage in a zone without sealing capacity?

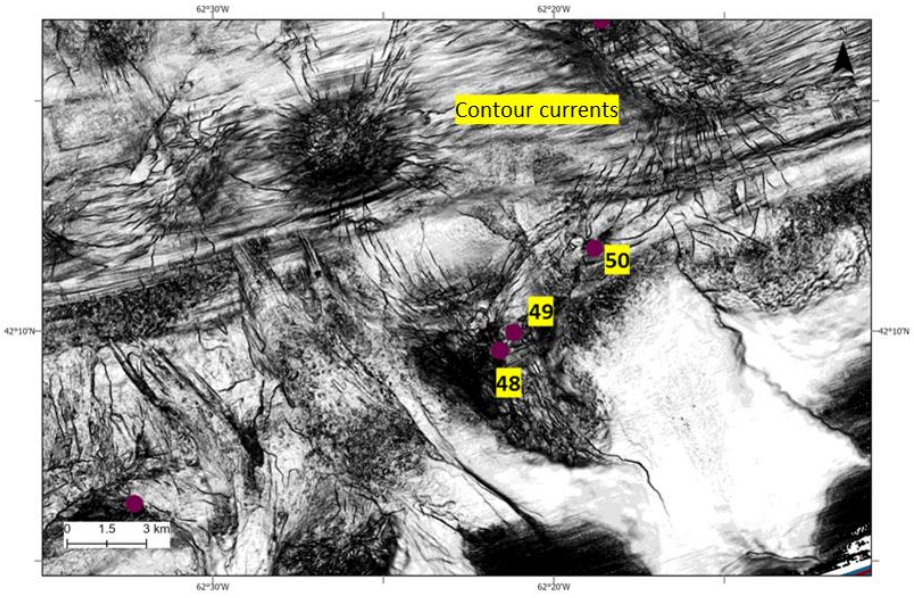

Figure 4.17E. Coherence attribute at 3000 m.

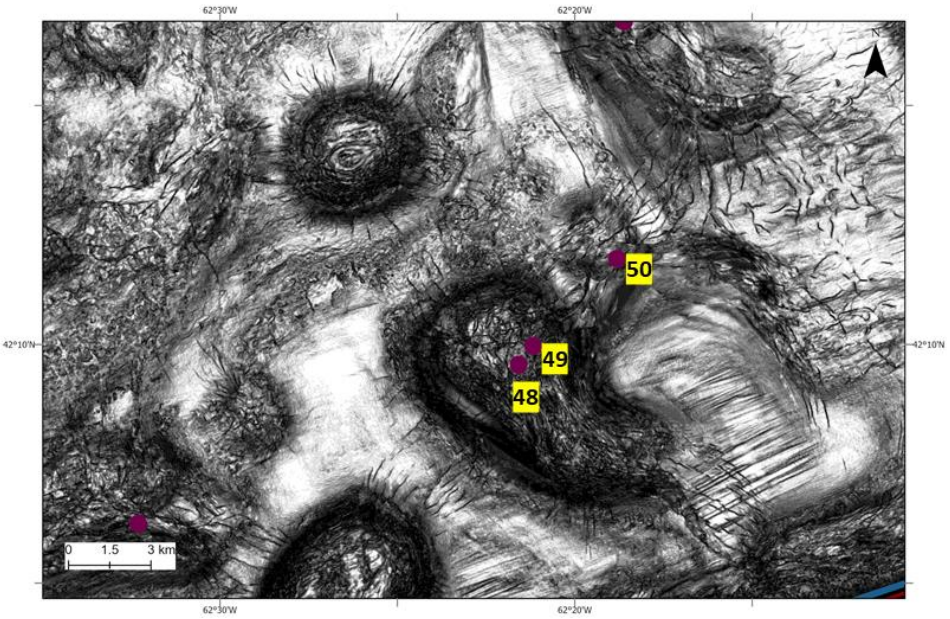

Figure 4.17F. Coherence attribute at 3500 m.

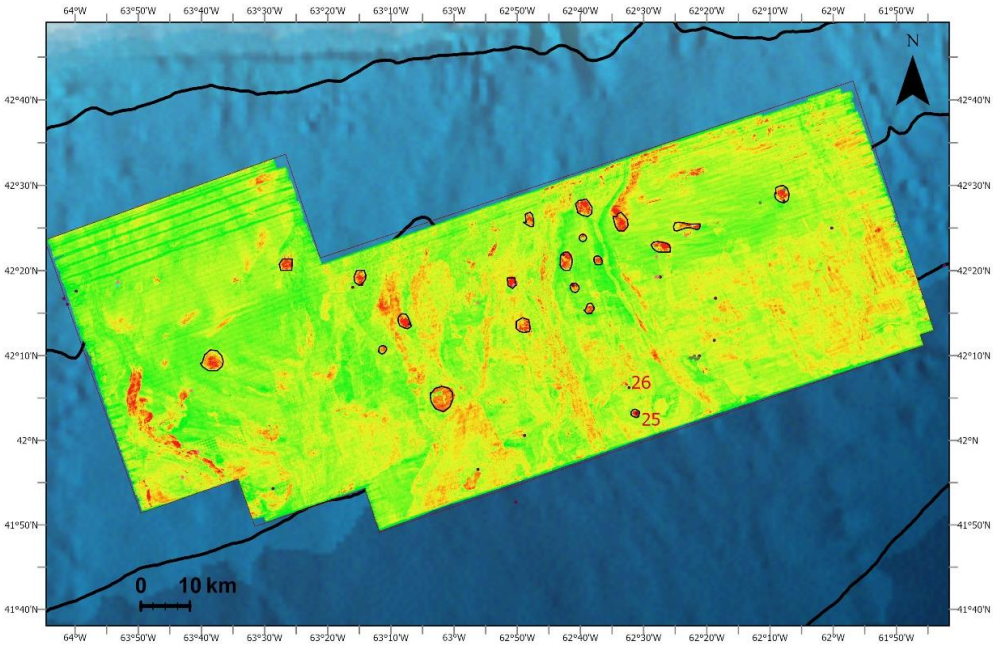

Figure 4.18A. The RMS amplitude showing locations for sample 2016 Sites 25 and 26.

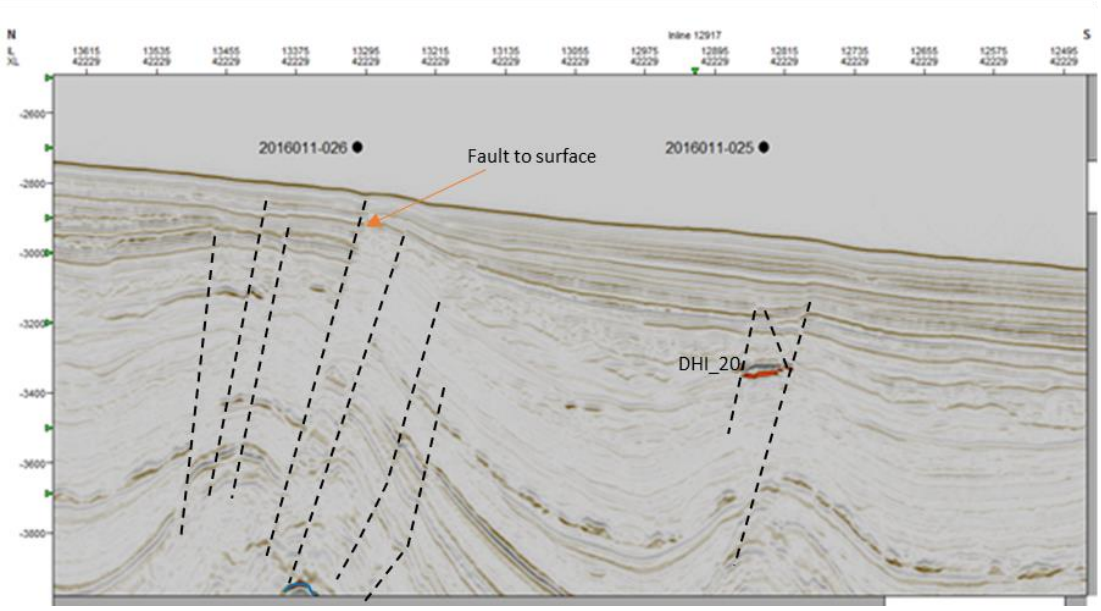

Figure 4.18B. Seismic crossline cross-section for Sites 2016-025 and -026

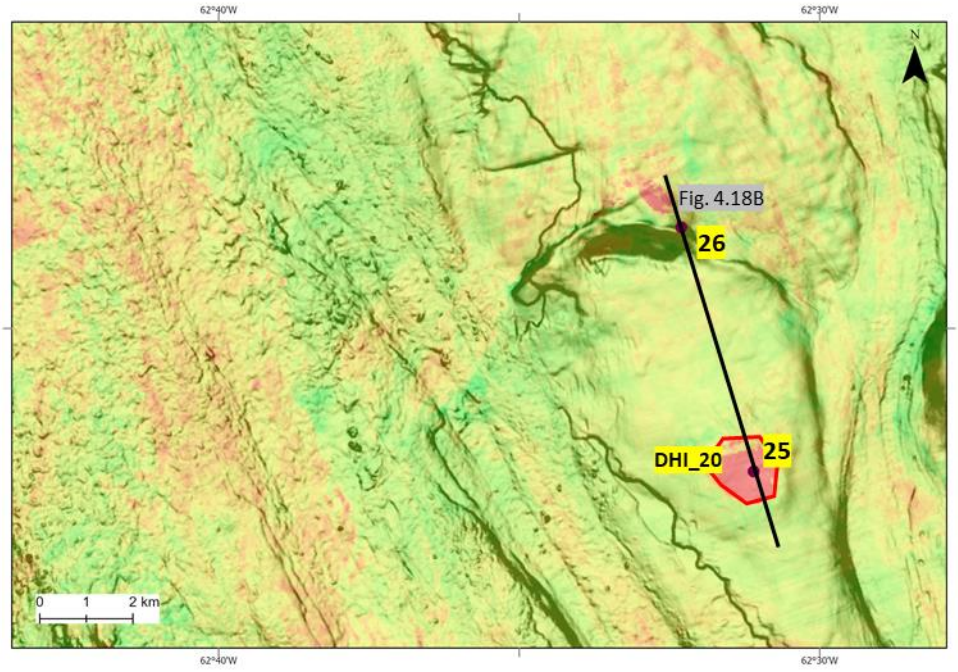

Figure 4.18C. The RMS amplitude map shows a high amplitude anomaly at Site 25 interpreted as DHI_20.

Sites 25 and 26 appear to be located between the Mohican and Moheida Channel Systems (see Deptuck and Kendell, 2020). The vertical seismic section indicates a fault originating deep in the subsurface and terminating at surface for Site 26 (Figure 4.18B). Site 25 appears to be on top of a high-amplitude seismic anomaly, but the size of the anomaly in the vertical section (Figure 4.18B) does not correspond to the impedance contrast observed in the RMS amplitude (Figure 4.118C). It is clear that the seismic section displayed here did not capture the full extent of the anomaly.

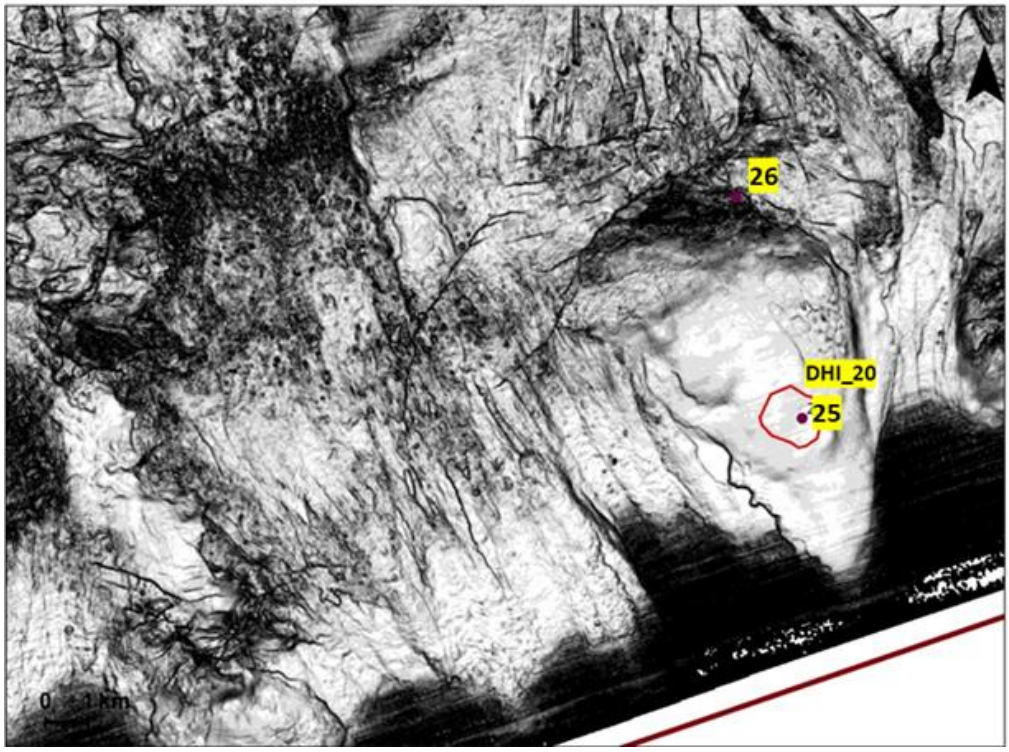

Figure 4.18D. Coherence attribute at 3000 m.

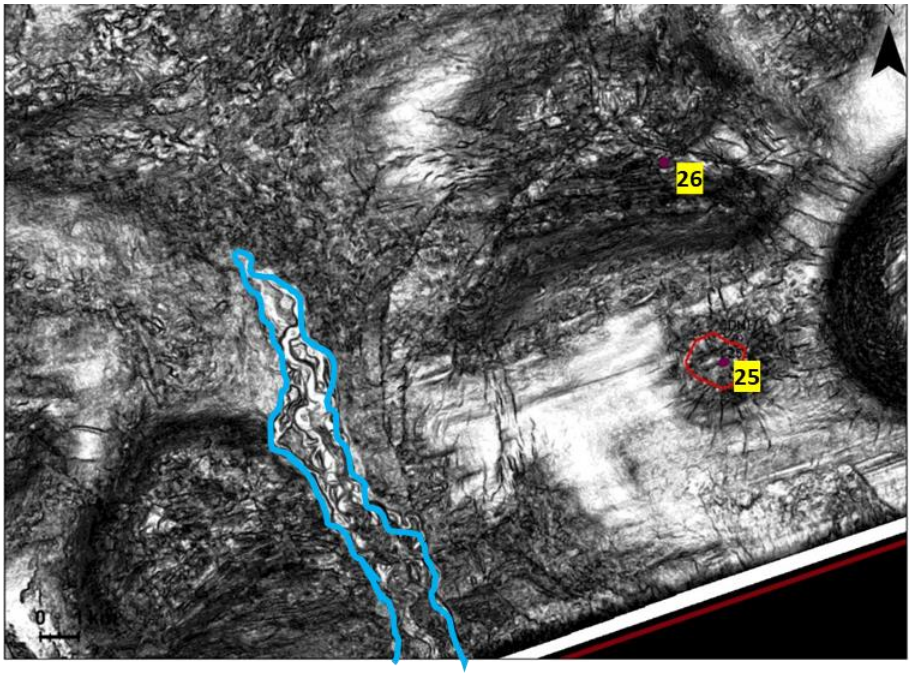

Figure 4.18E. Coherence attribute at 3500 m. The blue lines are a meandering canyon fill.

Site 26 was one of many sites with abundant light hydrocarbons but without correlation to a thermogenic source even though the core sediment had gas bubbles at the time of retrieval from the seabed (Fowler and Webb, 2017). The core recovered form a water depth of 2880 m at Site 25 intersected a large sandy dewatering layer. There are no noteworthy hydrocarbon signatures for this sample in the geochemistry report. It is plausible that gas is migrating through the sediment and is not being impeded or trapped in the sandy layers.

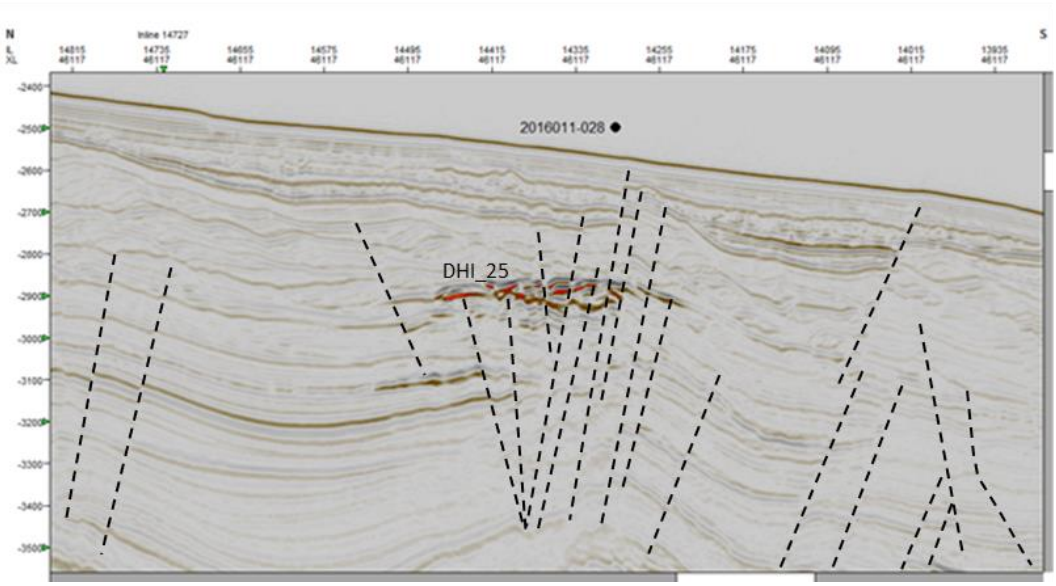

Figure 4.19A. Seismic crossline cross-section for 2016 Site 28 with a DHI about 400 m below the seafloor. This DHI was out of bounds for the horizon used to create the RMS surface.

The vertical seismic section for Site 2016-028 indicates the presence of a DHI in the near surface sediment (Figure 4.19A). A fault appears to cut through the anomaly and almost terminates at the ocean floor. There are no noteworthy signatures in the geochemical analysis for this core. Deeper in the subsurface, paleo-pockmarks are observed for this site implying the possibility of a paleo seep in this location.

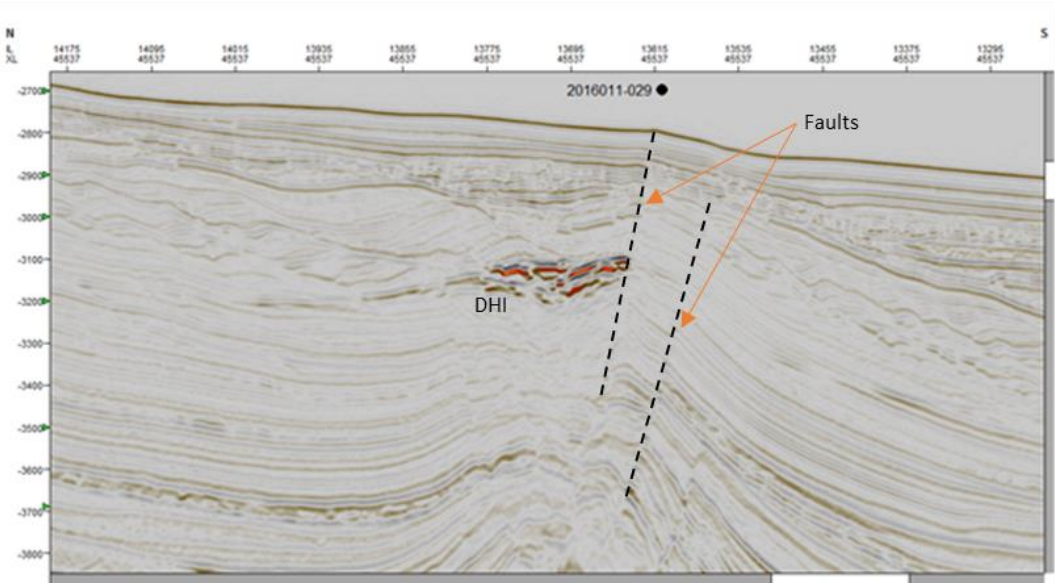

Figure 4.19B. Seismic crossline cross-section for Site 29 with a DHI about 400 m below the seafloor and a fault terminating at surface.

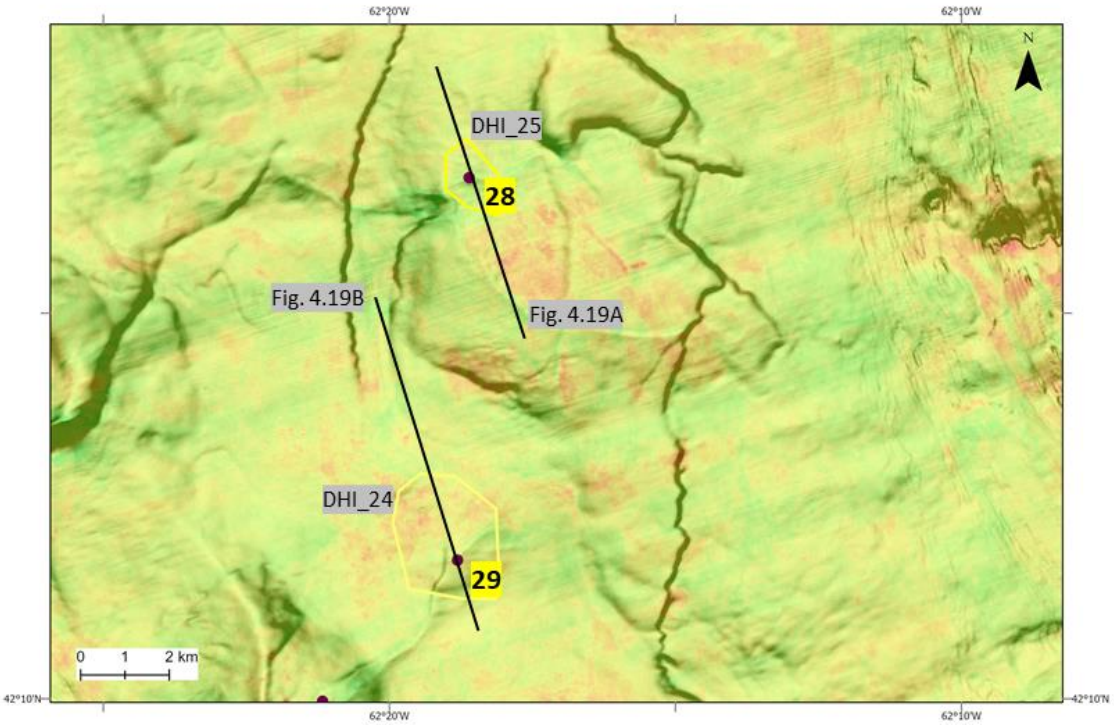

Figure 4.19C. An RMS amplitude snapshot map overlaid on a variance seafloor map for Cores 2016-28 and -29. DHI_24 and DHI_25 were not captured on the RMS amplitude map in this study. It is likely that it was outside the bounds of the horizon used to create the RMS map.

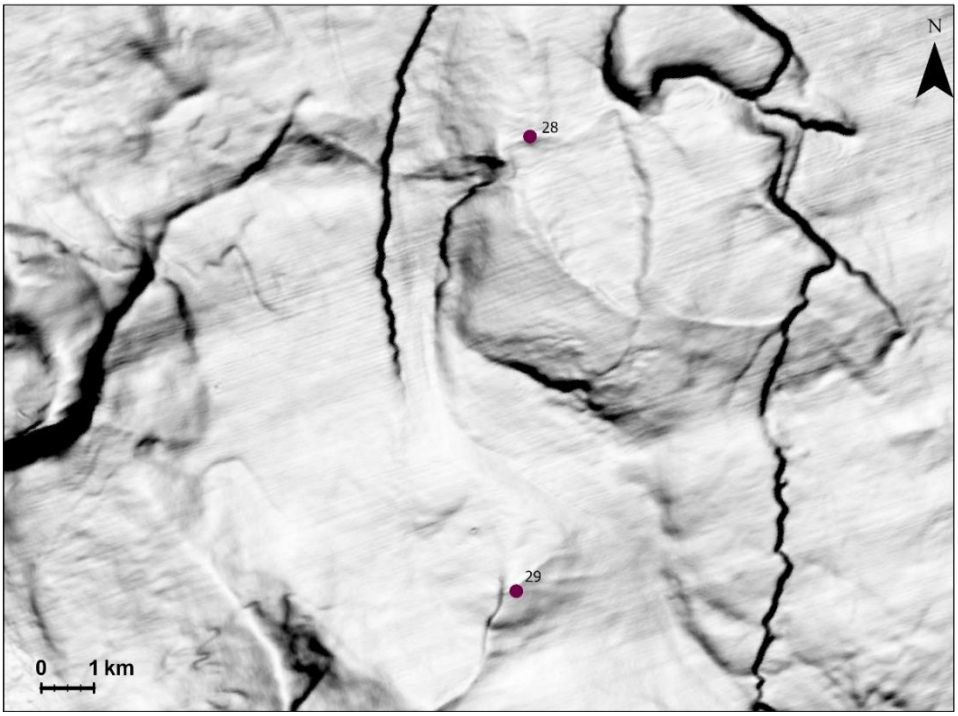

Figure 4.19D. Coherence attribute at seafloor surface.

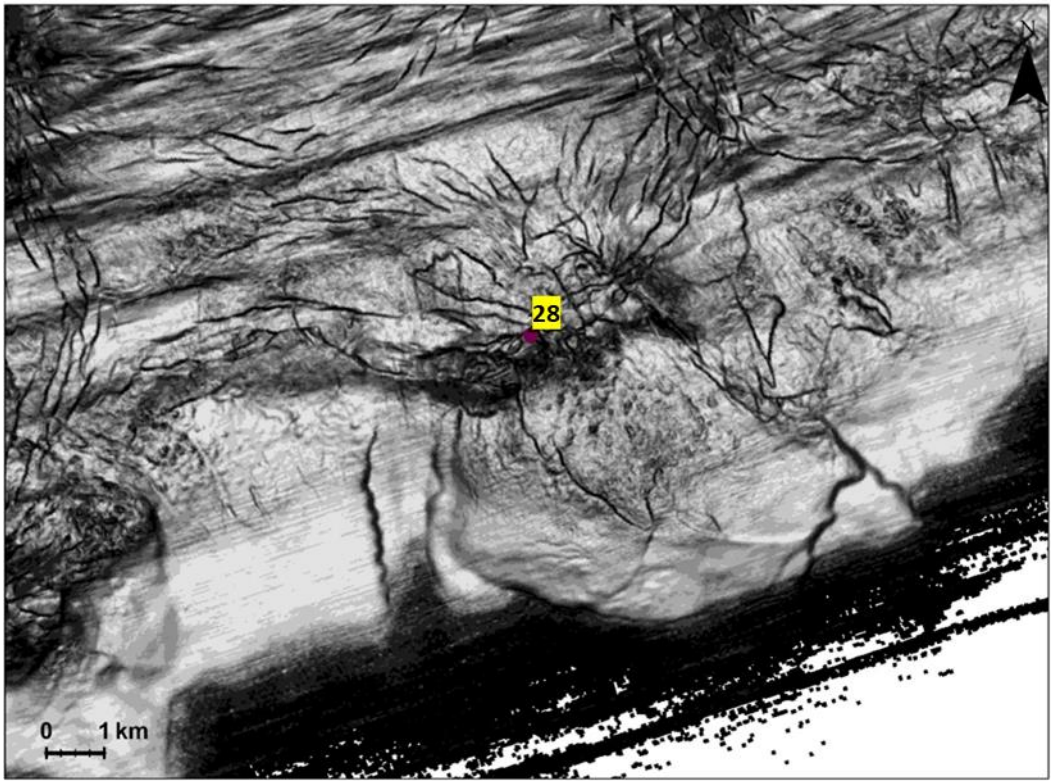

Figure 4.19E. Coherence attribute at 2700 m. Site 29 is in the water column at this depth.

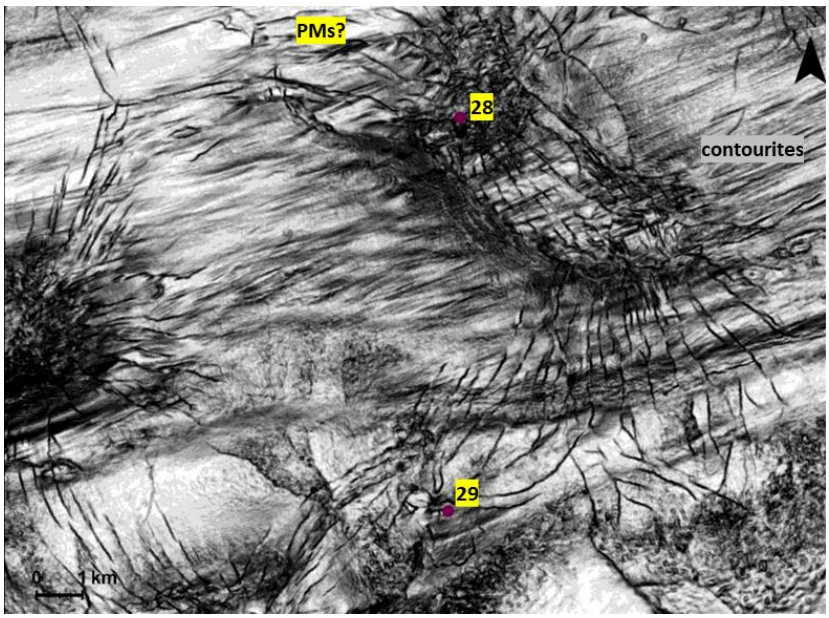

Figure 4.19F. Coherence attribute at 3000 m for Sites 28 and 29. Paleo-pockmark like features are observed near Site 28. These features could also be contourite-related crescent dunes. More interpretation of vertical seismic sections in the area is needed to confirm what the features are.

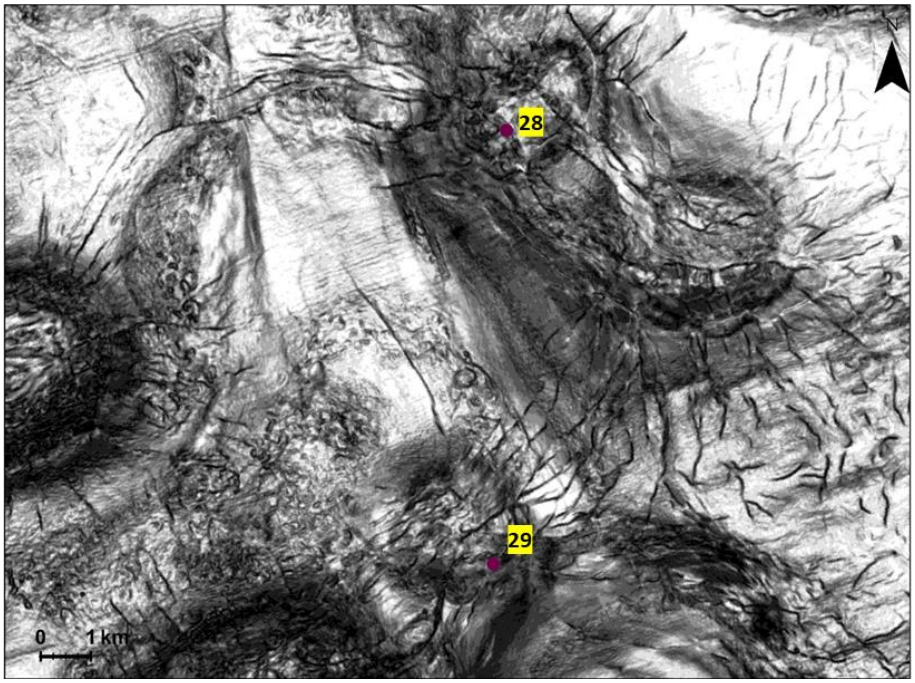

Figure 4.19G. Coherence attribute at 3500 m for Sites 28 and 29.

Site 2016-029 is south and downslope of Site 28. The vertical seismic section indicates the presence of a DHI in the near surface and faults from the deep subsurface that terminate at surface (Figure 4.19 A, B). The RMS amplitude map (Figure 4.19C) did

not capture the two DHIs as the horizon used to create the amplitude map was shallower than where DHIs_24 and 25 are showing. The coherence attribute at seafloor surface (Figure 4.19D) shows a smooth surface with slump scarps that could imply a transport corridor for sediment, and a gentle relief feature that reflects a buried salt body. Like in Site 28, the geochemical analysis for Site 29 did not indicate any evidence for the presence of petrogenic hydrocarbons.

Chapter 5 : Discussion and Conclusion

The geophysical data from the Shelburne 3D provides evidence for surface (e.g., pockmarks and fault networks) and near surface (e.g., DHIs, cross stratal faults) petroleum migration, contour currents, canyon systems, and paleo-pockmark features. Some of these features are related to sedimentation and salt or other structural deformation, and some are possibly or likely expressions of hydrocarbon migration from deeper within the basin. Based solely on the geophysical data no definitive evidence was collected for the presence of active cold seeps in the Shelburne 3D.

In the study area, various zones with amplitude anomalies are observable (Figure 3.18 RMS amplitude map). A major limitation in the use of RMS amplitude maps is that background noise of a surveyed area increases as all peaks are squared before finding their square root. In this case, aside from possible DHIs, observed amplitude anomalies are likely related to changes in lithology between shaly limestone, shale, and marls and from erosive processes related to sediment flow (OERA, 2019). Along canyon margins, anomalous amplitudes stand out that are most likely associated with tuning effects where incision surfaces merge with underlying strata (Deptuck and Kendell, 2020). Without vertical seismic profiles as guides, it becomes harder to differentiate acoustic anomalies related to DHIs, as seen in the RMS amplitude map. In this integration, side-by-side images of the different attributes and structural and stratigraphic features gave comprehensive insight to the interpretation. A limitation encountered in the seismic data attribute extraction is image resolution. At a certain scale, images blur and it becomes harder to pick out seafloor features. AUV data and sub bottom seismic profiles are options for better resolution at a sub-km scale.

Thirty-three sampling locations retrieved in the 2015, 2016, and 2018 cruises were considered in this study (Table 1). Eleven of these sites did not indicate a presence of a DHI in their vertical seismic cross sections (samples 2015 Site 4, 5, 8, 6, and 7; 2016 Site 13, 16, 22, 23, 26, 48, 49, and 50). Some of these sites showed geochemical evidence for the presence of hydrocarbon (e.g., 2015 Site 5 and 6). These locations had faults terminating at the surface or very near to the surface, which implies they had connectivity and were good conduits for migration of fluids to the surface. These locations could have a leaking reservoir or a charging source rock in the deeper subsurface but without mechanisms of sealing or trapping the migrating hydrocarbons after the leak. Some of the sites were interpreted as having pockmark fluid escape features.

For sites that have visible DHIs in the vertical seismic cross-sections, the geochemical analysis did not universally indicate a presence of hydrocarbons. Samples 2016 Sites 15 and 17 had DHIs with faults that terminated at surface, but the presence of hydrocarbons was not reported from the survey's geochemical analyses. Samples 2015 Site 10, 12, 13, 14, and 15 as well as 2016 Site 27 and 28 all had DHIs in the shallow sediment, but no hydrocarbon signatures. For Site 27 this outcome was unexpected given the concomitant presence of paleo-pockmarks that implies a transient or an intermittent seepage event(s).

Samples 2016 Site 18, 21, and 30 showed both DHIs in the near surface and had positive indications for hydrocarbons. The locations had a complex network of faults and fractures that would allow for migration of leaking hydrocarbons. The best locations for further investigation would be for samples 2016 Site 19 and 20, and 2018 Site 21.

Collectively, these sites had DHIs, a network of polygonal faults, and pockmarks. Based on these observations it is possible that cold seeps exist in these locations.

Overall, geochemical data for cores collected in the basin indicate some evidence for a working petroleum system in the deep-water Scotian Slope (Fowler and Webb, 2017, 2019; OERA, 2019). Basin modeling and well calibration from recent well completion reports indicate that there is at least one potential play for a petroleum system in the deep water (OERA, 2019). From the seismic data, DHI presence is one of the types of evidence for hydrocarbon migration to the surface from the subsurface and therefore implies the existence of a working petroleum system. Furthermore, pockmarks and polygonal faults (especially near the Cheshire well) also add credibility to this assumption.

Table 1. Summary table of cored samples in relation to DHI presence and corresponding geochemical signatures.

Figure	Core_ID	Geochemical Data	DHI Presence	Trap Type	Faulting	Indicator of Seepage on surface	Comments
4.2B	2015018_0004	HC Negative	NO	Stratigraphic (gas in sediment	Highly faulted in shallow sediment	Seafloor disturbances potentially associated to leakage from gas-charged sediment	Anomaly observed on vertical cross section is interpreted as a tuning effect or a change in lithology on erosive surface
4.2C	2015018_0005	HC Positive	NO	Combined stratigraphic and structural	Faults to surface	Faults to surface	Gas charged sediment
4.3B	2015018_0008	HC Negative	NO		Highly faulted in shallow sediment	Faults to surface	High amplitude anomaly on RMS from sediment transport (crevasse splay)
4.4C	2015018_0006	HC Positive	NO		Highly Faulted	Irregularities on seafloor	Zone of mass transport flow. It is plausible that the sediment is gas charged
4.4D	2015018_0007	HC Negative	NO		Some faulting	Washouts near sea floor and also above the crest of the diapir	Zone of mass transport flow. Gas charged sediment
4.5B	2016011_013	HC Negative	NO		Faults to surface	Paleo-pockmarks at 3500m	Downslope sediment transport zone
4.6B	2016011_015	No data	YES	Stratigraphic	Fault to near surface	Fault on edge of DHI that leads to near-surface	Sediment hosting DHI is overlain by a MTC/sediment flow
4.6D	2016011_016	No data	NO		Fault to surface		Canyon/channel system
4.7B	2016011_017	No data	YES	Structural	Fault to surface; some polygonal faulting	Depressions on seafloor surface on seismic section	
4.8B	2016011_23	HC Negative	NO		Fault to surface		Sampled near a salt apron. Very rough surface on seafloor
4.9B	2016011_22	HC Negative	NO		Faults to near surface		Deeper core, past the zone of disturbance might give more conclusive data on whether the depositional sediment is charged with diffuse gas from the subsurface.
4.10B	2016011_019	No data	YES	Structural	Some faulting	Pockmark features observed	This site looks promising in the search for a cold seep
4.10D	2016011_020	HC Negative	YES (?)	Stratigraphic		pockmark features observed	Not much faulting but sediment appears to be permeable
4.11B	2015018_0009	HC Positive	YES	Structural	Fault to surface		

Continued below

Figure	Core_ID	Geochemical Data	DHI Presence	Trap Type	Faulting	Indicator of Seepage on surface	Comments
4.11C	2015018_0010	HC Negative	YES	Sructural	Fault to surface	Fault to surface that could source from the DHI	
4.12B	2016011_018	HC Positive	YES	Structural	Fault to surface	Fault connectivity to surface	
4.12B	2016011_021	HC Positive	YES	Structural	Fault to surface	Fault connectivity to surface	
4.13B	2016011_027	HC Negative	YES	Structural	Faults to near surface	Pockmark -like depressions on surface	
4.13G	2015018_0013	HC Negative	YES	Stratigraphic	Fault to surface	Pockmark like features observed	Pockmark-like features observed at different depths
4.14B	2015018_0012	HC Negative	YES	Structural	Faults to surface	High connectivity of faults	Missed target?
4.14B	2015018_0014	HC Negative	YES	Structural	Faults to surface	High connectivity of faults	
4.14C	2015018_0015	HC Negative	YES	Combined stratigraphic and structural	Faults to surface	High fault interval	This site should be a candidate for revisit. Should compare metagenomic and lipidomic dataset which might have better sensitivity
4.15B	2016011_030	HC Positive	YES	Structural	Fault to surface	Highly faulted in shallow sediment just below the seabed	It is plauisble that the HCs migrated to the surface near this location via pockmarks, and there was lateral migration due to sediment drift.
4.17B	2016011_050	Slick	NO	NA	NA		slick sample
4.17B	2016011_048	HC Positive	NO		Faults to near surface		Gas Hydrate in core
4.17B	2016011_049	HC Positive	NO		Faults to near surface		Gas Hydrate in core
4.18B	2016011_025	HC Negative	YES(?)		Fault terminating near surface		Gas charged sandy sediment(?)
4.18B	2016011_026	HC Positive	NO		Fault to surface		Gas bubbles observed during core retrieval
4.19A	2016011_028	HC Negative	YES	Structural		Paleo-pockmarks at 3000m and 3500m	Paleoseep?
4.19B	2016011_029	HC Negative	YES	Structural	Fault to surface		

In integrating the disparate data types, we posed four questions to help characterize the petroleum system and active seep potential in the Shelburne 3D survey:

1. Is a working petroleum system present in the deep-water portion of the Scotian Slope? Based on the discussion above, it is highly likely a working petroleum system is present in the study area.

2. Is there a large enough volume of prospective source rock to generate and expel hydrocarbons? This component remains unconfirmed. While geophysical data might provide some clues about trap, reservoir, and seal, it does not provide much insight into source rock, generation, and expulsion of hydrocarbons and the hydrocarbon charge component of the play (Dembicki, 2020) and sources other than biogenic are likely located well below the interval studied in this project. Finding cold seeps in a prospect reduces charge risk in play analysis (Dembicki, 2020) and their presence has been used in offshore exploration programs for over five decades (Dembicki, 2020). Even so, authentication of seep presence does not prove economic hydrocarbon accumulations at depth and does not explain seal failure or the process of gas displacement from reservoirs (Wenger and Isaksen, 2002).

Hydrocarbon seeps are often small features, less than a few metres across, that episodically vent thermogenic or biogenic hydrocarbons at the seafloor. As such, they are not always easily recognized in seafloor extractions from 3D data due to lack of resolution (Dembicki and Samuel, 2007). In this study, visible features were limited to acoustic anomalies, faults, and fluid escape features. In such a case, piston core sampling of sediments containing leaked hydrocarbons can greatly improve the utility of this approach. The piston coring program in 2016 identified the likelihood of a seep near Site

48 and 49 (Fowler and Webb, 2019). Interestingly, while there was a slick collected in proximity of this site and gas hydrates observed within the sediment core, the confirmation for thermogenic hydrocarbons in the samples was still not definitive. This indicates that even this method has limitations.

Furthermore, it seems that there was not always a direct correlation between acoustic anomalies in the seismic data and gas concentrations in the sediment. It is plausible that the corers did not always penetrate the target sediment where hydrocarbon fluids were preserved, or also due to the spotty distribution of hydrocarbon concentration in the salt-rich basin. A common limitation with piston coring is hitting target features as the wireline deviates with depth as much as 500 m laterally with a 5° vertical deviation (Fowler and Hubert, 2020). This deviation can mean a lack of thermogenic geochemical signature in the analyzed sediment core even if sampling was attempted very close to a seep site (Abrams and Dahdah, 2011). Even when a core does hit a target point as observed on seismic data, the sampling depth may not be deep enough to acquire measurable hydrocarbon shows. A corer might sample shallower portions, far from saturated sediment, giving negative signatures in places with hydrocarbons. It is crucial that the corer retrieves sediment below the zone of maximum disturbance. Even then, if the seepage volume and rate is not significant enough to overwhelm sediment alteration process as described in Abrams (2005), the corer could still disprove presence of hydrocarbons in sediment that does in fact host hydrocarbons by retrieving sediment just a small distance away from hydrocarbon-hosting sediment. Geochemical data cannot be a sole indicator for a seep (Fowler and Webb, 2019), but can add great confidence to other data especially when the right targets are hit.

As both the geophysical and geochemical data give good indications, we naturally look to the geologic data and basin modelling models in the slope region. Wells are a good de-risking step to determine hydrocarbon shows or producible reserves. Basin modeling can aid in determining the possibility of hydrocarbon generation and expulsion. OERA (2019) mentions the possibility of hydrocarbons generated in potential Early Jurassic source rocks migrating vertically up to Cenozoic sediments and accumulating on top of salt diapirs. Based on well findings, any likely source rock that is charging the system must be older than Middle Jurassic (OERA, 2019). It is predicted that there is a source rock, but it remains to be found and proven.

3. Is an adequate amount of good reservoir rock available to receive these hydrocarbons? Reservoir presence is considered the main risk along the study area (OERA, 2019). Aside from the salt preventing connectivity of basins with sediment, numerous canyons along the slope appear to transfer sands further down the basin and into salt-induced minibasins and into deep water. Significant salt tectonism in the Shelburne subbasin has greatly restricted the drainage areas, structure of migration pathways, and in turn, charge efficiency (OERA, 2019). The salt bodies also influence potential hydrocarbon migration by limiting lateral migration and reducing connectivity between the minibasins. Migration is therefore expected to be mostly vertical along salt diapirs, and the generated hydrocarbons are highly unlikely to concentrate in large reservoirs. Under these conditions, it is believed a very rich source rock would be required to charge large traps, and there is still no direct evidence for the presence of a prolific source rock.

4. **Are there traps large enough and with sufficient closure to contain these hydrocarbons?** Like most salt basins (e.g., Pilcher et al., 2011; Weimer et al., 2017; Bourollec et al., 2017), numerous structural traps with special geometries (an effect of salt behaving as a fluid during basin evolution) are observed in the Shelburne Subbasin. However, the subbasin is in a relatively sediment-starved part of the margin and potential reservoirs remain elusive (OERA, 2019). Deptuck and Kendell (2020) discuss how the distal parts of Shelburne 3D volume host salt bodies covered with the least amount of sediment (<1 km).

Ultimately, this study shows that seismic data reveals features suggesting the presence of hydrocarbons, but the features remain inconclusive on defining the petroleum system model and economic potential present in the basin. All these models, while useful and applied in offshore Nova Scotia prospecting, carry substantial uncertainty. However, used with other tools, it can still de-risk the exploration process by acting as a guide, and delineating areas to focus for exploration. Finding unconfirmed source rocks in the deep-water basin and use of other technologies in seep hunting seem to be a necessary next step to fill in the gaps on the exploration potential of the deep-water portion of the Scotian Basin.

5.1 Future work

Integration of the datasets has helped to bring a better understanding of the dynamic nature of a structurally complex section of the Scotian Slope. The maps created will continue to be of use for work in the deep-water portion of the basin. In this study, a few sites are suggested for revisit in future cruises: 2015018-007; 2016011-013, -019, -027 and -30; 2018041-023. Additionally, three main leads are also suggested.

- In continuation of the de-risking theme, confirmation of detailed description of DHIs would be valuable information. In depth characterization of depositional elements and structural patterns to better explain flow features would be a worthy study to pursue. Fault interpretation can similarly add clarity to how DHIs formed and where they tend to be located within the basin, as well as potentially explain their absence via fault-related fluid leakage. In this study, the characterization was done at a high-level and greater detail is necessary. This study only mapped DHIs up to 3200 m, but there are more DHIs further outboard from the shelf in 3800 m water depth. Mapping these in one horizon would have been too thick to make sensible deductions for this study. It is suggested that the other DHIs are mapped and the analyzed together with the existing datasets. The DHI horizon mapped in this study also indicates a possible continuous geologic event associated with mass transport processes that is trapping the DHIs in the study area. Further investigation is encouraged for this hypothesis.
- Microbiological data collected from the 2015-2018 coring cruises could be added to the database. This data would be helpful in understanding the microbial ecosystem in the Scotian Basin. If there do exist thermophilic bacteria that could be an indirect indicator of seeps, the knowledge would be useful in the de-risking process. Other biological disciplines would also find it useful to have a baseline library of microbes in the slope region.
- The information from this study could use to visualize geohazard studies in the deep-water portion. Knowledge of existing gas pockets and highly faulted zones would be useful information in infrastructure considerations in the offshore.

5.1 References

Abrams, M.A. 1992. Geophysical and geochemical evidence for subsurface hydrocarbon leakage in the Bering Sea, Alaska. *Marine and Petroleum Geology Bulletin*, 9: 208–221.

Abrams, M.A. 2005. Significance of hydrocarbon seepage relative to subsurface petroleum generation and entrapment. *Marine and Petroleum Geology Bulletin*, 22(4): 457–478.

Abrams, M.A. 2020. Marine seepage variability and its impact on evaluating the surface migrated hydrocarbon seep signal. *Marine and Petroleum Geology*, 121.

Abrams, M. and Dahdah, N. 2011. Surface sediment hydrocarbons as indicators of surface hydrocarbons – field calibration of existing and new surface geochemistry methods in the Marco Polo Area Gulf of Mexico. *American Association Petroleum Geology Bulletin*, 95(11): 1907–1935.

Adam, J. and Krezsek, C. 2012. Basin-scale salt tectonic processes of the Laurentian Basin, Eastern Canada: insights from integrated regional 2D seismic interpretation and 4D physical experiments. *Geological Society, London, Special Publications*, 363: 331–360.

Albertz, M., Beaumont, C., Shimeld, J.W., Ings, S.J. and Gradman, S. 2010. An investigation of salt tectonic structural styles in the Scotian Basin, offshore Atlantic Canada: 1. Comparison of observations with geometrically simple numerical models. *Tectonics*, 29 (TC4017).

Albertz, M. and Beaumont, C. 2010. An investigation of salt tectonic structural styles in the Scotian Basin, offshore Atlantic Canada: 2. Comparison of observations with geometrically complex numerical models. *Tectonics*. 29 (TC4018).

Alistair, R.B. 2011. Interpretation of 3D seismic data, 7TH edn. The American Association Anstey, N.A. 1978. Seismic exploration for sandstone reservoir. International Human Resources Development Corporation.

Avseth, P., Mukerji, T. and Mavko, G. 2005. Quantitative seismic interpretation. *Cambridge University Press*, Cambridge, pp 168–170.

Berthelsen, A. 1978. The Methodology of kineto-stratigraphy as applied to glacial geology. *Bulletin of the Geological Society of Denmark*, 27**:** 25–38.

Bolchert, G., Weimer, P. and McBride, B.C. 2000. Structural and stratigraphic controls on petroleum seeps, Green Canyon and Ewing Bank, northern Gulf of Mexico: implications for petroleum migration. *Gulf Coast Association of Geological Societies Transactions*, (I):65–74.

Boles, J. R., Garven, P. G., and Chen, J. 2004. Evolution of a hydrocarbon migration pathway along basin-bounding faults: Evidence from fault cement: *American Association of Petroleum Geology Bulletin*, 88: 947–970.

Bouroullec, R., Weimer, P., and Serrano, O. 2017. Petroleum geology of the Mississippi Canyon, Atwater Valley, western DeSoto canyon, and western Lloyd Ridge protraction areas, northern deep-water Gulf of Mexico: Traps, reservoirs, and tectono-stratigraphic evolution. *American Association of Petroleum Geology Bulletin*, 101(7): 1073–1108.

Brooks, J.M. and Carey, B.D. 1986. Offshore surface geochemical exploration. *Oil Gas Journal*, 84:66—72.

Brown, A.R. 1996. Seismic attributes and their classification. *The Leading Edge*, 15(10): 1090—1195.

Brown, D. 2018. Exploration and Production History of the Nova Scotia Offshore Area. *CNSOPB Geoscience Report*, 5p. Available online at https://www.cnsopb.ns.ca/sites/default/files/resource/exploration_production_history_of_ns_offshore_-_december_2018_0.pdf

Bump, P.A., Hovorka, S.D. and Meckel, T.A. 2021. Common risk segment mapping: Streamlining exploration for carbon storage sites, with application to coastal Texas and Louisiana. *International Journal of Greenhouse Gas Control*, 111(103457).

Burrough, P.A. 1986. Principles of Geographical Information Systems for Land Resources Assessment. *Clarendon Press, Oxford*, 193p.

Callow, B., Bull, J.M., Provenzano, G., Bottner, C., Birinci, H., Robinson, A., Henstock, T., Minshull, T.A., Bayrakci, G., Lichtschlag, A., Roche, B., Yilo, N., Gehrmann, R., Karstens, J., Falcon-Suarez, I.H. and Berndt, C. 2021. Seismic chimney characterisation in the North Sea – Implications for pockmark formation and shallow gas migration. *Marine and Petroleum Geology*, 133(9): 105301.

Campbell, D.C., Shimeld, J. and Deptuck, M.E., and Mosher, D.C. 2015. Seismic stratigraphic framework and depositional history of a large Upper Cretaceous depocenter off southwest Nova Scotia, Canada. *Marine and Petroleum Geology*, 65:22-42.

Campbell, D. C. and MacDonald, A. W. A. 2016. CCGS Hudson Expedition 2015-018 Geological investigation of potential seabed seeps along the Scotian Slope, June 25 - July 9, 2015. *Geological Survey of Canada, Open File* 8116, 75 p. https://doi.org/10.4095/299390

Campbell, D.C., 2019. CCGS Hudson Expedition 2016-011, phase 2. Cold seep investigations on the Scotian Slope, offshore Nova Scotia, June 15–July 6, 2016; *Geological Survey of Canada, Open File* 8525, 88 p. https://doi.org/10.4095/313603

Campbell, D.C., and Normandeau, A., 2019. CCGS Hudson Expedition 2018-041: high-resolution investigation of deepwater seabed seeps and landslides along the Scotian Slope, offshore Nova Scotia, May 26 – June 15, 2018; *Geological Survey of Canada, Open File* 8567, 66 p. https://doi.org/10.4095/314695

Carlson, P.R., Golan-Bac, M.S., Karl, H.A. and Kvenvolden, K.A. 1985. Seismic and geochemical evidence for shallow gas in sediment on Navarin continental margin. Bering Sea, *American Association Petroleum Geology Bulletin* 69: 422–436.

Cartwright, J., Aplin, A. and Huuse, M. 2007. Seal bypass system. *American Association of Petroleum Geology Bulletin*, 91(8): 1141–1166.

Cathles, L.M., Su, Z., and Chen, D. 2010. The physics of gas chimney and pockmark formation, with implications for assessment of seafloor hazards and gas sequestration. *Marine and Petroleum Geology*, 27(1): 82–91.

Chavez, I., Piper, D.J.W. and Pe-Piper, G. 2018. Correlation of the Aptian Naskapi Member of the Scotian Basin and its regional implications, *Canadian Journal of Earth Sciences 2018*, 55:514-535, https://doi.org/10.1139/cjes-2017-020

Chopra, S. and Marfut, K.J. 2005a. Seismic Attributes – A historical perspective. *Geophysics*, 70 (5): 3S0–28S0.

Chopra, S and Marfut, K.J. 2005b. Seismic Attributes for Prospect Identification and Reservoir Characterization. *Society of Exploration Geophysicists: Geophysical Development Series* V.11, 464p.

CNSOPB–Canada Nova Scotia Offshore Petroleum Board. 2000. Technical Summaries of Scotian Shelf: Significant and Commercial Discoveries.

CNSOPB– Canada Nova Scotia Offshore Petroleum Board. 2018. Exploration and Production History of the Nova Scotia Offshore Area. December 2018. 5p.

Cullen, J., Mosher, D.C., Louden, K. 2008. The Mohican Channel Gas Hydrate Zone, Scotian Slope: Geophysical Structure. *Proceedings of the 6th International Conference on Gas Hydrates* (ICGH 2008), Vancouver, British Columbia, Canada, July 6–10, 2008.

Cummings, D.C. 2004. Sedimentology and Stratigraphy of an Ancient Progradational Terrigenous Clastic Shelf Margin, Mississauga Formation (Upper Jurassic-Lower Cretaceous), Offshore Nova Scotia, Canada, PhD Thesis, University of Ottawa, Ontario, Canada.

Cummings, D.C., and Arnott, R.W.C. 2005. Growth-faulted shelf margin deltas: a new (but old) play type, offshore Nova Scotia. *Bulletin of Canadian Petroleum Geology*, 53(3): 211–236.

Dembicki, H. and Samuel, B.M. 2007. Identification, characterization, and ground-truthing of deepwater thermogenic hydrocarbon macro-seepage utilizing high-resolution AUV geophysical data. In: *Offshore Technology Conference Paper* 18556.

Dembicki, H. 2020. Reducing the risk of finding a working petroleum system using SAR imaging, sea surface slick sampling, and geophysical seafloor characterization: an example from the eastern Black Sea Basin, offshore Georgia. *Marine and Petroleum Geology*, 115, 104276.

Deptuck, M.E., Kendell, K. and Smith, B. 2009. Complex deepwater fold-belts in the SW Sable Subbasin, offshore Nova Scotia. Frontiers and Innovation. *2009 CSPG CSEG CWLS Convention Calgary.*

Deptuck, M.E. 2010a. The 'slope detachment zone' on the western Scotian Slope, offshore Nova Scotia: structural style, timing, and implications for margin evolution. In *Conjugate Margins II, Abstract volume* IV: 87–95.

Deptuck, M.E. 2010b. Key structural elements in the southwestern most Sable Subbasin, offshore Nova Scotia, Canada. *CNSOPB Geoscience Open File Report* 2010-001PF.

Deptuck, M.E., and Campbell, D.C. 2012. Widespread erosion and mass failure from the 51Ma Montagnais marine bolide impact off southwestern Nova Scotia, Canada. *Canadian Journal of Earth Sciences*. 49: 1567—1594.

Deptuck, M.E., Brown, D.E., and Altheim, B. 2015. Call for Bids NS15-1 – Exploration history, geologic setting, and exploration potential: Western and Central regions. *CNSOPB Geoscience Open File Report*, 2015-001MF, 49p.

Deptuck, M.E., and Kendell, K.L. 2020. Atlas of 3D seismic surfaces and thickness maps, central and southwestern Scotian Slope, *Canada-Nova Scotia Offshore Petroleum Board Geoscience Open File Report*: 2020-001MF to 006MF.

Ding, F., Spiess, V., MacDonald, I.R., Bruning, M., Fekete, N. and Bohrmann, G. 2010. Shallow sediment deformation styles in north-western Campeche Knolls, Gulf of

Mexico, and their controls on the occurrence of hydrocarbon seepage. *Marine Petroleum Geology*, 27: 959–972.
Eliuk, L.S., 1978. The Abenaki Formation, Nova Scotia Shelf, Canada – A Depositionaland Diagenetic Model for a Mesozoic Carbonate Platform: *Bulletin of Canadian Petroleum Geology*. 26(4): 424–514.
Eliuk, L. 2008. Regional Setting of the late Jurassic Deep Panuke Field, Offshore NovaScotia, Canada – Cuttings based Sequence Stratigraphy and Depositional Facies Associations Abenaki Formation Carbonate Margin. Central Atlantic Margin – Conjugate Margin Conference – Halifax 2008, 186–208.
Enachescu, M. E., and Hogg, J. (2005). Exploring for Atlantic Canada's Next Giant Petroleum Discovery: *Recorder*, 30(5): 19–30.
EnCana 2006. Deep Panuke Offshore Gas Development Plan. Vol. 2, Halifax, Nova Scotia.
Fensome, R.A., Crux, J.A., Gard, I.G., MacRae, R.A., Williams, G.L., Thomas, F.C., Fiorini, F., and Wach, G. 2008. The last 100 million years on the Scotian Margin, Offshore Eastern Canada. In *Atlantic Geology* 44. An event-stratigraphic scheme emphasizing biostratigraphic data. p93- 126.
Fowler, M. and Webb, J. 2015. Report on Geochemical Analyses of Piston Core Samples, Offshore Nova Scotia.
Fowler, M. and Webb, J. 2017. Geochemistry Data Report for 2016 Scotian Slope Piston Coring Program. 620p.
Fowler, M. and Webb, J. 2019. Geochemistry Data Report for 2018 Scotian Slope Coring Program. 306p. https://oera.ca/research/piston-coring-geochemistry-program
Fowler, M., and Hubert, C. 2020. Geochemistry and Microbiology in Seep Prospecting. *GEOexPRO*, 17(2).
Gartrell, A., Lils, M. and Underschultz, J. 2002. Controls on the trap integrity of the Skua oil field, Timor Sea, in M. Keep and S. J. Moss, eds., The sedimentary basins of Western Australia 3: *Proceedings of the Petroleum Exploration Society of Australia Symposium, Perth*, p. 389–407.
Gay, A., Lopez, M., Berndt, C. and Ranne, M. 2007. Geological controls on focused fluid flow associated with seafloor seeps in the Lower Congo Basin. *Marine Geology*, 244(1-4): 68–92.
Gay, A., Takano, Y., Gilhooly III, W.P., Berndt, C., Heeschen, K., Suzuki, N., Saegusa, S., Nakagawa, F., Tsunogai, U. and Jiang, S.Y. 2011. Geophysical and geochemical evidence of large-scale fluid flow within shallow sediments in the eastern Gulf of Mexico, offshore Louisiana. *Geofluids* 11: 34–47.
Gemmer, L., Beaumont, C. and Ings, S.J. 2005. Dynamic modelling of passive margin salt tectonics: effects of water loading, sediment properties and sedimentation patterns, *Basin Research*, 17: 383–402.
Geological Survey of Canada. 1991. East Coast Basin Atlas Series: Scotian Shelf. 152p.
Gould, K., Pe-Piper, G. and Piper, D.J.W. 2010. Relationship of diagenetic chlorite rims to depositional facies in the Lower Cretaceous reservoir sandstones of the Scotian Basin. In *Sedimentology*, 57: 587–610.
Harland, N., Hogg, J., Riddy, R., Syhlonyk, G., Uswak, G. J. Weissenberger and R.Wierzbicki. 2002. A Major Discovery at the Panuke Field Jurassic Abenaki Formation Offshore Nova Scotia: *CSPG Convention Abstracts*.

Harrington, P. 1985. Formation of pockmarks by pore-water escape. *Geo-Marine Letters*, 5: 193–197.

Heggland, R. 1998. Gas seepage as an indicator of deeper prospective reservoirs; a study based on exploration 3D seismic data. *Marine and Petroleum Geology*, 5(1): 1–9.

Hintze, W.H. 1971. Depiction of faults on stratigraphic isopach maps. *The American Association Petroleum Geologists Bulletin*, 55(6): 871–879.

Hogg. J.R., Dolph, D.A., Mackidd, D. and Michel, K. 2001. Petroleum Systems of Deep-Water Basins–Global and Gulf of Mexico Experience, R.H. Fillon, N.C. Rosen, P. Weimer, A. Lowrie, H. Pettingill, R.L. Phair, H.H. Roberts, H.H. van Hoom.

Hood, K. C., Wenger, L. M., Gross, O. P., and S. C. Harrison, 2002. Hydrocarbon systems analysis of the northern Gulf of Mexico: Delineation of hydrocarbon migration pathways using seeps and seismic imaging. *In* Surface exploration case histories: Applications of geochemistry, magnetics, and remote sensing, D. Schumacher and L.A. LeSchack, eds., *American Association of Petroleum Geologists* Studies in Geology No. 48 and *SEG Geophysical References Series* No. 11: 25–40.

Hou, D., Pang, X., Xiao, J., Shang, J., Shi, H., Wang, J., Shu, Y. and Zu, J. 2008. Geological and geochemical evidence on the identification of natural gas migration through fault system, Baiyun Sag, Pearl River Mouth Basin. *Earth Science Frontiers*, 15: 81–87.

Hovland, M., 2012. The Geomorphology and Nature of Seabed Seepage Processes, Bathymetry and Its Applications, Dr. Philippe Blondel (Ed.), ISBN: 978-953-307-959-2, *InTech.*

Hovland, M., Heggland, R., De Vries, M.H., and Tjelta, T.I. 2010. Unit-pockmarks and their potential significance for predicting fluid flow. *Marine and Petroleum Geology*, 27: 1190–1199.

Hovland, M., Jensen, S. and Fichler, C. 2012. Methane and minor oil macro-seep systems—their complexity and environmental significance. *Marine Geology* 332–334: 163–173.

Huang, B., Xiao, X., Li, X. and Cai, D. 2009. Spatial distribution and geochemistry of the nearshore gas seepages and their implications to natural gas migration in the Yinggehai Basin. *Offshore South China Sea Marine and Petroleum Geology*, 26: 928–935.

Ings, S.J. and Shimeld, J.W. 2006. A new conceptual model for the structural evolution of a regional salt detachment on the northeast Scotian margin, offshore eastern Canada, *AAPG Bulletin*, 90:1407–1423.

Ings, S.J., Gemmer, L. and Beaumont, C. 2009. Passive Margin Salt Tectonics Driven by Progradation. *AAPG Bulletin*, 81(3): 398–423.

Jansa, L.F., Pe-Piper, G., Robertson, P.B., and Freidenreich, O. 1989. Montagnais: A submarine impact structure on the Scotian shelf, eastern Canada. *Geological Society of America Bulletin*, 101: 450–463.

Jansa, L.F., and Wade, J.A. 1975. Paleogeography and sedimentation in the Mesozoic and Cenozoic, southeastern Canada. *In* Canada's continental margins and off-Shore petroleum exploration. Edited by C.J. Yorath, E.R. Parker, and D.J. Glass. *Canadian Society of Petroleum Geologists*, Calgary. pp. 79–102.

Johansen, C., Macelloni, L., Natter, M., Silva, M., Woosley, A., Diercks, A.R., Hill, J., Viso, R., Marty, E., Lobodin, V.V., Shed, W., Joye, S.B. and MacDonal, I.R. 2020. Hydrocarbon migration pathway and methane budget for a Gulf of Mexico natural seep site: green canyon 600. *Earth and Planetary Science Letters*, 545, 116411.

Judd, A. and Hovland, M. 2007. Seabed fluid flow around the world. In *Seabed Fluid Flow: The Impact on Geology, Biology and the Marine Environment* (pp. 45–133). Cambridge: Cambridge University Press.

Keen, C. 2000. Causes and consequences of tectonically driven Cretaceous/Tertiary uplift on the Grand Banks.

Kendell, K.L. 2012. Variations in salt expulsion style within the Sable Canopy Complex, central Scotian margin. *Canadian Journal of Earth Sciences*, 49: 1504 –1522. doi: 10.1139/e2012-069.

Kennicutt M.C. 2017. Oil and Gas seeps in the Gulf of Mexico. In: Ward C. (Eds) *Habitats and Biota of the Gulf of Mexico*: Before the Deepwater Horizon Oil Spill. Springer, New York, NY.

Keppie, J.D. 2000. Geological map of the Province of Nova Scotia; Nova Scotia Department of Natural Resources, Minerals and Energy Branch, Map ME 2000-1, scale 1:500 000. Available online as DP ME43, Version 2, 2006 at http://www.novascotia.ca/natr/meb/download/dp043.htm.

Kidston, A.G., Brown, D.E., Smith, B.M. and Altheim, B. 2002. Hydrocarbon Potential of The Deep-Water Scotian Slope: *Canada-Nova Scotia Offshore Petroleum Board (CNSOPB Report)*, Halifax, 111p.

Kidston, A.G., Brown, D.E., Smith, B.M., and Altheim, B. (2005). The Upper Jurassic Abenaki Formation Offshore Nova Scotia: A Seismic and Geologic Perspective. *Canada-Nova Scotia Offshore Petroleum Board*, Halifax, 165p.

Kidston, A.G., Brenton, M.S., Brown, D.E., Makrides, C. and Altheim, B. 2007. Nova Scotia Deepwater Wells, Post Drill Analysis, 1982-2004. *CNSOPB Report*, Halifax, 181p.

Koson, S., Chenrai, P., and Choowong, M. 2014. Seismic attributes and seismic geomorphology. *Bulletin of Earth Sciences of Thailand*, 6(1): 1–9.

Kvenvolden, K.A., Vogel, T.M., and Gardner, J.V. 1981. Geochemical prospecting for hydrocarbons in the outer continental shelf, southern Bering Sea, Alaska. *Journal of Geochemical Exploration*, 14: 209–219.

Laubmeyer, G. 1933. A new geophysical prospecting method, especially for deposits of Hydrocarbons. *Petroleum*, 28(18): 1–4.

Lee, J. 2018. "Glacial Lithofacies and Stratigraphy", Chapter 11 in *Past Glacial Environments* (Second edition), Elsevier, pp. 377–429.

Leythauser, D., Schaefer, R.G. and Yukler, A. 1982. Role of diffusion in primary migration of hydrocarbons. *AAPG Bulletin*, 66(4): 408–429.

Leythauser, D., Schwark, L., and Keuser, C. 2000. Geological conditions and geochemical effects of secondary petroleum migration and accumulation. *Marine and Petroleum Geology* 17: 857–859.

Liner, C.L. 2004. Elements of 3D seismology, 2nd Ed. PennWell Books, Tulsa, OK.

Link, W.K. 1952. Significance of oil and gas seeps in world oil exploration. *AAPG Bulletin*, 36: 1505–1541.

Løseth, H., Gading, M. and Wensaas, L. 2009. Hydrocarbon leakage interpreted on seismic data. *Marine and Petroleum Geology*, 26**:** 1304–1319.

Losh, S., Eglinton, L., Schoell, M. and J. Wood, 1999. Vertical and lateral fluid flow related to a large growth fault, Eugene Island Block 330 field, offshore Louisiana: *AAPG Bulletin*, 83: 244–276.

Louden, K. 2002. Tectonic Evolution of the East Coast of Canada. *Canadian Society of Exploration Geophysicists "Recorder*", 27(2): 37–48.

Macgregor, D.S. 1993. Relationships between seepage, tectonics and subsurface petroleum reservoirs. *Marine and Petroleum Geology*. 10:606–619.

Macgregor, D.S. 1996. Factors controlling the destruction or preservation of giant light oilfields. *Petroleum Geoscience* 2 (3): 197–217.

MacLean, B.C. 1991. Depth to pre-Mesozoic basement and oceanic layer 2, East Coast Basin Atlas Series, Scotian Shelf, *Geological Survey of Canada*, page 79.

MacLean, B.C., and Wade, J.A. 1993. Seismic Markers and Stratigraphic Picks in the Scotian Basin Wells. East Coast Basin Atlas Series, *Geological Survey of Canada*, 276p.

Magoon, L.B., and Dow, W.G. 1994. The petroleum system – From source to trap. *AAPG Memoir*, 60: 3–24.

McIver, N.L. 1972. Cenozoic and Mesozoic Stratigraphy of the Nova Scotia Shelf. *Canadian Journal of Earth Sciences*, 9: 54–70.

Marfut, K.J., and Alves, T.M. 2015. Pitfalls and limitations in seismic attribute interpretation of tectonic features. *Interpretation*, 3(1): 1F-TF1.

McQuillin, R., Bacon, M. and Barclay, W. 1984. An introduction to seismic interpretation: reflection Seismic in *petroleum exploration*, 2nd edn., Graham and Trotman Ltd, London.

Mosher, David. C. 2008. Bottom simulating reflectors on Canada's East Coast Margin: Evidence for gas hydrate. *Proceedings of the 6th International Conference on Gas Hydrates* (ICGH 2008), Vancouver, British Columbia, Canada.

Mukhopadhay, P.K., Brown, D., Kidston, A., Bowman, T., Faber, J. and Harvey, P. 2003. Petroleum Systems of Deepwater Scotian Basin, Eastern Canada: Challenges for Finding Oil versus Gas Provinces. *2003 Offshore Technology Conference, Houston, Texas*, May 5-8, 2003.

Mukhopadhyay, P.K., Wade, J.A. and Kruge, M.A. 1995. "Organic facies and maturation of Jurassic/Cretaceous rocks, possible oil-source rock correlation based on pyrolysis of asphaltenes, Scotian Basin, Canada". *Organic Geochemistry*, 22 (1): 85–104.

Mukhopadhyay, P.K. 1993. "Analyses and interpretation of geochemical and source rock data from Scotian Shelf wells". *Geological Survey of Canada Open File Report* 2804.

Mukhopadhyay, P.K. 1990. "Characterization and maturation of selected oil and condensate samples and correlation with source beds, Scotian Shelf." *Geological Survey of Canada Open File Report* 2620.

Mukhopadhyay, P.K. and Wade, J.A. 1990. "Organic facies and maturation of sediments from the three Scotian Shelf Wells". *Bulletin of Canadian Petroleum Geology* 38 (4): 407–424.

Murillo, C.A. 2011. Overview of Eastern and Atlantic Canada's Petroleum Industry and Economic Impacts of Offshore Atlantic Projects [2010-2035]: *Canadian Energy Research Institute*. Published report. https://ceri.ca/assets/files/Study_127_Full_Report.pdf

Nagle, J., Pe-Piper, G., Piper, D.J.W. and Saint-Ange, F. 2019. Predictive modelling of sandstone reservoir distribution in the SW Scotian Basin, *AGS 45th Colloquium*.

Nanda N.C. 2016a, Seismic Interpretation Methods. In: *Seismic Data Interpretation and Evaluation for Hydrocarbon Exploration and Production*. Springer, Cham, 37-72.

Nanda N.C. 2016b, Tectonics and Seismic Interpretation. In: *Seismic Data Interpretation and Evaluation for Hydrocarbon Exploration and Production*. Springer, Cham, 73–89.

Nanda, N.C. 2021. Direct Hydrocarbon Indicators (DHI). In: *Seismic Data Interpretation and Evaluation for Hydrocarbon Exploration and Production*. Advances in Oil and Gas Exploration & Production. Springer, Cham.

Natural Resources Canada 2009. Geology of the Scotian Margin. www.nrcan.gc.ca.

Nord-gard Bolas, H. M., and C. Hermanrud, 2003. Hydrocarbon leakage processes and trap retention capacities offshore Norway: *Petroleum Geoscience*, 9: 321–332.

OERA (2015) Southwest Nova Scotia Expansion: Georges Bank and Shelburne Subbasin Study. *Nova Scotia Department of Energy Report*. https://oera.ca/research/sw-nova-scotiaexpansion-atlas-2015

OERA (Offshore Energy Research Association) 2019. Shelburne Subbasin Postmortem Analysis Review of Cheshire L-97 and Monterey Jack E-93. Comparison with OETR 2011 Play Fairway Analysis. https://oera.ca/sites/default/files/202001/Shelburne_subbasin_Postmortem_Analysis_FINAL_Resize.pdf

OETRA: Offshore Energy Technical Research Association. 2011. Play Fairway Analysis Atlas – Offshore Nova Scotia. Nova Scotia Department of Energy Report, *NSDOE Records Storage File* No. 88-11-0004-01, 347p.

Oyeyemi, K.D. and Aizebeokhai, A.P. 2015. Seismic attributes analysis for reservoir characterization: offshore Niger Delta. *Petroleum and Coal*, 57(6): 619–628.

Phipps, G.G. and Carson, T.G. 1982. The exploration significance of seismic DHI analysis in Malay Basin. In: *Proceedings Offshore Technology Conference* No. 14, 3-6 May 1982, Houston, Texas, 2: 391–402.

Hovla, J.D., Kang, M.H., and Han, H.C. 2013. First order seismic attributes for clastic seismic Facies interpretation: Examples from the East China Sea. *Journal of Asian Earth Sciences* 66: 34–54.

Pilcher, R.S., Kilsdonk, B., and Trude, J. 2011. Primary basins and their boundaries in the deep-water northern Gulf of Mexico: Origin, trap types, and petroleum system implications. *AAPG Bulletin*, 95(2): 219–240.

Piper, D.J.W., Pe-Piper, G., and Ingram, S.C. 2004. Early Cretaceous sediment failure in the southwestern Sable Subbasin, offshore Nova Scotia. *Bulletin of American Association of Petroleum Geologists*, 88(7): 991–1006.

Piper, D.J.W., Notfall, R., and Pe-Piper, G. 2010. Allochthonous prodeltaic sediment Facies in the Lower Cretaceous at the Tantallon M-41 well: Implications for the Deep-water Scotian Basin. *Bulletin of American Association of Petroleum Geologists*, 94(1) 87–104.

Pramanik, A.G., Singh, V., Srivastava, A.K. and Rakesh, K. 2002. Stratigraphic Inversion for enhancing vertical resolution. *Geohorizons*, **7**(2): 8–18.

Pramanik, A.G., Srivastava, A.K., Singh, V. and Katiyar, R. 2003. Stratigraphic interpretation using post-stack inversion: case histories from Indian Basins: In: *Expanded abstract, 65th EAGE conference* held on June 2—6, Stavanger, p52.

Reilly II, J.F., MacDonald, I.R., Biegert, E.K. and Brooks, J.M. 1996. Geologic controls on the distribution of chemosynthetic communities in the Gulf of Mexico. In: Schumacher, D., Abrams, M.A. (Eds.), *Hydrocarbon Migration and its Near Surface Effects. AAPG Memoir*, 66: 39–62.

Roberts, H.H., Aharon, P., Carney, R., Larkin, J. and Sassen, R. 1990. Sea floor response to hydrocarbon seeps, Louisiana continental slope. *Geo-Marine Letters*, 10: 232–243.

Roden, R., Forrest, M. and Holeywell, R. 2012. Relating seismic interpretation to reserve/resource calculations: insights from a DHI consortium. *The Leading Edge* 31(9): 1066–1074.

Rollet, N., Logan, G.A., Kennard, J.M., O'Brien, P.E., Jones, A.T. and Sexton, M. 2006. Characterization and correlation of active hydrocarbon seepage using geophysical data sets. An example from the tropical, carbonate Yampi Shelf, Northwest Australia. *Marine and Petroleum Geology* 23: 145–164.

RPS. 2013. Environmental observation report., Shell Canada Limited: Shelburne Basin 3D Seismic Survey. Available online at www.cnsopb.ns.ca/sites/default/files/resource/environmental_report_final.pdf

Shaw, J., Piper, D., Fader G., King, E., Todd, G., Bell, T., Batterson, M. and Courtney, R. 2004. A conceptual model of the deglaciation of Atlantic Canada.

Shell Canada Ltd., 2017. Monterey Jack E-43/E-43A End of Well Report. *Canada-Nova Scotia Offshore Petroleum Board* File No. D405.

Shell Canada Ltd., 2018. Cheshire L-97/L-97A End of Well Report. *Canada-Nova Scotia Offshore Petroleum Board* File No. D404.

Shimeld, J. 2004. A comparison of salt tectonic subprovinces beneath the Scotian Slope and Laurentian Fan. *24th Annual GCS-SEPM Foundation, Bob F. Perkins Research Conference*, Houston. 291–306.

Smith, B.M., Makrides, C., Altheim, B. and Kendell, K. 2014. Resource Assessment of undeveloped Significant Discoveries on the Scotian Shelf. *Canada-Nova Scotia Offshore Petroleum Board*, 182p. https://www.cnsopb.ns.ca/sites/default/files/resource/sda_report__finalhighquality_april_3_2014.pdf

Swift, S.A. 1987. Late Cretaceous-Cenozoic Development of Outer Continental Margin, Southwestern Nova Scotia. *American Association of Petroleum Geologists Bulletin*, 71(6): 678–701.

Taner, M.T., Koehler, F., and Sheriff, R.E. 1979. Complex Seismic Trace Analysis. *Geophysics* 44 (6):1041.

Taner, M.T., Schuelke, J.S., Doherty, R.O. and Baysal, E. 1995. Seismic attributes revisited. In: Expanded abstract, *Society of Exploration Geophysicists*, pp 1104–1106.

Taner, M.T. 2001. Seismic attributes: Canadian Society of Exploration Geophysicists. *Recorder*, 26(9): 48–56.

Thomas, F.C. 2005. Oligocene benthic foraminifera from the Paleogene Wenonah Canyon, Scotian Shelf – normal versus canyon assemblages. *Atlantic Geology*, 41: 1–16.

Thrasher, J., Fleet, A., Hay, S.J., Hovland, M. and Duppenbecker, S. 1996. Understanding geology is the key to using seepage in exploration: the spectrum of seepage styles. In: Schumacher, D., Abrams, M.A. (Eds.), Hydrocarbon Migration and its Near Surface Effects. *AAPG Memoir*, 66: 223–242.

Tissot, B.P., and Welte, D.H. 1984. Petroleum Formation and Occurrence. 2nd Edition, Springer-Verlag, Berlin, 699p.

Vendeville, B.C. 2005. Salt tectonics driven by sediment progradation: Part I – Mechanics and kinematics. *AAPG Bulletin*, 89(8): 1071–1079.

Wade, J. A., and MacLean B. C. 1990a. The geology of the southeastern margin of Canada. Geology of the continental margin of eastern Canada: *Geological Survey of Canada*, Geology of Canada, 2: 167–238.

Wade, J.A., and MacLean, B.C. 1990b. Aspects of the Geology of the Scotian Basin from Recent Seismic and Well Data. In *Geology of the Continental Margins of Eastern Canada*: *Geological Survey of Canada, Geology of Canada*, 2: 190–238.

Weston, J.F. and MacRae, R.A., Ascoli, P., Cooper, M.K.E., Fensome, R.A., Shaw, D., and Williams G.L. 2012. A revised biostratigraphic and well log sequence stratigraphic framework for the Scotian Margin, offshore eastern Canada. *Canadian Journal of Earth Sciences*, 49: 1417–1462.

Weimer, P., Zimmerman, E., Cossey, S.P., Hirsh, H., Snyder, B., Leibovitz, M., and Adson, J. 2017. Atlas of fields and discoveries, central Mississippi Canyon, Atwater Valley, northwestern Lloyd Ridge, and western DeSoto canyon protraction areas, northern deep-water Gulf of Mexico. *AAPG Bulletin*, 101(7): 995–1002.

Welsink, H.J. 1989. Tectono-stratigraphy of the passive margin off Nova Scotia, *AAPG Memoir* 46.

Wenger, Lloyd and Isaksen, Gary. 2002. Control of Hydrocarbon Seepage Intensity on Level of Biodegradation in Sea Bottom Sediments. *Organic Geochemistry*, 33**:** 1277–1292.

Whelan, J., Eglinton, L., Cathles III, L., Losh, S. and Roberts, H. 2005. Surface and subsurface manifestations of gas movement through a N-S transect of the Gulf of Mexico. *Marine and Petroleum Geology*, 22(4): 479–497.

Wierzbicki, R., Dravis, J.J., Al-Aasm, I., and Harland, N. 2006. Burial dolomitization and dissolution of Upper Jurassic Abenaki platform carbonates, Deep Panuke reservoir, Nova Scotia, Canada. *American Association of Petroleum Geologists Bulletin*, 90: 1843–1861.

Withjack, M.O., and Schlische, R.W. 2006. A Review of Tectonics Events on the Passive Margin of Eastern North America. *25th Annual Bob F. Perkings Research Conf.,* 203–235.

Zhang, Y., Pe-Piper, G. and Piper, D.J.W. 2014. Sediment geochemistry as a provenance indicator: Unravelling the cryptic signatures of polycyclic sources, climate change, tectonism and volcanism, *Sedimentology*, 61, 383–410, doi: 10.1111/sed.12066.

Appendix I: Coordinate Systems in ArcMap

Checking for a Coordinate System:

1. Right click on the title of the Map Layer in the Table of Contents. Click on properties at the bottom of the pop-up menu
2. Click on the Source tab
3. In the Data Source Section, choose the Geographic Coordinate System or Projected coordinate system label. This will tell the current coordinate system being used by the map layer.
4. The other map layers can be checked to confirm they are using the same Coordinate System. If not, they can be changed to match each other.

Changing a Coordinate System in a Map Layer

1. Open ArcToolbox
2. Open Data Management Tools – Projections and Transformations – Feature – Project. The project dialog box will appear:
    a. Under Input Data Set or Feature Class, choose the Map Layer whose projection you wish to change. It can be an entirely new Map Layer or Shapefile or one that is already being used in a Map Project.
    b. Under Output Data Set or Feature Class, check to make sure that the file is being saved in the same folder as the rest of your Map and Data Layers. If your data is in a Geodatabase, you can save the newly projected Map Layer directly into the Geodatabase by browsing to its location. Rename the new Map Layer so that you will recognize it and be able to distinguish it from the Map Layer you are changing.
    c. Under Output Coordinate System, click on the Properties button (looks like a sheet of paper with a pointing finger hovering over it). The Spatial References Properties dialog box will appear. Click the Select button. The
    d. Browse for Coordinate System dialog box will appear.

3. Choose the Projected Coordinate System folder or the Geographic Coordinate system folder, depending upon the Coordinate Systems of your other files and how you want to match them.
4. Click the Apply button to apply the chosen Coordinate System. Then click OK twice

If you changed the name of the Shapefile/Map layer in the Projection process, you would have to add this new Map Layer to your map and/or Geodatabase and remove the old Map Layer that uses the incorrect Coordinate System.

Appendix II: 3D Seismic Cross Sections

This supplementary appendix contains extra Inline and crossline seismic traces that cut across/along samples collected in 2015, 2016 and 2018 that did not make it in the main text. All seismic sections are shown with permission from NSDNRR.

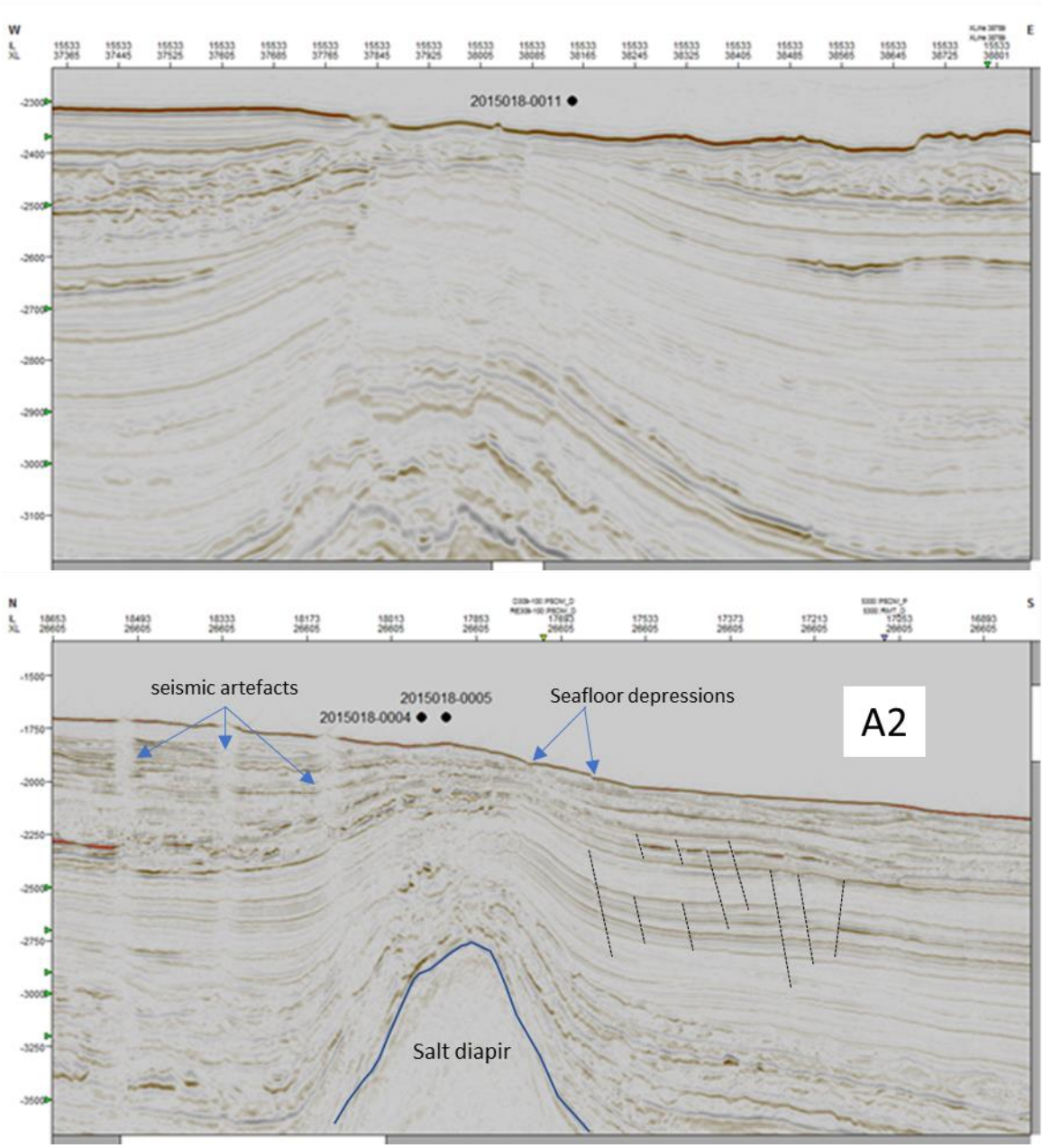

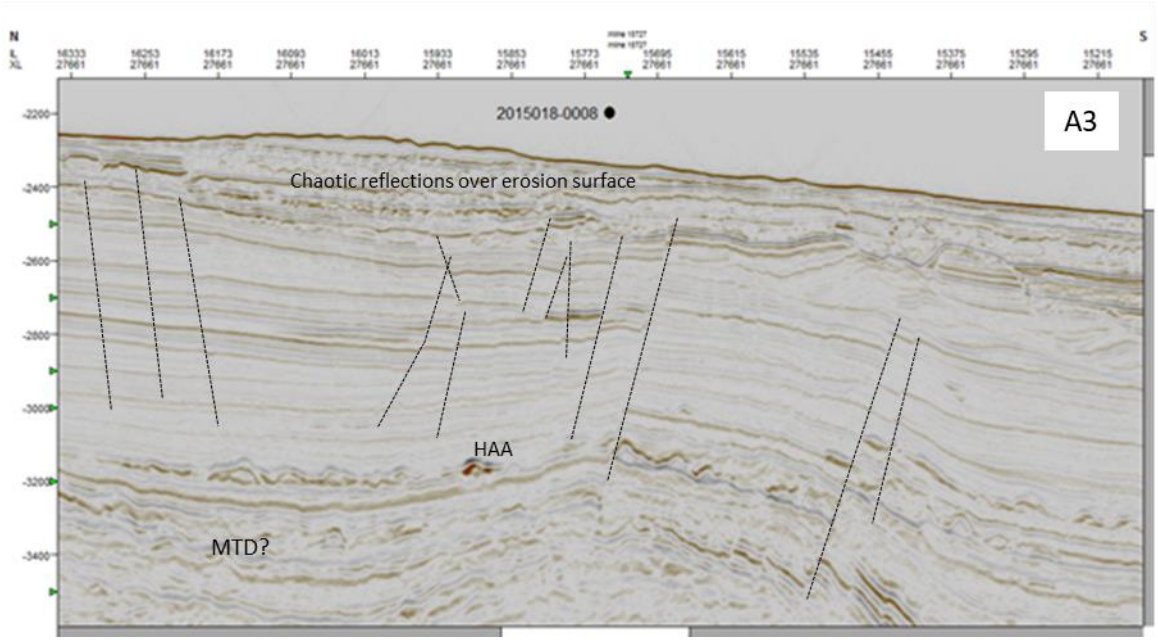
N
S
2015018-0008
A3
Chaotic reflections over erosion surface
HAA
MTD?

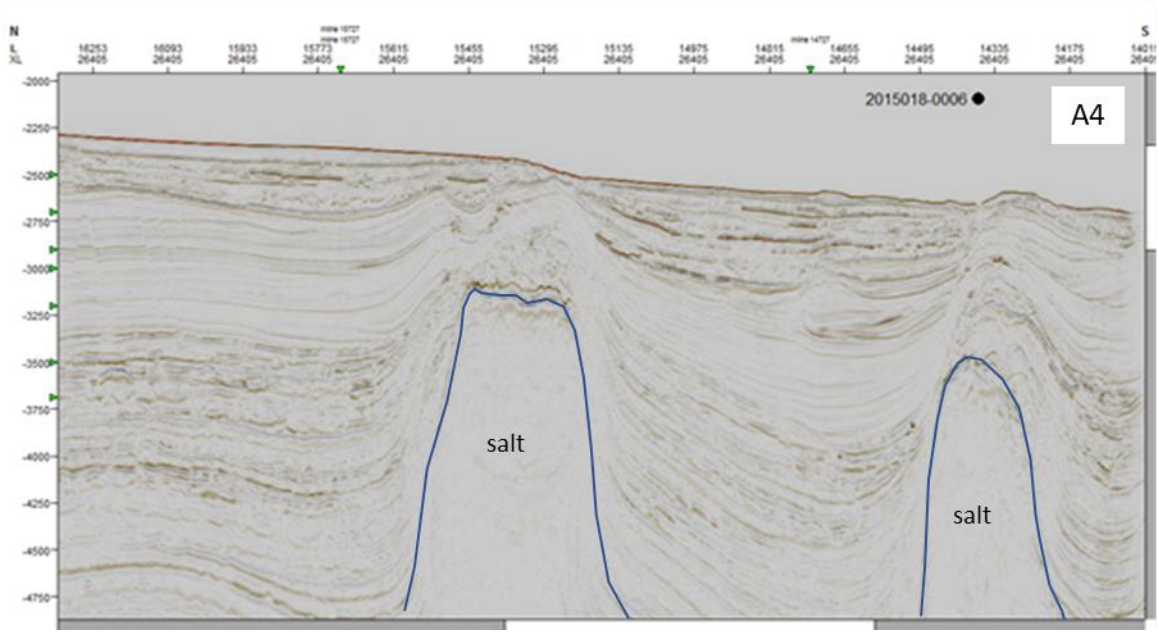
N
S
2015018-0006
A4
salt
salt

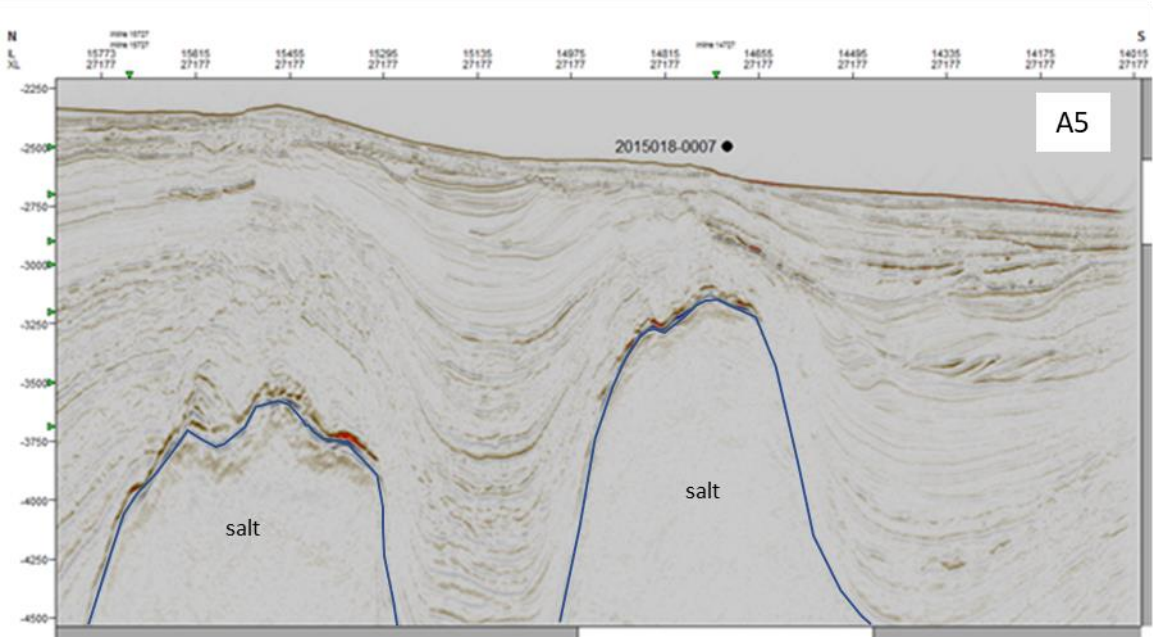
A5
2015018-0007
salt
salt

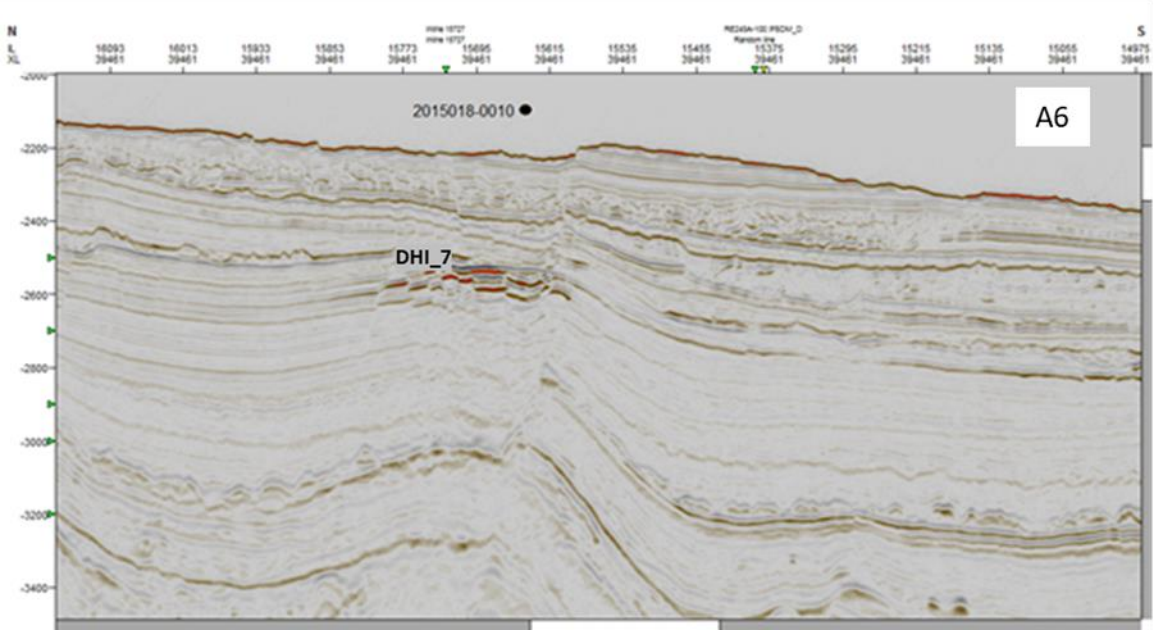
A6
2015018-0010
DHI_7

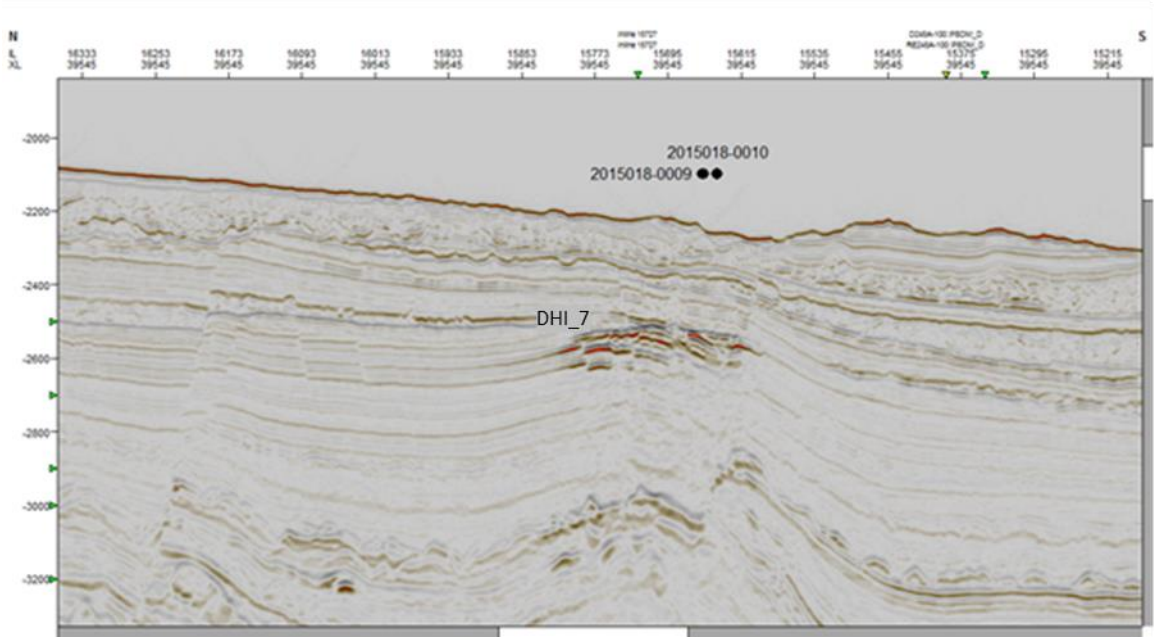
N
S
2015018-0010
2015018-0009
DHI_7

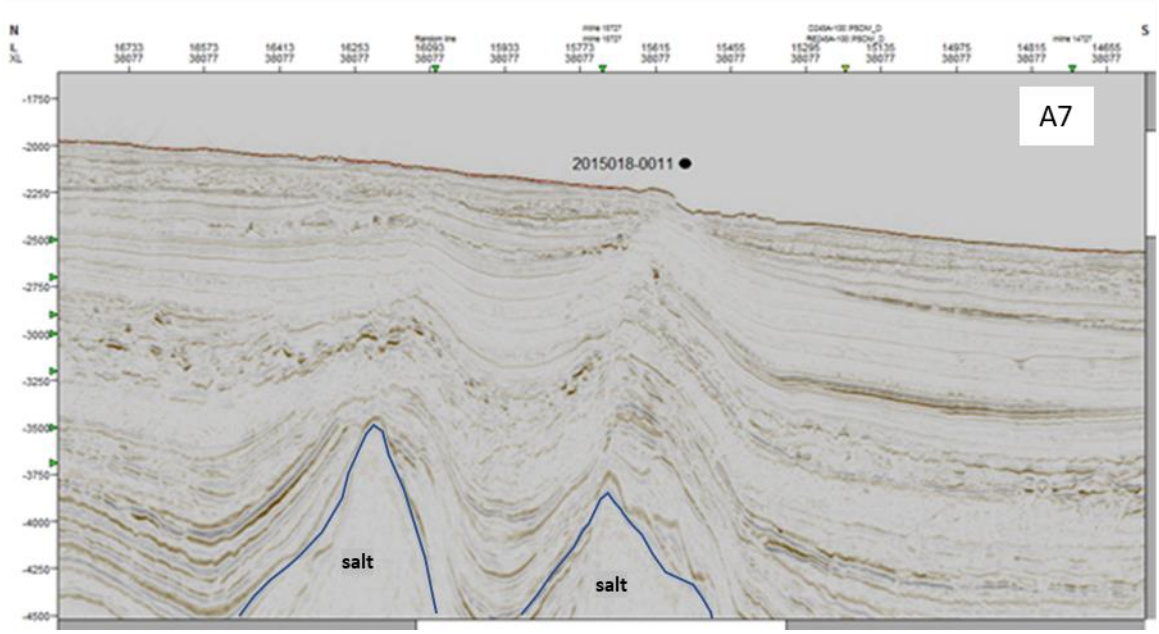
N
S
A7
2015018-0011
salt
salt

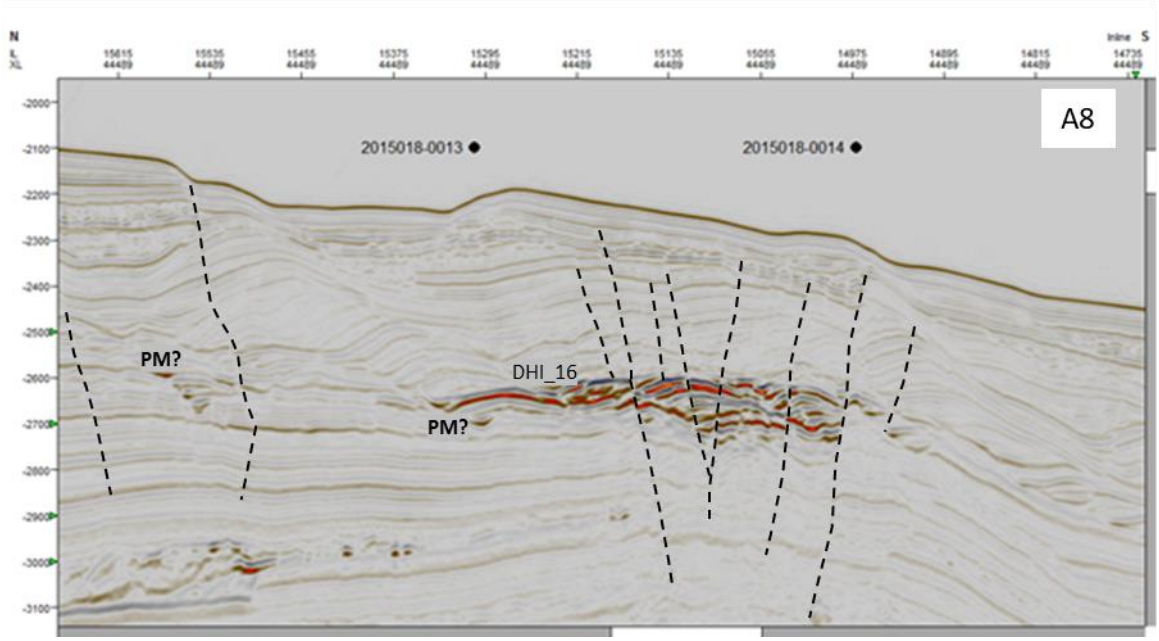
A8
2015018-0013
2015018-0014
PM?
DHI_16
PM?

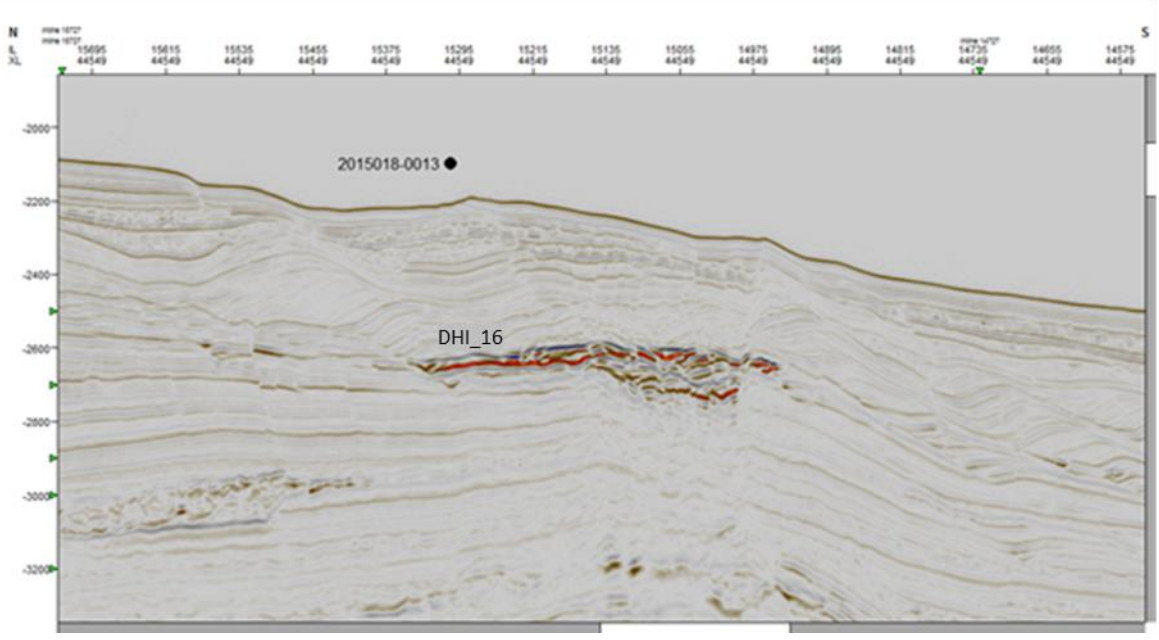
2015018-0013
DHI_16

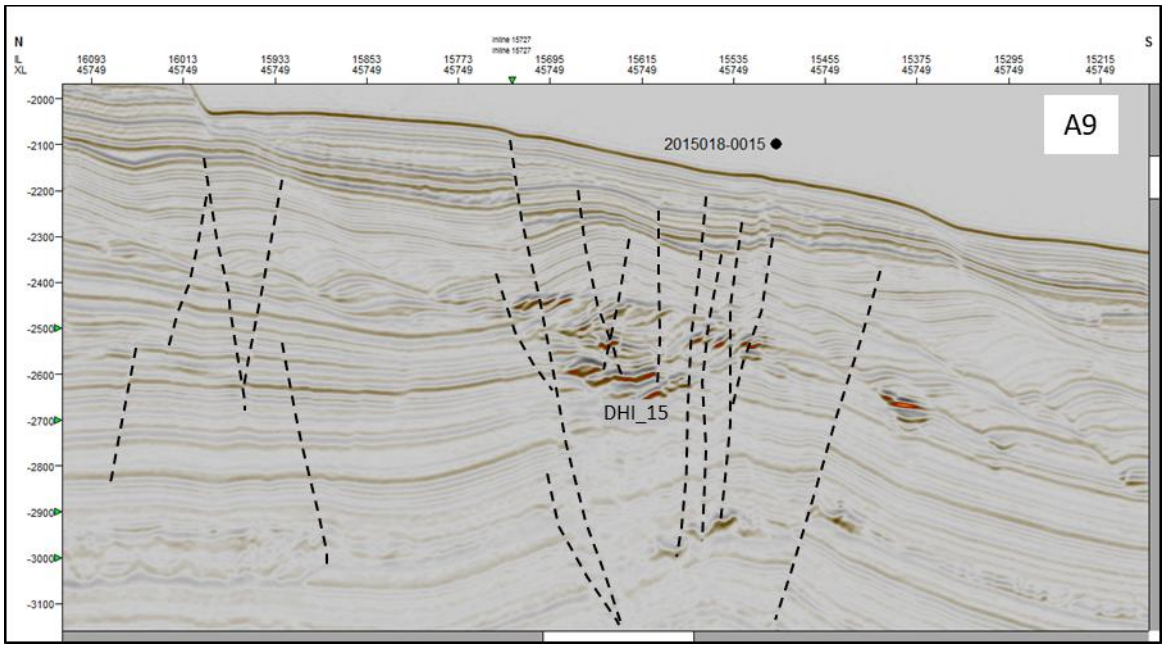
N
S
IL
XL
16093 45749
16013 45749
15933 45749
15853 45749
15773 45749
15695 45749
15615 45749
15535 45749
15455 45749
15375 45749
15295 45749
15215 45749
-2000
-2100
-2200
-2300
-2400
-2500
-2600
-2700
-2800
-2900
-3000
-3100
A9
2015018-0015
DHI_15

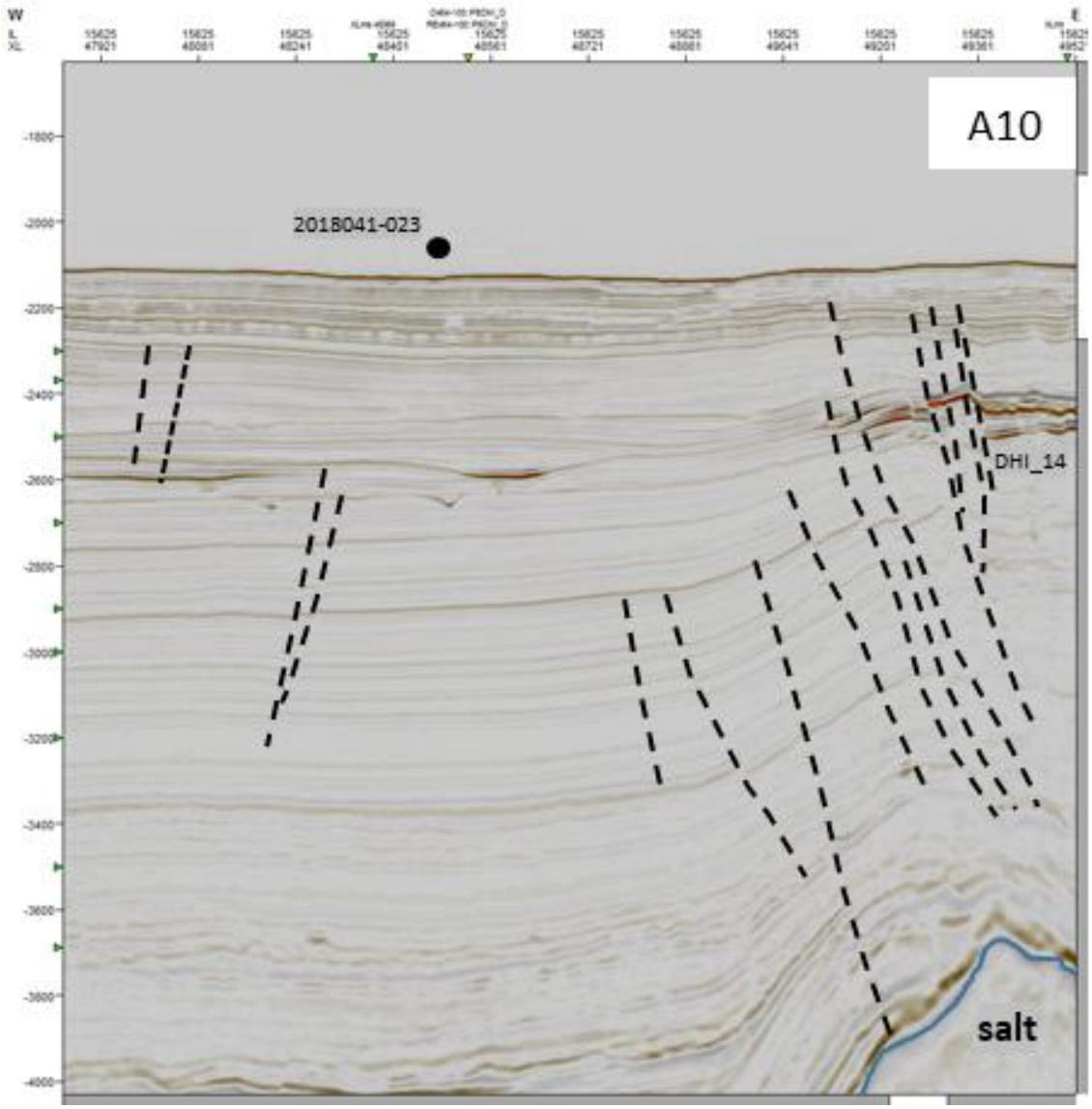
A10
2018041-023
DHI_14
salt

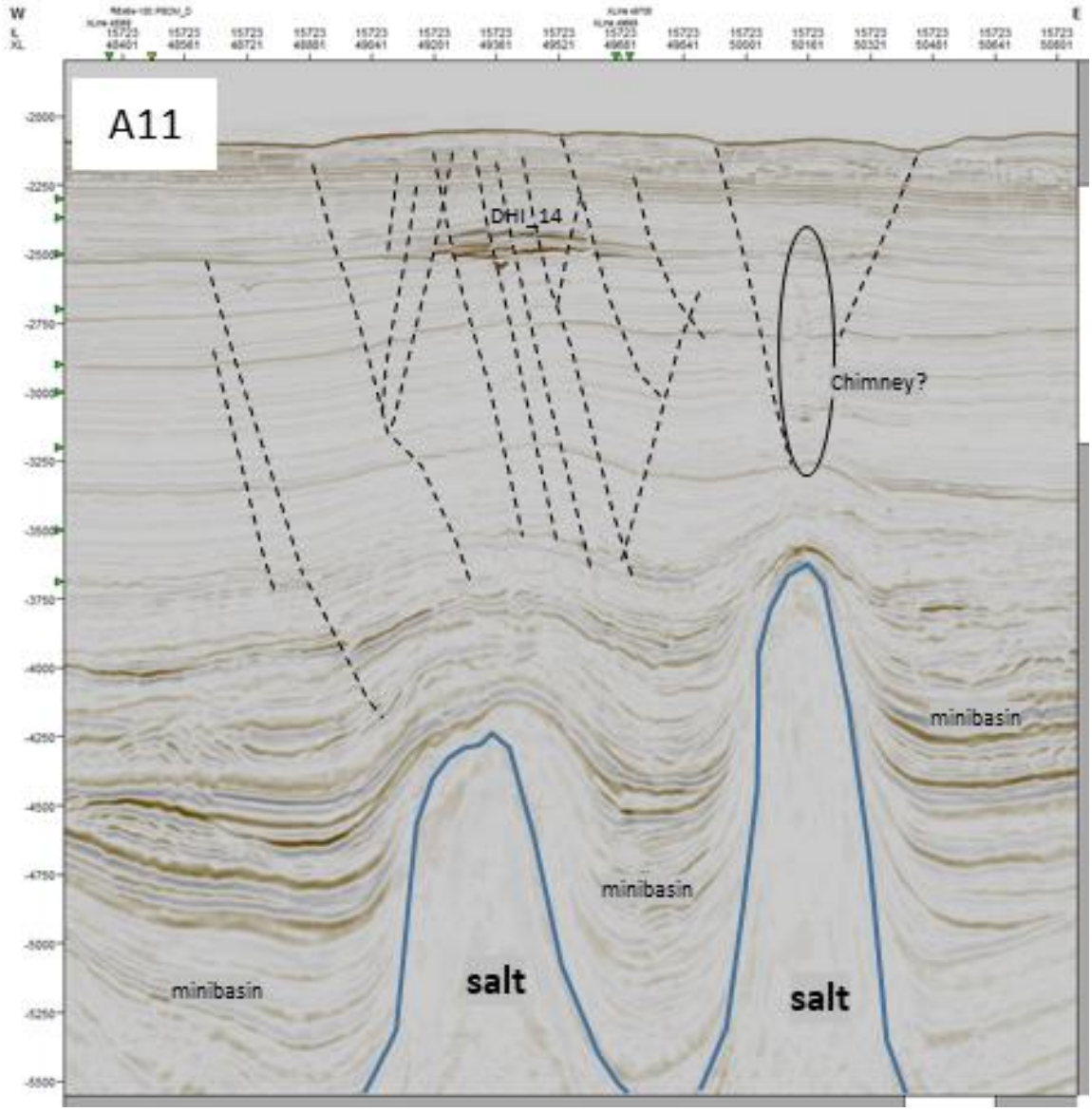
A11
DHI_14
Chimney?
minibasin
minibasin
minibasin
salt
salt

2018_021

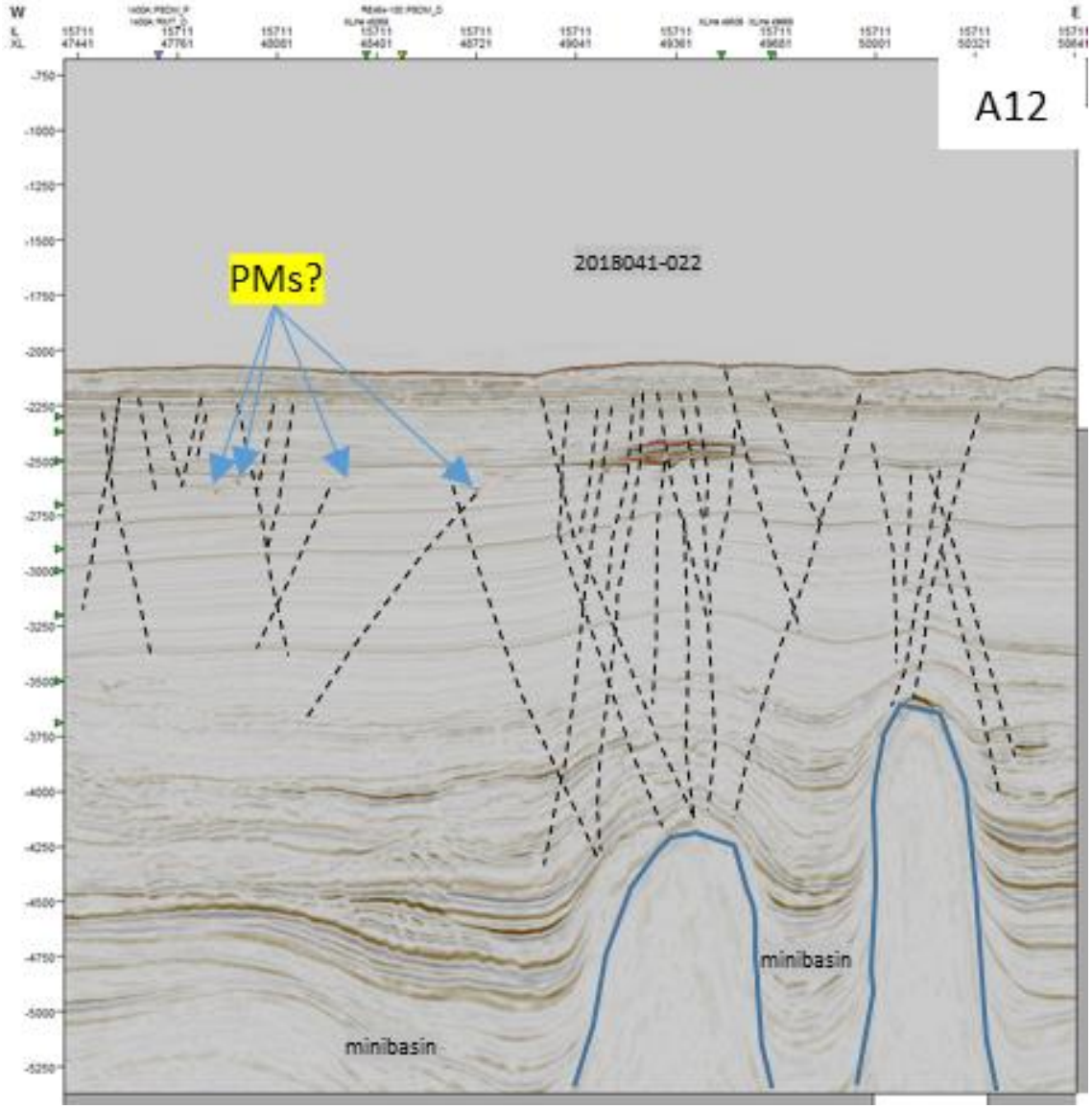

2018_22/ DHI_14

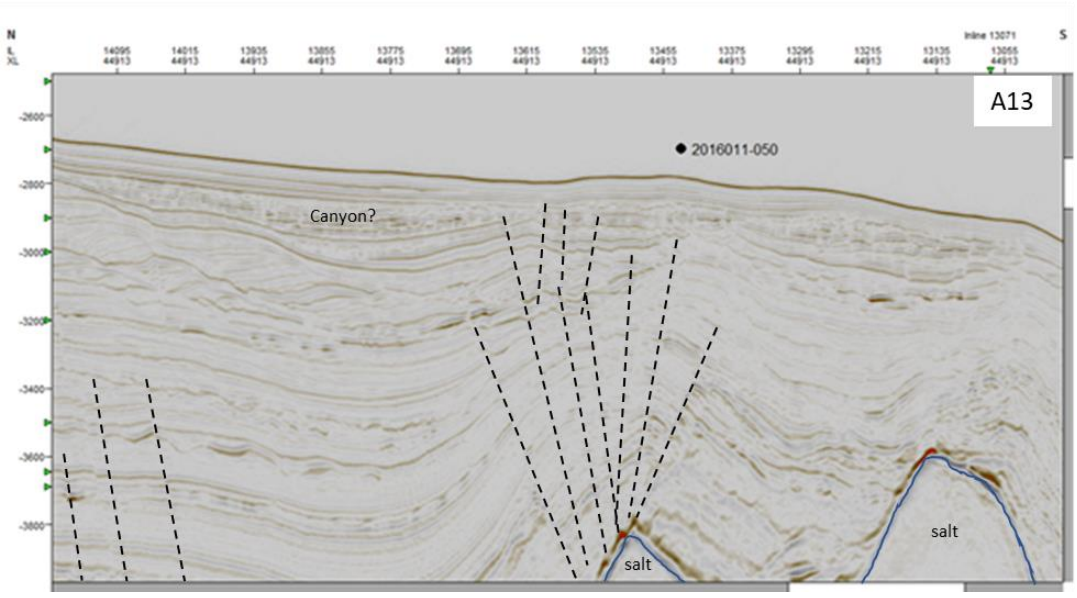
A13
2016011-050
Canyon?
salt
salt

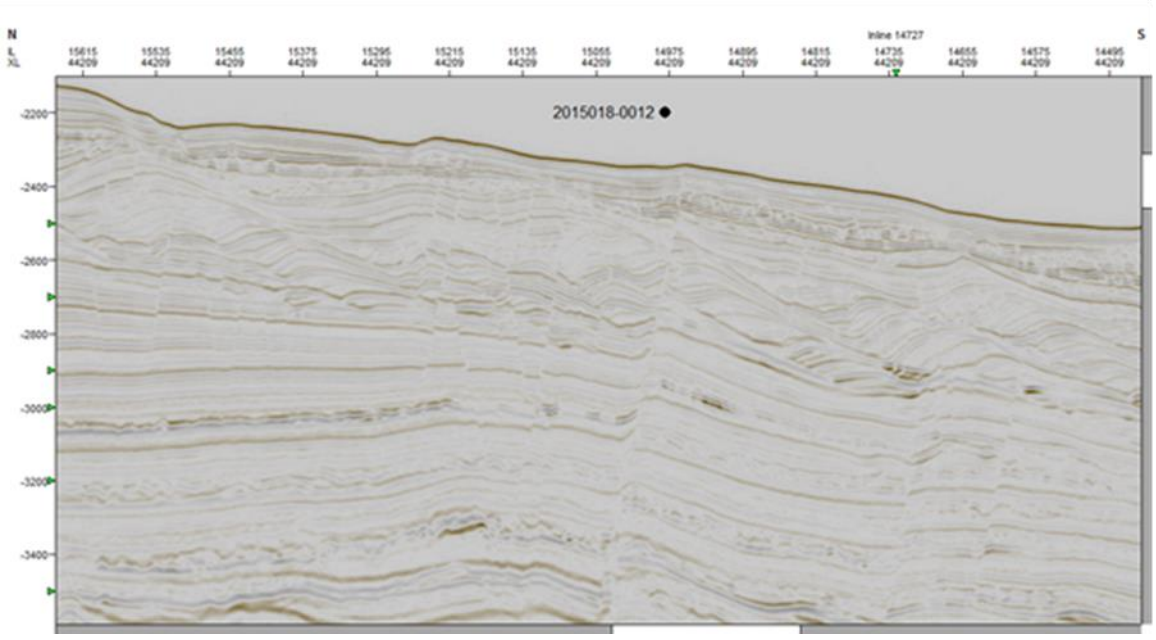
2015018-0012

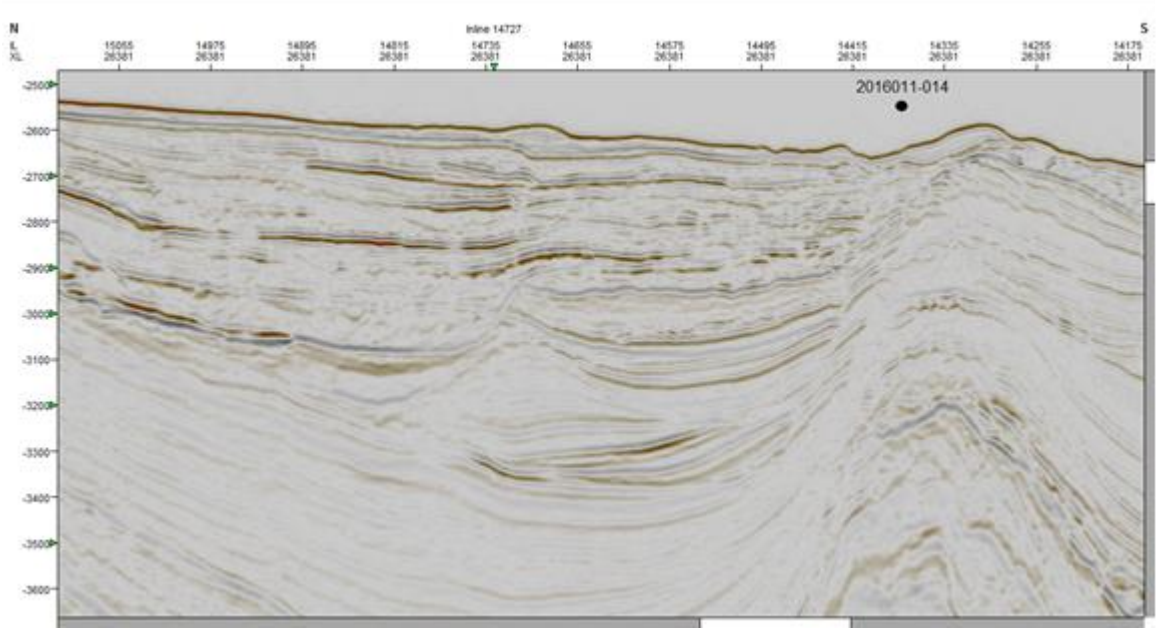
N
Inline 14727
S
IL
XL
2016011-014

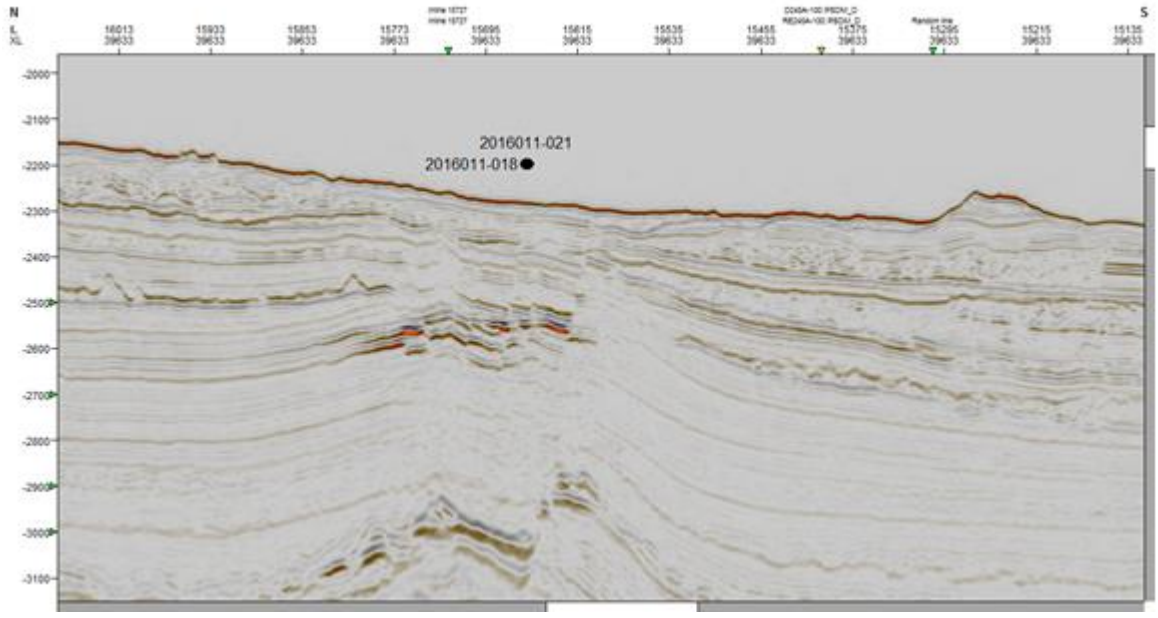
N
S
IL
XL
2016011-021
2016011-018

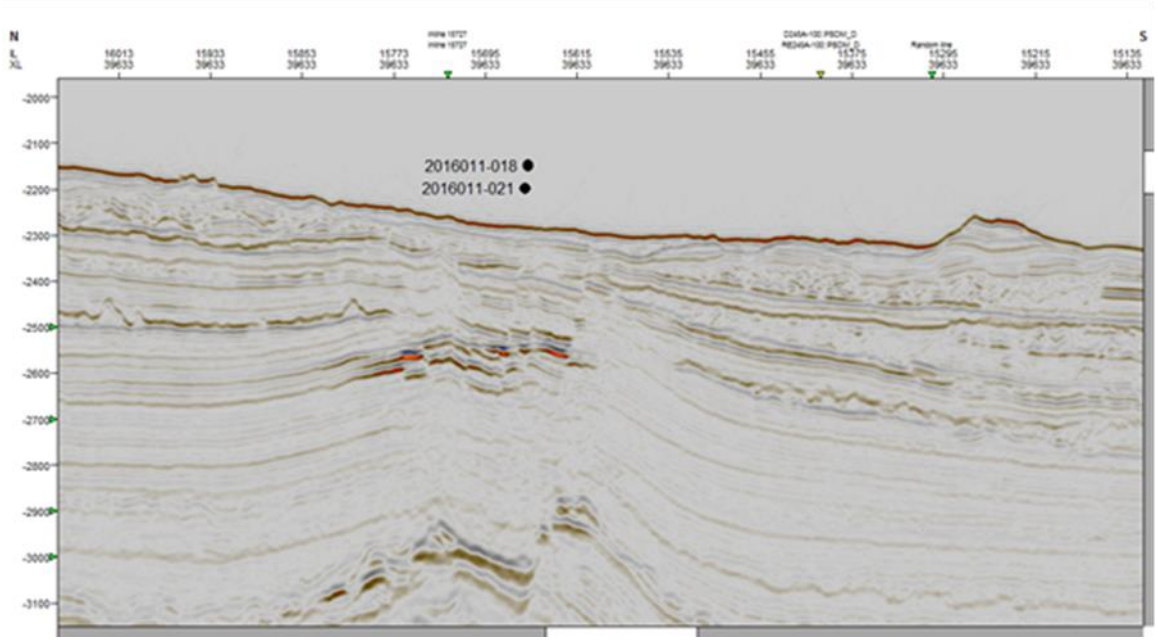
N
S
2016011-018
2016011-021

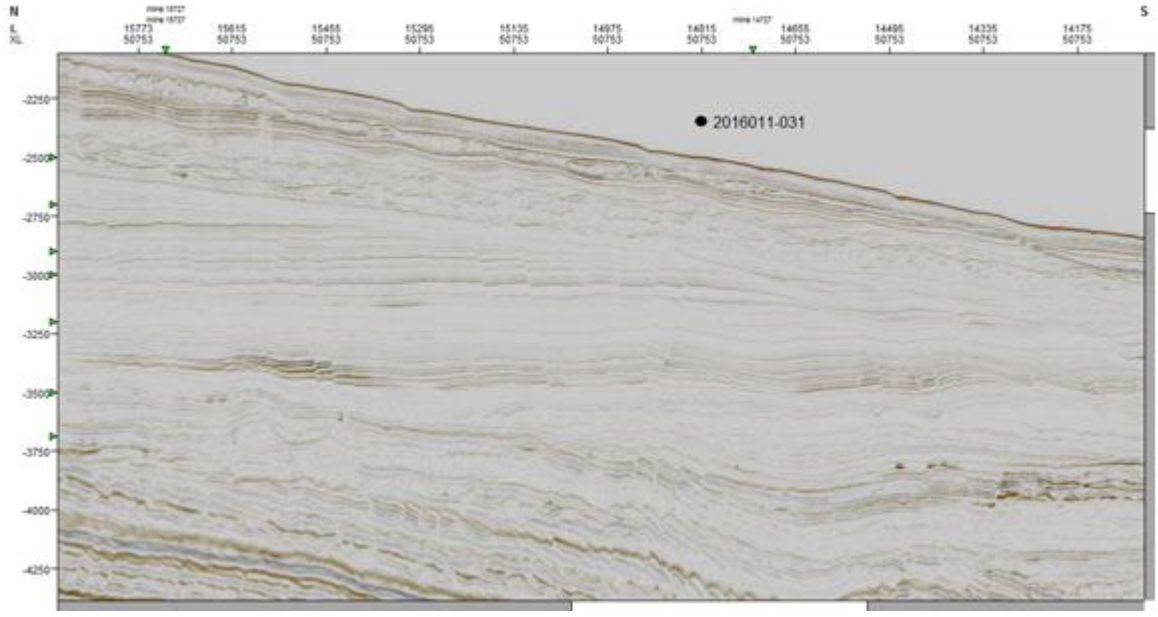
N
S
2016011-031

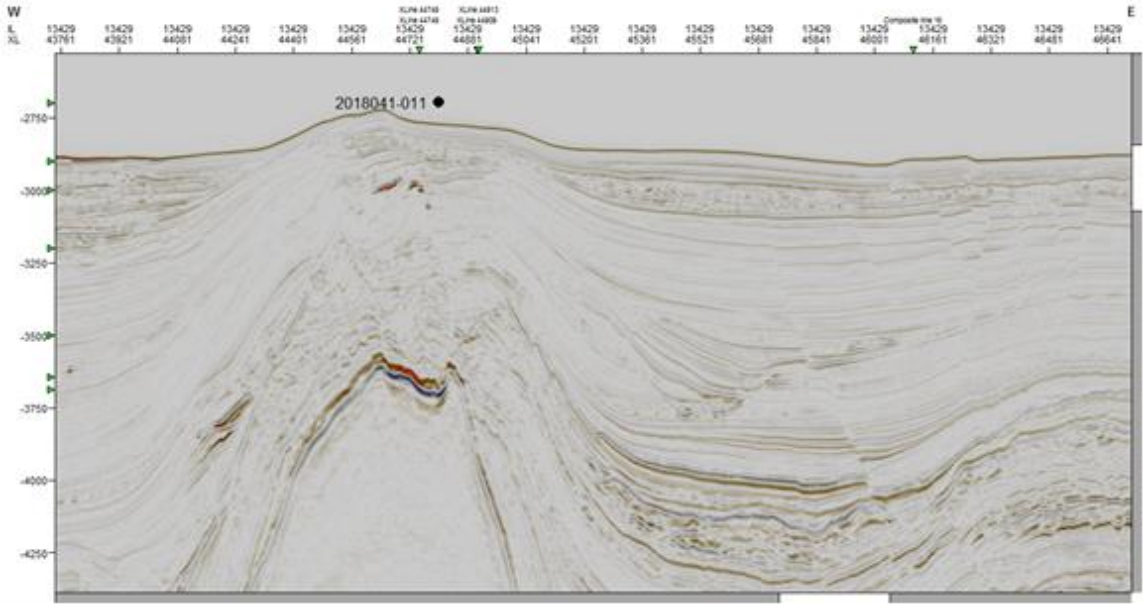
W
E
2018041-011

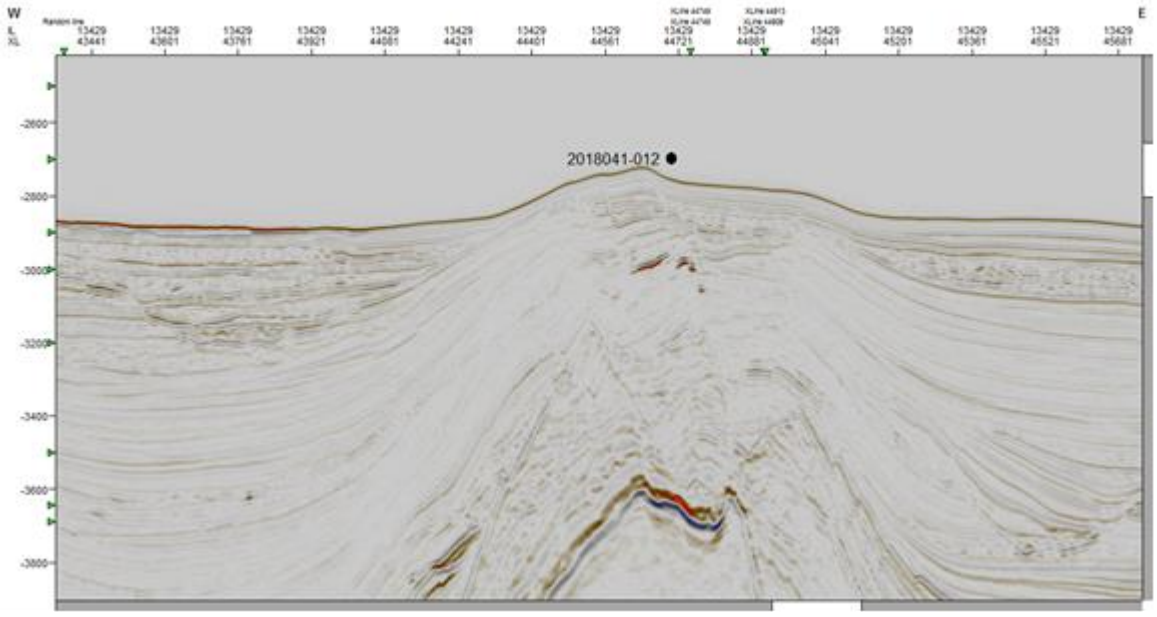
W
E
2018041-012

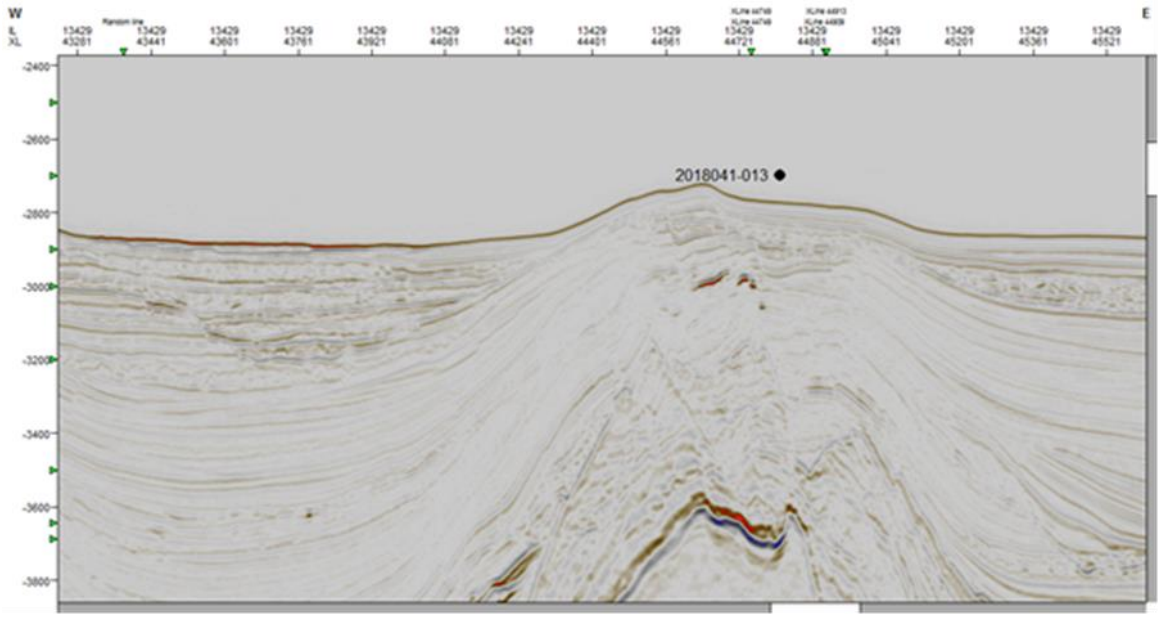
W
E
2018041-013

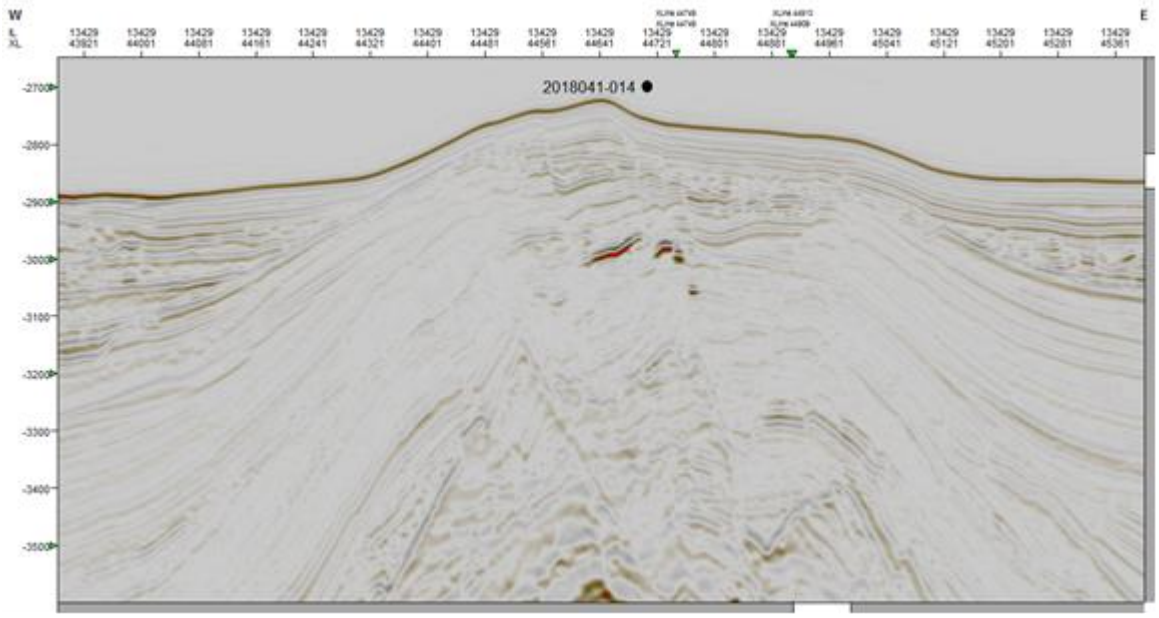
W
E
2018041-014

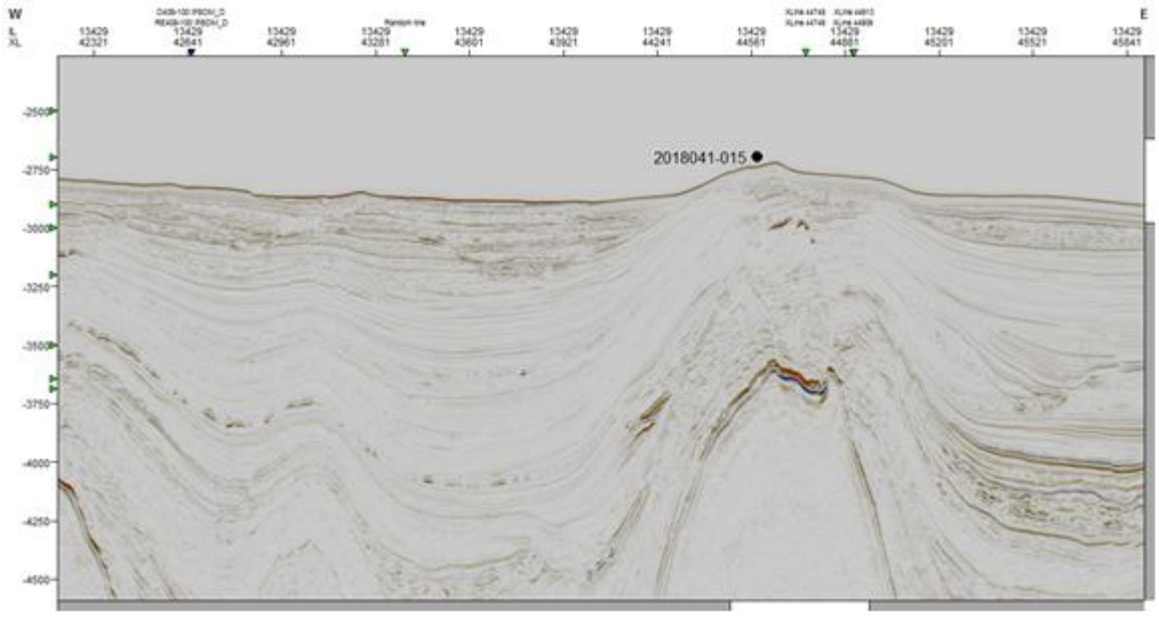
W
E
IL
XL
2018041-015

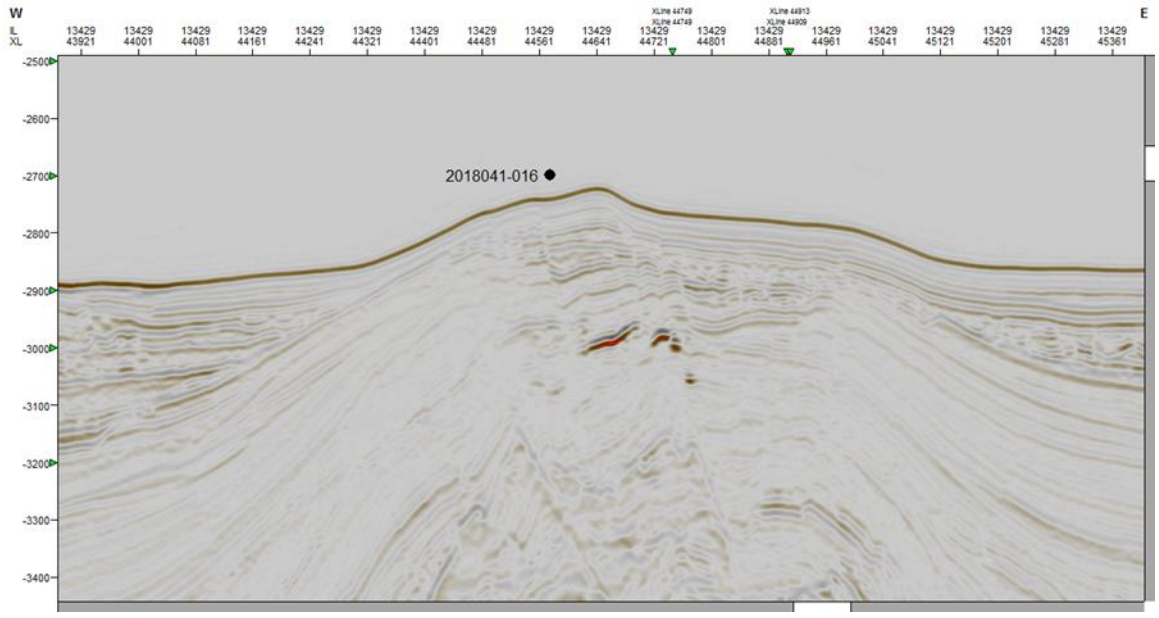
W
E
IL
XL
2018041-016

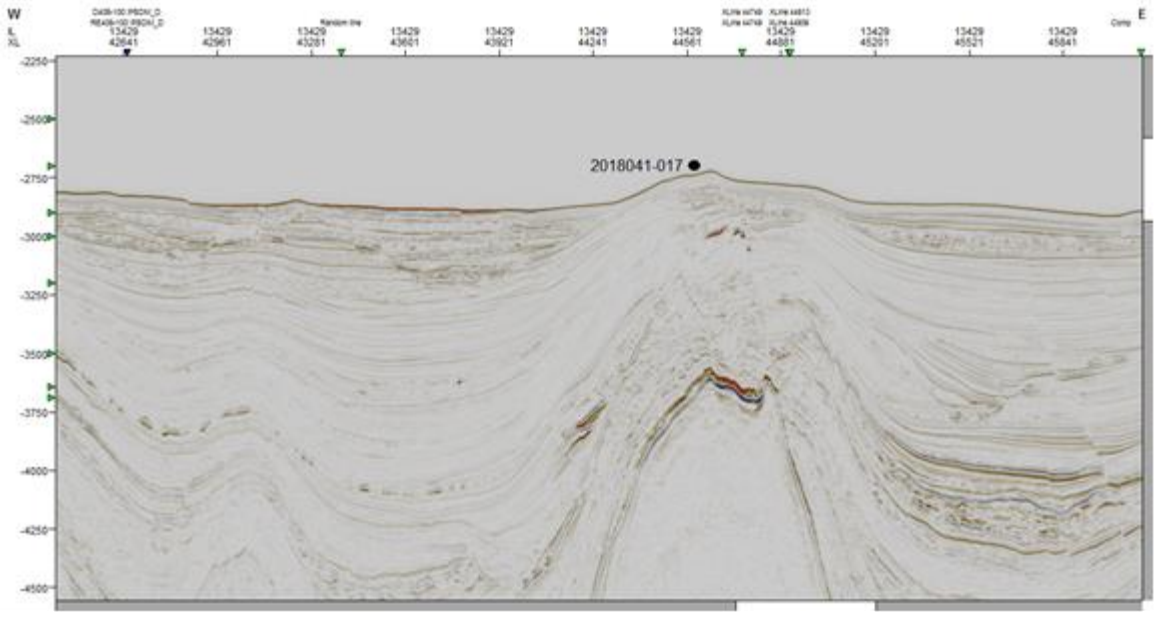
W
E
IL
XL
2018041-017

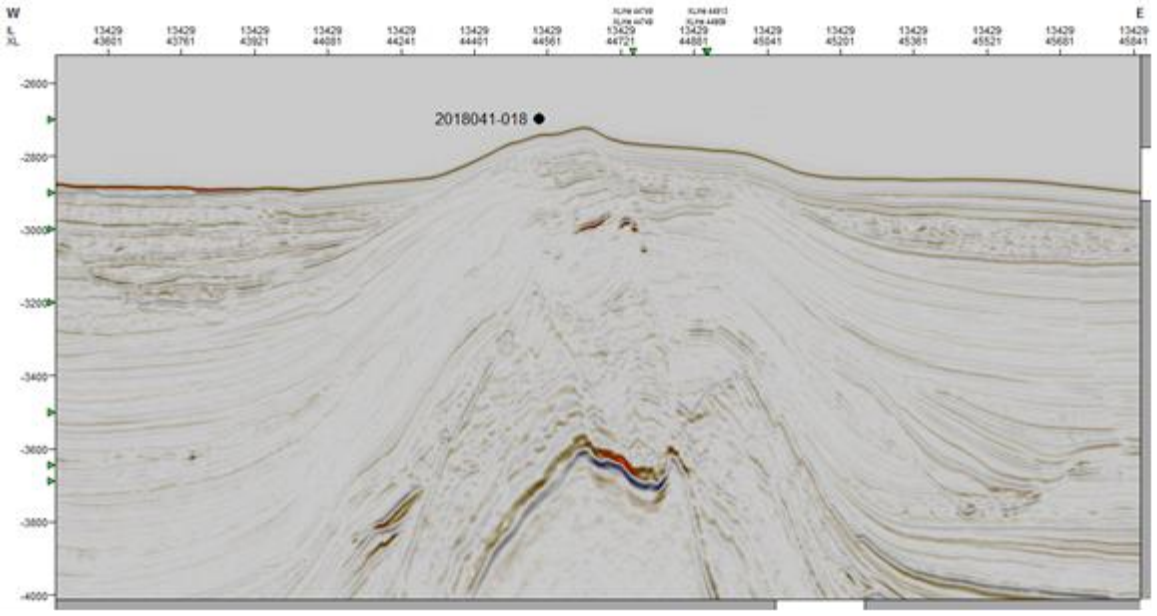
W
E
IL
XL
2018041-018

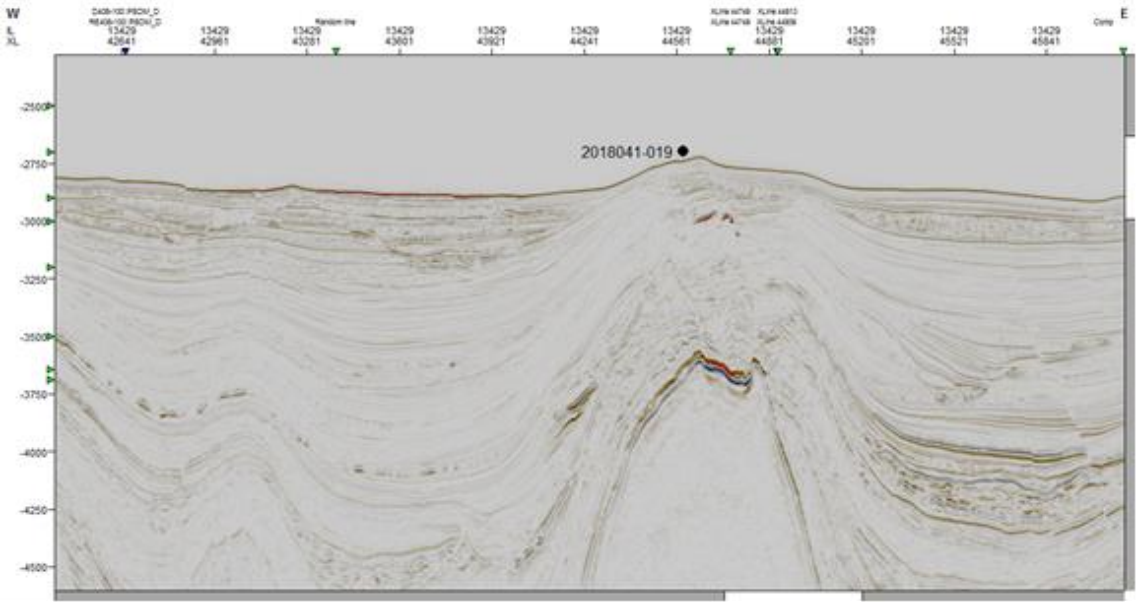
W
E
2018041-019

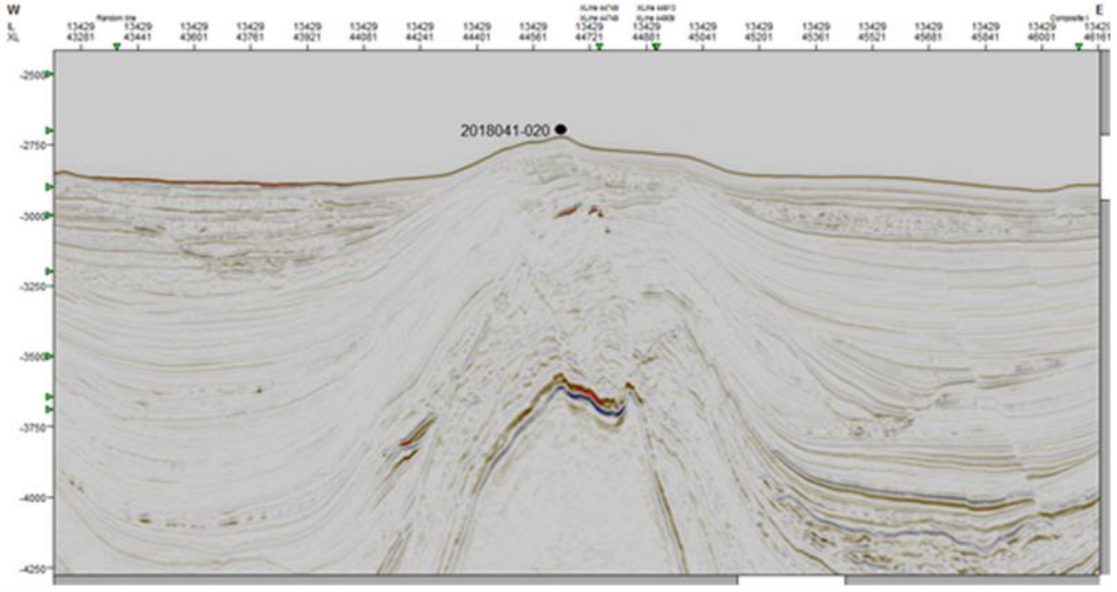
W
E
2018041-020

Appendix II: Coherence Maps

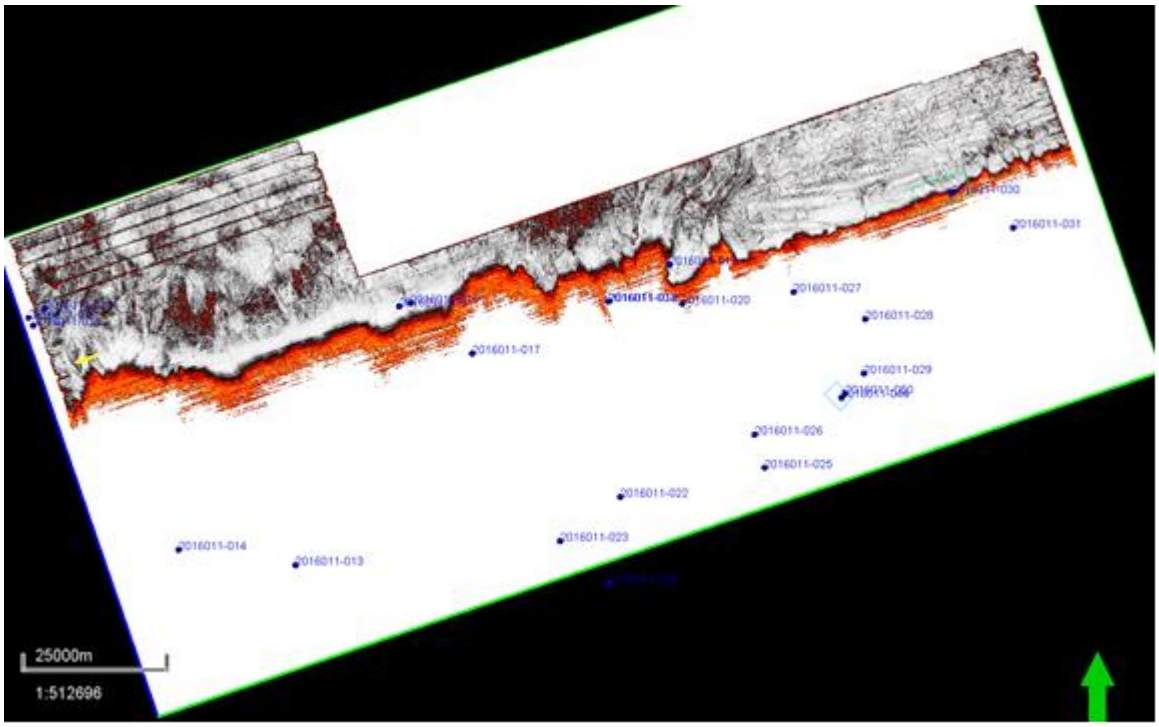

Z = -2100

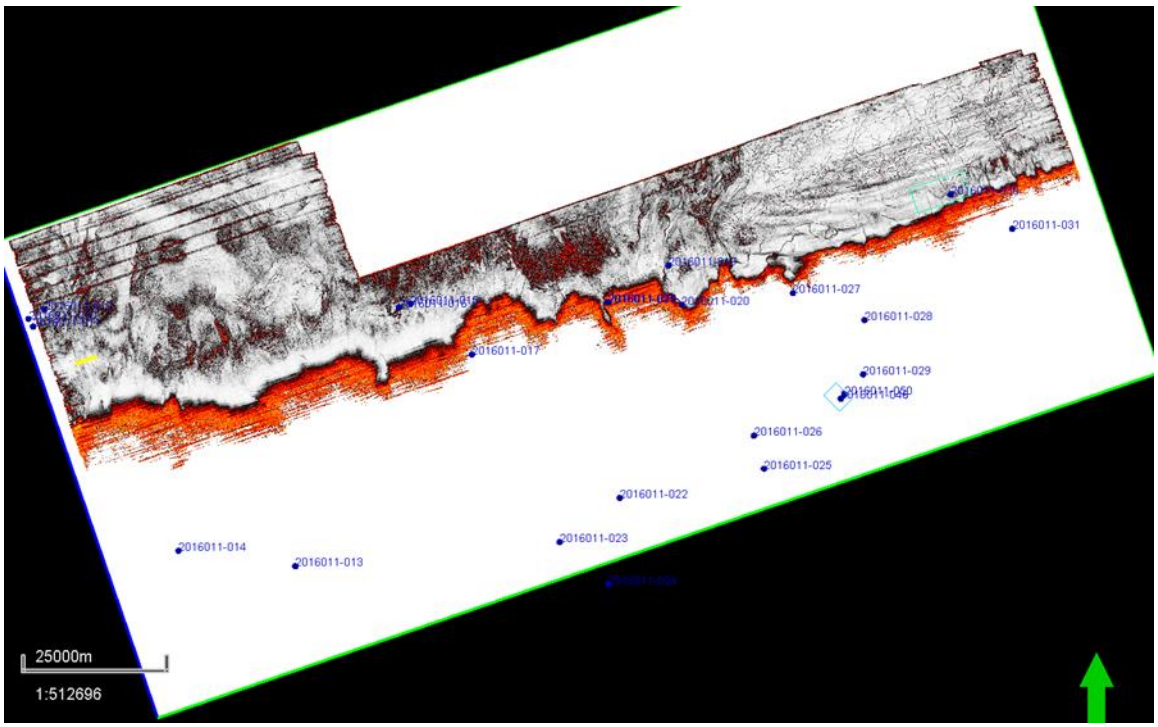

Z = -2200

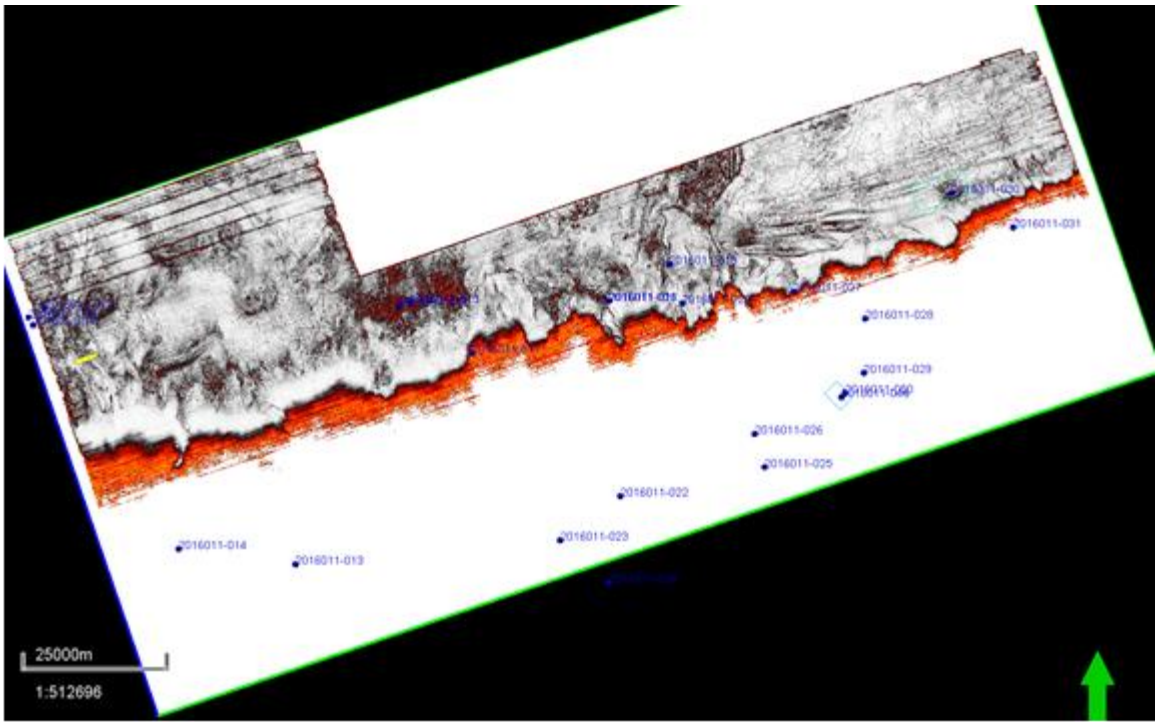
2016011-031
2016011-028
2016011-029
2016011-026
2016011-025
2016011-022
2016011-023
2016011-014
2016011-013
25000m
1:512696

Z = -2300

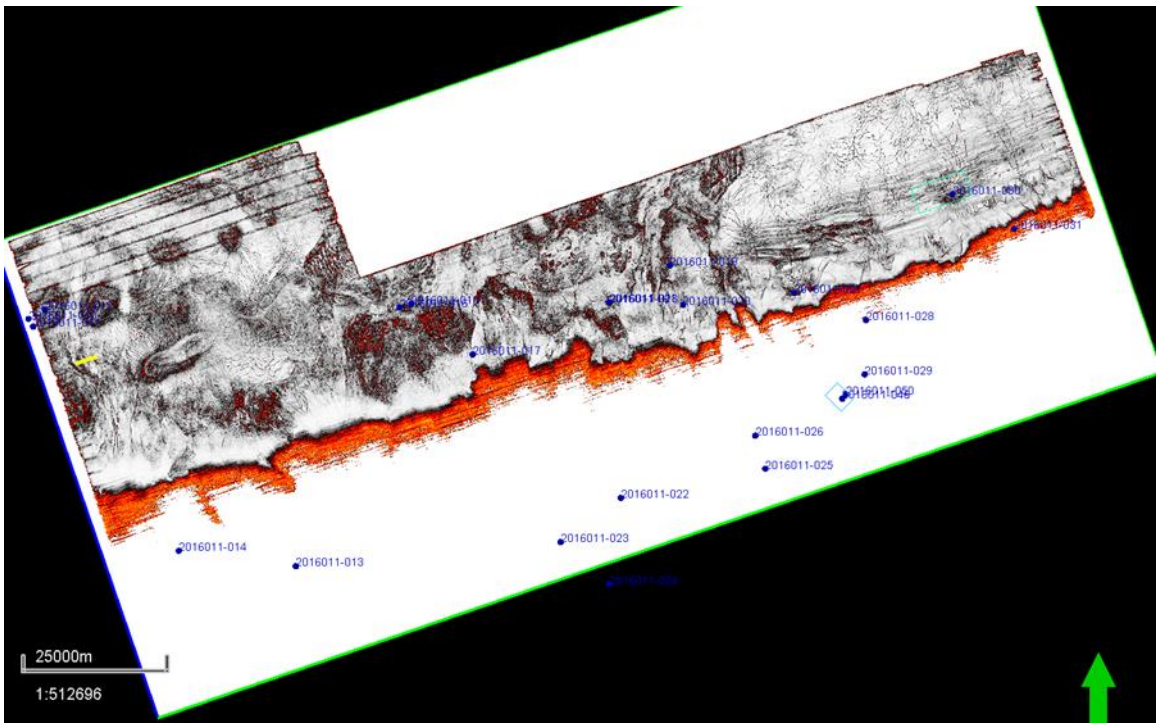
2016011-031
2016011-028
2016011-029
2016011-026
2016011-025
2016011-022
2016011-023
2016011-014
2016011-013
25000m
1:512696

Z = -2400

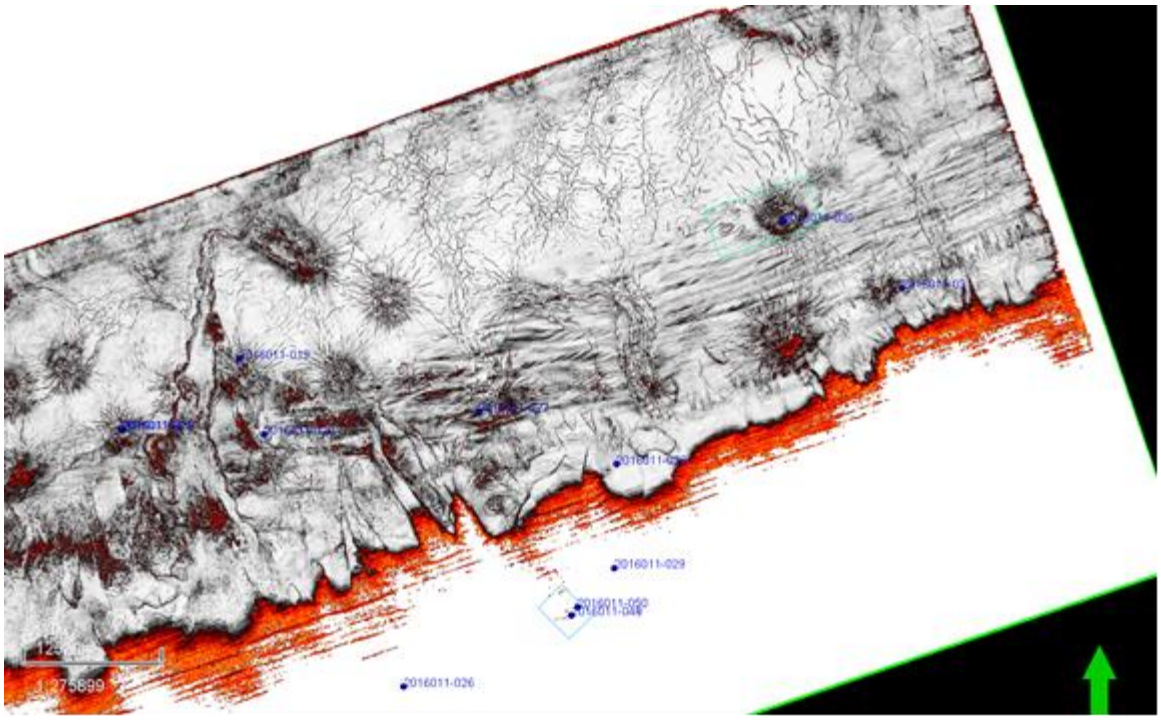
2016011-029
2016011-026

Z = -2500

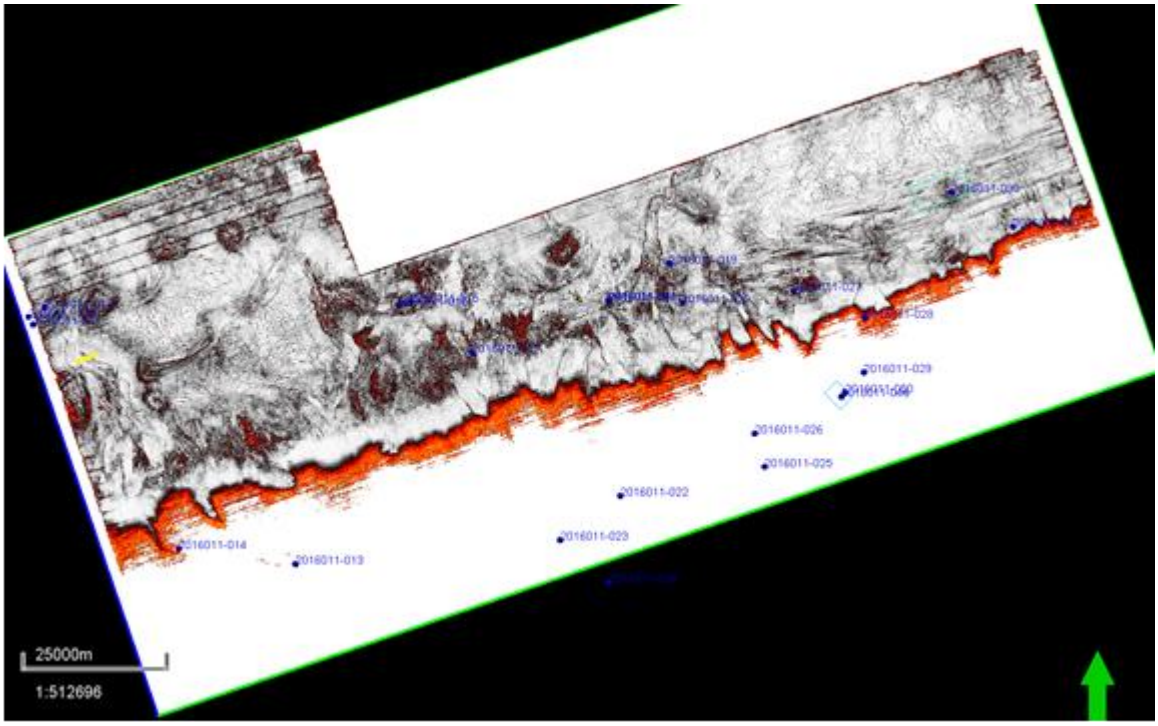
2016011-029
2016011-026
2016011-025
2016011-022
2016011-023
2016011-014
2016011-013
25000m
1:512696

Z = -2600

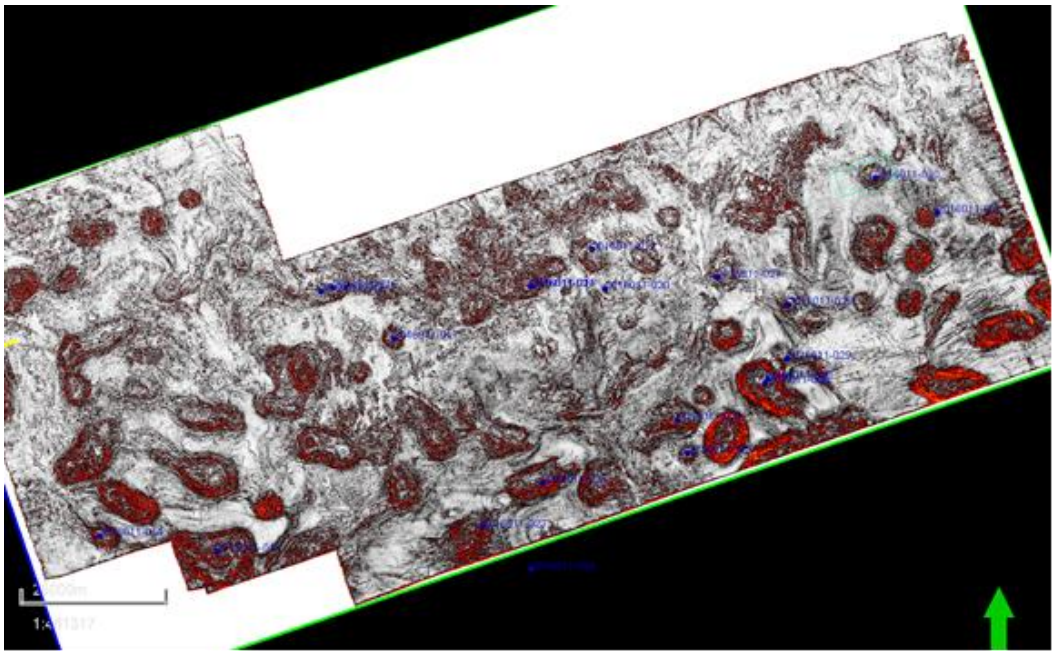

Z = -3600

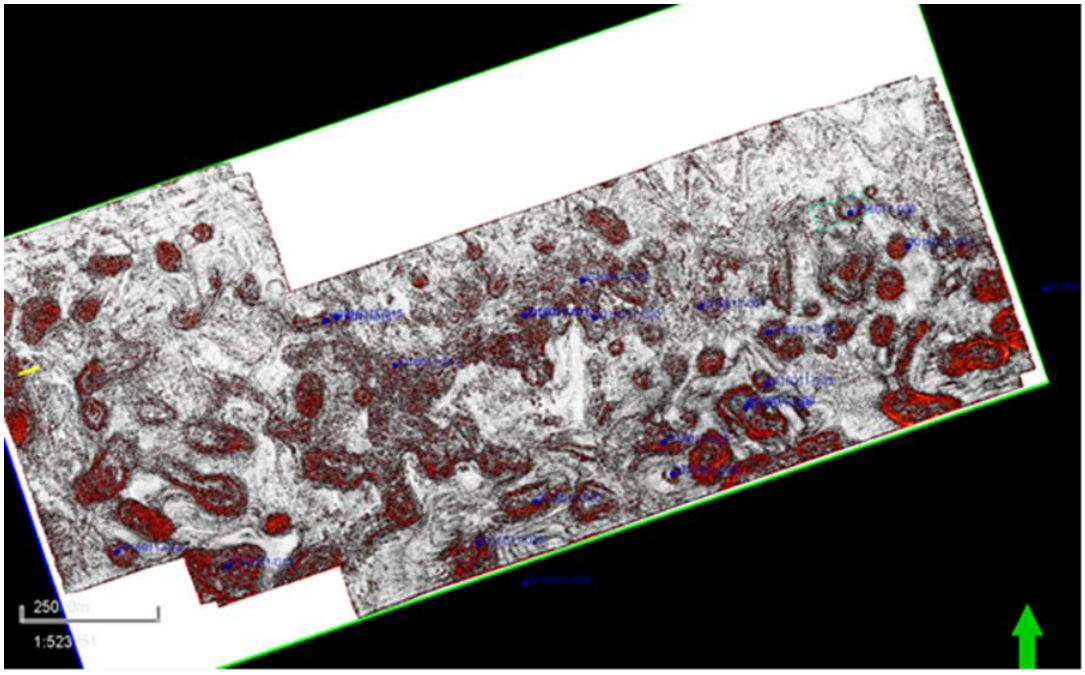

Z = -3800

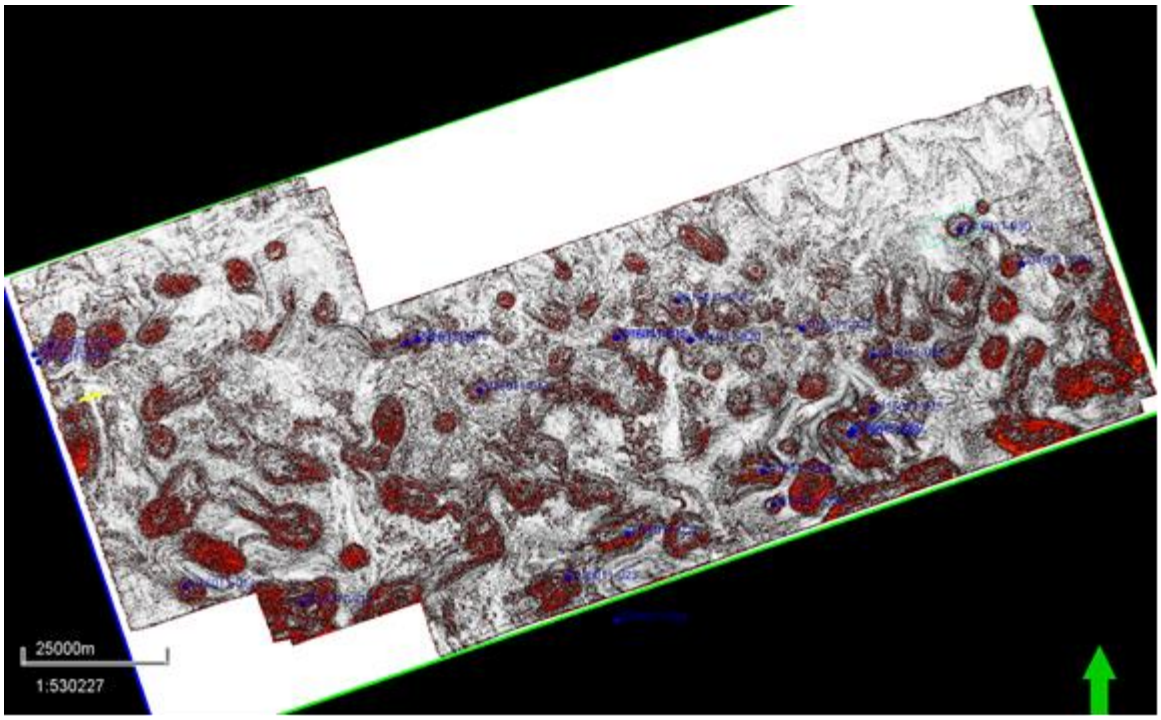

Z = -3900

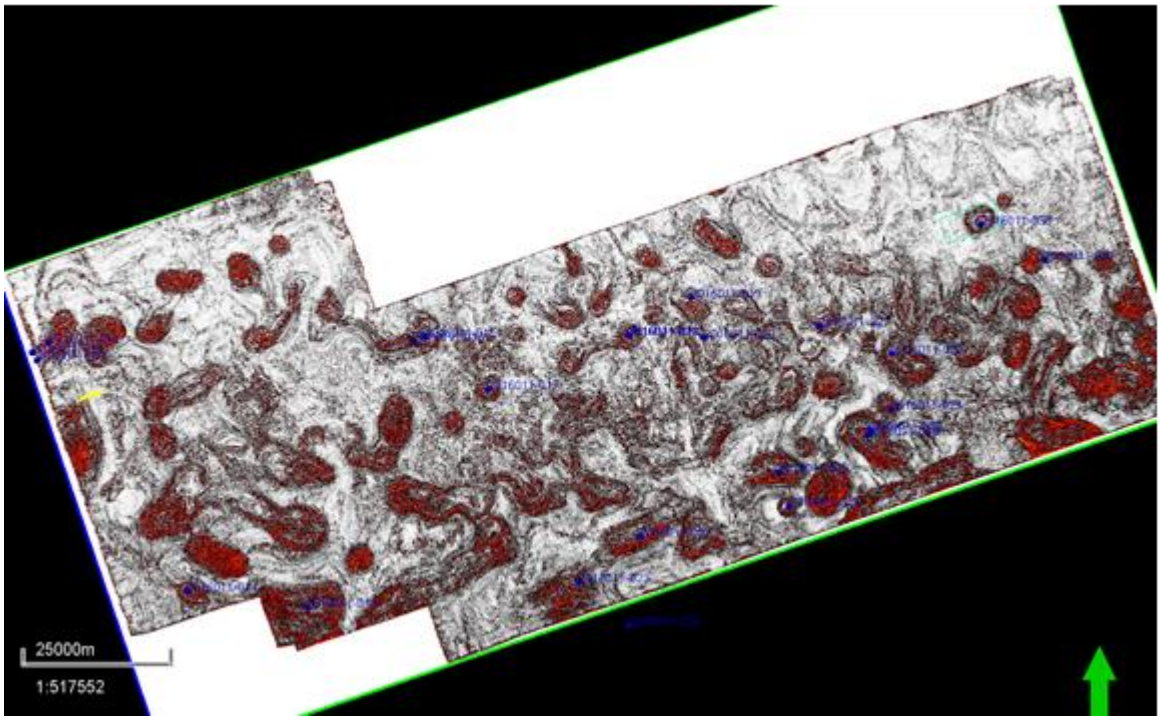

Z = -4000

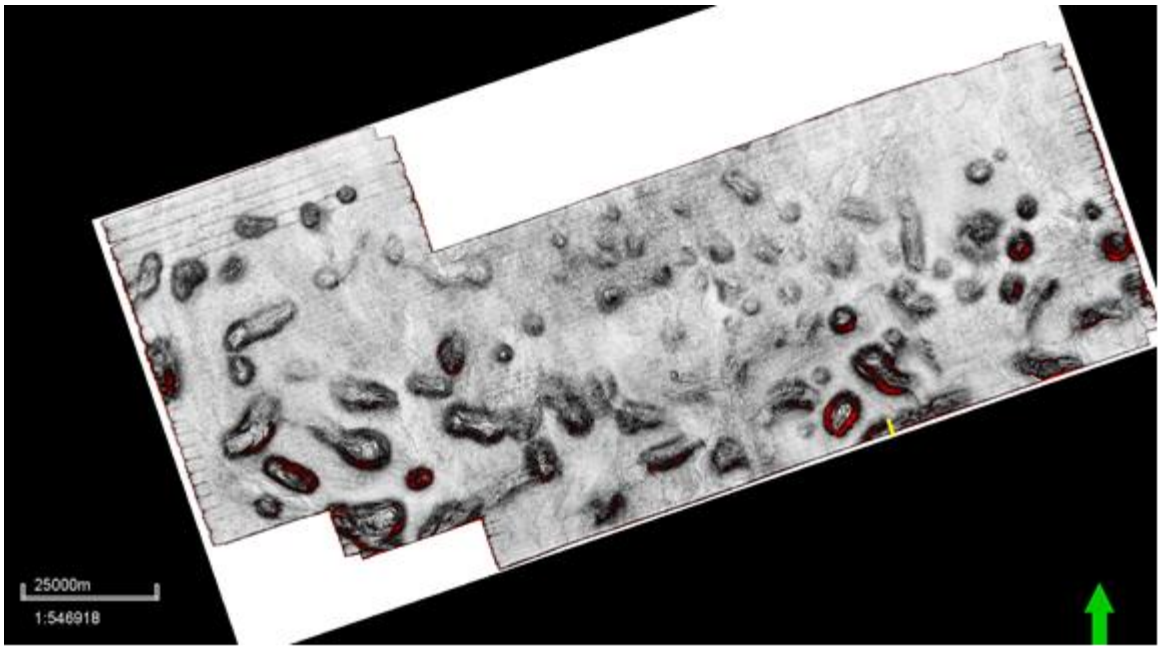

Flattened coherence maps (Flattened to seafloor)

2D -2500 (INTERACTIVE PARAMETER)

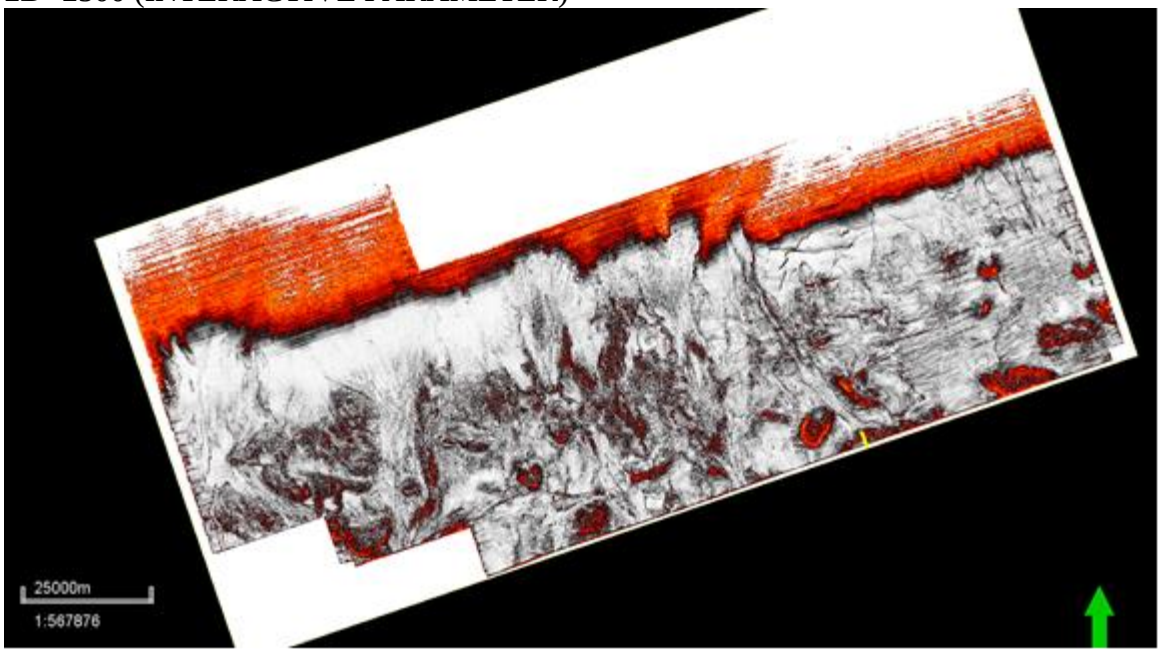

2D -2500

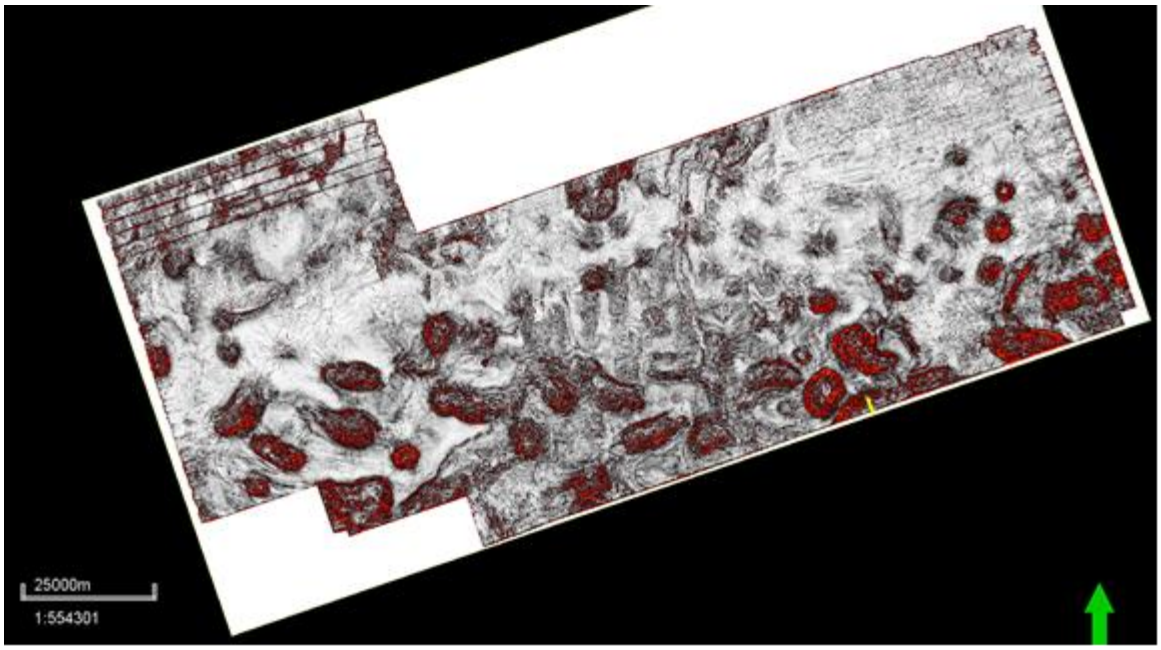

2D -3000

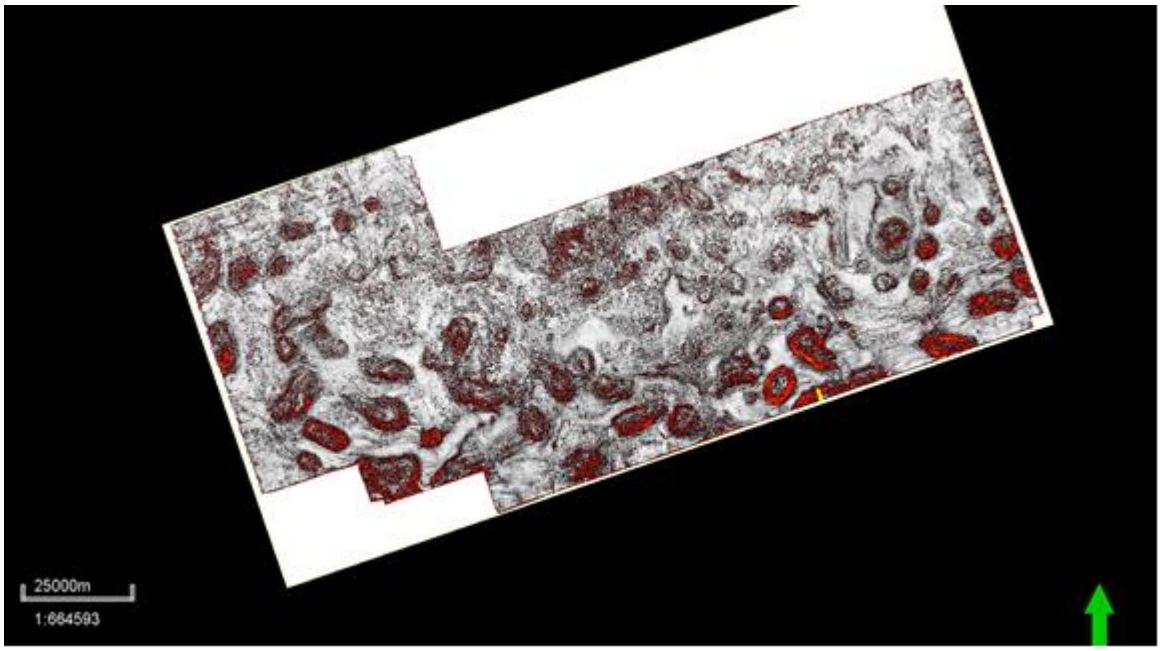

2D -3500

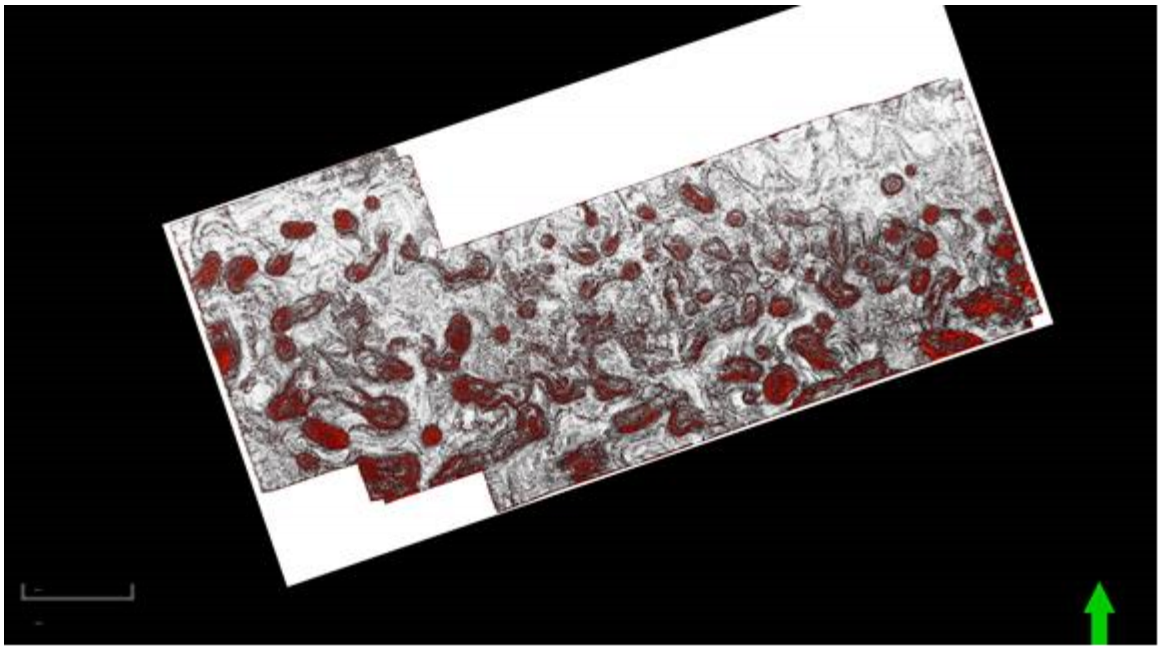

2D -4000

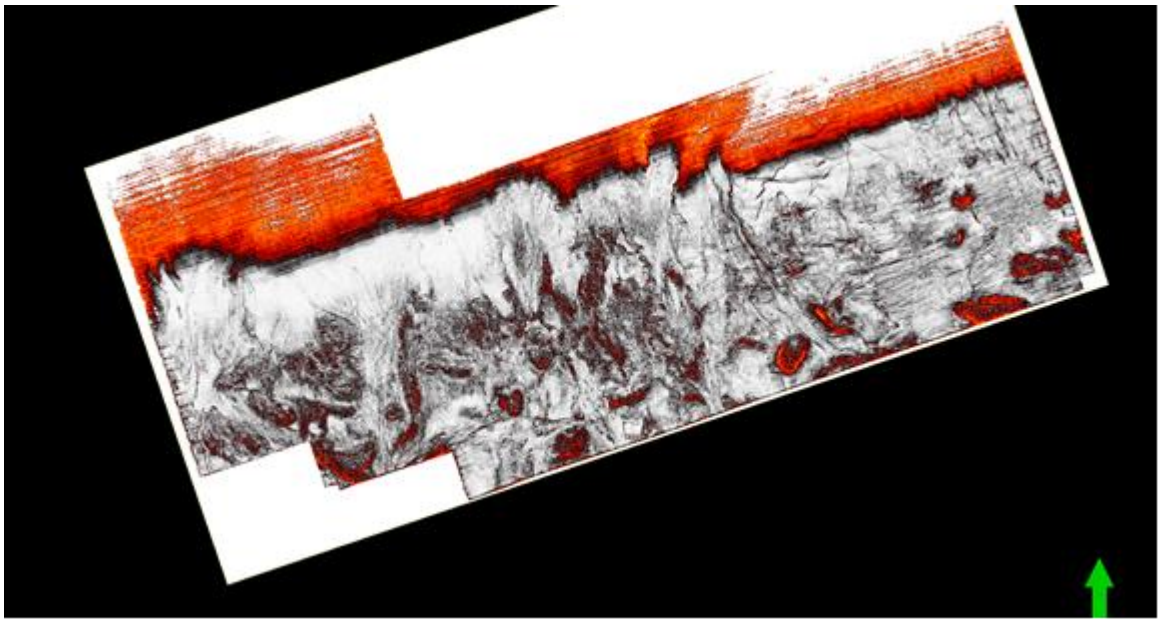

3D -2500

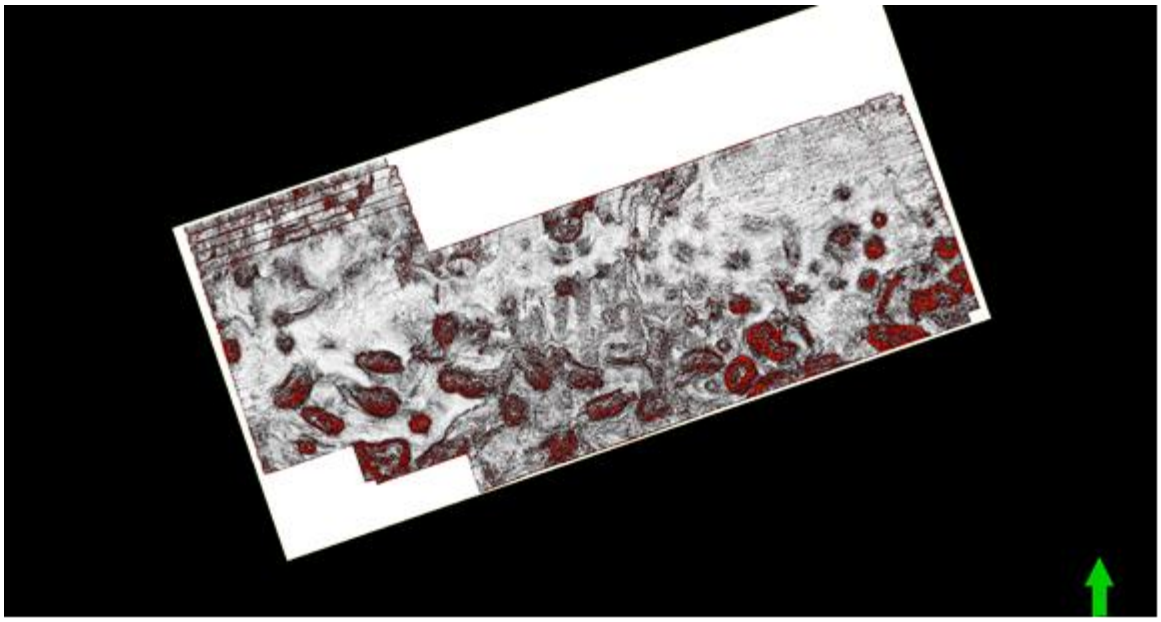

3D -3000

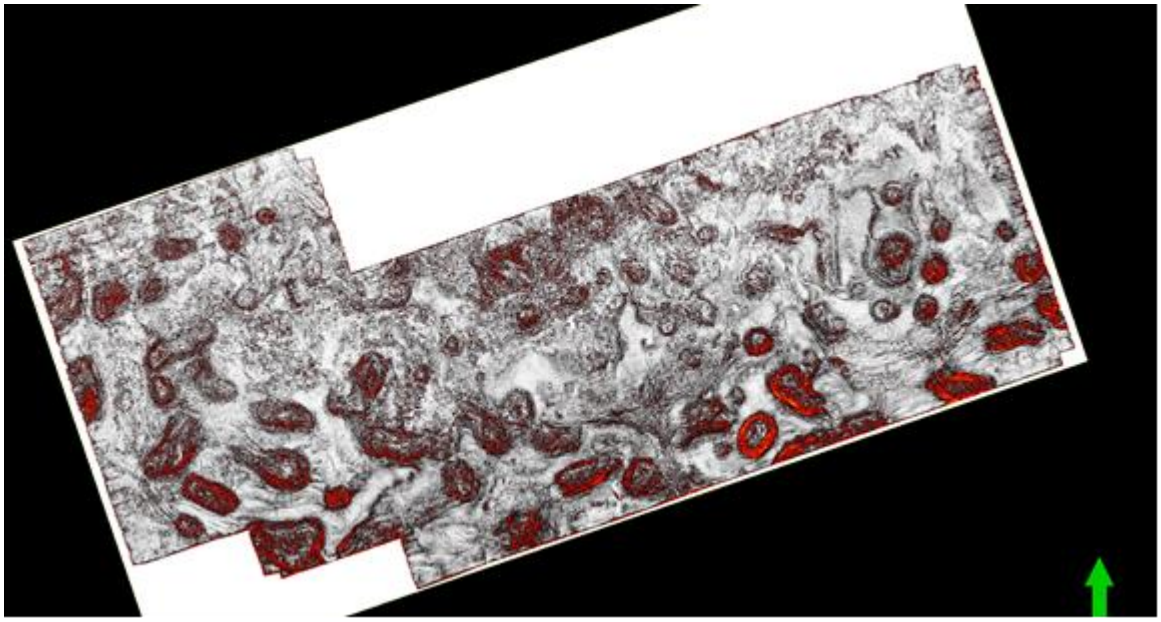

3D -3500

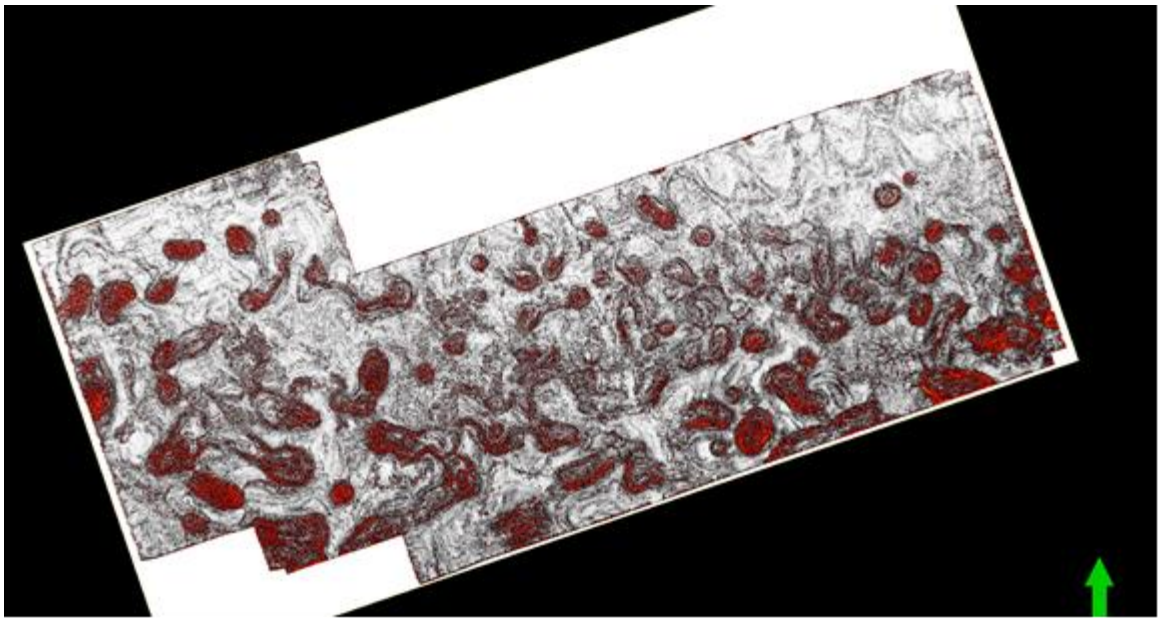

3D -4000

-2700 WITH FLATTENED SEAFLOOR

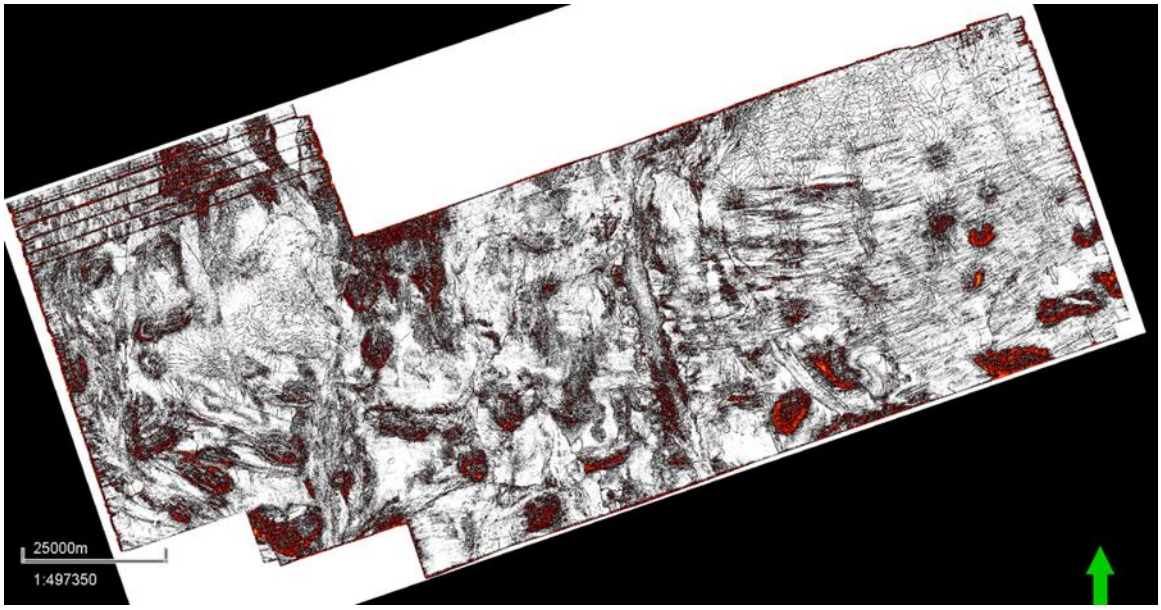

Appendix IV: Directory of Wells

CNSOPB Directory of Wells
Nova Scotia Offshore Area

	A	B	C	D	E	F	G	H	I	J	K	L	M	N	O	P	Q
1	Well No.	D #	Well Name	Well Name 2	Company	Drilling Unit	Latitude (N)	Longitude (W)	Spud Date	Well Termination Date	RT Elevation (m)	Water Depth (m)	Total Depth (m MD)	Total Depth (ft MD)	Well Type	Well Classification	Well Status
2	1	1	Sable Island	C-67	Mobil et al	Bawden Rig 18	43°56'04.90"	59°55'01.40"	7-Jun-67	2-Jan-68	8.2	3.9	4,604	15,106	Exploratory	dry hole	P&A
3	2	2	Onondaga	E-84	Shell	Sedneth 1	43°43'16.13"	60°13'17.18"	1-Sep-69	11-Nov-69	25.9	57.9	3,988	13,085	Exploratory	gas well	P&A
4	3	3	Oneida	O-25	Shell	Sedneth 1	43°14'57.36"	61°33'36.49"	16-Nov-69	10-Feb-70	25.9	82.3	4,120	13,516	Exploratory	dry hole	P&A
5	4	4	Naskapi	N-30	Shell	Sedneth 1	43°29'46.79"	62°33'59.55"	16-Feb-70	19-Mar-70	26.0	95.1	2,205	7,235	Exploratory	dry hole	P&A
6	5	5	Mohawk	B-93	Shell	Sedco H	42°42'10.52"	64°43'53.50"	3-May-70	23-May-70	31.4	117.0	2,126	6,975	Exploratory	dry hole	P&A
7	6	6	Cree	E-35	Shell	Sedco H	43°44'20.79"	60°35'55.87"	8-Sep-70	3-Nov-70	31.4	53.3	3,984	13,070	Exploratory	gas show	P&A
8	7	7	Mic Mac	J-77	Shell	Sedneth 1	44°36'42.82"	59°26'10.87"	25-Mar-70	24-May-70	26.0	62.8	3,886	12,750	Exploratory	oil show	P&A
9	8	8	Mic Mac	H-86	Shell	Sedneth 1	44°35'27.78"	59°27'03.13"	31-Aug-70	2-Dec-70	25.9	54.3	4,785	15,700	Exploratory	dry hole	P&A
10	9	9	Missisauga	H-54	Shell	Sedneth 1	44°23'20.39"	59°22'47.56"	26-May-70	20-Jul-70	25.9	102.1	4,202	13,787	Exploratory	dry hole	P&A
11	10	10	Abenaki	J-56	Shell	Sedneth 1	44°15'44.59"	59°53'03.02"	4-Dec-70	13-Mar-71	25.9	106.7	4,569	14,991	Exploratory	dry hole	P&A
12	11	11	Huron	P-96	Shell	Sedneth 1	44°35'47.11"	58°28'50.64"	22-Jul-70	27-Aug-70	25.9	57.9	3,018	9,903	Exploratory	dry hole	P&A
13	12	12	Triumph	P-50	Shell	Sedneth 1	43°39'51.62"	59°51'02.36"	4-Aug-71	10-Oct-71	25.9	90.2	4,595	15,077	Exploratory	gas show	P&A
14	13	13	Esperanto	K-78	Mobil et al	Sedco H	44°47'31.26"	58°11'19.24"	9-Mar-71	24-Apr-71	31.4	68.8	3,540	11,615	Exploratory	dry hole	P&A
15	14	16	Abenaki	L-57	Shell	Sedco H	44°16'34.49"	59°53'39.64"	28-May-70	6-Jul-70	31.4	108.8	2,178	7,147	Exploratory	dry hole	P&A
16	15	17	Argo	F-38	Shell	Sedco H	45°27'23.22"	58°50'24.34"	17-Dec-70	19-Feb-71	31.4	71.6	3,386	11,110	Exploratory	dry hole	P&A
17	16	18	Wyandot	E-53	Shell	Sedco H	44°52'20.70"	59°23'54.05"	7-Nov-70	14-Dec-70	31.4	121.0	3,049	10,005	Exploratory	oil show	P&A
18	17	19	Erie	D-26	Shell	Sedneth 1	44°55'03.52"	59°34'29.82"	16-Mar-71	11-Apr-71	25.9	98.1	2,376	7,795	Exploratory	oil show	P&A
19	18	20	Crow	F-52	Shell	Sedneth 1	45°21'24.23"	59°08'22.73"	12-Apr-71	27-Apr-71	25.9	94.5	1,507	4,943	Exploratory	dry hole	P&A
20	19	22	Onondaga	O-95	Shell	Sedco H	43°44'48.10"	60°13'52.60"	9-Jul-70	16-Aug-70	31.4	53.9	3,314	10,874	Delineation	gas show	P&A
21	20	23	Fox	I-22	Shell	Sedco H	45°21'33.58"	59°33'16.03"	20-Feb-71	3-Mar-71	31.4	83.8	0,829	2,722	Exploratory	dry hole	P&A
22	21	24	Iroquois	J-17	Shell	Sedco H	44°26'31.38"	59°47'12.29"	18-Aug-70	6-Sep-70	31.4	59.4	2,086	6,845	Exploratory	dry hole	P&A
23	22	27	Dauntless	D-35	Mobil et al	Sedco H	44°44'08.26"	57°20'46.62"	26-Apr-71	16-Jul-71	31.4	69.2	4,741	15,555	Exploratory	dry hole	P&A
24	23	29	Sauk	A-57	Shell	Sedneth 1	44°16'05.70"	58°37'44.41"	30-Apr-71	10-Jul-71	25.9	60.0	4,575	15,010	Exploratory	dry hole	P&A
25	24	30	Chippewa	L-75	Shell	Sedneth 1	44°34'35.87"	58°41'50.54"	12-Jul-71	12-Aug-71	29.9	70.1	2,126	6,972	Exploratory	dry hole	P&A
26	25	33	Onondaga	F-75	Shell	Sedco H	43°44'17.84"	60°11'36.25"	28-Jul-71	7-Sep-71	31.4	56.4	3,891	12,765	Delineation	dry hole	P&A
27	26	34	Eurydice	P-36	Shell	Sedco H	45°25'47.30"	60°04'46.97"	15-Sep-71	24-Oct-71	29.9	164.6	2,965	9,728	Exploratory	dry hole	P&A
28	27	39	Sable Island	E-48	Mobil et al	Bawden Rig 14	43°57'20.35"	60°07'24.44"	28-May-71	15-Oct-71	6.4	na	3,603	11,820	Exploratory	oil well & gas	P&A
29	28	68	Chippewa	G-67	Shell	Sedco H	44°36'20.50"	58°39'44.62"	28-Oct-71	18-Dec-71	24.7	67.7	3,670	12,040	Exploratory	dry hole	P&A
30	29	69	Sable Island	O-47	Mobil et al	Bawden Rig 14	43°56'56.70"	60°06'38.08"	13-Dec-71	1-Jul-72	7.0	1.8	4,198	13,775	Delineation	dry hole	P&A
31	30	70	Marmora	C-34	Shell	Sedneth 1	43°43'13.79"	60°05'21.93"	15-Jan-72	31-Mar-72	25.9	57.6	4,038	13,248	Exploratory	gas show	P&A
32	31	74	Mohican	I-100	Shell	Sedco H	42°59'39.04"	62°28'51.32"	27-Dec-71	10-Mar-72	29.9	153.3	4,393	14,414	Exploratory	dry hole	P&A
33	32	75	Primrose	N-50	Shell	Sedco H	43°59'48.43"	59°06'51.63"	14-Mar-72	21-Apr-72	29.9	90.8	1,713	5,622	Exploratory	oil well & gas	P&A
34	33	80	Eagle	D-21	Shell et al	Sedco H	43°50'06.73"	59°34'09.21"	22-Apr-72	2-Jul-72	29.9	51.2	4,660	15,290	Exploratory	gas show	P&A
35	34	81	Sable Island	1H-58	Mobil et al	Bawden Rig 9	43°57'27.17"	60°07'37.81"	3-Jun-72	27-Aug-72	10.7	na	3,039	9,971	Exploratory	oil well & gas	P&A
36	35	85	Thebaud	P-84	Mobil et al	Sedco H	43°53'59.53"	60°12'19.34"	8-Jul-72	13-Oct-72	28.6	25.9	4,115	13,500	Exploratory	gas well	P&A
37	36	86/97	Primrose	A-41/1a A-	Shell	Sedco H	44°00'05.68"	59°06'18.26"	15-Oct-72	27-Jan-73	29.9	109.7	3,616	11,865	Delineation	gas show	P&A
38	37	88	Sable Island	2H-58	Mobil et al	Bawden Rig 9	43°57'27.14"	60°07'37.75"	6-Oct-72	31-Dec-72	10.6	na	2,758	9,050	Delineation	oil well & gas	P&A
39	38	91	Sable Island	3H-58	Mobil et al	Bawden Rig 9	43°57'27.21"	60°07'37.88"	1-Jan-73	21-Mar-73	10.6	na	3,740	12,270	Delineation	oil well & gas	P&A
40	39	94	Bluenose	G-47	Mobil et al	Sedco J	44°06'20.79"	59°21'27.35"	25-Jan-73	25-Apr-73	29.9	81.4	4,587	15,050	Exploratory	gas show	P&A
41	40	95	Primrose	F-41	Shell	Sedco H	44°00'29.55"	59°07'06.52"	30-Jan-73	5-Mar-73	29.9	68.6	2,592	8,505	Delineation	gas show	P&A
42	41	96	Cohasset	D-42	Mobil Tetco	Sedco J	43°51'06.52"	60°37'13.89"	27-Apr-73	16-Jul-73	31.4	41.1	4,427	14,525	Exploratory	oil well	P&A
43	42	98	Marmora	P-35	Shell et al	Sedco H	43°44'59.36"	60°04'47.58"	6-Mar-73	21-Apr-73	29.9	53.3	4,093	13,428	Exploratory	dry hole	P&A

CNSOPB Directory of Wells
Nova Scotia Offshore Area

	A	B	C	D	E	F	G	H	I	J	K	L	M	N	O	P	Q
1	Well No.	D #	Well Name	Well Name 2	Company	Drilling Unit	Latitude (N)	Longitude (W)	Spud Date	Well Termination Date	RT Elevation (m)	Water Depth (m)	Total Depth (m MD)	Total Depth (ft MD)	Well Type	Well Classification	Well Status
44	43	99	Tuscarora	C-61	Shell et al	Sedco H	44°40'10.35"	58°55'10.85"	23-Apr-73	2-Jun-73	29.9	78.9	3,939	12,925	Exploratory	dry hole	P&A
45	44	101	Sable Island	4H-58	Mobil et al	Bawden Rig 9	43°57'27.24"	60°07'37.95"	22-Mar-73	11-Aug-73	10.6	na	4,519	14,827	Delineation	oil well & gas	P&A
46	45	103	Cap Rouge	F-52	Shell et al	Sedco H	47°11'20.29"	61°08'15.24"	8-Jun-73	3-Sep-73	31.1	56.7	5,059	16,598	Exploratory	dry hole	P&A
47	46	112	Sable Island	5H-58	Mobil et al	Bawden Rig 9	43°57'27.10"	60°07'37.68"	15-Aug-73	18-Sep-73	10.6	na	2,478	8,130	Delineation	oil well & gas	P&A
48	47	118	Sable Island	6H-58	Mobil et al	Bawden Rig 9	43°57'27.07"	60°07'37.61"	22-Sep-73	18-Oct-73	10.6	na	2,355	7,727	Delineation	dry hole	P&A
49	48	121	Ojibwa	E-07	Union et al	Sedco H	43°46'20.44"	61°46'14.42"	4-Feb-74	28-Feb-74	29.9	75.6	2,330	7,643	Exploratory	dry hole	P&A
50	49	123	Citnalta	I-59	Mobil et al	Sedco J	44°08'42.58"	59°37'32.11"	4-Feb-74	29-Apr-74	29.9	94.5	4,575	15,010	Exploratory	gas well	P&A
51	50	125	Demascota	G-32	Shell	Sedco H	43°41'27.19"	60°49'54.00"	1-Mar-74	20-May-74	29.9	54.3	4,672	15,329	Exploratory	dry hole	P&A
52	51	126	Intrepid	L-80	Texaco et al	Sedco J	43°49'35.78"	59°56'43.83'	18-May-74	15-Aug-74	31.4	43.6	4,162	13,655	Exploratory	gas well	P&A
53	52	129	Sambro	I-29	Union et al	Sedco H	43°38'35.29"	62°48'08.52"	23-May-74	27-Jun-74	29.9	193.5	3,069	10,071	Exploratory	dry hole	P&A
54	53	130	Hercules	G-15	Union et al	Sedco H	45°34'20.65"	58°47'13.06"	23-Jul-74	1-Aug-74	29.9	115.8	1,081	3,547	Exploratory	dry hole	P&A
55	54	131	Jason	F-20	Union et al	Sedco H	45°29'05.45"	58°32'28.27"	3-Jul-74	22-Jul-74	29.9	112.8	2,483	8,146	Exploratory	dry hole	P&A
56	55	134	North Sydney	P-05	Murphy et al	Sedco H	46°34'46.24"	59°45'01.80"	10-Aug-74	6-Sep-74	29.9	62.8	1,661	5,449	Exploratory	gas show	P&A
57	56	140	Montagnais	I-94	Union et al	Sedco H	42°53'40.71"	64°13'46.51"	12-Sep-74	29-Sep-74	29.9	112.8	1,646	5,400	Exploratory	dry hole	P&A
58	57	144	Adventure	F-80	Mobil et al	Sedco J	45°19'27.54"	57°56'22.80"	13-Jan-75	22-Feb-75	29.9	98.8	1,999	6,559	Exploratory	dry hole	P&A
59	58	146	Sachem	D-76	Mobil	Sedco J	44°35'09.22"	57°41'58.29"	17-May-75	30-Jul-75	29.9	58.5	4,878	16,006	Exploratory	dry hole	P&A
60	59	158	Onondaga	B-96	Shell	Sedco H	43°45'08.21"	60°14'09.76"	12-Jan-76	21-Mar-76	29.9	60.4	3,758	12,328	Delineation	dry hole	P&A
61	60	160	Mic Mac	D-89	Shell et al	Sedco H	44°38'08.86"	59°28'18.93"	26-Mar-76	4-May-76	29.9	85.3	3,261	10,700	Exploratory	dry hole	P&A
62	61	162	Hesper	I-52	Petrocan et al	Sedco H	44°41'40.33"	57°52'32.24"	8-May-76	5-Jun-76	29.9	42.1	2,804	9,200	Exploratory	dry hole	P&A
63	62	163	North Sydney	F-24	Shell et al	Sedco H	46°33'23.13"	59°48'45.47"	9-Jun-76	14-Jun-76	29.9	59.7	1,707	5,600	Exploratory	gas show	P&A
64	63	164	Wenonah	J-75	Petrocan et al	Sedco H	43°34'34.44"	60°26'13.73"	26-Sep-76	15-Nov-76	29.9	66.7	3,670	12,040	Exploratory	dry hole	P&A
65	64	165	Penobscot	L-30	Petrocan et al	Sedco H	44°09'43.55"	60°04'09.33"	18-Jul-76	23-Sep-76	29.9	137.5	4,267	14,000	Exploratory	oil & gas show	P&A
66	65	168	Moheida	P-15	Petrocan et al	Sedco H	43°04'56.32"	62°16'44.33"	18-Nov-76	15-Feb-77	29.9	111.9	4,298	14,100	Exploratory	dry hole	P&A
67	66	169	Penobscot	B-41	Petrocan et al	Sedco H	44°10'02.44"	60°06'32.72"	18-Feb-77	30-Mar-77	29.9	117.9	3,444	11,300	Exploratory	dry hole	P&A
68	67	170	Migrant	N-20	Mobil	Gulftide	43°59'56.24"	60°17'18.23"	29-Jul-77	23-Jan-78	26.1	13.7	4,669	15,318	Exploratory	gas show	P&A
69	68	171	Acadia	K-62	Chevron	Ben Ocean	42°51'43.54"	61°55'02.08"	11-Apr-78	2-Aug-78	12.8	866.2	5,286	17,343	Exploratory	dry hole	P&A
70	69	172	Thebaud	I-94	Mobil	Gulftide	43°53'43.67"	60°13'38.13"	26-Feb-78	3-Jul-78	29.9	28.0	3,962	13,000	Delineation	gas well	P&A
71	70	174	Cohasset	P-42	Mobil	Gulftide	43°51'50.32"	60°36'18.23"	9-Jun-78	10-Jul-78	30.5	34.1	2,591	8,500	Delineation	dry hole	P&A
72	71	177	Cohasset	L-97	Mobil et al	Gulftide	43°56'37.19"	60°29'58.55"	13-Jul-78	13-Nov-78	32.9	21.6	4,872	15,984	Exploratory	gas show	P&A
73	72	178	Venture	D-23	Mobil	Gulftide	44°02'14.86"	59°34'24.72"	28-Nov-78	16-Jun-79	31.7	20.1	4,945	16,224	Exploratory	gas well	P&A
74	73	195	Venture	B-13	Mobil et al	Rowan Juneau	44°02'11.61"	59°32'03.54"	17-Aug-80	6-Jun-81	33.8	24.7	5,368	17,611	Delineation	gas well	P&A
75	74	202	Venture	B-43	Mobil et al	Rowan Juneau	44°02'00.72"	59°36'37.37"	6-Jul-81	25-Apr-82	33.8	20.4	5,872	19,265	Delineation	gas well	P&A
76	75	207	Banquereau	C-21	Petrocan	Bow Drill I	44°10'07.52"	58°34'00.24'	2-Dec-81	1-Aug-82	27.0	83.0	4,991	16,374	Exploratory	gas well	P&A
77	76	213	Olympia	A-12	Mobil-Pex-Tex	Zapata Scotian	44°01'03.27"	59°46'44.09"	23-Apr-82	10-Jan-83	38.0	40.0	6,064	19,895	Exploratory	gas well	P&A
78	77	214	N Banquereau	I-13	Petrocan et al	Bow Drill I	44°12'33.16"	58°31'49.38"	2-Aug-82	28-Dec-82	25.0	91.0	5,188	17,021	Exploratory	dry hole	P&A
79	78	216	West Esperanto	B-78	Petocan et al	Vinland	44°47'03.40"	58°26'11.22"	22-Aug-82	5-May-83	23.3	91.1	5,703	18,711	Exploratory	dry hole	P&A
80	79	217	South Venture	O-59	Mobil et al	Rowan Juneau	43°58'52.83"	59°38'08.49"	29-Apr-82	2-Jan-83	35.4	24.0	6,176	20,262	Exploratory	gas well	P&A
81	80	219	Shubenacadie	H-100	Shell et al	Sedco 709	42°49'28.43"	61°28'42.81"	5-Nov-82	12-Feb-83	24.1	1476.5	4,200	13,780	Exploratory	dry hole	P&A
82	81	223	Bluenose	2G-47	Mobil et al	John Shaw	44°06'22.30"	59°21'23.05"	30-Dec-82	5-Sep-83	24.4	85.3	5,797	19,019	Exploratory	gas show	P&A
83	82	224	Venture	B-52	Mobil et al	Rowan Juneau	44°01'12.88"	59°38'07.76"	19-Jan-83	27-Oct-83	34.0	19.5	5,960	19,554	Delineation	gas well	P&A
84	83	225	Arcadia	J-16	Mobil et al	Zapata Scotian	44°05'43.59"	59°31'58.19"	27-Jan-83	19-Jul-83	38.1	55.5	6,005	19,701	Exploratory	gas well	P&A
85	84	226	Glenelg	J-48	Shell Petrocan	Sedco 709	43°37'38.57"	60°06'24.84"	22-Feb-83	7-Nov-83	24.0	83.7	5,148	16,890	Exploratory	gas well	P&A
86	85	227	S.W. Banquereau	F-34	Petrocan et al	Bow Drill I	44°03'15.62"	58°50'21.60"	20-Feb-83	30-Aug-83	24.9	173.9	6,309	20,699	Exploratory	gas show	P&A
87	86	228	Uniacke	G-72	Shell Pex et al	Vinland	44°11'29.17"	59°41'09.75"	9-May-83	4-Apr-84	23.5	152.9	5,735	18,815	Exploratory	gas well	P&A
88	87	231	Glooscap	C-63	Husky/	Bow Drill II	43°12'09.83"	62°09'56.75"	7-Aug-83	3-Jan-84	22.9	99.0	4,542	14,902	Exploratory	dry hole	P&A

CNSOPB Directory of Wells
Nova Scotia Offshore Area

	A	B	C	D	E	F	G	H	I	J	K	L	M	N	O	P	Q
1	Well No.	D #	Well Name	Well Name 2	Company	Drilling Unit	Latitude (N)	Longitude (W)	Spud Date	Well Termination Date	RT Elevation (m)	Water Depth (m)	Total Depth (m MD)	Total Depth (ft MD)	Well Type	Well Classification	Well Status
89	88	232	Venture	H-22	Mobil et al	Zapata Scotian	44°01'24.13"	59°33'06.14"	26-Jul-83	16-Apr-84	38.1	24.0	5,944	19,501	Delineation	gas well	P&A
90	89	235	St. Paul	P-91	Petrocan et al	Bow Drill I	47°10'57.88"	60°13'36.83"	2-Sep-83	31-Dec-83	24.9	173.9	2,885	9,465	Exploratory	dry hole	P&A
91	90	239	Alma	F-67	Shell Pex et al	Sedco 709	43°36'17.98"	60°39'56.75"	2-Dec-83	5-Jul-84	24	68	5,054	16,581	Exploratory	gas well	P&A
92	91	240	Louisbourg	J-47	Home et al	Glomar	44°26'43.08"	58°21'26.02"	25-Nov-83	13-Oct-84	38.2	63.1	6,043	19,826	Exploratory	gas show	P&A
93	92	242	Chebucto	K-90	Husky/	Bow Drill II	43°39'44.73"	59°42'51.52"	6-Jan-84	2-Aug-84	22.8	86.2	5,235	17,175	Exploratory	gas well	P&A
94	93	243	South Griffin	J-13	Bow Valley/	Rowan Gorilla I	44°22'37.77"	58°01'54.76"	8-Jan-84	20-Aug-84	39.6	63.4	5,911	19,393	Exploratory	dry hole	P&A
95	94	244	Bonnet	P-23	Pex et al	Bow Drill I	42°22'48.64"	65°03'01.89"	14-Jan-84	4-Apr-84	25.0	133.5	4,336	14,226	Exploratory	dry hole	P&A
96	95	248	Dover	A-43	Petrocan et al	Bow Drill I	44°22'09.02"	60°06'09.28"	17-Apr-84	10-Jul-84	25.0	116.0	4,525	14,846	Exploratory	dry hole	P&A
97	96	249	West Venture	N-91	Mobil et al	Zapata Scotian	44°00'45.82"	59°44'27.36"	19-Apr-84	7-Jul-85	39.3	38.1	5,547	18,199	Exploratory	gas well	P&A
98	97	250	South Desbarres	O-76	Shell PCI et al	Vinland	44°05'56.07"	59°55'59.02"	17-Apr-84	13-Oct-84	23.7	69.0	6,039	19,813	Exploratory	dry hole	P&A
99	98	251	Evangeline	H-98	Husky/	Bow Drill III	43°17'25.27"	60°58'48.40"	27-Mar-84	16-Jun-84	23.5	175.0	3,365	11,040	Exploratory	dry hole	P&A
100	98	re-entered	Evangeline	H-98	Husky/	Bow Drill II	43°17'26.85"	60°58'50.60"	8-Aug-84	1-Nov-84	20.1	175.0	5,044	16,549	Exploratory	dry hole	P&A
101	99	252	West Venture	C-62	Mobil et al	Rowan Juneau	44°01'02.78"	59°40'00.93"	19-May-84	23-Mar-85	33.8	16.0	5,522	18,117	Exploratory	gas well	P&A
102	100	256	Glenelg	E-58	Shell/PCI et al	Sedco 709	43°37'17.51"	60°08'51.63"	7-Jul-84	20-Oct-84	24.0	79.0	4,192	13,753	Delineation	gas well	P&A
103	101	257	Hesper	P-52	BVH et al	Rowan Gorilla I	44°41'50.95"	57°52'47.72"	22-Aug-84	1-May-85	40.5	44.5	5,679	15,632	Exploratory	dry hole	P&A
104	102	260	Citadel	H-52	Home et al	Glomar	44°11'25.07"	58°52'39.87"	18-Dec-84	29-May-85	38.3	65.3	5,666	18,589	Exploratory	dry hole	P&A
105	103	261	Glenelg	H-38	Shell PCI et al	Sedco 709	43°37'19.33"	60°04'48.61"	26-Oct-84	26-Jan-85	24.1	89.3	4,865	15,961	Delineation	dry hole	P&A
106	104	267	Alma	K-85	Shell PCI et al	Sedco 709	43°34'44.32"	60°43'01.69"	29-Jan-85	10-Apr-85	24	65.3	3,602	11,817	Delineation	gas well	P&A
107	105	268	Albatross	B-13	Pex/Tex et al	Sedco 710	42°42'10.68"	63°02'11.83"	12-Dec-84	28-Mar-85	24.0	1,341.0	4,046	13,274	Exploratory	dry hole	P&A
108	106	269	West Venture	N-01	Mobil et al	Rowan Gorilla III	44°00'58.80"	59°45'51.69"	20-Jan-85	30-Jun-85	38.1	40.1	3,632	11,916	Service Relief	dry hole	P&A
109	107	271	Thebaud	I-93	Mobil et al	Rowan Juneau	43°52'44.54"	60°13'50.94"	27-Mar-85	30-Sep-85	37.0	31.0	5,166	16,949	Delineation	gas well	P&A
110	108	272	Peskowesk	A-99	Shell/PCI et al	Sedco 706	44°28'13.84"	58°58'40.98"	22-Apr-85	13-Jun-85	27.5	62.0	4,024	13,202	Exploratory	dry hole	P&A
111	109	275	Kegeshook	G-67	Shell/PCI et al	Glomar	44°06'28.87"	60°24'31.26"	11-Jun-85	30-Jul-85	37.0	62.0	3,540	11,614	Exploratory	dry hole	P&A
112	110	276	Merigomish	C-52	Shell/PCI et al	Sedco 706	43°31'02.62"	60°38'33.78"	15-Jun-85	12-Aug-85	27.5	75.0	3,950	12,959	Exploratory	dry hole	P&A
113	111	277	West Olympia	O-51	Mobil et al	Rowan Gorilla I	44°00'47.80"	59°53'03.64"	23-Jun-85	9-Nov-85	38.0	38.4	4,816	15,800	Exploratory	gas well	P&A
114	112	280	Shelburne	G-29	Pex et al	Sedco 710	42°38'26.87"	63°33'33.46"	31-Mar-85	16-Sep-85	25.0	1153.5	4,005	13,140	Exploratory	dry hole	P&A
115	113	281	North Triumph	G-43	Shell/PCI et al	Sedco 709	43°42'19.06"	59°51'23.02"	26-Sep-85	31-Jan-86	24.0	73.6	4,504	14,777	Exploratory	gas well	P&A
116	114	289	North Triumph	B-52	Shell/PCI et al	John Shaw	43°41'02.38'	59°52'56.87"	24-Jan-86	29-Mar-86	24.0	81.0	3,960	12,992	Delineation	gas well	P&A
117	115	293	Tantallon	M-41	Shell/PCI et al	Sedco 709	43°50'55.96"	58°22'23.99"	15-Feb-86	18-Apr-86	24.0	1516.0	5,602	18,379	Exploratory	dry hole	P&A
118	116	294	Cohasset	A-52	Petrocan et al	Rowan Gorilla I	43°51'08.11"	60°37'43.46"	19-Dec-85	26-Mar-86	40.0	36.0	2,847	9,340	Delineation	oil well	P&A
119	117	295	Thebaud	C-74	Mobil et al	Rowan Gorilla I	43°53'05.34"	60°11'35.62"	29-Mar-86	26-Sep-86	41.8	29.6	5,150	16,896	Delineation	gas well	P&A
120	118	296	W. Chebucto	K-20	HBV et al	Bow Drill II	43°39'44.63"	59°47'32.44"	5-Apr-86	11-Aug-86	22.8	93.6	5,369	17,614	Exploratory	gas show	P&A
121	119	299	Glenelg	N-49	Shell/PCI et al	Vinland	43°38'59.43"	60°07'02.10"	1-Jun-86	4-Aug-86	23.2	72.3	4,040	13,254	Delineation	gas well	P&A
122	120	300	Panuke	B-90	Shell et al	Vinland	43°49'11.99"	60°42'34.59"	6-Aug-86	24-Sep-86	23.0	47.0	3,445	11,302	Exploratory	oil well	P&A
123	121	304	Whycocomagh	N-90	Canterra et al	Sedco 710	43°39'50.83"	60°28'03.71"	20-Apr-87	26-May-87	24.1	67.7	3,535	11,597	Exploratory	dry hole	P&A
124	122	305	Como	P-21	Petrocan et al	Rowan Gorilla I	43°50'45.87"	60°48'19.28"	15-May-87	1-Jul-87	40.2	39.0	3,540	11,614	Exploratory	dry hole	P&A
125	123	307	Panuke	F-99	Petrocan et al	Rowan Gorilla I	43°48'24.90"	60°44'34.01"	2-Jul-87	24-Aug-87	40.2	45.1	2,507	8,225	Delineation	oil well	P&A
126	124	312	South Sable	B-44	Mobil et al	Rowan Gorilla I	43°53'06.56"	59°51'42.09"	27-Mar-88	13-Jul-88	42.1	35.9	5,208	17,085	Exploratory	gas well	P&A
127	125	319	Lawrence	D-14	LASMO NSRL	Rowan Gorilla III	43°53'04.79"	60°32'51.84"	14-Jan-91	24-Feb-91	40.0	30.0	2,850	9,350	Exploratory	dry hole	P&A
128	126	320	Balmoral	M-32	LASMO NSRL	Rowan Gorilla III	43°51'54.89"	60°35'46.73"	26-Feb-91	9-Apr-91	38.0	34.0	2,525	8,284	Exploratory	oil well	P&A
129	127	321	Panuke PP1	J-99	LASMO NSRL	Rowan Gorilla III	43°48'40.14"	60°44'00.25"	11-May-91	2-Jul-91	47.2	44.7	3,031	9,945	Development	oil well	P&A
130	128	322	Panuke PP2	J-99	LASMO NSRL	Rowan Gorilla III	43°48'40.20"	60°44'00.26"	18-Jul-91	4-Jan-92	47.2	44.7	2,435	7,989	Development	oil well	P&A
131	129	323	Panuke PP3	J-99	LASMO NSRL	Rowan Gorilla III	43°48'40.23"	60°44'00.19"	3-Jul-91	2-Feb-92	47.2	44.7	2,685	9,909	Development	oil well	P&A
132	130	324	Panuke PI-1	J-99	LASMO NSRL	Rowan Gorilla III	43°48'40.19'	60°44'00.13"	9-Jul-91	18-Jul-91	47.2	44.0	1,082	3,550	Development	oil well	P&A
133	131	325	Panuke PP4	J-99	LASMO NSRL	Rowan Gorilla III	43°48'40.14"	60°44'00.17"	27-Jun-92	25-Jul-92	47.2	44.0	2,292	7,520	Development	oil well	P&A
134	132	326	Panuke PP4B	J-99	LASMO NSRL	Rowan Gorilla III	43°48'40.14"	60°44'00.17"	4-Aug-92	11-Oct-92	47.2	44.0	3,054	10,020	Development	oil well	P&A
135	133	327	Panuke PP4C	J-99	LASMO NSRL	Rowan Gorilla III	43°48'40.14"	60°44'00.17"	11-Oct-92	14-Nov-92	47.2	44.0	3,047	9,997	Development	oil well	P&A
136	134	328	Cohasset CP1	P-51	LASMO NSRL	Rowan Gorilla III	43°50'57.15"	60°37'39.99"	8-May-93	5-Jun-93	41.5	43.0	2,472	8,110	Development	oil well	P&A

CNSOPB Directory of Wells
Nova Scotia Offshore Area

	A	B	C	D	E	F	G	H	I	J	K	L	M	N	O	P	Q
1	Well No.	D #	Well Name	Well Name 2	Company	Drilling Unit	Latitude (N)	Longitude (W)	Spud Date	Well Termination Date	RT Elevation (m)	Water Depth (m)	Total Depth (m MD)	Total Depth (ft MD)	Well Type	Well Classification	Well Status
137	135	329	Panuke PP4A	J-99	LASMO NSRL	Rowan Gorilla III	43°48'40.14"	60°44'00.17"	25-Jul-92	2-Aug-92	47.2	44.0	1,776	5,827	Development	oil well	P&A
138	136	330	Cohasset CP2	P-51	LASMO NSRL	Rowan Gorilla III	43°50'57.06"	60°37'40.17"	5-Jun-93	29-Jun-93	41.5	43.0	2,337	7,667	Development	oil well	P&A
139	137	331	Cohasset CP3	P-51	LASMO NSRL	Rowan Gorilla III	43°50'57.11'	60°37'39.90"	30-Jun-93	29-Jul-93	41.5	43.0	2,750	9,023	Development	oil well	P&A
140	138	332	Cohasset CP4	P-51	LASMO NSRL	Rowan Gorilla III	43°50'57.16"	60°37'40.22"	30-Jul-93	19-Aug-93	41.5	43.0	2,525	8,284	Development	oil well	P&A
141	139	333	Cohasset CP5	P-51	LASMO NSRL	Rowan Gorilla III	43°50'57.05'	60°37'39.95"	19-Aug-93	10-Dec-93	41.5	43.0	2,613	8,573	Development	oil well	P&A
142	140	334	Cohasset CP6	P-51	LASMO NSRL	Rowan Gorilla III	43°50'57.02"	60°37'40.09"	25-Aug-93	13-Sep-93	41.5	43.0	3,067	10,063	Development	oil well	P&A
143	141	335	Cohasset CP6A	P-51	LASMO NSRL	Rowan Gorilla III	43°50'57.02"	60°37'40.09"	19-Sep-93	30-Sep-93	41.5	43.0	2,660	8,728	Development	oil well	P&A
144	142	336	Cohasset CP6B	P-51	LASMO NSRL	Rowan Gorilla III	43°50'57.02"	60°37'40.09"	5-Oct-93	23-Oct-93	41.5	43.0	2,595	8,414	Development	oil well	P&A
145	143	337	Cohasset CP7	P-51	LASMO NSRL	Rowan Gorilla III	43°50'56.99"	60°37'39.99"	24-Oct-93	21-Nov-93	41.5	43.0	3,376	11,076	Development	oil well	P&A
146	144	338	Cohasset CP7A	P-51	LASMO NSRL	Rowan Gorilla III	43°50'56.99"	60°37'39.99"	11-Dec-93	28-Dec-93	41.5	43.0	2,740	8,990	Development	oil well	P&A
147	145	339	Cohasset CP8	P-51	LASMO NSRL	Rowan Gorilla III	43°50'57.21"	60°37'39.94"	29-Sep-94	24-Nov-94	41.5	43.0	2,555	8,383	Development	oil well	P&A
148	146	340	Cohasset CP9	P-51	LASMO NSRL	Rowan Gorilla III	43°50'57.12"	60°37'40.13"	10-Oct-94	29-Nov-94	41.5	43.0	2,560	8,399	Development	oil well	P&A
149	147	341	Cohasset CP3A	P-51	PanCanadian NS Ltd	Rowan Gorilla III	43°50'57.11"	60°37'39.90"	23-Oct-95	15-Feb-96	41.5	43.0	4,620	15,158	Development	oil well	P&A
150	148	342	Cohasset CP10	P-51	PanCanadian NS Ltd	Rowan Gorilla III	43°50'57.09"	60°37'40.04"	29-Jun-96	26-Jul-96	41.5	43.0	2,833	9,294	Development	oil well	P&A
151	149	343	Cohasset CP10A	P-51	PanCanadian NS Ltd	Rowan Gorilla III	43°50'57.09"	60°37'40.04"	29-Oct-96	28-Nov-96	41.5	43.0	3,107	10,194	Development	oil well	P&A
152	150	344	Cohasset CP10B	P-51	PanCanadian NS Ltd	Rowan Gorilla III	43°50'57.09"	60°37'40.04"	5-Jan-97	9-Feb-97	41.5	43.0	2,485	8,153	Development	oil well	P&A
153	151	345	Cohasset CP6C	P-51	PanCanadian NS Ltd	Rowan Gorilla III	43°50'57.02"	60°37'40.09"	6-May-97	30-Jun-97	41.5	43.0	2,639	8,658	Development	oil well	P&A
154	152	346	Panuke PP3A	J-99	PanCanadian NS Ltd	Rowan Gorilla III	43°48'40.23"	60°44'00.19"	15-Mar-98	13-Apr-98	47.2	44.6	3,305	10,843	Development	oil well	P&A
155	153	347	Panuke PP3B	J-99	PanCanadian NS Ltd	Rowan Gorilla III	43°48'40.23"	60°44'00.19"	29-Apr-98	12-Jun-98	47.2	44.6	4,097	13,442	Development	oil well	P&A
156	154	348	Grand Pre	G-08	PanCanadian	Rowan Gorilla II	43°57'24.10"	60°30'30.79"	4-May-98	2-Jun-98	42.4	20.1	2,382	7,815	Exploratory	dry hole	P&A
157	155	349	Venture 1	O-32	SOEI	Rowan Gorilla II	44°01'59.38"	59°34'57.19"	20-Jun-98	5-Nov-99	40.0	22.0	5,314	17,434	Development	gas well	P&A
158	156	350	Venture 2	O-32	SOEI	Rowan Gorilla II	44°01'59.48"	59°34'57.06"	12-Jun-98	30-Jun-01	40.0	22.0	5,586	18,327	Development	gas well	P&A
159	157	351	Venture 3	O-32	SOEI	Rowan Gorilla II	44°01'59.47"	59°34'57.20"	18-Jun-98	29-Oct-99	40.0	22.0	5,110	16,765	Development	gas well	P&A
160	158	352	Venture 4	O-32	SOEI	Rowan Gorilla II	44°01'59.39"	59°34'57.05"	16-Jun-98	23-Oct-99	40.0	22.0	5,469	17,943	Development	gas well	P&A
161	159	353	Venture 5	O-32	SOEI	Rowan Gorilla II	44°01'59.46"	59°34'57.34"	14-Jun-98	12-Apr-00	40.0	22.0	6,029	19,780	Development	gas well	P&A
162	160	354	Panuke PP3C	J-99	PanCanadian	Rowan Gorilla III	43°48'40.23"	60°44'00.19"	17-Jul-98	12-Apr-99	47.2	44.7	4,163	13,658	Development	gas well	P&A
163	161	355	Thebaud 1	E-74	SOEI	Galaxy II	43°53'28.21"	60°11'59.68"	15-Nov-98	25-Jul-00	45.0	29.2	4,700	15,420	Development	gas well	P&A
164	162	356	Thebaud 2	E-74	SOEI	Galaxy II	43°53'28.08"	60°11'59.70"	18-Nov-98	13-Sep-99	45.0	29.2	4,394	14,416	Development	gas well	P&A
165	163	357	Thebaud 3	E-74	SOEI	Galaxy II	43°53'28.35"	60°11'59.66"	22-Nov-98	26-Jul-99	45.0	29.2	4,523	14,839	Development	gas well	P&A
166	164	358	Thebaud 4	E-74	SOEI	Galaxy II	43°53'28.21"	60°11'59.87"	20-Nov-98	NA	45.0	29.2	458	1,503	Development	gas well	P&A
167	165	359	Thebaud 5	E-74	SOEI	Galaxy II	43°53'28.21"	60°11'59.49"	16-Dec-98	15-Apr-00	45.0	29.2	5,015	16,453	Development	gas well	P&A
168	166	360	Panuke PI-1A	J-99	PanCanadian/ NSRL	Rowan Gorilla III	43°48'40.18"	60°44'00.13"	27-Aug-99	11-Nov-99	47.2	44.0	4,033	13,232	Exploratory/Delineation	gas well	P&A
169	167	361	North Triumph 1	P-42	SOEI	Galaxy II	43°41'58.31"	59°51'18.86"	4-Oct-99	4-Dec-99	54.7	75.4	3,805	12,484	Development	gas well	P&A
170	168	362	Panuke PI-1B	J-99	PanCanadian	Rowan Gorilla III	43°48'40.18"	60°44'00.13"	11-Nov-99	19-Feb-00	47.2	44.0	4,046	13,274	Exploratory/Delineation	gas well	P&A
171	169	363	North Triumph 2	P-42	SOEI	Rowan Gorilla II	43°41'58.19"	59°51'18.99"	20-May-00	5-Jul-00	45.1	75.5	3,937	12,917	Development	gas well	P&A
172	170	364	Panuke	H-08	PanCanadian	Rowan Gorilla III	43°47'21.21"	60°45'19.93"	25-May-00	19-Aug-00	39.5	36.5	3,682	12,080	Delineation	gas well	P&A
173	171	365	Emma	N-03	Mobil Oil	Galaxy II	44°02'47.78"	60°00'53.78"	2-Aug-00	1-Nov-00	45.7	50.6	4,600	15,092	Exploratory	dry hole	P&A
174	172	366	Panuke	M-79	PanCanadian	Rowan Gorilla IV	43°48'48.81"	60°41'47.42"	12-Jul-00	2-Oct-00	46.0	43.5	4,598	15,085	Exploratory	gas well	P&A

CNSOPB Directory of Wells
Nova Scotia Offshore Area

	A	B	C	D	E	F	G	H	I	J	K	L	M	N	O	P	Q
1	Well No.	D #	Well Name	Well Name 2	Company	Drilling Unit	Latitude (N)	Longitude (W)	Spud Date	Well Termination Date	RT Elevation (m)	Water Depth (m)	Total Depth (m MD)	Total Depth (ft MD)	Well Type	Well Classification	Well Status
175	173	367	Panuke	F-09	PanCanadian	Rowan Gorilla III	43°48'22.47"	60°45'57.64"	23-Aug-00	11-Nov-00	39.9	42.0	3,815	12,516	Exploratory	gas show	P&A
176	174	368	Panuke	M-79A	PanCanadian	Rowan Gorilla V	43°48'48.81"	60°41'57.42"	11-Oct-00	17-Dec-00	46.0	43.5	3,934	12,907	Exploratory	gas well	P&A
177	175	369	Adamant	N-97	Mobil et al	Galaxy II	43°56'48.08"	60°14'27.66"	5-Nov-00	4-Feb-01	48.7	16.9	4,708	15,666	Exploratory	gas show	P&A
178	176	370	Musquodoboit	E-23	PanCanadian	Rowan Gorilla V	43°42'15.82"	60°49'09.99"	1-Jul-01	2-Sep-01	47.1	47.3	3,818	12,526	Exploratory	dry hole	P&A
179	177	371	Thebaud 6	E-74	SOEI	Galaxy II	43°53'28.14"	60°11'59.78"	10-Aug-01	9-Nov-01	55.0	29.2	4,011	13,159	Development	gas well	P&A
180	178	372	Southampton	A-25	PanCanadian	Rowan Gorilla V	43°34'09.66"	60°18'16.67"	3-Sep-01	12-Dec-01	82.0	47.0	5,058	16,594	Exploratory	dry hole	P&A
181	179	373	Onondaga	B-84	Shell Canada	Galaxy II	43°43'08.92"	60°12'41.51"	17-Nov-01	12-May-02	45.7	59.7	5,019	16,466	Exploratory	gas well	P&A
182	180	374	Annapolis	B-24	Marathon Cda	West Navion	43°23'07.91"	59°48'38.15"	26-Dec-01	24-Apr-02	35.5	1,737.0	3,496	11,470	Exploratory	gas show	P&A
183	181	375	Queensland	M-88	PanCanadian-	Rowan Gorilla V	43°47'55.26"	60°43'11.19"	14-Dec-01	10-Feb-02	47.0	38.0	4,443	14,577	Exploratory	gas show	P&A
184	182	376	Venture 6	O-32	ExxonMobil	Galaxy II	44°01'59.55"	59°34'57.35"	16-May-02	23-Oct-02	57.2	22.5	6,025	19,767	Development	gas well	P&A
185	183	377	Newburn	H-23	Chevron Cda	Deepwater	43°12'16.43"	60°48'21.20"	22-May-02	21-Aug-02	24.0	977.0	6,070	19,915	Exploratory	gas show	P&A
186	184	378	Annapolis	G-24	Marathon Cda	West Navion	43°23'22.94"	59°48'29.19"	17-Apr-02	16-Aug-02	35.5	1,711.0	6,182	20,282	Exploratory	gas well	P&A
187	185	379	Marquis	L-35	Canadian Sup.	Rowan Gorilla V	44°04'37.57"	60°20'52.72"	6-Jul-02	14-Sep-02	56.0	48.0	4,552	14,934	Exploratory	dry hole	P&A
188	186	380	Marquis	L-35A	Canadian Sup.	Rowan Gorilla V	44°04'37.57"	60°20'52.72"	27-Aug-02	14-Sep-02	56.0	48.0	4,552	14,934	Exploratory	dry hole	P&A
189	187	382	South Venture 1	P-60	ExxonMobil	Galaxy II	43°59'50.36"	59°37'41.40"	29-Oct-02	15-Jan-03	48.7	23.0	4,439	14,564	Development	gas well	P&A
190	188	383	Torbrook	C-15	EnCana Corp.	Eirik Raude	42°34'02.60"	62°17'35.64"	16-Nov-02	14-Jan-03	25.0	1674.5	3,600	11,811	Exploratory	dry hole	P&A
191	189	384	Glenelg	H-59	ExxonMobil	Galaxy II	43°38'15.67"	60°07'47.15"	19-Jan-03	17-Mar-03	48.7	75.0	4,116	13,503	Development	gas well	P&A
192	190	385	Alma 1	N-76	ExxonMobil	Galaxy II	43°35'46.74"	60°41'21.92"	4-May-03	9-Nov-03	46.4	66.6	4,851	15,915	Development	gas well	P&A
193	191	386	Margaree	F-70	EnCana Corp.	Rowan Gorilla V	43°49'24.46"	60°39'54.85"	21-May-03	6-Aug-03	47.6	42.5	3,677	12,064	Exploratory	gas well	P&A
194	192	387	Alma 2	N-76	ExxonMobil	Galaxy II	43°35'46.23"	60°41'22.73"	17-Jun-03	28-Nov-03	46.4	66.6	3,790	12,434	Development	gas well	P&A
195	193	388	Balvenie	B-79	Imperial Oil	Eirik Raude	43°08'01.29"	60°10'56.84"	6-Jul-03	6-Sep-03	25.0	1803.0	4,750	15,584	Exploratory	dry hole	P&A
196	194	390	MarCoh	D-41	EnCana Corp.	Rowan Gorilla V	43°50'09.48"	60°37'21.56"	28-Aug-03	23-Oct-03	47.6	43.4	3,625	11,893	Exploratory	gas well	P&A
197	195	391	Weymouth	A-45	EnCana Shell	Eirik Raude	43°04'01.09"	60°36'16.81"	27-Oct-03	8-Mar-04	25.0	1689.7	6,520	21,391	Exploratory	dry hole	P&A
198	196	392	Mariner	I-85	Candian Sup/	Rowan Gorilla V	44°04'30.74"	59°42'07.20"	19-Nov-03	16-Mar-04	47.0	55.5	5,408	17,743	Exploratory	gas show	P&A
199	197	393	Cree	I-34	ExxonMobil	Rowan Gorilla V	43°43'41.48"	60°34'42.62"	15-May-04	14-Aug-04	49.0	57.0	3,945	12,943	Exploratory	dry hole	P&A
200	198	394	Crimson	F-81	Marathon Cda	Deepwater	43°20'22.29"	59°42'57.03"	18-Jun-04	27-Aug-04	21.4	2091.5	6,676	21,404	Exploratory	gas show	P&A
201	199	395	South Venture 2	P-60	ExxonMobil	Galaxy II	43°59'50.34"	59°37'41.52"	8-Jun-04	24-Jun-05	55.5	22.9	5,315	17,438	Development	gas well	P&A
202	200	396	South Venture 3	P-60	ExxonMobil	Galaxy II	43°59'50.47"	59°37'41.55"	25-Mar-05	1-Jul-05	55.9	22.9	4,666	15,308	Development	gas well	P&A
203	201	397	Venture 7	O-32	ExxonMobil	Galaxy II	44°01'59.56"	59°34'57.21"	5-Aug-05	24-Dec-05	60.2	22.0	6,483	21,270	Development	gas well	P&A
204	202	398	Dominion	J-14	Encana-Marauder	Rowan Gorilla VI	43°53'33.32"	60°31'54.21"	18-Nov-05	30-Jan-06	47.5	29.5	3,700	12,139	Exploratory	dry hole	P&A
205	203	399	Alma 3	N-76	ExxonMobil	Galaxy II	43°35'46.72"	60°41'21.69"	8-Feb-06	11-Apr-06	56.7	66.6	3,380	11,089	Development	gas well	P&A
206	204	400	Dominion	J-14A	Encana-Marauder	Rowan Gorilla VI	43°53'33.33"	60°31'54.21"	30-Dec-05	24-Jan-06	47.5	29.5	4,440	14,567	Exploratory	dry hole	P&A
207	205	401	Alma 4	N-76	ExxonMobil	Rowan Gorilla III	43°35'46.66"	60°41'20.18"	08-Jun-09	14-Aug-09	49.7	66.6	3,985	13,074	Development	gas well	P&A
208	206	402	Margaree	E-70	EnCana	Rowan Gorilla III	43°49'16.94"	60°40'20.18"	12-Jan-10	31-Mar-10	40.9	41.0	2,539	8,330	Development	injector	P&A
209	207	403	Alma 4A	N-76	ExxonMobil	Rowan Gorilla III	43°35'46.66"	60°41'21.77"	08-Aug-09	05-Oct-09	40.9	66.6	4,329	14,202	Development	gas well	P&A
210	208	404	Cheshire	L-97/L-97A	Shell Canada Ltd.	Stena IceMax	42°26'37.99"	62°14'56.83"	23-Oct-15	22-Sep-16	31.7	2,141.5	7,068	23,188	Exploratory	dry hole	P&A
211	209	405	Monterey Jack	E-43/E-43A	Shell Canada Ltd.	Stena IceMax	42°12'16.43"	63°37'29.96"	25-Sep-16	21-Jan-17	31.7	2,117.8	6,692	21,955	Exploratory	dry hole	P&A
212	210	406	Aspy	D-11/D-11A	BP Canada Energy Group	West Aquarius	42° 50' 0.336"	60° 17' 52.169"	22-Apr-18	11-Dec-18	31.0	2771.0	7,400	24,278	Exploratory	dry hole	P&A